이학박사 학위논문

Discovery of Inhibitors of a Protein–RNA (Lin28–*let-7*) Interaction and Antimalarial Agents Through the Development of High-Throughput Screening

고효율 생리활성 탐색 방법의 개발을 통한 단백질–RNA 상호작용 저해제 및 항말라리아 화합물의 발굴

2015 년 8 월

서울대학교 대학원
생물물리 및 화학생물학과
임동현

Abstract

One of the greatest challenges in the field of chemical biology is the identification of novel bioactive small molecules. These molecules can serve as specific bioprobes for the mechanistic studies of biological systems or therapeutic candidates with unique modes of action. There are two main approaches for identifying bioactive small molecules. In the target-based approach, a target biomacromolecule that plays crucial roles in a disease model is selected. High-throughput biochemical assays identify small molecules that modulate the function of the disease-related target. Finally, the desired phenotypic changes induced by the active small molecules are investigated. In the phenotype-based approach, a phenotype related to a disease model is selected, and small molecules that induce the changes in the phenotype are selected. Target identification process can reveal the mechanism of the action of chemical modulators.

Efficient discovery of bioactive small molecules would be possible by combining advantages of each method. Regardless of the type of high-throughput screening, however, the successful discovery of new small molecule modulators has been significantly influenced by the molecular diversity of small molecule screening libraries. Therefore, a new strategy to construct a small molecule library is presented in chapter 1 with the purpose of modulating new therapeutic targets such as protein–protein interactions.

The library members contained two distinct hetereocycles connected in a single molecule with stereodivergent linkers. Pyrimidine-, pyrazole-, or pyrazolopyrimidine-based carbohybrids were constructed through condensations of the key intermediates, 2-*C*-formyl glycals, with various

dinucleophiles. Fused-triazole scaffolds were obtained through intramolecular 1,3-dipolar cycloadditions after selective functionalization of the carbohybrid polyol moieties with azide and alkyne functionalities. Overall, this synthetic method affords two distinct privileged substructures in a single molecule, connected by stereodivergent diol linkers derived from abundant natural chiral sources, carbohydrates. The resulting vicinal diols in the linker were further modified to achieve unique connectivities between the two privileged structures for maximized three-dimensional shape diversity. The diversity was verified through principal moment inertial analysis and the structure alignment of tenergy-minimized compounds.

In chapter 2, a target-based approach is exemplified in an attempt to identify inhibitors of a protein–miRNA (Lin28–*let-7*) interaction, an important therapeutic target.

MicroRNAs (miRNAs) regulate gene expression by targeting most protein-coding transcripts. As a result, miRNAs are involved in every important cellular process in animal. Dysregulation of miRNA biogenesis is associated with many human diseases. *Let-7* miRNA family is well known for its tumor suppression function, and it is down-regulated in many cancers. Lin28 protein is abnormally expressed in many cancer cells, and the protein bind primary and precursor *let-7* miRNAs to inhibit their maturation. In this study, FRET-based high throughput screening system was constructed in order to identify inhibitors of the Lin28–*let-7* interaction. Unnatural amino acid mutagenesis and bioorthogonal chemistry enabled site-specific fluorescent labeling of Lin28, resulting in a highly robust and reliable Lin28–*let-7* binding assays. High-throughput screening using the assay identified flavone-based natural products as inhibitors of the protein–miRNA interaction. Biophysical studies

revealed that inhibitors specifically bind Lin28 to block the access of *let-7* miRNAs.

In chapter 3, discovery of 2-aminopyrimidine-based antimalarial agents using a high-content phenotype-based screening is presented. New antimalarial agents that exhibit multistage activities against drug-resistant strains of malaria parasites represent good starting points for developing next-generation antimalarial therapies. In order to discover such agents, an image-based parasitological screening method for defining drug effects on different asexual life cycle stages of *Plasmodium falciparum* was developed. High-throughput screening of the in house chemical library using this image-based approach led to the identification of carbohybrid-based 2-aminopyrimidine compounds with fast-acting growth inhibitory activities against three laboratory strains of multidrug-resistant *P. falciparum*. Structure−activity relationship study led to the identification of two derivatives (**8aA** and **11aA**) as the most promising antimalarial candidates, targeting all major blood stages of multidrug-resistant *P. falciparum* parasites.

Table of Contents

Chapter 1. Synthesis of Molecular Frameworks Containing Two Distinct Heterocycles Connected in a Single Molecule with Enhanced Three-Dimensional Shape Diversity

1.1. Introduction……1
1.2. Results and Discussion
1.2.1. Preparation of pyrimidine- and pyrazole-based carbohybrids…….5
1.2.2. Construction of fused triazoles through intramolecular 1,3-dipolar cycloadditions……7
1.2.3. Modification of the linker to maximize skeletal diversity in 3D space ……..12
1.3. Conclusion……18
1.4. Experimental Section……19
1.5. References……25
1.6. Acknowledgements……30
1.7. Supporting Information……32

Chapter 2. Discovery of Small Molecule Inhibitors of Lin28–*let-7* Interactions Through the Development of a FRET-based High-Throughput Screening

2.1. Introduction……58
2.2. Results and Discussion
2.2.1. A design strategy for FRET-based binding assay to detect Lin28–*let-7* interaction……61
2.2.2. Site-specific fluorescent labeling of Lin28A through unnatural amino acid mutagenesis……64

2.2.3. Validation of the binding assay and application to high-throughput screening of small molecule library……..…70
2.2.4. Discovery of flavones as inhibitors of Lin28–*let*-*7* interactions and their mode of action……..…74
2.3. Conclusion…….77
2.4. Experimental Section…….78
2.5. References……..…….…….…….82
2.6. Acknowledgements…….…..……85
2.7. Supporting Information……..…86

Chapter 3. Discovery of Carbohybrid-Based 2-Aminopyrimidine Analogues As a New Class of Rapid-Acting Antimalarial Agents Using Image-Based Cytological Profiling Assay

3.1. Introduction……..…….90
3.2. Results and Discussion
3.2.1 A novel image-based cytological profiling assay……..…….…..…92
3.2.2. Discovery of carbohybrid-based aminopyrimidines as a new antimalarial drug class…….95
3.2.3. Novel *in vivo* antimalarial activity of carbohybrids in a mouse malaria model…….103
3.3. Conclusion……105
3.4. Experimental Section…….……..……106
3.5. References.…….……116
3.6. Acknowledgements.……120
3.7. Supporting Information…….……..122

Abstract in Korean…….129
Appendix…….132

List of Tables

Table 1.1. Synthesis of pyrimidine-, pyrazole-, and pyrazolopyrimidine-based carbohybrids……..…….…..…..…….6

Table 1.2. New molecular frameworks containing two distinct privileged substructures in a single hybrid molecule obtained through pathway I…..….11

Table 1.3. New molecular frameworks containing two distinct privileged structures in a single hybrid molecule obtained through pathways II and III..12

Table 1.4. Deprotection of PMB groups in the linker…….……13

Table 2.1. Structure-activity relationship of selected flavones against Lin28A–*let-7a-1* and Lin28B–*let-7a-1* interaction determined by EMSA……..…75

Table 3.1. Antimalarial and cytotoxicity profiles of 2-aminopyrimidine-based hit compounds…….…….…….……96

Table 3.2. Antimalarial and cytotoxicity profiles of 2-aminopyrimidine-based hit compounds…….100

Table 3.3. Microsomal stability and *in vivo* pharmacokinetic properties of candidate compounds **8aA** and **11aA**…….103

List of Figures

Figure 1.1. Bioactive small molecules containing carbohybrid, pyrimidine, pyrazole, pyrazolopyrimidine, and triazole substructures…….…….3

Figure 1.2. New molecular frameworks containing two distinct privileged structures connected with stereodivergent linkers…….…….5

Figure 1.3. 3-dimensional shape diversity of the chimera molecules.…..……17

Figure 2.1. Regulation of *let-7* biogensis by Drosha, Dicer, and Lin28 proteins ……..….60

Figure 2.2. Schematic model of the Lin28–*let-7* binding and a design strategy to construct a FRET-based turn-on binding assay……64

Figure 2.3. Optimization of the Lin28A AzF mutant expression……67

Figure 2.4. Labeling of crude lysates from three Lin28A AzF mutants using DIBO-Alexa555 or BCN-Cy3…….…….69

Figure 2.5. Site-specific labeling of Lin28A AzF mutants with BCN-Cy3…70

Figure 2.6. Validation of the binding assay…….……71

Figure 2.7. Application of the binding assay to high-throughput screening and EMSA for hit confirmation…….……..……..…73

Figure 2.8. Luteolin and myricetin as inhibitors of the Lin28A–*let-7a-1* interactions……74

Figure 2.9. Inhibitory activity of flavones against Lin28B–*let-7a-1* interaction and Lin28A–*let-7g* interaction…….…….……76

Figure 3.1. Stage-specific activities of selected antimalarial agents as determined using a novel image-based cytological profiling method…..……94

Figure 3.2. Cellular modes of action of 2-aminopyrimidine-based carbohybrid compounds……97

Figure 3.3. Speed of action and stage-specificity of derivatives **8aA** and **11aA** ……102

Figure 3.4. Chemical structures and probit analyses of *in vivo* parasitaemia reduction effects of carbohybrid-based 2-aminopyrimidine **8aA** and **11aA** derivatives……..…..…….104

Figure 3.5. Light microscopy images of Day 4 blood smears from *P. chabaudi*-infected mice showing *in vivo* antimalarial activity of derivative **8aA** and **11aA**…….105

List of Schemes

Scheme 1.1. Synthesis of intermediates (**6–8**) that harbor β-azido hydroxyl functionality……..……..……..….9

Scheme 1.2. Synthesis of fused 1,2,3-triazoles……10

Scheme 1.3. Modification of the linker to maximize skeletal diversity in 3D space……14

Scheme 3.1. Synthesis of carbohybrid-based molecular frameworks…….98

Scheme 3.2. Synthesis of compound **14bA** and **15bA**……99

List of Abbreviations

HTS High-throughput screening

pDOS Privileged-substructure-based diversity-oriented synthesis

3D 3-Dimensional

DMF Dimethylformamide

PMB *p*-Methoxybenzyl

PPI Protein–protein interaction

DDQ 2,3-Dichloro-5,6-dicyanobenzoquinone

CDI 1,1-Carbonyldiimidazole

PMI Principal moments of inertia

miRNA microRNA

Pri-miRNA Primary microRNA

Pre-miRNA Precursor microRNA

PreE Pre-element

EMSA Electrophoretic mobility shift assay

FRET Förster resonance energy transfer

CSD Cold shock domain

AzF 4-Azido-L-phenylalanine

aaRS Aminoacyl tRNA synthetase

RF1 Release factor 1

EF-Tu Elongation factor Tu

IPTG Isopropyl β-D-1-thiogalactopyranoside

DIBO Dibenzocyclooctyne

BCN Bicyclononyne

P. falciparum *Plasmodium falciparum*

P. chabaudi *Plasmodium chabaudi*

DAPI 4',6-Diamidino-2-phenylindole

ART Artemisinin

CQ Chloroquine

E64 *trans*-Epoxysuccinyl-L-leucylamido-(4-guanidino)butane

GlcNAc *N*-Acetylglucosamine

SI Selectivity index

hpi Hour postinvasion

IP Intraperitoneal

Chapter 1. Synthesis of Molecular Frameworks Containing Two Distinct Heterocycles Connected in a Single Molecule with Enhanced Three-Dimensional Shape Diversity

Chem. Eur. J. **2013**, 19, 7100–7108.

1.1. Introduction

One of the greatest challenges in the field of chemical biology is the identification of new small molecule modulators that can selectively perturb the function of gene products.[1] Such chemical modulators can serve as specific bioprobes for the mechanistic studies of mysterious biological systems at the molecular level, which is the main concept of chemical genetics.[2] In addition, these small-molecule modulators can open new doors for the development of new therapeutic agents with unique modes of action.[3] The discovery of new bioactive small molecules has been achieved by means of high-throughput screening (HTS) against various biological targets, which can be classified into two major approaches: target-based enzymatic assays and discovery-driven phenotypic assays.[4] Recently, the screening paradigm has shifted toward phenotypic screening as the dominant strategy for discovering new first-in-class therapeutics.[5] Therefore, image-based high-content screening (HCS) has received increased attention in the pharmaceutical industry and academia to expand the repertoire of "druggable" targets.[6]

Regardless of the type of HTS, the successful discovery of new small-molecule modulators has been significantly influenced by the molecular diversity of small-molecule screening libraries.[7] Therefore, it is essential to efficiently construct a collection of drug-like small molecules with maximum

molecular diversity. To this end, synthetic chemists have adopted a diversity-oriented synthesis (DOS) approach that aims at the efficient generation of complex and drug-like compound libraries that contain large numbers of structurally diverse molecular frameworks.[8] Our research group have been particularly interested in the development of divergent and robust synthetic pathways for the efficient construction of a drug-like small-molecule library through the creative assembly of polyheterocycles embedded with privileged substructures including benzopyrans,[9a] benzodiazepines,[9b] acetal-fused pyranopyrones,[9c] and tetrahydroindazolones.[9d] This approach was named privileged-substructure-based diversity-oriented synthesis (pDOS).[10] It is worth mentioning that new polyheterocycles embedded with privileged substructures showed enhanced selectivities and high relevance in multiple biological assays, which was confirmed by the successful identification of specific small-molecule modulators for various biological targets, including anticancer, antiosteoporosis, and antidiabetic agents.[11]

Among the synthetic pathways developed thus far, I pursued the further elaboration of a particular molecular framework, namely, carbohybrids. These are defined as acyclic polyols fused with various privileged heterocycles, which are widely dispersed in nature and have interesting biological activities (Figure 1.1). For example, bengazoles are antifungal marine natural products that contain a unique bisoxazole moiety connected to a carbohydrate-like acyclic polyol.[12] Many iminoalditols with acyclic polyol chains have been identified as inhibitors of glycosyltransferases and glycosidases for diverse therapeutic applications.[13] Sialic acid and its derivatives are polyol-fused heterocyclic molecules widely distributed in nature.[14] On the basis of these interesting structural motifs, an efficient one-pot protocol has been developed

for the synthesis of acyclo-*C*-nucleosides as carbohybrids starting from 2-*C*-formyl glycals.[15] The synthetic method overcame the limitations of previously reported protocols that used 2-*C*-formyl glycals, such as poor yields and the use of strong base. With this powerful method in hand, I envisioned the further expansion of the carbohybrid collection through the creation of new molecular frameworks through the incorporation of various diversity elements, including skeletal, stereochemical, and substituent diversity. In fact, a new type of carbohybrid, elaborated through the modification of a glycosidic linkage at the polyol moiety, has been identified in *Proteus* bacteria (Figure 1.1).[16]

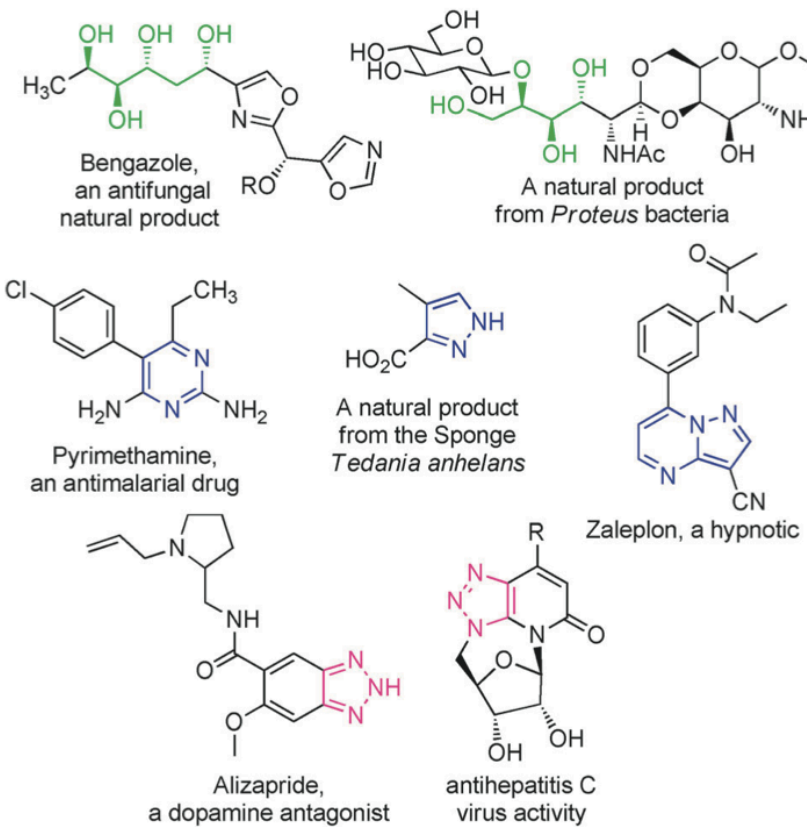

Figure 1.1. Bioactive small molecules containing carbohybrid, pyrimidine, pyrazole, pyrazolopyrimidine, and triazole substructures.

Herein, I report a systematic modification of carbohybrid collections to create new molecular frameworks that contain two distinct privileged substructures in a single molecule. Acyclic polyols fused with pyrimidines, pyrazoles, or pyrazolopyrimidines served as primary carbohybrid skeletons; such heterocycles are privileged substructures frequently observed in bioactive natural products and pharmaceutical agents (Figure 1.1).[17] I also identified 1,2,3-triazoles fused with diverse heterocycles as modification elements for carbohybrids because they are abundant in many bioactive compounds. In fact, there are only a half dozen reports on the synthesis of a fused 1,2,3-triazole-based compound library, and the strategies for their preparation are still in the early stages of development.[18] As shown in Figure 1.2, carbohybrid-derived new molecular frameworks contain two privileged substructures connected with stereodivergent vicinal diols. New synthetic schemes were designed to construct fused triazoles through the intramolecular 1,3-dipolar cycloaddition of azido and alkyne functionalities, which can be installed at the desired positions of the polyol moiety. The intramolecular cycloaddition reaction is quite an efficient transformation and is tolerant of a broad range of substrates.

Next, I aimed to modify the stereodivergent vicinal diol functionality in the linker with various chemical reactions, which would provide new kinds of skeletal diversity through the creation of additional molecular scaffolds. The various tetherings of the chirally enriched vicinal diols allowed the specific display of the two privileged heterocycles in a diverse three-dimensional (3D) space owing to the conformational restriction of the rotatable bonds in the linker region. In this chapter, I describe in detail my stereodivergent synthetic strategy to control the spatial orientation of privileged heterocycles using carbohybrid molecular frameworks.

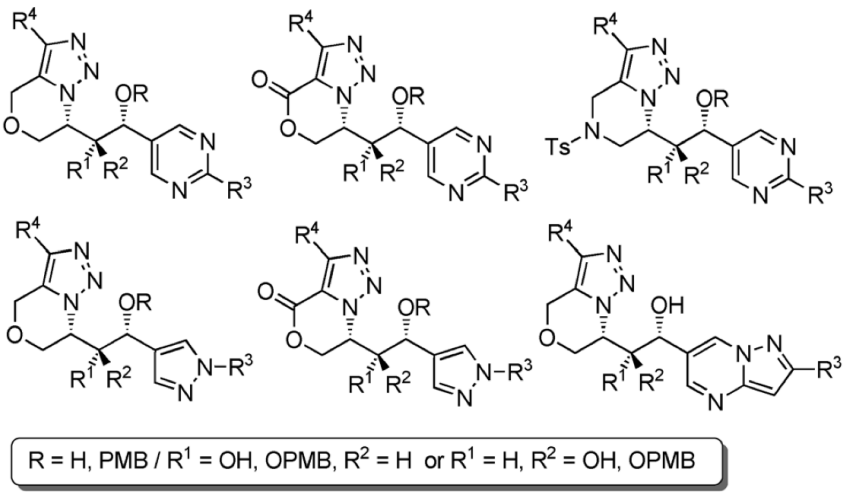

Figure 1.2. New molecular frameworks containing two distinct privileged structures connected with stereodivergent linkers.

1.2. Results and Discussion

1.2.1. Preparation of pyrimidine- and pyrazole-based carbohybrids

The efficient one-pot synthesis of pyrimidine-, pyrazole-, and pyrazolopyrimidine-based carbohybrids has been reported using 2-*C*-formyl glycals as starting materials.[15] In this study, I sought to diversify the polyheterocyclic skeletons through the introduction of fused triazoles in these carbohybrids. Hence, I prepared the key intermediates **1** and **2** through the selective protection of hydroxyl groups on D-glucal and D-galactal, and a subsequent Vilsmeier–Haack formylation. In brief, the primary hydroxyl group at the C-6 position was protected with a trityl group, and two of the secondary hydroxyl groups were orthogonally protected with *p*-methoxy-benzyl (PMB) groups. After formylation in the presence of $POCl_3$ in

dimethylformamide (DMF), the intermediates **1** and **2** were transformed into acyclic polyol-fused pyrimidines **3**, pyrazoles **4**, and pyrazolopyrimidines **5** through the imine formation with dinucleophiles followed by nucleophilic sugar-ring opening.

As shown in Table 1.1, this transformation preserved its broad scope of substrate generality and afforded various polyheterocycles in moderate to good yields. The dinucleophilic condensation of 2-*C*-formyl D-glucal **1** along with ring opening gave almost an identical result to that of 2-*C*-formyl D-galactal **2** in terms of yield and the reaction time under the same conditions (Table 1.1, entries 1 and 2).

Table 1.1. Synthesis of pyrimidine-, pyrazole-, and pyrazolopyrimidine-based carbohybrids.

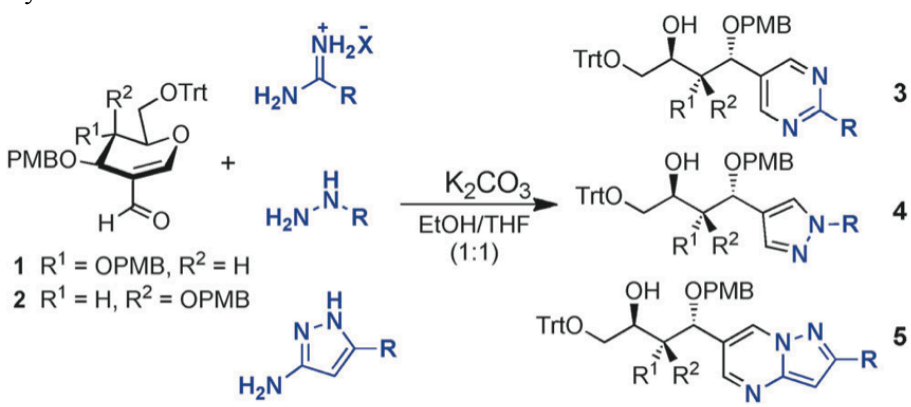

Entry	R^1	R^2	R	Conditions	Yield [%]	Product
1	OPMB	H	NMe_2	RT, 16 h	85	**3a**
2	H	OPMB	NMe_2	RT, 16 h	80	**3b**
3	H	OPMB	*p*-chlorophenyl	RT, 21 h	52	**3c**
4	H	OPMB	NH_2	80 °C, 21 h	68	**3d**
5	H	OPMB	methyl	RT, 14 h	94	**4a**
6	H	OPMB	phenyl	80 °C, 12 h	55	**4b**
7	H	OPMB	methyl	80 °C, 11 h	70	**5a**
8	H	OPMB	phenyl	80 °C, 12 h	44	**5b**

In previous reports, it was clearly demonstrated that both 2-*C*-formyl D-glucal and 2-*C*-formyl D-galactal were coupled with various dinucleophiles in a similar pattern.[15] Therefore, in this research I focused on the formation of fused triazoles and the subsequent diversification in spatial orientation of privileged heterocycles using galactal-based carbohybrids (Table 1.1, entries 2–8). When substituted guanidines and benzamidines were used in a salt form, I generated the free bases of dinucleophiles in the presence of K_2CO_3, which afforded the polyol-fused pyrimidines **3a–d** in moderate to respectable yields (Table 1.1, entries1–4). Synthesis of the pyrazole-based carbohybrid **4a** was successfully achieved in excellent yields by means of the cyclocondensation with methylhydrazine under the basic co-solvent conditions at room temperature (Table 1.1, entry 5). In the case of phenylhydrazine, the desired product **4b** was not observed under identical conditions, probably owing to the inherently poor nucleophilicity of arylhydrazines. However, thermal activation at 80 °C allowed the formation of the desired product **4b** in modest yield (Table 1.1, entry 6). In the case of 5-substituted 3-aminopyrazoles, the conventional heating at 80 °C was also required to obtain the desired pyrazolopyrimidines **5a,b** in moderate to good yields (Table1.1, entries 7 and 8). As observed in the arylhydrazine cases, the presence of a phenyl substituent at the C-5 position of 3-aminopyrazole lowered its reactivity and caused a significant reduction in yield.

1.2.2. Construction of fused triazoles through intramolecular 1,3-dipolar cycloadditions

There are many reports on privileged structures as core skeletons for the

synthesis of potentially bioactive small molecules and as key binding motifs for various biopolymers, especially enzymes and proteins.[19] Therefore, pDOS[10] has been proposed as an efficient strategy for the construction of new polyheterocyclic molecular frameworks that contain privileged substructures to systematically perturb various biological processes, including protein–protein interactions (PPIs). Along this line, I envisioned that the linking of two privileged substructures in a single hybrid molecule might be a powerful strategy to modulate potential PPIs. Each privileged substructure in these hybrid molecules can serve as a binding motif for different PPI partners, which could increase the possibility of perturbing a specific protein–protein interaction in the complex signaling networks.

With the robust and general transformation of key intermediates **1** and **2** with various dinucleophiles, including substituted guanidines, benzamidines, hydrazines, and 3-aminopyrazoles, I pursued the further modification of my resulting carbohybrids. The construction of new core skeletons through the connection of two distinct privileged substructures in a single molecule using various linkers has never been explored in the fields of molecular diversity and diversity-oriented synthesis. Inspired by their abundance in many bioactive compounds[18b,d] and the early developmental stage of drug-like fused 1,2,3-triazole libraries,[18a,c–f] I designed the strategic linkage of fused 1,2,3-triazoles at the other ends of acyclic *C*-nucleosides **3–5** (Figure 1.2).

As shown in Scheme 1.1, the free secondary hydroxyl groups in **3–5**, generated by the cyclocondensations with dinucleophiles, were mesylated, and the trityl-protected primary alcohol was unmasked in the presence of *p*-toluenesulfonic acid in methanol. Then, nucleophilic substitution of the *O*-mesyl group with NaN_3 in DMF afforded intermediates **6–8** that bore β-azido

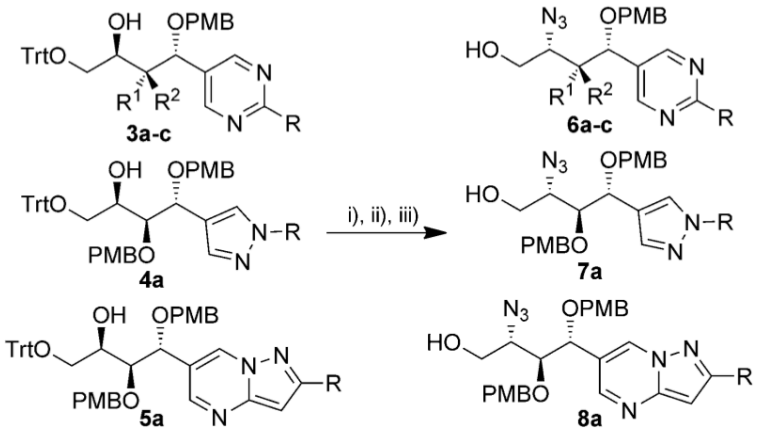

Scheme 1.1. Synthesis of intermediates (**6–8**) that harbor β-azido hydroxyl functionality. i) MsCl, TEA, CH_2Cl_2, 0 °C–RT; ii) *p*-TsOH, MeOH, RT; iii) NaN_3, DMF, 100 °C. **3a**, **6a**: R=NMe_2, R^1 =OPMB, R^2 =H, 62%; **3b**, **6b**: R=NMe_2, R^1 =H, R^2 =OPMB, 88%; **3c**, **6c**: R=*p*-chlorophenyl, R^1 =H, R^2 =OPMB, 73%; **4a**, **7a**: R=Me, 67%; **5a**, **8a**: R=Me, 75%.

hydroxyl functionality in excellent three-step yields. Owing to the mild reaction conditions, no deterioration of chiral enrichment was observed, which might have been caused by the epoxide-associated epimerization through neighboring-group participation. For the formation of the fused triazoles, alkyne functionality was then introduced by the reactions of the hydroxyl groups in **6–8** with various alkyne building blocks. As shown in Scheme 1.2, the nucleophilic substitution of various alkynyl halides with the β-azido hydroxyl moiety in the presence of NaH afforded the corresponding ether intermediates, which underwent the intramolecular 1,3-dipolar cycloadditions in toluene heated to reflux without further purification to yield the desired morpholine-fused triazoles **9** in moderate to excellent yields (Scheme 1.2, pathway I). The hydroxyl moieties in **6–8** were also converted to ester linkages through Mitsunobu reactions with alkynyl acids, and the subsequent intramolecular 1,3-dipolar cycloadditions yielded 2-morpholine-fused triazoles

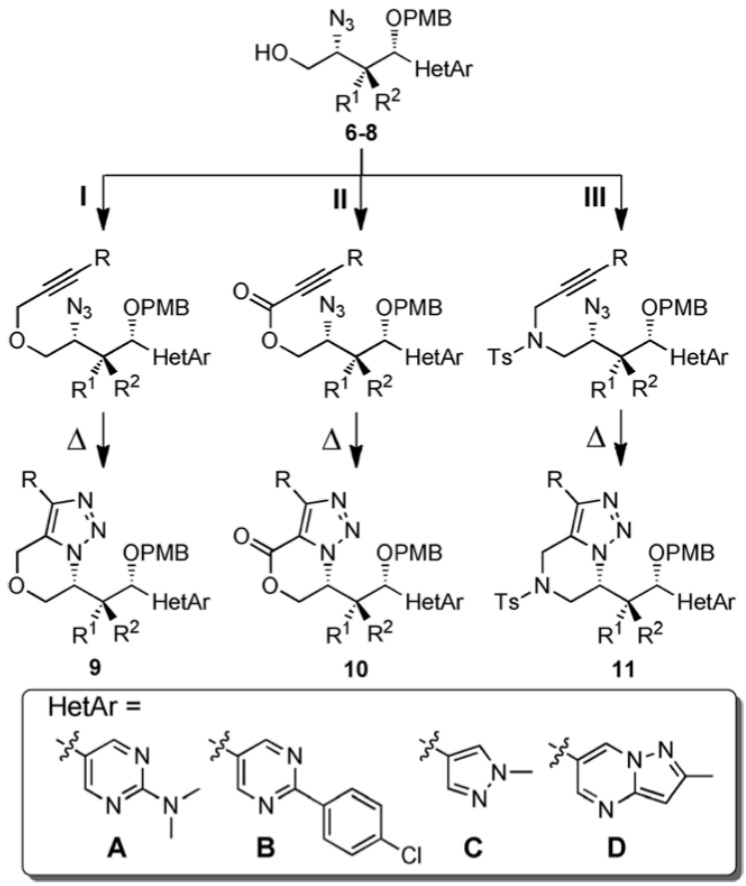

Scheme 1.2. Synthesis of fused 1,2,3-triazoles. I) Haloalkynes, NaH, DMF (S_N2-type O-alkylation), then heating in toluene at reflux. II) Alkynyl acids, diisopropyl azodicarboxylate (DIAD), PPh_3, THF (Mitsunobu reaction), then microwave irradiation, 150 W, 120 °C, DMF. III) Alkynyl sulfonamides, DIAD, PPh_3, THF (Mitsunobu reaction), then heating in toluene at reflux.

10 in excellent yields (Scheme 1.2, pathway II). Alkynyl sulfonamides were successfully introduced under Mitsunobu conditions, and the subsequent intramolecular cycloaddition in toluene heated to reflux afforded piperazine-fused triazoles **11** in high yields (Scheme 1.2, pathway III). Unlike Huisgen cycloaddition, these intramolecular 1,3-dipolar cycloadditions selectively formed single 1,5-regioisomers without copper catalyst, regardless of alkynyl substituents due to the restricted geometries. However, it is worth mentioning

Table 1.2. New molecular frameworks containing two distinct privileged substructures in a single hybrid molecule obtained through pathway I.

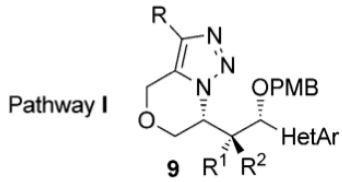

Entry	HetAr	R^1	R^2	R	Yield [%]	Product
1	**A**	OPMB	H	hydrogen	65	**9a**
2	**A**	OPMB	H	methyl	89	**9b**
3	**A**	OPMB	H	ethyl	90	**9c**
4	**A**	OPMB	H	phenyl	65	**9d**
5	**A**	OPMB	H	3-methoxyphenyl	73	**9e**
6	**A**	OPMB	H	1-naphthalene	67	**9f**
7	**A**	H	OPMB	hydrogen	78	**9g**
8	**A**	H	OPMB	methyl	80	**9h**
9	**A**	H	OPMB	ethyl	89	**9i**
10	**A**	H	OPMB	phenyl	64	**9j**
11	**A**	H	OPMB	4-fluorophenyl	58	**9k**
12	**A**	H	OPMB	4-methoxyphenyl	84	**9l**
13	**A**	H	OPMB	2-thienyl	42	**9m**
14	**B**	H	OPMB	methyl	77	**9n**
15	**C**	H	OPMB	methyl	60	**9o**
16	**D**	H	OPMB	methyl	88	**9p**

that the cycloaddition reaction rate was much slower in the case of the ester intermediates (Scheme 1.2, pathway II) than the other substrates under conventional reflux conditions. Instead, microwave irradiation in DMF for 3 min at 150 W and 120 °C was sufficient to convert all the ester intermediates to the desired 1,2,3-triazoles in good yields.

As shown in Tables 1.2 and 1.3, I successfully achieved the efficient synthesis of new chimera compounds (**9–11**) that contained various fused triazoles and privileged heterocycles connected with chirally enriched vicinal diols. This synthetic route is modular enough to construct any combination of fused 1,2,3-triazoles with privileged polyheterocycles, which dramatically

enhances the expandability of their molecular diversity. In addition, I can envision the access to all possible diastereomers of final compounds by using different starting D- and L-hexoses.

Table 1.3. New molecular frameworks containing two distinct privileged structures in a single hybrid molecule obtained through pathways II and III.

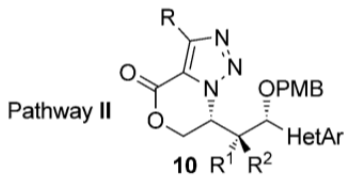

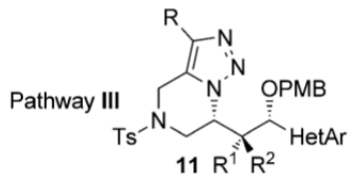

Entry	Path	HetAr	R^1	R^2	R	Yield [%]	Product
1	II	**A**	OPMB	H	methyl	95	**10a**
2	II	**A**	H	OPMB	methyl	72	**10b**
3	II	**B**	H	OPMB	methyl	92	**10c**
4	II	**B**	H	OPMB	ethyl	90	**10d**
5	II	**C**	H	OPMB	methyl	73	**10e**
6	II	**C**	H	OPMB	phenyl	77	**10f**
7	III	**A**	OPMB	H	hydrogen	58	**11a**
8	III	**A**	OPMB	H	phenyl	73	**11b**
9	III	**A**	OPMB	H	4-methylphenyl	70	**11c**
10	III	**A**	OPMB	H	4-cyanophenyl	71	**11d**

1.2.3. Modification of the linker to maximize skeletal diversity in 3D space

After the successful construction of new chimera compounds that contained fused 1,2,3-triazoles and privileged heterocycles connected with chirally enriched vicinal diols, I pursued the introduction of a new diversity element. This was to be achieved through molecular-shape transformation by using various chemical reactions of the stereodivergent vicinal diols in the linker. In fact, the actual arrangement of privileged substructures in 3D space might be critical to potential interactions with biopolymers.[20] By interlocking vicinal

diols in the linkers of my chimera compounds, the projection of two privileged structures could be dramatically changed, and the potential interaction of these unique skeletons to biopolymers can be quite specific due to their limited conformational freedom with a prepaid entropic penalty. The generation of molecular-shape diversity might lead to the diversification of biological activity, with a similar set of appendages in a complementary 3D fashion. To this end, the PMB protecting groups were removed in the presence of 20% trifluoroacetic acid in dichloromethane to release free vicinal diols in excellent yields (Table 1.4).

Table 1.4. Deprotection of PMB groups in the linker.

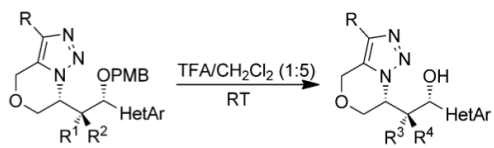

9 **12**

Entry	SM	HetAr	R^1	R^2	R^3	R^4	R	Yield [%]	Product
1	**9a**	**A**	OPMB	H	OH	H	hydrogen	99	**12a**
2	**9b**	**A**	OPMB	H	OH	H	methyl	92	**12b**
3	**9c**	**A**	OPMB	H	OH	H	ethyl	92	**12c**
4	**9g**	**A**	H	OPMB	H	OH	hydrogen	99	**12g**
5	**9h**	**A**	H	OPMB	H	OH	methyl	88	**12h**
6	**9i**	**A**	H	OPMB	H	OH	ethyl	99	**12i**
7	**9j**	**A**	H	OPMB	H	OH	phenyl	96	**12j**
8	**9k**	**A**	H	OPMB	H	OH	4-fluorophenyl	96	**12k**
9	**9l**	**A**	H	OPMB	H	OH	4-methoxyphenyl	89	**12l**
10	**9m**	**A**	H	OPMB	H	OH	2-thienyl	76	**12m**
11	**9n**	**B**	H	OPMB	H	OH	methyl	94	**12n**
12	**9o**	**C**	H	OPMB	H	OH	methyl	99	**12o**

As shown in Scheme 1.3, the resulting vicinal diols were modified through various chemical transformations to uniquely position the two privileged substructures in 3D space. For example, the acetal exchange reaction of the glucal-derived (*R*,*R*)-vicinal diol **12b** with *p*-anisaldehyde dimethyl acetal

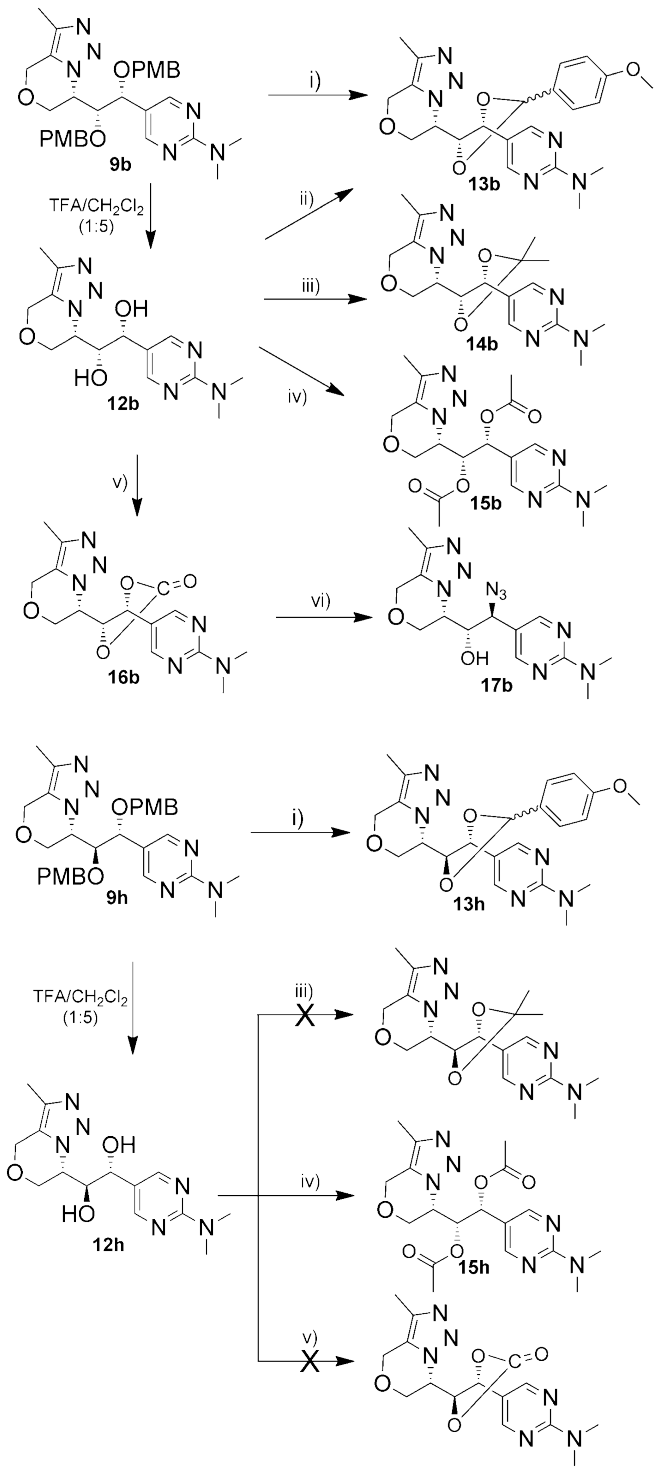

Scheme 1.3. Modification of the linker to maximize skeletal diversity in 3D space. i) DDQ, CH_2Cl_2, 0 °C–RT; **13b**, 59% d.r.=81:19; **13h**, 33%, d.r.= 66:34. ii) Anisaldehyde dimethyl acetal, *p*-TsOH, CH_2Cl_2, RT; **13b**, 55%, d.r. = 71:29. iii) 2,2-

Dimethoxypropane, *p*-TsOH, acetone, RT; **14 b**, 85%. iv) Acetic anhydride, TEA, 4-dimethylaminopyridine (DMAP), CH_2Cl_2, RT; **15b**, 95%; **15h**, 89%. v) CDI, CH_2Cl_2, RT; **16b**, 79%. vi) NaN_3, H_2O, DMF, 110 °C; **17b**, 49%.

afforded the chimera compound **13b** that contained *p*-methoxyphenyl acetal as a 71:29 diastereomeric mixture as determined by ^{1}H NMR spectroscopy. Interestingly, **13b** can also be obtained by 2,3-dichloro-5,6-dicyano-benzoquinone (DDQ) treatment of PMB-protected **9b** in anhydrous CH_2Cl_2 with a similar 81:19 diastereomeric ratio. When the galactal-derived (*R*,*S*)-vicinal diol compound **9h** with PMB protecting groups was treated with DDQ, a different *p*-methoxyphenyl acetal-containing chimera compound **13h** was obtained, with a diastereomeric ratio of 66 :34. The glucal-derived (*R*,*R*)-vicinal diol **12b** was tolerant of various diol-based chemical transformations. For example, the acid-catalyzed acetal exchange reaction of **12b** with 2,2-dimethoxypropane provided dimethyl acetal **14b** in high yield, and the treatment of **12b** with 1,1-carbonyldiimidazole (CDI) in CH_2Cl_2 allowed the formation of carbonate **16b** in good yield. However, the galactal-derived (*R*,*S*)-vicinal diol **12h** did not undergo the ring-forming exchange reaction to the dimethyl acetal under identical conditions (Scheme 3, route iii), possibly due to $A_{1,2}$-strain-like repulsion between two privileged heterocycles upon acetal-based cyclization of the vicinal diol. Similarly, the carbonate compound synthesized by the treatment of **12h** with CDI was transiently generated, but readily decomposed back to the starting compound **12h** at room temperature, which demonstrated the instability of the tethered five-membered ring system from galactal-derived (*R*,*S*)-vicinal diols (Figure 3c).

The further diversification of stereodivergent vicinal diols was carried out through nucleophilic ring opening of the cyclic carbonate **16b** with NaN_3 to

yield the monohydroxy azido compound **17b**.[21] To maximize the molecular shape diversity of my compound collections, the stereodivergent vicinal diols were modified with acetylation to provide **15b** and **15h** as a linear version of my chimera compounds.

Overall, the vicinal diol modifications introduced new skeletal diversity in my compound collection: two heterocyclic substructures could be uniquely oriented in 3D space through the tethering process of vicinal diols. To visualize the shape diversity I achieved, I selected eight representative chimera compounds (**9h**, **12b**, **13b**, **13h**, **14b**, **15b**, **16b**, and **17b**) with identical appendages that differed with respect to stereochemistry and/or tethering moiety of vicinal diols. The eight compounds were virtually modeled in 3D space, and their energy-minimized molecular structures were superimposed and aligned with respect to the pyrimidine group. As shown in Figure 1.3a, the orientations of morpholine-fused triazoles diverged significantly in 3D space through the rigidified linker regions, which emphasized the importance of the shape diversity in my chimera compounds and the associated spatial display of two privileged substructures within a single molecule. Moreover, to quantify the discrete shape differences of eight representative compounds in 3D space, I performed the normalized principal moments of inertia (PMI) analysis.[22] The PMI analysis has been used to capture the shape-based distribution of the small molecule library. The points in the resulting plot occupy an isosceles triangle defined by the vertices (0,1), (0.5,0.5), and (1,1), which correspond to the shape of a rod, disc, and sphere, respectively. As shown in Figure 1.3b, my representative compounds were dispersed in the PMI plot, which indicates that my linker diversification strategy of stereodivergent vicinal diols allows access

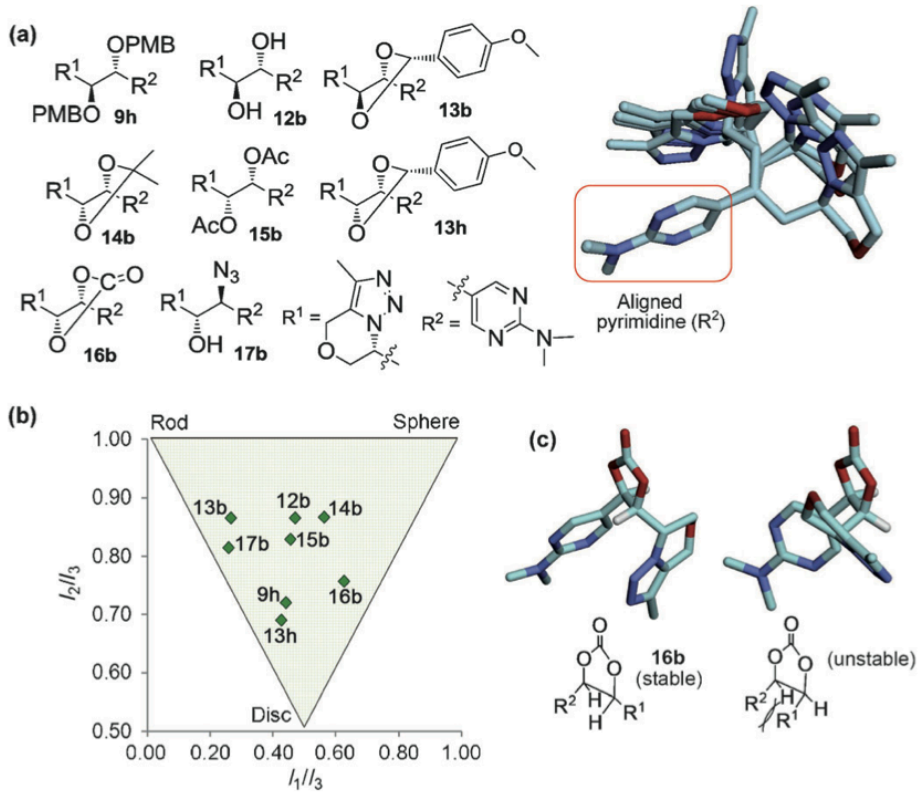

Figure 1.3. 3-dimensional shape diversity of the chimera molecules. (a) Overlay of eight representative molecules. Energy-minimized conformers were aligned with respect to the pyrimidine moiety. Branching linker atoms are not shown in this figure for clarity. (b) PMI plot depicting the eight representative compounds. (c) The structural differences in energy-minimized conformers of glucal-derived (*R*,*R*)-carbonate **16b** and unstable galactal-derived (*R*,*S*)-carbonate.

to different chemical spaces by means of the unique display of two privileged substructures in 3D space.

The differences in the stereochemistry and linker tethering lead to the significant shape and skeletal diversity of final compounds, thus emphasizing the importance of the unique design of molecular frameworks and their connectivity. It is worth mentioning that the overall shape of a small molecule is the most fundamental element that influences its specific modulation of

biological functions and signaling pathways. Indeed, a substantial "shape space" coverage (in other words, molecular-shape diversity) has been correlated with a broad range of perturbations in biological activities.[22] In this study, I demonstrated that the shape space coverage of chimera carbohybrids that contain two unique privileged substructures could be expanded through the tethering of the stereodivergent vicinal diols in the linker region. Therefore, in the field of diversity-oriented synthesis, my linker-diversification strategy affords a new way to access molecular-shape diversity in 3D space and a new tool to expand this molecular diversity without significant changes in substituents.

1.3. Conclusion

New molecular frameworks were developed through the systematic incorporation of two distinct privileged substructures in a single molecule. As substituents of carbohybrids, pyrimidines, pyrazoles, and pyrazolopyrimidines were synthesized by means of the condensations of common intermediates, 2-*C*-formyl glycals, with the corresponding dinucleophiles in simple one-pot procedures. To enhance the biological relevance of these compounds, particularly with respect to the potential perturbations of protein–protein interactions, privileged fused triazoles were introduced at the other end of the resulting carbohybrids. The β-azido hydroxyl moieties in the key intermediates were prepared by selective polyol modifications, and the primary hydroxyl groups were modified with various alkyne building blocks. The resulting intermediates, which contain both azido and alkyne functionalities, were then subjected to intramolecular copper-free 1,3-dipolar cycloaddition by

conventional heating or microwave irradiation to efficiently yield the fused 1,2,3-triazoles as a single 1,5-regioisomer. The key feature of these carbohybrids was the connection of two privileged heterocycles with a stereochemically enriched vicinal diol linker, which was further utilized for the expansion of molecular-shape diversity through tethering of the stereodivergent vicinal diols using various chemical reactions. This allowed the unique orientation of privileged substructures in 3D space. This linker-diversification strategy offers a new diversity element through molecular shape transformation without substituent changes. PMI analysis and the structure alignment of energy-minimized representative compounds clearly demonstrated the importance of stereochemistry and linker-modification chemistry of vicinal diols. The molecular recognition of bioactive small molecules by biopolymers is significantly influenced by their 3D conformations.[23] Therefore, the linker-diversification strategy and my new molecular frameworks can provide a valuable platform on which to build molecular diversity in 3D space, ultimately leading to the identification of specific bioactive small molecules, particularly protein–protein interaction modulators.

1.4. Experimental Section

General methods. All commercially available reagents and solvents were used without further purification unless noted otherwise. All the solvents were purchased form commercial venders. ^{1}H and ^{13}C NMR spectra were obtained using Bruker DRX-300 (Bruker Biospin, Germany), Agilent 400-MR DD2 (Agilent, USA), or Varian Inova-500 (Varian Assoc., Palo Alto, USA)

instruments. Chemical shifts were reported in ppm from tetramethylsilane (TMS) as internal standard or the residual solvent peak ($CDCl_3$; ^1H: δ = 7.26 ppm; ^{13}C: δ = 77.23 ppm). Multiplicity was indicated as follows: s (singlet), d (doublet), t (triplet), q (quartet), m (multiplet), dd (doublet of doublet), dt (doublet of triplet), td (triplet of doublet), brs (broad singlet), and so on. Coupling constants are reported in hertz. Mass spectrometric analysis was performed using a Finnigan Surveyor MSQ Plus LC/MS (Thermo) with electrospray ionization (ESI). Microwave reaction was performed using a CEM Discover Benchmate microwave synthesizer. The conversion of starting materials was monitored by thin-layer chromatography (TLC) using precoated glass-backed plates (silica gel 60; F_{254} = 0.25 mm), and the reaction components were visualized by observation under UV light (254 and 365 nm) or by treatment of TLC plates with visualizing agents such as $KMnO_4$, phosphomolybdic acid, ceric sulfate, and ninhydrin followed by heating. Products were purified by flash column chromatography on silica gel (230–400 mesh) using a mixture of EtOAc/hexane or MeOH/CH_2Cl_2 as eluents. The energy-minimized structures of molecules were obtained by Vconf Interface v2.0 using default parameters and visualized by Discovery Studio 3.0. The principal moment of inertia (PMI) of the energy-minimized structures was calculated using PreADMET v2.0 and visualized by a PMI plot as described previously.[22a]

General procedure for the preparation of pyrimidine-, pyrazole-, and pyrazolopyrimidine-based carbohybrids 3–5. A solution of 2-*C*-formyl glycal **1** or **2** (100 mg) in THF (3 mL) was added to a stirred solution of dinucleophile (2 equiv.) and K_2CO_3 (5 equiv.) in ethanol (3 mL). The reaction mixture was stirred at room temperature or 80 °C until the full conversion of

starting materials monitored by TLC. The solvent was removed under reduced pressure and the residue was partitioned between ethyl acetate and water. The aqueous layer was extracted with ethyl acetate twice, and the combined organic layer was dried over anhydrous Na_2SO_4. The filtrate was condensed under reduced pressure and subjected to flash column chromatography. Carbohybrid **3b**: Prepared from **2** and 1,1-dime-thylguanidine sulfate salt, amorphous white solid. Yield: 80%; $[\alpha]_D^{25}$ = 9.69 (c = 0.91, $CHCl_3$); R_f = 0.17 (EtOAc/hexane 1:2); ^{1}H NMR (500 MHz, $CDCl_3$): δ = 8.24 (s, 2 H), 7.42 (d, *J* = 8.1 Hz, 6 H), 7.30–7.22 (m, 9H), 7.15 (d, *J* = 8.6 Hz, 2H), 6.82–6.78 (m, 4H), 6.69 (d, *J* = 8.3 Hz, 2H), 4.40 (d, *J* = 11.2Hz, 1H), 4.24 (d, *J* = 7.6Hz, 1H), 4.18 (d, *J* = 11.2 Hz, 1 H), 4.11–4.05 (m, 3 H), 3.78 (s, 3 H), 3.76 (s, 3 H), 3.73 (dd, *J* = 7.6, 2.4 Hz, 1H), 3.27 (dd, *J* = 9.3, 6.1 Hz, 1H), 3.21 (s, 6H), 3.08 (dd, *J* = 9.3, 6.4 Hz, 1H), 2.39 ppm (d, *J* = 7.6 Hz, 1H); ^{13}C NMR (125 MHz, $CDCl_3$): δ = 162.4, 159.5, 159.4, 157.9, 144.1, 130.2, 129.8, 129.7, 128.9, 128.0, 127.2, 119.1, 114.0, 113.8, 86.9, 81.0, 76.5, 74.3, 70.3, 70.0, 64.7, 60.6, 55.5, 37.4, 14.4 ppm; HRMS (FAB+): m/z calculated for $C_{45}H_{47}N_3O_6$ $[M+H]^+$: 726.3543; found: 726.3536.

General procedure for the preparation of key intermediates 6–8 that harbor β-azido hydroxyl functionality. Triethylamine (TEA; 3 equiv.) and MsCl (Ms = mesylate; 2 equiv.) were added to a stirred solution of primary carbohybrid **3–5** (1 equiv.) in anhydrous CH_2Cl_2 at 0 °C. The mixture was stirred at 0 °C for 2 h, diluted with CH_2Cl_2 and washed with brine. The aqueous layer was extracted with CH_2Cl_2, and the combined organic layer was dried over anhydrous Na_2SO_4. After removal of the organic solvent under reduced pressure, the crude mesylated product was dissolved in methanol, followed by the addition of *p*-TsOH (1.5 equiv.). After stirring for 8 h at room

temperature, the solvent was removed under the reduced pressure, and the residue was partitioned between ethyl acetate and saturated $NaHCO_3$ solution. The aqueous layer was extracted with ethyl acetate twice, and the combined organic layer was dried over anhydrous Na_2SO_4. The filtrate was condensed under reduced pressure and subjected to flash column chromatography. The detritylated product (1 equiv.) was dissolved in DMF and NaN_3 (5 equiv.) was added, after which the mixture was stirred at 100 °C for 12 h. The solvent was removed and the residue was partitioned between ethyl acetate and water. The aqueous layer was extracted with ethyl acetate, and the combined organic layer was dried over anhydrous Na_2SO_4. The filtrate was condensed under reduced pressure and subjected to flash column chromatography to obtain key intermediates **6–8**. Intermediate **6a**: Prepared from carbohybrid **3a**, white syrup. Yield: 62%; $[\alpha]_D^{25}$ = 55.11 (c = 0.74, $CHCl_3$) ; R_f = 0.19 (EtOAc/hexane 1:1) ; ^{1}H NMR (500 MHz, $CDCl_3$): δ = 8.31 (s, 2 H), 7.22–7.18 (m, 4 H), 6.86–6.84 (m, 4 H), 4.63 (s, 2 H), 4.47–4.43 (m, 2 H), 4.23 (d, *J* = 11.2 Hz, 1H), 3.80 (s, 6H), 3.65 (t, *J* = 5.4 Hz, 1H), 3.60 (d, *J* = 4.9 Hz, 2H), 3.26 (q, *J* = 5.1 Hz, 1H), 3.22 (s, 6H), 1.94 ppm (brs, 1 H) ; ^{13}C NMR (125 MHz, $CDCl_3$): δ = 162.4, 159.51, 159.49, 157.6, 130.3, 129.9, 129.8, 129.6, 117.9, 114.0, 113.9, 81.1, 78.4, 74.9, 70.6, 63.5, 62.3, 55.39, 55.36, 37.3 ppm; HRMS (FAB+): m/z calculated for $C_{26}H_{32}N_6O_5$ $[M+H]^+$: 509.2512; found: 509.2515.

General procedure for the preparation of morpholine-fused triazoles 9. NaH (2 equiv.) was added to a stirred solution of key intermediates **6–8** in anhydrous DMF at 0 °C. After stirring the mixture for 15 min at 0 °C, alkynyl halide (1.5 equiv.) was added, and the mixture was stirred at room temperature for 5 h. The solvent was removed under reduced pressure, and the residue was

partitioned between ethyl acetate and brine. The aqueous layer was extracted with ethyl acetate, and the combined organic layer was dried over anhydrous Na_2SO_4. The filtrate was condensed under reduced pressure and dissolved in toluene. The mixture was heated to reflux for 4 h. After removal of the solvent, the residue was subjected to flash column chromatography. In some cases, the crude mixture in DMF was heated to 110 °C to give morpholine-fused triazoles **9** in a one-pot manner. After completion of the reaction, the purification step was the same as described above. Triazole **9b**: prepared from intermediate **6a** and 1-bromo-2-butyne; white solid. Yield: 89%; $[\alpha]_D^{25}$ = –60.08 (c = 0.58, $CHCl_3$) ; R_f = 0.09 (EtOAc/hexane 1:1) ; ^{1}H NMR (500 MHz, $CDCl_3$): δ = 8.25 (s, 2 H), 7.15–7.10 (m, 4 H), 6.80–6.78 (m, 4 H), 4.62–4.50 (m, 4 H), 4.45–4.40 (m, 2 H), 4.34 (d, *J* = 11.2 Hz, 1 H), 4.15–4.10 (m, 3 H), 3.76–3.74 (m, 7 H), 3.18 (s, 6 H), 2.08 ppm (s, 3 H) ; ^{13}C NMR (125 MHz, $CDCl_3$): δ = 162.1, 159.4, 159.3, 157.7, 136.6, 130.2, 129.84, 129.79, 129.7, 127.5, 117.7, 113.8, 80.4, 77.4, 74.8, 70.0, 64.7, 62.0, 56.0, 55.33, 55.31, 37.2, 9.8 ppm; HRMS (FAB+): m/z calculated for $C_{30}H_{36}N_6O_5$ $[M+H]^+$: 561.2825; found: 561.2821.

General procedure for the preparation of 2-morpholione-fused triazoles 10. Diisopropyl azodicarboxylate (1.2 equiv.) was added slowly to a stirred solution of key intermediates **6–8** (1 equiv.), triphenylphosphane (1.2 equiv.), and akynic acids (1.2 equiv.) in anhydrous THF at 0 °C. The mixture was stirred at 0 °C for 1.5 h. After removal of the solvent, the residue was subjected to flash column chromatography to give ester intermediates. They were dissolved in DMF and heated in a capped microwave vessel under microwave irradiation (150 W, 120 °C) for 3 min. After removal of the solvent, the residue was subjected to flash column chromatography. Triazole **10a**:

Prepared from intermediate **6a** and 2-butynoic acid, Yellow solid, Yield: 95%; $[\alpha]_D^{25}$ = –16.09 (c = 0.61, $CHCl_3$), R_f= 0.19 (EtOAc/hexane 1:1); ^{1}H NMR (300 MHz, $CDCl_3$): δ = 8.42 (s, 2 H), 7.14 (d, *J* = 8.7 Hz, 2 H), 7.03 (d, *J* = 8.7 Hz, 2 H), 6.85–6.76 (m, 4 H), 4.68–4.64 (m, 1H), 4.54 (d, *J* = 5.8 Hz, 1H), 4.46–4.40 (m, 3H), 4.33 (d, *J* = 10.5 Hz, 1H), 4.23 (d, *J* = 10.5 Hz, 1H), 4.16 (d, *J* = 11.1 Hz, 1H), 3.92–3.89 (m, 1H), 3.79 (s, 3H), 3.78 (s, 3H), 3.22 (s, 6H), 2.54 ppm (s, 3H); ^{13}C NMR (75 MHz, $CDCl_3$): δ = 162.6, 159.8, 159.7, 158.1, 156.7, 148.9, 131.0, 130.1, 129.2, 128.4, 121.8, 117.0, 114.1, 114.0, 79.3, 77.4, 74.9, 70.6, 68.5, 55.7, 55.5, 55.4, 37.3, 11.4 ppm; HRMS (FAB+): m/z calculated for $C_{30}H_{34}N_6O_6$ $[M+H]^+$: 575.2618; found: 575.2622.

General procedure for the preparation of piperazine-fused triazoles 11. Diisopropyl azodicarboxylate (1.5 equiv.) was added slowly to a stirred solution of key intermediates **6–8** (1 equiv.), triphenylphosphane (1.5 equiv.), and akynic sulfonamides (1.5 equiv.) in anhydrous THF at 0 °C. The mixture was stirred at room temperature for 12 h. After removal of the solvent, the residue was subjected to flash column chromatography, and the resulting intermediate was stirred in toluene heated at reflux for 3 h. After removal of the solvent, the residue was subjected to flash column chromatography. Triazole **11b**: prepared from intermediate **6a** and 4-methyl-*N*-(3-phenylprop-2-yn-1-yl)benzenesulfonamide, yellow solid. Yield: 73%; $[\alpha]_D^{25}$ = –50.39 (c = 0.46, $CHCl_3$); R_f= 0.20 (EtOAc/hexane 2:3); ^{1}H NMR (400 MHz, $CDCl_3$): δ = 8.39 (s, 2H), 7.60–7.55 (m, 4H), 7.46–7.43 (m, 2H), 7.37–7.32 (m, 3H), 7.08–7.03 (m, 4H), 6.77–6.71 (m, 4 H), 4.72–4.67 (m, 2 H), 4.46 (d, *J* = 11.7 Hz, 1 H), 4.34–4.19 (m, 3 H), 4.15–4.09 (m, 2 H), 4.02 (d, *J* = 11.7 Hz, 1 H), 3.71 (s, 3 H), 3.69 (s, 3 H), 3.52 (dd, *J* = 13.1, 5.7 Hz, 1 H), 3.17–3.13 (m, 7 H), 2.46 ppm (s, 3 H); ^{13}C NMR (100 MHz, $CDCl_3$): δ = 162.4, 159.59, 159.57, 157.9,

144.9, 141.9, 132.8, 130.8, 130.6, 130.4, 129.5, 129.1, 129.0, 128.2. 127.8, 126.3, 125.4, 117.5, 113.99, 113.98, 80.2, 75.1, 74.8, 69.8, 57.2, 55.4, 55.3, 44.4, 42.8, 37.3, 21.8 ppm; HRMS (FAB+): m/z calculated for $C_{42}H_{45}N_7O_6S$ $[M+H]^+$: 776.3230; found: 776.3234.

1.5. References

[1] a) Schreiber, S. L. Small molecules: the missing link in the central dogma. *Nat. Chem. Biol.* **2005**, 1, 64–66; b) Hübel, K; Lessmann, T; Waldmann, H. Chemical biology–identification of small molecule modulators of cellular activity by natural product inspired synthesis. *Chem. Soc. Rev.* **2008**, 37, 1361–1374.

[2] a) Lehμr, J.; Stockwell, B. R.; Giaever, G.; Nislow, C. Combination chemical genetics. *Nat. Chem. Biol.* **2008**, 4, 674–681; b) O'Connor, C. J.; Laraia, L.; Spring, D. R. Chemical genetics. *Chem. Soc. Rev.* **2011**, 40, 4332–4345.

[3] a) Dandapani, S.; Marcaurelle, L. A. Grand challenge commentary: accessing new chemical space for 'undruggable' targets. *Nat. Chem. Biol.* **2010**, 6, 861–863; b) Schreiber, S. L. Organic synthesis toward small-molecule probes and drugs. *P. Natl. Acad. Sci. USA* **2011**, 108, 6699–6702.

[4] Cong, F.; Cheung, A. K.; Huang, S. M. A. Chemical genetics–based target identification in drug discovery. *Annu. Rev. Pharmacol.* **2012**, 52, 57–78.

[5] Swinney, D. C.; Anthony J. How were new medicines discovered? *Nat. Rev. Drug. Discov.* **2011**, 10, 507–519.

[6] a) Zock, J. M. Applications of high content screening in life science research. *Comb. Chem. High Throughput Screening Comb. Chem. High. T. Scr.*

2009, 12, 870–876; b) Zanella, F.; Lorens, J. B.; Link W. High content screening: seeing is believing. *Trends Biotechnol.* **2010**, 28, 237–245; c) Soleilhac, E.; Nadon, R.; Lafanechere, L. High-content screening for the discovery of pharmacological compounds: advantages, challenges and potential benefits of recent technological developments. *Expert Opin. Drug Discovery* **2010**, 5, 135–144.

[7] a) Drewry, D. H.; Macarron, R. Enhancements of screening collections to address areas of unmet medical need: an industry perspective. *Curr. Opin. Chem. Biol.* **2010**, 14, 289–298; b) Marcaurelle, L. A.; Foley, M. A. The evolving role of molecular diversity in drug discovery. *Curr. Opin. Biol.* **2010**, 14, 285–288.

[8] a) Schreiber, S. L. Target-oriented and diversity-oriented organic synthesis in drug discovery. *Science* **2000**, 287, 1964–1969; b) Burke, M. D.; Schreiber, S. L. A planning strategy for diversity-oriented synthesis. *Angew. Chem. Int. Ed.* **2004**, 43, 46–58; c) Spandl, R. J.; Bender, A.; Spring, D. R. Diversity-oriented synthesis; a spectrum of approaches and results. *Org. Biomol. Chem.* **2008**, 6, 1149–1158; d) Galloway, W. R. J. D.; Isidro-Llobet, A.; Spring, D. R. Diversity-oriented synthesis as a tool for the discovery of novel biologically active small molecules. *Nat. Commun.* **2010,** 1, 80; e) O'Connor, C. J.; Beckmann, H. S. G.; Spring, D. R. Diversity-oriented synthesis: producing chemical tools for dissecting biology. *Chem. Soc. Rev.* **2012**, 41, 4444–4456.

[9] a) Ko, S. K.; Jang, H. J.; Kim, E.; Park, S.B. Concise and diversity-oriented synthesis of novel scaffolds embedded with privileged benzopyran motif. *Chem. Commun.* **2006**, 2962–2964; b) Lee, S. C.; Park, S. B. Novel application of Leuckart–Wallach reaction for synthesis of tetrahydro-1,4-benzodiazepin-5-ones library. *Chem. Commun.* **2007**, 3714–3716; c) Sagar, R.;

Park, J.; Koh, M.; Park, S. B. Diastereoselective synthesis of polycyclic acetal-fused pyrano[3,2-c]pyran-5(2H)-one derivatives. *J. Org. Chem.* **2009**, 74, 2171–2174; d) Kim, J.; Song, H.; Park, S. B. Orthogonal regioselective synthesis of *N*-Alkyl-3-substituted tetrahydroindazolones. *Eur. J. Org. Chem.* **2010**, 3815–3822.

[10] Oh, S.; Park, S.B. A design strategy for drug-like polyheterocycles with privileged substructures for discovery of specific small-molecule modulators. *Chem. Commun.* **2011**, 47, 12754–12761.

[11] a) Oh, S.; Kim, S. J.; Hwang, J. H.; Lee, H. Y.; Ryu, M. J.; Park, J.; Kim, S. J.; Jo, Y. S.; Kim, Y. K.; Lee, C. H.; Kweon, K. R.; Shong, M.; Park, S. B. Antidiabetic and antiobesity effects of ampkinone (**6f**), a novel small molecule activator of AMP-activated protein kinase. *J. Med. Chem.* **2010**, 53, 7405–7413; b) Oh, S.; Nam, H. J.; Park, S.; Beak, S. H.; Park, S. B. Development of a benzopyran-containing androgen receptor antagonist to treat antiandrogen-resistant prostate cancer. *ChemMedChem* **2010**, 5, 529–533; c) Zhu, M.; Kim, M. H.; Lee, S.; Bae, S. J.; Kim, S. H.; Park, S. B. Discovery of novel benzopyranyl tetracycles that act as inhibitors of osteoclastogenesis induced by receptor activator of NF-κB ligand. *J. Med. Chem.* **2010**, 53, 8760–8764; d) Oh, S.; Cho, S.W.; Yang, J. Y.; Sun, H. J.; Chung, Y. S.; Shin, C. S.; Park, S. B. Discovery of a novel benzopyranyl compound as a potent *in vitro* and *in vivo* osteogenic agent. *MedChemComm* **2011**, 2, 76–80; e) Cho, T.-J.; Kim, J.; Kwon, S.-K.; Oh, K.; Lee, J.-a.; Lee, D.-S.; Cho, J.; Park, S. B. A potent small-molecule inducer of chondrogenic differentiation of human bone marrow-derived mesenchymal stem cells. *Chem. Sci.* **2012**, 3, 3071–3075.

[12] Searle, P. A.; Richter, R. K.; Molinski, T. F. Bengazoles C−G from the sponge *Jaspis* sp. synthesis of the side chain and determination of absolute

donfiguration. *J. Org. Chem.* **1996**, 61, 4073–4079.

[13] a) Carmona, A. T.; Fuentes, J.; Robina, I.; Garcia, E. R.; Demange, R.; Vogel, P.; Winters, A.L. Stereoselective syntheses of 1,4-dideoxy-1,4-imino-octitols and novel tetrahydroxyindolizidines. *J. Org. Chem.* **2003**, 68, 3874–3883; b) Lundt, I.; Steiner, A. J.; Stutz, A. E.; Tarling, C. A.; Ully, S.; Withers, S. G.; Wrodnigg, T. M. Fluorescently tagged iminoalditol glycosidase inhibitors as novel biological probes and diagnostics. *Bioorg. Med. Chem.* **2006**, 14, 1737–1742.

[14] a) Klefel, M. J.; von Itzstein, M. Recent advances in the synthesis of sialic acid derivatives and sialylmimetics as biological probes. *Chem. Rev.* **2002**, 102, 471–490; b) Angata, T.; Varki, A. chemical diversity in the sialic acids and related α-keto acids: an evolutionary perspective. *Chem. Rev.* **2002**, 102, 439–469.

[15] a) Sagar, R.; Park, S. B. Facile and efficient synthesis of carbohybrids as stereodivergent druglike small molecules. *J. Org. Chem.* **2008**, 73, 3270–3273; b) Sagar, R.; Kim, M. J.; Park, S. B. An improved synthesis of pyrimidine- and pyrazole-based acyclo-*C*-nucleosides as carbohybrids. *Tetrahedron Lett.* **2008**, 49, 5080–5083.

[16] a) Vinogradov, E.; Bock, K. A new type of glycosidic linkage: an open-chain acetal-linked *N*-acetylgalactosamine in the core part of the lipopolysaccharides from *Proteus* microorganisms. *Angew. Chem. Int. Ed.* **1999**, 38, 671–674 ; b) Hindsgaul, O. Carbohydrate chemistry: Sugars out in the open. *Nature* **1999**, 399, 644–645.

[17] a) Bekhit, A. A.; Hymete, A.; Bekhit, A. E. A.; Damtew, A.; Aboul-Enein, H. Y. Pyrazoles as promising scaffold for the synthesis of anti-inflammatory and/or antimicrobial agent: a review. *Mini-Rev. Med. Chem.* **2010**, 10, 1014–

1033; b) Parameswaran, P. S.; Naik, C. G.; Hegde, V. R. Secondary metabolites from the sponge *Tedania anhelans*: isolation and characterization of two novel pyrazole acids and other metabolites. *J. Nat. Prod.* **1997**, 60, 802–803; c) Lagoja, I. M. Pyrimidine as constituent of natural biologically active compounds. Chem. *Biodiversity* **2005**, 2, 1–50; d) Sirichaiwat, C.; Intaraudom, C.; Kamchonwongpaisan, S.; Vanichtanankul, J.; Thebtaranonth, Y.; Yuthavong, Y. Target guided synthesis of 5-benzyl-2,4-diamonopyrimidines: their antimalarial activities and binding affinities to wild type and mutant dihydrofolate reductases from *Plasmodium falciparum*. *J. Med. Chem.* **2004**, 47, 345–354; e) Weitzel, K. W.; Wickman, J. M.; Augustin, S. G.; Strom, J. G. Zaleplon: a pyrazolopyrimidine sedative-hypnotic agent for the treatment of insomnia. *Clin. Ther.* **2000**, 22, 1254–1267.

[18] a) Baindur, N; Chadha, N.; Player, M. R. Solution-phase synthesis of a library of 3,5,7-trisubstituted 3H-[1,2,3]triazolo[4,5-d]pyrimidines. *J. Comb. Chem.* **2003**, 5, 653–659; b) Wang, P. Y.; Du, J. F.; Rachakonda, S.; Chun, B. K.; Tharnish, P. M.; Stuyver, L. J.; Otto, M. J.; Schinazi, R. F.; Watanabe, K. A. Synthesis and structure−activity relationships of novel anti-hepatitis C Agents: N^3,5'-Cyclo-4-(β-d-ribofuranosyl)-vic-triazolo[4,5-b]pyridin-5-one derivatives. *J. Med. Chem.* **2005**, 48, 6454–6460 ; c) Gao, Y. N.; Lam, Y. L. [3+2] Cycloaddition reactions in the synthesis of triazolo[4,5-b]pyridin-5-ones and pyrrolo[3,4-b]pyridin-2-ones. *J. Comb. Chem.* **2008**, 10, 327–332; d) Majumdar, K. C.; Ray, K. Synthesis of 1,2,3-triazole-fused heterocycles via intramolecular azide-alkyne cycloaddition reactions. *Synthesis-Stuttgart* **2011**, 3767–3783; e) Donald, J. R.; Wood, R. R.; Martin, S. F. Application of a sequential multicomponent assembly process/Huisgen cycloaddition strategy to the preparation of libraries of 1,2,3-triazole-fused 1,4-benzodiazepines. *ACS*

Comb. Sci. **2012**, 14, 135–143; f) Fosso, M. Y.; Chan, K. Y.; Gregory, R.; Chang, C. W. T. Library synthesis and antibacterial investigation of cationic anthraquinone analogs. *ACS. Comb. Sci.* **2012**, 14, 231–235.

[19] a) Duarte, C. D.; Barreiro, E. J.; Fraga, C. A. M. Privileged structures: a useful concept for the rational design of new lead drug candidates. *Mini-Rev. Med. Chem.* **2007**, 7, 1108–1119 ; b) Welsch, M. E.; Snyder, S. A.; Stockwell, B. R. Privileged scaffolds for library design and drug discovery. *Curr. Opin. Chem. Biol.* **2010**, 14, 347–361.

[20] Burke, M. D.; Berger, E. M.; Schreiber, S. L. Generating diverse skeletons of small molecules combinatorially. *Science* **2003**, 302, 613–618.

[21] Chang, H. T.; Sharpless, K. B.; A practical route to enantiopure 1,2-aminoalcohols. *Tetrahedron Lett.* **1996**, 37, 3219–3222.

[22] a) Sauer, W. H. B.; Schwarz, M. K. Molecular shape diversity of combinatorial libraries: a prerequisite for broad bioactivity. *J. Chem. Inf. Comput. Sci.* **2003**, 43, 987–1003; b) Kopp, F.; Stratton, C. F.; Akella, L. B.; Tan, D. S. A diversity-oriented synthesis approach to macrocycles via oxidative ring expansion. *Nat. Chem. Biol.* **2012**, 8, 358–365.

[23] Hung, A. W.; Ramek, A.; Wang, Y. K.; Kaya, T.; Wilson, J. A.; Clemons, P. A.; Young, D. W. Route to three-dimensional fragments using diversity-oriented synthesis. *Proc. Natl. Acad. Sci. USA* **2011**, 108, 6799–6804.

1.6. Acknowledgements

This work was supported by the Bio & Medical Technology Development Program (2012M3A9C4048780), the Global Frontier Project Grant (2011-0032150), the WCU program (R31-10032), and the Basic Research

Laboratory (2010-0019766) funded by the National Research Foundation of Korea (NRF). I am grateful for fellowships awarded by the Hi Seoul Fellowship.

1.7. Supporting Information

Synthesis of 2-*C*-formyl-3,4-di-*O*-(*p*-methoxybenzyl)-6-*O*-trityl-D-glucal 1. **Tritylation:** To a stirred solution of D-glucal (500 mg, 1 equiv.) in anhydrous pyridine (2.5 mL) was added trityl chloride (1.2 equiv.) and 4-(dimethylamino)pyridine (DMAP, 0.1 equiv.). After stirring at room temperature for 24 h, the mixture was partitioned between ethyl acetate and water. The aqueous layer was extracted with water and the combined organic layer was washed with 10 % $CuSO_4$ aqueous solution to remove pyridine. The organic layer was dried over anhydrous Na_2SO_4 and the filtrate was condensed under reduced pressure followed by flash column chromatography to obtain 6-*O*-trityl-D-glucal. Yield = 63%. **PMB protection:** To a stirred solution of 6-*O*-trityl-D-glucal (1000 mg, 1 equiv.) in anhydrous DMF (10 mL), NaH (4.8 equiv.) was added slowly at 0 °C. After stirring the mixture for 15 min, *p*-methoxybenzyl chloride (2.4 equiv.) and tetrabutylammonium chloride (0.05 equiv.) was added. The mixture was stirred for 3 h at room temperature and partitioned between diethyl ether and water. The aqueous layer was extracted with diethyl ether and the combined organic layer was dried over anhydrous Na_2SO_4. The filtrate was condensed under reduced pressure and subjected to flash column chromatography to obtain 3,4-di-*O*-(*p*-methoxybenzyl)-6-*O*-trityl-D-glucal. Yield = 97%. **Formylation:** To a stirred solution of 3,4-di-*O*-(*p*-methoxybenzyl)-6-*O*-trityl-D-glucal (1000 mg, 1 equiv.) in anhydrous DMF (10 mL), $POCl_3$ (3 equiv.) was added dropwise at 0 °C. After stirring the mixture for 10 h at room temperature, the reaction was quenched by transferring the mixture slowly to the saturated cold $NaHCO_3$ aqueous solution. The aqueous layer was extracted with ethyl acetate and the combined organic layer was washed with brine. The organic layer was dried over anhydrous Na_2SO_4 and the filtrate was condensed under reduced pressure followed by flash column chromatography to obtain 2-*C*-formyl-3,4-di-*O*-(*p*-methoxybenzyl)-6-*O*-trityl-D-glucal **1** as a white solid. Yield: 63%; $[\alpha]_D^{22}$ = +18.61 (c = 1.07, $CHCl_3$); R_f= 0.67 (EtOAc : Hexane = 1 : 1); ^{1}H NMR (500 MHz, $CDCl_3$) δ 9.35 (s, 1H), 7.38–7.36 (m, 6H), 7.33 (s, 1H), 7.27–7.23 (m, 9H), 7.12 (d, *J* = 8.8 Hz, 2H), 6.98 (d, *J* = 8.3 Hz, 2H), 6.84 (d, *J* = 8.8 Hz,

2H), 6.74 (d, *J* = 8.8 Hz, 2H), 4.53–4.50 (m, 1H), 4.45–4.30 (m, 5H), 3.80 (s, 3H), 3.78 (s, 3H), 3.71–3.69 (m, 1H), 3.60 (dd, *J* = 11.2, 7.8 Hz, 1H), 3.20 (dd, *J* = 11.0, 4.2 Hz, 1H); ^{13}C NMR (125 MHz, $CDCl_3$) 190.5, 164.5, 159.6, 159.3, 143.9, 130.5, 129.7, 129.6, 129.5, 129.2, 128.8, 128.0, 127.3, 118.1, 114.1, 113.9, 87.2, 80.0, 72.2, 71.4, 71.2, 65.5, 62.9, 55.4.

Synthesis of 2-*C*-formyl-3,4-di-*O*-(*p*-methoxylbenzyl)-6-*O*-trityl-D-galactal 2.

Tritylation: To a stirred solution of D-galactal (1 equiv.) and trityl chloride (1.2 equiv.) in anhydrous DCM was added diisopropylethylamine (DIPEA, 1.5 equiv.) and 4-(dimethylamino)pyridine (DMAP, 0.1 equiv.). After stirring at room temperature for 24 h, the mixture was diluted with DCM and washed with brine. The organic layer was dried over anhydrous Na_2SO_4 and the filtrate was condensed under reduced pressure followed by flash column chromatography to obtain 6-*O*-trityl-D-galactal. Yield = 89%. **PMB protection:** The same procedure as the above was applied to obtain 3,4-di-*O*-(*p*-methoxybenzyl)-6-*O*-trityl-D-galactal. Yield = 95%. **Formylation:** The same procedure as the above was applied to obtain 2-*C*-formyl-3,4-di-*O*-(*p*-methoxybenzyl)-6-*O*-trityl-D-galactal. Yield = 64%; $[\alpha]_D^{22}$ = +20.09 (c = 1.05, $CHCl_3$); R_f = 0.64 (EtOAc : Hexane = 1 : 1); ^{1}H NMR (500 MHz, $CDCl_3$) δ 9.25 (s, 1H), 7.38–7.36 (m, 6H), 7.25–7.20 (m, 9H), 7.12 (s, 1H), 7.10 (d, *J* = 8.3 Hz, 2H), 7.00 (d, *J* = 8.6 Hz, 2H), 6.83 (d, *J* = 8.6 Hz, 2H), 6.73 (d, *J* = 8.6 Hz, 2H), 4.64–4.61 (m, 1H), 4.52 (d, *J* = 11.7 Hz, 1H), 4.49 (s, 2H), 4.44 (dd, *J* = 3.5, 1.3 Hz, 1H), 4.39 (d, *J* = 11.7 Hz, 1H), 3.801 (s, 3H), 3.797 (s, 3H), 3.72–3.68 (m, 2H), 3.58 (dd, *J* = 11.7, 1.7 Hz, 1H); ^{13}C NMR (125 MHz, $CDCl_3$) 189.6, 164.6, 164.5, 159.5, 159.0, 144.1, 131.1, 129.8, 129.4, 129.3, 128.9, 127.9, 127.1, 119.5, 114.0, 113.6, 87.0, 79.2, 73.3, 72.9, 71.2, 65.0, 55.5, 55.4; LRMS (ESI) *m/z* calculated for $C_{45}H_{47}N_3O_6$ $[M+Na]^+$: 679.27; found: 679.27.

Synthesis of pyrimidine-, pyrazole- and pyrazolopyrimidine-based carbohybrids 3–5. The synthetic procedure is described at the Experimental Section.

Compound **3a**: Prepared from 1,1-dimethylguanidine sulfate salt; White solid; Yield = 85%; $[\alpha]_D^{21}$ = –51.96 (c = 1.62, $CHCl_3$); R_f= 0.53 (EtOAc : Hexane = 1 : 1); ^{1}H NMR (500 MHz, $CDCl_3$) δ 8.24 (s, 2H), 7.41–7.40 (m, 6H), 7.30–7.22 (m, 9H), 7.10 (d, *J* = 8.8 Hz, 2H), 6.89 (d, *J* = 8.3 Hz, 2H), 6.80 (d, *J* = 8.3 Hz, 2H), 6.70 (d, *J* = 8.3 Hz, 2H), 4.39–4.37 (m, 2H), 4.22–4.14 (m, 2H), 4.02–3.99 (m, 2H), 3.78 (s, 3H), 3.77 (s, 3H), 3.58 (dd, *J* = 6.4, 2.9 Hz, 1H), 3.25–3.24 (m, 2H), 3.22 (s, 6H), 2.96 (d, *J* = 5.9 Hz, 1H); ^{13}C NMR (125 MHz, $CDCl_3$) 162.4, 159.6, 159.4, 157.8, 143.9, 130.3, 130.1, 129.8, 129.5, 128.9, 128.1, 127.3, 118.1, 114.1, 113.8, 86.8, 80.5, 76.6, 73.6, 70.52, 70.48, 64.8, 55.5, 55.4, 37.4; LRMS (ESI) *m/z* calculated for $C_{45}H_{47}N_3O_6$ $[M+H]^+$: 726.35; found: 726.10.

Compound **3b**: Prepared from 1,1-dimethylguanidine sulfate salt; White solid; Yield = 80%; $[\alpha]_D^{25}$ = –9.69 (c = 0.91, $CHCl_3$); R_f= 0.17 (EtOAc : Hexane = 1 : 2); ^{1}H NMR (500 MHz, $CDCl_3$) δ 8.24 (s, 2H), 7.42 (d, *J* = 8.1 Hz, 6H), 7.30–7.22 (m, 9H), 7.15 (d, *J* = 8.6 Hz, 2H), 6.82–6.78 (m, 4H), 6.69 (d, *J* = 8.3 Hz, 2H), 4.40 (d, *J* = 11.2 Hz, 1H), 4.24 (d, *J* = 7.6 Hz, 1H), 4.18 (d, *J* = 11.2 Hz, 1H), 4.11–4.05 (m, 3H), 3.78 (s, 3H), 3.76 (s, 3H), 3.73 (dd, *J* = 7.6, 2.4 Hz, 1H), 3.27 (dd, *J* = 9.3, 6.1 Hz, 1H), 3.21 (s, 6H), 3.08 (dd, *J* = 9.3, 6.4 Hz, 1H), 2.39 (d, *J* = 7.6 Hz, 1H); ^{13}C NMR (125 MHz, $CDCl_3$) δ 162.4, 159.5, 159.4, 157.9, 144.1, 130.2, 129.8, 129.7, 128.9, 128.0, 127.2, 119.1, 114.0, 113.8, 86.9, 81.0, 76.5, 74.3, 70.3, 70.0, 64.7, 60.6, 55.5, 37.4, 14.4; HRMS (FAB+) *m/z* calculated for $C_{45}H_{47}N_3O_6$ $[M+H]^+$: 726.3543; found: 726.3536.

Compound **3c**: Prepared from 4-chlorobenzamidine hydriodide; Amorphous white solid; Yield = 52%; $[\alpha]_D^{23}$ = +3.16 (c = 1.32, $CHCl_3$); R_f= 0.66 (EtOAc : Hexane = 1 : 1); ^{1}H NMR (500 MHz, $CDCl_3$) δ 8.66 (s, 2H), 8.41 (d, *J* = 8.3 Hz, 2H), 7.48 (d, *J* = 8.6 Hz, 2H), 7.45–7.43 (m, 6H), 7.31–7.28 (m, 6H), 7.26–7.23 (m, 3H), 7.17 (d, *J* = 8.6 Hz, 2H), 6.83 (d, *J* = 8.6 Hz, 2H), 6.68 (d, *J* = 8.5 Hz, 2H), 6.60 (d, *J* = 8.6 Hz, 2H), 4.47 (d, *J* = 8.1 Hz, 1H), 4.43 (d, *J* = 11.2 Hz, 1H), 4.29 (d, *J* = 11.2 Hz, 1H), 4.18–4.14 (m, 1H), 4.08 (d, *J* = 10.8 Hz, 1H), 3.91 (d, *J* = 10.8 Hz, 1H), 3.80–3.78 (m, 1H), 3.78 (s, 3H), 3.64 (s,

3H), 3.36 (dd, *J* = 9.3, 6.4 Hz, 1H), 3.10 (dd, *J* = 9.0, 6.8 Hz, 1H), 2.32 (d, *J* = 8.3 Hz, 1H); ^{13}C NMR (125 MHz, $CDCl_3$) δ 163.4, 159.7, 159.5, 157.2, 143.9, 137.2, 136.1, 130.9, 130.3, 129.9, 129.7, 129.2, 129.1, 129.0, 128.9, 128.1, 127.4, 114.1, 113.8, 87.1, 80.6, 76.3, 74.4, 71.4, 69.8, 64.6, 55.5, 55.3; LRMS (ESI) *m/z* calculated for $C_{49}H_{45}ClN_2O_6$ $[M+H]^+$: 793.30; found: 793.39.

Compound **3d**: Prepared from guanidine hydrochloride; Amorphous white solid; Yield = 68%; $[\alpha]_D^{24}$ = –13.52 (c = 1.07, $CHCl_3$); R_f = 0.25 (EtOAc : Hexane = 3 : 1, 1% TEA); ^{1}H NMR (500 MHz, $CDCl_3$) δ 8.20 (s, 2H), 7.44–7.42 (m, 6H), 7.30–7.22 (m, 9H), 7.15 (d, *J* = 8.6 Hz, 2H), 6.82 (d, *J* = 8.3 Hz, 2H), 6.77 (d, *J* = 8.6 Hz, 2H), 6.70 (d, *J* = 8.3 Hz, 2H), 5.22 (d, *J* = 8.1 Hz, 2H), 4.40 (d, *J* = 11.2 Hz, 1H), 4.28(d, *J* = 7.6 Hz, 1H), 4.21 (d, *J* = 11.2 Hz, 1H), 4.12–4.02 (m, 3H), 3.78 (s, 3H), 3.75 (s, 3H), 3.73–3.71 (m, 1H), 3.28 (dd, *J* = 9.2, 6.2 Hz, 1H), 3.10 (dd, *J* = 9.3, 6.6 Hz, 1H), 2.51 (t, *J* = 7.8 Hz, 1H); ^{13}C NMR (100 MHz, $CDCl_3$) δ 163.0, 159.52, 159.48, 158.4, 144.0, 130.2, 129.7, 129.5, 129.4, 128.9, 128.1, 127.3, 122.3, 114.1, 113.8, 86.9, 80.9, 76.3, 74.4, 70.7, 69.9, 64.7, 55.5, 55.4; LRMS (ESI) *m/z* calculated for $C_{49}H_{45}ClN_2O_6$ $[M+H]^+$: 698.32; found: 698.31.

Compound **4a**: Prepared from methylhydrazine; White solid; Yield = 94%; $[\alpha]_D^{22}$ = –31.35 (c = 1.51, $CHCl_3$); R_f = 0.20 (EtOAc : Hexane = 1 : 1); ^{1}H NMR (500 MHz, $CDCl_3$) δ 7.42–7.40 (m, 6H), 7.34 (s, 1H), 7.29–7.21 (m, 10 H), 7.15 (d, *J* = 8.6 Hz, 2H), 6.92 (d, *J* = 8.6 Hz, 2H), 6.79 (d, *J* = 8.8 Hz, 2H), 6.76 (d, *J* = 8.8 Hz, 2H), 4.45 (d, *J* = 11.5 Hz, 1H), 4.42 (d, *J* = 6.4 Hz, 1H), 4.31–4.21 (m, 3H), 3.97–3.93 (m, 1H), 3.87 (s, 3H), 3.80–3.76 (m, 7H), 3.16–3.10 (m, 2H), 2.62 (d, *J* = 5.9 Hz, 1H); ^{13}C NMR (125 MHz, $CDCl_3$) δ 159.31, 159.26, 144.0, 139.2, 130.24, 130.16, 130.0, 129.7, 129.5, 128.8, 128.0, 127.1, 119.8, 113.9, 113.7, 86.7, 81.3, 74.2, 72.9, 70.4, 70.0, 64.6, 55.39, 55.36, 39.13; LRMS (ESI) *m/z* calculated for $C_{43}H_{44}N_2O_6$ $[M+H]^+$: 685.33; found: 685.37.

Compound **4b**: Prepared from phenylhydrazine; Amorphous yellow solid; Yield = 55%; $[\alpha]_D^{21}$ = –23.25 (c =0.57, $CHCl_3$); R_f = 0.68 (EtOAc : Hexane =

1 : 1); ^{1}H NMR (500 MHz, $CDCl_3$) δ 7.77 (s, 1H), 7.64–7.62 (m, 3H), 7.46–7.42 (m, 7H), 7.29–7.21 (m, 11H), 7.18 (d, *J* = 8.6 Hz, 2H), 6.88 (d, *J* = 8.6 Hz, 2H), 6.81 (d, *J* = 8.6 Hz, 2H), 6.69 (d, *J* = 8.6 Hz, 2H), 4.53–4.50 (m, 2H), 4.30 (d, *J* = 11.5 Hz, 1H), 4.26 (s, 2H), 4.04–4.01 (m, 1H), 3.81 (dd, *J* = 6.6, 2.9 Hz, 1H), 3.78–3.76 (m, 4H), 3.71 (s, 3H), 3.22 (dd, *J* = 9.3, 5.9 Hz, 1H), 3.15 (dd, *J* = 9.5, 5.8 Hz, 1H); ^{13}C NMR (125 MHz, $CDCl_3$) δ 159.43, 159.39, 144.1, 141.0, 140.2, 130.11, 130.07, 129.7, 129.6, 128.9, 128.8, 128.0, 127.2, 126.6, 126.4, 122.2, 119.0, 114.0, 113.8, 86.9, 71.3, 74.4, 72.9, 70.5, 70.4, 64.7, 55.5, 55.4; LRMS (ESI) *m/z* calculated for $C_{48}H_{46}N_2O_6$ $[M+H]^+$: 747.34; found: 747.30.

Compound **5a**: Prepared from 3-amino-5-methylpyrazole; Amorphous white solid; Yield = 70%; $[\alpha]_D^{23}$ = +5.16 (c =0.90, $CHCl_3$); R_f = 0.40 (EtOAc : Hexane = 1 : 1); ^{1}H NMR (500 MHz, $CDCl_3$) δ 8.40 (s, 1H), 8.31 (d, *J* = 2.0 Hz, 1H), 7.47–7.44 (m, 5H), 7.37 (d, *J* = 7.6 Hz, 1H), 7.31–7.23 (m, 9H), 7.16 (d, *J* = 8.3 Hz, 2H), 6.82 (d, *J* = 8.6 Hz, 2H), 6.65 (d, *J* = 8.6 Hz, 2H), 6.52–6.48 (m, 3H), 4.44–4.42 (m, 2H), 4.28 (d, *J* = 11.0 Hz, 1H), 4.18 (t, *J* = 5.7 Hz, 1H), 4.11 (d, *J* = 11.0 Hz, 1H), 3.91 (d, *J* = 11.2 Hz, 1H), 3.79–3.75 (m, 4H), 3.70 (s, 3H), 3.37 (dd, *J* = 9.3, 6.1 Hz, 1H), 3.10 (dd, *J* = 9.2, 7.2 Hz, 1H), 2.53 (s, 3H); ^{13}C NMR (125 MHz, $CDCl_3$) δ 159.6, 159.3, 155.5, 149.9, 148.9, 143.9, 133.5, 130.2, 129.8, 129.1, 128.9, 128.8, 128.7, 128.1, 127.3, 119.6, 114.1, 113.5, 96.1, 87.1, 80.4, 75.9, 74.3, 71.3, 69.7, 64.5, 55.4, 55.2, 14.7; LRMS (ESI) *m/z* calculated for $C_{46}H_{45}N_3O_6$ $[M+H]^+$: 736.34; found: 736.51.

Compound **5b**: Prepared from 3-amino-5-phenylpyrazole; Amorphous yellow solid; Yield = 44%; $[\alpha]_D^{20}$ = +7.56 (c =0.56, $CHCl_3$); R_f = 0.13 (EtOAc : Hexane = 1 : 2); ^{1}H NMR (500 MHz, $CDCl_3$) δ 8.46 (s, 1H), 8.34 (s, 1H), 8.01 (d, *J* = 8.1 Hz, 2H), 7.50–7.40 (m, 9H), 7.32–7.23 (m, 9H), 7.18 (d, *J* = 8.1 Hz, 2H), 6.98 (s, 1H), 6.83 (d, *J* = 8.3 Hz, 2H), 6.66 (d, *J* = 7.8 Hz, 2H), 6.50 (d, *J* = 8.3 Hz, 2H), 4.48–4.44 (m, 2H), 4.30 (d, *J* = 11.0 Hz, 1H), 4.20 (t, *J* = 6.1 Hz, 1H), 4.14 (d, *J* = 11.0 Hz, 1H), 3.93 (d, *J* = 11.0 Hz, 1H), 3.81 (d, *J* = 8.3 Hz, 1H), 3.77 (s, 3H), 3.56 (s, 3H), 3.41–3.38 (m, 1H), 3.11 (t, *J* = 8.1 Hz, 1H); ^{13}C NMR (125 MHz, $CDCl_3$) δ 159.7, 159.4, 156.6, 150.3, 149.6, 143.9, 133.7,

132.9, 130.2, 129.8, 129.2, 129.0. 128.8, 128.1, 127.3, 126.7, 120.4, 114.1, 113.6, 93.7, 87.1, 80.4, 75.9, 74.3, 71.4, 69.7, 64.6, 55.5, 55.1, 14.4; LRMS (ESI) *m/z* calculated for $C_{51}H_{47}N_3O_6$ $[M+H]^+$: 798.35; found: 798.31.

Synthesis of key intermediates with β-azido hydroxyl groups 6–8. The synthetic procedure is described at the Experimental section.

Compound **6a**: Prepared from compound **3a**; White syrup; Yield = 62%; $[\alpha]_D^{25}$ = –55.11 (c = 0.74, $CHCl_3$); R_f= 0.19 (EtOAc : Hexane = 1 : 1); ^{1}H NMR (500 MHz, $CDCl_3$) δ 8.31 (s, 2H), 7.22–7.18 (m, 4H), 6.86–6.84 (m, 4H), 4.63 (s, 2H), 4.47–4.43 (m, 2H), 4.23 (d, *J* = 11.2 Hz, 1H), 3.80 (s, 6H), 3.65 (t, *J* = 5.4 Hz, 1H), 3.60 (d, *J* = 4.9 Hz, 2H), 3.26 (q, *J* = 5.1 Hz, 1H), 3.22 (s, 6H), 1.94 (bs, 1H); ^{13}C NMR (125 MHz, $CDCl_3$) δ 162.4, 159.51, 159.49, 157.6, 130.3, 129.9, 129.8, 129.6, 117.9, 114.0, 113.9, 81.1, 78.4, 74.9, 70.6, 63.5, 62.3, 55.39, 55.36, 37.3; HRMS (FAB+) *m/z* calculated for $C_{26}H_{32}N_6O_5$ $[M+H]^+$: 509.2512; found: 509.2515.

Compound **6b**: Prepared from compound **3b**; Yellow syrup; Yield = 88%; $[\alpha]_D^{23}$ = –43.99 (c =0.54, $CHCl_3$); R_f= 0.31 (EtOAc : Hexane = 1 : 1); ^{1}H NMR (500 MHz, $CDCl_3$) δ 8.29 (s, 2H), 7.18 (d, *J* = 8.6 Hz, 2H), 7.07 (d, *J* = 8.3 Hz, 2H), 6.87 (d, *J* = 8.6 Hz, 2H), 6.79 (d, *J* = 8.6 Hz, 2H), 4.52 (d, *J* = 11.0 Hz, 1H), 4.43–4.39 (m, 2H), 4.32 (d, *J* = 6.1 Hz, 1H), 4.18 (d, *J* = 11.2 Hz, 1H), 3.80–3.75 (m, 9H), 3.53 (q, *J* = 5.0 Hz, 1H), 3.23 (s, 6H), 2.18 (bs, 1H); ^{13}C NMR (125 MHz, $CDCl_3$) δ 162.5, 159.6, 158.1, 130.3, 129.8, 129.50, 129.46, 117.7, 114.1, 114.0, 81.3, 74.5, 70.4, 63.4, 62.2, 55.5, 55.4, 37.4; LRMS (ESI) *m/z* calculated for $C_{51}H_{47}N_3O_6$ $[M+H]^+$: 509.25; found: 509.11.

Compound **6c**: Prepared from compound **3c**; White solid; Yield = 73%; $[\alpha]_D^{22}$ = –46.71 (c =0.38, $CHCl_3$); R_f= 0.58 (EtOAc : Hexane = 1 : 1); ^{1}H NMR (500 MHz, $CDCl_3$) δ 8.71 (s, 2H), 8.42 (d, *J* = 8.8 Hz, 2H), 7.49 (d, *J* = 8.6 Hz, 2H), 7.19 (d, *J* = 8.6 Hz, 2H), 6.98 (d, *J* = 8.8 Hz, 2H), 6.88 (d, *J* = 8.8 Hz, 2H), 6.72 (d, *J* = 8.8 Hz, 2H), 4.56–4.53 (m, 2H), 4.45 (d, *J* = 11.2 Hz, 1H), 4.37 (d, *J* = 11.2 Hz, 1H), 4.27 (d, *J* = 11.0 Hz, 1H), 3.84–3.77 (m, 6H), 3.70 (s, 3H),

3.63–3.60 (m, 1H), 2.09–2.05 (m, 1H); ^{13}C NMR (125 MHz, $CDCl_3$) δ 163.7, 159.8, 159.7, 157.4, 137.3, 136.0, 130.3, 130.0, 129.7, 129.6, 129.1, 128.8, 114.2, 114.1, 80.2, 76.9, 74.2, 71.3, 63.5, 62.2, 55.5, 55.4; LRMS (ESI) *m/z* calculated for $C_{30}H_{30}ClN_5O_5$ $[M+H]^+$: 576.20; found: 576.48.

Compound **7a**: Prepared from compound **4a**; White solid; Yield = 67%; $[\alpha]_D^{21}$ = –57.73 (c =0.88, $CHCl_3$); R_f= 0.17 (EtOAc : Hexane = 1 : 1); ^{1}H NMR (500 MHz, $CDCl_3$) δ 7.51 (s, 1H), 7.35 (s, 1H), 7.20 (d, *J* = 8.6 Hz, 2H), 7.14 (d, *J* = 8.6 Hz, 2H), 6.88–6.83 (m, 4H), 4.58–4.46 (m, 4H), 4.25 (d, *J* = 11.2 Hz, 1H), 3.89 (s, 3H), 3.82–3.72 (m, 9H), 3.45 (q, *J* = 5.5 Hz, 1H), 2.63 (bs, 1H); ^{13}C NMR (125 MHz, $CDCl_3$) δ 159.5, 159.4, 139.5, 130.10, 130.07, 130.05, 130.0, 129.6, 118.6, 134.99, 113.96, 81.4, 74.4, 73.8, 70.2, 63.5, 62.2, 55.4, 39.2 ; LRMS (ESI) *m/z* calculated for $C_{24}H_{29}N_5O_5$ $[M+H]^+$: 468.22; found: 468.36.

Compound **8a**: Prepared from compound **5a**; White solid; Yield = 75%; $[\alpha]_D^{22}$ = –36.93 (c = 1.04, $CHCl_3$); R_f= 0.21 (EtOAc : Hexane = 1 : 1); ^{1}H NMR (500 MHz, $CDCl_3$) δ 8.43 (s, 1H), 8.35 (s, 1H), 7.16 (d, *J* = 7.6 Hz, 2H), 6.94 (d, *J* = 8.6 Hz, 2H), 6.85 (d, *J* = 7.8 Hz, 2H), 6.64 (d, *J* = 7.8 Hz, 2H), 6.49 (s, 1H), 4.55 (d, *J* = 11.2 Hz, 1H), 4.49 (dd, *J* = 6.6, 1.2 Hz, 1H), 4.44 (d, *J* = 11.2 Hz, 1H), 4.37 (dd, *J* = 11.1, 1.1 Hz, 1H), 4.26 (d, *J* = 11.2 Hz, 1H), 3.82–3.77 (m, 6H), 3.73 (s, 3H), 3.64–3.61 (m, 2H), 2.53 (s, 3H); ^{13}C NMR (125 MHz, $CDCl_3$) δ 159.8, 159.6, 155.8, 149.8, 149.2, 133.7, 130.2, 129.9, 128.8, 118.2, 114.2, 113.9, 96.3, 80.2, 77.4, 76.7, 74.1, 71.1, 63.6, 62.0, 55.5, 55.3, 14.8; LRMS (ESI) *m/z* calculated for $C_{27}H_{30}N_6O_5$ $[M+H]^+$: 519.24; found: 519.43.

Synthesis of morpholine-fused triazoles 9. The synthetic procedure is described at the Experimental Section.

Compound **9a**: Prepared from compound **6a** and 3-chloro-1-propyne; Yellow syrup; Yield = 65%; $[\alpha]_D^{21}$ = –65.18 (c = 0.55, $CHCl_3$); R_f= 0.43 (MeOH : DCM = 1 : 20); ^{1}H NMR (500 MHz, $CDCl_3$) δ 8.33 (s, 2H), 7.34 (s, 1H), 7.13–7.10 (m, 4H), 6.81–6.78 (m, 4H), 4.76–4.64 (m, 3H), 4.50–4.44 (m, 2H),

4.41–4.31 (m, 2H), 4.12 (d, *J* = 10.5 Hz, 1H), 4.08–4.05 (m, 2H), 3.82 (dd, *J* = 12.5, 3.9 Hz, 1H), 3.78 (s, 6H), 3.20 (s, 6H); ^{13}C NMR (125 MHz, $CDCl_3$) δ 162.3, 159.51, 159.46, 157.9, 131.3, 130.3, 130.0, 129.8, 129.6, 128.0, 117.9, 113.94, 113.90, 80.4, 74.8, 70.3, 65.5, 62.3, 56.4, 56.2, 55.44, 55.38, 37.3; LRMS (ESI) *m/z* calculated for $C_{29}H_{34}N_6O_5$ $[M+H]^+$: 547.27; found: 547.53.

Compound **9b**: Prepared from compound **6a** and 1-bromo-2-butyne; Slightly yellow solid; Yield = 93%; $[\alpha]_D^{25}$ = –60.08 (c =0.58, $CHCl_3$); R_f = 0.09 (EtOAc : Hexane = 1 : 1); ^{1}H NMR (500 MHz, $CDCl_3$) δ 8.25 (s, 2H), 7.15–7.10 (m, 4H), 6.80–6.78 (m, 4H), 4.62–4.50 (m, 4H), 4.45–4.40 (m, 2H), 4.34 (d, J = 11.2 Hz, 1 H), 4.15–4.10 (m, 3H), 3.76–3.74 (m, 7H), 3.18 (s, 6H), 2.08 (s, 3H) ; ^{13}C NMR (125 MHz, $CDCl_3$) δ 162.1, 159.4, 159.3, 157.7, 136.6, 130.2, 129.84, 129.79, 129.7, 127.5, 117.7, 113.8, 80.4, 77.4, 74.8, 70.0, 64.7, 62.0, 56.0, 55.33, 55.31, 37.2, 9.8; HRMS (FAB+) *m/z* calculated for $C_{30}H_{36}N_6O_5$ $[M+H]^+$: 561.2825; found: 561.2821.

Compound **9c**: Prepared from compound **6a** and 1-bromo-2-pentyne; White solid; Yield = 90%; $[\alpha]_D^{23}$ = –54.55 (c = 0.37, $CHCl_3$); R_f = 0.11 (EtOAc : Hexane = 1 : 1); ^{1}H NMR (500 MHz, $CDCl_3$) δ 8.27 (s, 2H), 7.16–7.11 (m, 4H), 6.82–6.80 (m, 4H), 4.65–4.54 (m, 4H), 4.47 (q, *J* = 4.4 Hz, 1H), 4.43 (d, *J* = 11.0 Hz, 1H), 4.35 (d, *J* = 11.2 Hz, 1H), 4.17–4.11 (m, 3H), 3.78–3.76 (m, 7H), 3.19 (s, 6H), 2.56–2.46 (m, 2H), 1.17 (t, *J* = 7.7 Hz, 3H); ^{13}C NMR (125 MHz, $CDCl_3$) δ 162.2, 159.5, 159.4, 157.9, 142.5, 130.3, 129.93, 129.91, 129.86, 127.1, 117.9, 113.9, 80.5, 77.6, 74.9, 70.2, 64.9, 62.3, 56.2, 55.43, 55.41, 37.3, 18.5, 13.2; LRMS (ESI) *m/z* calculated for $C_{31}H_{38}N_6O_5$ $[M+H]^+$: 575.30; found: 575.29.

Compound **9d**: Prepared from compound **6a** and 3-chloro-1-phenyl-1-propyne; Yellow solid; Yield = 65%; $[\alpha]_D^{21}$ = –27.24 (c =0.66, $CHCl_3$); R_f = 0.33 (EtOAc : Hexane = 1 : 1); ^{1}H NMR (400 MHz, $CDCl_3$) δ 8.21 (s, 2H), 7.53–7.50 (m, 2H), 7.42 (t, *J* = 7.6 Hz, 2H), 7.34–7.29 (m, 1H), 7.21–7.19 (m, 2H), 7.13–7.11 (m, 2H), 6.84–6.78 (m, 4H), 4.81 (s, 2H), 4.71 (d, *J* = 11.0 Hz, 1H), 4.60–4.53 (m, 3H), 4.37–4.29 (m, 3H), 4.13 (d, *J* = 11.3 Hz, 1H), 3.85 (dd, *J* =

12.1, 4.3 Hz, 1H), 3.78 (s, 3H), 3.73 (s, 3H), 2.96 (s, 6H); ^{13}C NMR (100 MHz, $CDCl_3$) δ 161.9, 159.6, 159.4, 157.7, 140.9, 130.8, 130.2, 129.92, 129.89, 128.9, 127.9, 127.5, 126.1, 117.4, 113.99, 113.95, 80.5, 77.7, 75.0, 70.0, 64.2, 63.3, 56.3, 55.42, 55.40, 37.01; LRMS (ESI) *m/z* calculated for $C_{35}H_{38}N_6O_5$ $[M+H]^+$: 623.30; found: 623.53.

Compound **9e**: Prepared from compound **6a** and 3-bromo-1-(3-methoxyphenyl)-1-propyne (**S1**); Yellow solid; Yield = 73%; $[\alpha]_D^{22}$ = –27.72 (c = 0.39, $CHCl_3$); R_f= 0.28 (EtOAc : Hexane = 1 : 1); ^{1}H NMR (500 MHz, $CDCl_3$) δ 8.22 (s, 2H), 7.32 (t, *J* = 7.8 Hz, 1H), 7.24–7.23 (m, 1H), 7.19 (d, *J* = 8.3 Hz, 2H), 7.12 (d, *J* = 8.8 Hz, 2H), 6.95 (d, *J* = 7.3 Hz, 1H), 6.87 (dd, *J* = 8.1, 2.7 Hz, 1H), 6.83–6.78 (m, 4H), 4.80 (s, 2H), 4.69 (d, *J* = 10.8 Hz, 1H), 4.61–4.57 (m, 2H), 4.53 (d, *J* = 11.2 Hz, 1H), 4.36 (d, *J* = 11.2 Hz, 1H), 4.33 (dd, *J* = 6.4, 4.9 Hz, 1H), 4.29 (dd, *J* = 12.7, 3.9 Hz, 1H), 4.13 (d, *J* = 11.7 Hz, 1H), 3.87 (s, 3H), 3.84 (dd, *J* = 12.5, 4.2 Hz, 1H), 3.77 (s, 3H), 3.73 (s, 3H), 2.99 (s, 6H); ^{13}C NMR (125 MHz, $CDCl_3$) δ 160.2, 159.6, 159.5, 157.7, 140.9, 132.2, 130.2, 129.94, 129.91, 129.88, 129.7, 118.4, 117.4, 114.1, 114.01, 113.98, 113.86, 111.4, 80.5, 77.7, 75.0, 70.0, 64.3, 63.3, 56.3, 55.57, 55.42, 55.40, 37.0; LRMS (ESI) *m/z* calculated for $C_{36}H_{40}N_6O_6$ $[M+H]^+$: 653.31; found: 653.06.

Compound **9f**: Prepared from compound **6a** and 1-(3-bromo-1-propynyl)naphthalene; Yellow solid; Yield = 67%; $[\alpha]_D^{22}$ = –25.19 (c =0.41, $CHCl_3$); R_f= 0.26 (EtOAc : Hexane = 1 : 1); ^{1}H NMR (300 MHz, $CDCl_3$) δ 8.38 (s, 2H), 8.17–8.13 (m, 1H), 7.92–7.86 (m, 2H), 7.54–7.47 (m, 3H), 7.29–7.15 (m, 5H), 6.85–6.80 (m, 4H), 4.80 (d, *J* = 6.2 Hz, 1H), 4.73–4.60 (m, 4H), 4.52 (d, *J* = 10.9 Hz, 1H), 4.41 (d, *J* = 11.3 Hz, 1H), 4.28–4.18 (m, 3H), 3.93 (dd, *J* = 12.4, 4.5 Hz, 1H), 3.78 (s, 3H), 3.74 (s, 3H), 3.13 (s, 6H); ^{13}C NMR (75 MHz, $CDCl_3$) δ 162.2, 159.6, 159.5, 158.0, 140.9, 134.1, 131.5, 130.3, 130.0, 129.9, 129.8, 129.6, 129.1, 128.6, 127.8, 127.3, 126.9, 126.3, 125.9, 125.3, 117.9, 114.0, 80.5, 77.8, 77.4, 75.0, 70.3, 65.3, 63.2, 56.5, 55.4, 37.3; LRMS (ESI) *m/z* calculated for $C_{39}H_{40}N_6O_5$ $[M+H]^+$: 673.31; found: 673.64.

Compound **9g**: Prepared from compound **6b** and 3-chloro-1-propyne; White solid; Yield = 78%; $[\alpha]_D^{24}$ = –71.27 (c = 0.41, $CHCl_3$); R_f = 0.52 (EtOAc : Hexane = 3 : 1); ^{1}H NMR (500 MHz, $CDCl_3$) δ 8.38 (s, 2H), 7.52 (s, 1H), 7.17 (d, *J* = 8.1 Hz, 2H), 6.87 (d, *J* = 8.3 Hz, 2H), 6.77 (d, *J* = 8.3 Hz, 2H), 6.68 (d, *J* = 8.1 Hz, 2H), 4.90–4.87 (m, 2H), 4.75 (d, *J* = 14.7 Hz, 1H), 4.62 (dd, *J* = 7.2, 3.5 Hz, 1H), 4.46 (d, *J* = 11.5 Hz, 1H), 4.24 (d, *J* = 7.6 Hz, 1H), 4.12 (d, *J* = 11.5 Hz, 1H), 4.04–4.00 (m, 2H), 3.90–3.87 (m, 2H), 3.80 (s, 3H), 3.75 (s, 3H), 3.23 (s, 6H); ^{13}C NMR (125 MHz, $CDCl_3$) δ 162.6, 159.7, 159.4, 158.2, 132.3, 130.1, 130.0, 129.5, 129.3, 128.5, 117.9, 114.2, 113.8, 80.9, 76.1, 74.8, 70.0, 63.9, 62.4, 56.6, 55.5, 55.4, 37.4; LRMS (ESI) *m/z* calculated $C_{29}H_{34}N_6O_5$ $[M+H]^+$: 547.27; found: 547.52.

Compound **9h**: Prepared from compound **6b** and 1-bromo-2-butyne; White solid; Yield = 79%; $[\alpha]_D^{22}$ = –67.51 (c = 1.23, $CHCl_3$); R_f = 0.16 (EtOAc : Hexane = 2 : 1); ^{1}H NMR (500 MHz, $CDCl_3$) δ 8.37 (s, 2H), 7.16 (d, *J* = 8.6 Hz, 2H), 6.86 (d, *J* = 8.6 Hz, 2H), 6.79 (d, *J* = 8.6 Hz, 2H), 6.68 (d, *J* = 8.6 Hz, 2H), 4.81–4.75 (m, 2H), 4.65 (d, *J* = 14.7 Hz, 1H), 4.57 (dd, *J* = 7.5, 4.0 Hz, 1H), 4.44 (d, *J* = 11.5 Hz, 1H), 4.24 (d, *J* = 7.3 Hz, 1H), 4.10 (d, *J* = 11.5 Hz, 1H), 4.04–3.98 (m, 2H), 3.94 (d, *J* = 10.8 Hz, 1H), 3.85–3.80 (m, 4H), 3.75 (s, 3H), 3.22 (s, 6H), 2.25 (s, 3H); ^{13}C NMR (125 MHz, $CDCl_3$) δ 162.5, 159.6, 159.3, 158.2, 137.2, 130.03, 129.97, 129.6, 129.4, 128.6, 117.9, 114.1, 113.7, 80.8, 76.2, 74.8, 69.9, 63.7, 62.3, 56.5, 55.5, 55.4, 37.4, 10.3; LRMS (ESI) *m/z* calculated for $C_{30}H_{36}N_6O_5$ $[M+H]^+$: 561.28; found: 561.21.

Compound **9i**: Prepared from compound **6b** and 1-bromo-2-pentyne; White solid; Yield = 89%; $[\alpha]_D^{22}$ = –63.84 (c = 0.29, $CHCl_3$); R_f = 0.64 (MeOH : DCM = 1 : 10); ^{1}H NMR (500 MHz, $CDCl_3$) δ 8.38 (s, 2H), 7.16 (d, *J* = 8.3 Hz, 2H), 6.85 (d, *J* = 8.6 Hz, 2H), 6.78 (d, *J* = 8.6 Hz, 2H), 6.68 (d, *J* = 8.6 Hz, 2H), 4.81–4.78 (m, 2H), 4.68 (d, *J* = 14.6 Hz, 1H), 4.58 (dd, *J* = 7.3, 4.2 Hz, 1H), 4.45 (d, *J* = 11.5 Hz, 1H), 4.25 (d, *J* = 7.3 Hz, 1H), 4.11 (d, *J* = 11.2 Hz, 1H), 4.03–3.98 (m, 2H), 3.93 (d, *J* = 10.5 Hz, 1H), 3.84 (dd, J = 12.0, 4.6 Hz, 1H), 3.79 (s, 3H), 3.74 (s, 3H), 3.22 (s, 6H), 2.69–2.63 (m, 2H), 1.24 (t, *J* = 7.7 Hz, 3H); ^{13}C NMR (125 MHz, $CDCl_3$) δ 162.5, 159.6, 159.3, 158.2, 143.1,

130.0, 129.9, 129.6, 129.4, 128.1, 117.9, 114.1, 113.7, 80.9, 76.2, 74.8, 69.9, 63.7, 62.4, 56.6, 55.5, 55.3, 37.4, 18.7, 13.7; LRMS (ESI) *m/z* calculated for $C_{31}H_{38}N_6O_5$ $[M+H]^+$: 575.30; found: 575.57.

Compound **9j**: Prepared from compound **6b** and 3-Chloro-1-phenyl-1-propyne; White solid; Yield = 64%; $[\alpha]_D^{23}$ = –44.25 (c =0.30, $CHCl_3$); R_f = 0.40 (EtOAc : Hexane = 1 : 1); ^{1}H NMR (500 MHz, $CDCl_3$) δ 8.41 (s, 2H), 7.62 (d, *J* = 7.8 Hz, 2H), 7.45 (t, *J* = 7.6 Hz, 2H), 7.34 (m, 1H), 7.18 (d, *J* = 8.3 Hz, 2H), 6.86 (d, *J* = 8.3 Hz, 2H), 6.79 (d, *J* = 8.3 Hz, 2H), 6.63 (d, *J* = 8.3 Hz, 2H), 5.01 (d, *J* = 14.9 Hz, 1H), 4.92–4.88 (m, 2H), 4.65 (dd, *J* = 7.2, 3.8 Hz, 1H), 4.48 (d, *J* = 11.2 Hz, 1H), 4.28 (d, *J* = 7.6 Hz, 1H), 4.13 (d, *J* = 11.2 Hz, 1H), 4.08–3.98 (m, 3H), 3.91 (dd, *J* = 12.1, 4.8 Hz, 1H), 3.79 (s, 3H), 3.67 (s, 3H), 3.24 (s, 6H); ^{13}C NMR (125 MHz, $CDCl_3$) δ 162.5, 159.7, 159.3, 158.2, 141.7, 131.1, 130.0, 129.5, 129.3, 129.1, 128.8, 128.0, 126.3, 117.9, 114.1, 113.7, 81.1, 76.2, 75.0, 70.0, 63.6, 63.4, 56.9, 55.5, 55.3, 37.4; LRMS (ESI) *m/z* calculated for $C_{35}H_{38}N_6O_5$ $[M+H]^+$: 623.30; found: 623.57.

Compound **9k**: Prepared from compound **6b** and 3-bromo-1-(4-fluorophenyl)-1-propyne (**S2**); Slightly yellow solid; Yield = 58%; $[\alpha]_D^{22}$ = –37.23 (c = 0.18, $CHCl_3$); R_f= 0.17 (EtOAc : Hexane = 1 : 2); ^{1}H NMR (500 MHz, $CDCl_3$) δ 8.40 (s, 2H), 7.59–7.56 (m, 2H), 7.18–7.13 (m, 4H), 6.86 (d, *J* = 8.6 Hz, 2H), 6.78 (d, *J* = 8.6 Hz, 2H), 6.63 (d, *J* = 8.6 Hz, 2H), 4.99–4.85 (m, 3H), 4.64 (dd, *J* = 7.6, 3.9 Hz, 1H), 4.48 (d, *J* = 11.5 Hz, 1H), 4.27 (d, *J* = 7.6 Hz, 1H), 4.13 (d, *J* = 11.2 Hz, 1H), 4.07–3.98 (m, 3H), 3.91 (dd, *J* = 12.0, 4.9 Hz, 1H), 3.80 (s, 3H), 3. 68 (s, 3H), 3.24 (s, 6H); ^{13}C NMR (125 MHz, $CDCl_3$) δ 162.57 (d, *J* = 247.5 Hz), 162.55, 159.7, 159.3, 158.2, 140.9, 130.04, 129.98, 129.5, 129.3, 128.5, 128.0 (d, *J* = 7.9 Hz), 127.3 (d, *J* = 3.3 Hz), 117.8, 116.2 (d, *J* = 21.5 Hz), 114.1, 113.7, 81.2, 76.1, 75.0, 70.0, 63.6, 63.2, 56.9, 55.5, 55.3, 37.4; LRMS (ESI) *m/z* calculated for $C_{35}H_{37}FN_6O_5$ $[M+H]^+$: 641.29; found: 641.46.

Compound **9l**: Prepared from compound **6b** and 3-bromo-1-(4-methoxyphenyl)-1-propyne (**S3**); White solid; Yield = 84%; $[\alpha]_D^{23}$ = –33.07 (c =0.60, $CHCl_3$); R_f = 0.56 (MeOH : DCM = 1 : 10); ^{1}H NMR (500 MHz,

$CDCl_3$) 8.41 (s, 2H), 7.54 (d, *J* = 8.8 Hz, 2H), 7.17 (d, *J* = 8.3 Hz, 2H), 6.99 (d, *J* = 8.8 Hz, 2H), 6.86 (d, *J* = 8.6 Hz, 2H), 6.79 (d, *J* = 8.6 Hz, 2H), 6.63 (d, *J* = 8.6 Hz, 2H), 4.98 (d, *J* = 14.7 Hz, 1H), 4.91–4.86 (m, 2H), 4.63 (dd, *J* = 7.6, 3.9 Hz, 1H), 4.47 (d, *J* = 11.2 Hz, 1H), 4.28 (d, *J* = 7.3 Hz, 1H), 4.13 (d, *J* = 11.5 Hz, 1H), 4.08–4.04 (m, 2H), 4.00–3.98 (m, 1H), 3.90 (dd, *J* = 12.1, 4.5 Hz, 1H), 3.85 (s, 3H), 3.79 (s, 3H), 3.69 (s, 3H), 3.23 (s, 6H); ^{13}C NMR (125 MHz, $CDCl_3$) δ 162.5, 159.7, 159.5, 159.3, 158.2, 141.6, 130.04, 130.00, 129.5, 129.4, 127.9, 127.6, 123.7, 117.9, 114.6, 114.1, 113.7, 81.1, 76.2, 75.0, 70.0, 63.6, 63.3, 56.9, 55.54, 55.48, 55.3, 37.4; LRMS (ESI) *m/z* calculated for $C_{36}H_{40}N_6O_6$ $[M+H]^+$: 653.31; found: 653.45.

Compound **9m**: Prepared from compound **6b** and 3-bromo-1-(2-thienyl)-1-propyne (**S4**); Yellow solid; Yield = 42%; $[\alpha]_D^{22}$ = –34.10 (c = 0.27, $CHCl_3$); R_f = 0.23 (EtOAc : Hexane = 1 : 2); ^{1}H NMR (500 MHz, $CDCl_3$) δ 8.40 (s, 2H), 7.33 (d, *J* = 4.9 Hz, 1H), 7.18–7.16 (m, 3H), 7.12–7.10 (m, 1H), 6.87–6.85 (m, 2H), 6.81–6.79 (m, 2H), 6.65–6.64 (m, 2H), 4.98 (d, *J* = 15.2 Hz, 1H), 4.89–4.87 (m, 1H), 4.83 (d, *J* = 15.2 Hz, 1H), 4.62–4.60 (m, 1H), 4.47 (d, *J* = 11.5 Hz, 1H), 4.28 (d, *J* = 7.3 Hz, 1H), 4.13 (d, *J* = 11.2 Hz, 1H), 4.08–4.00 (m, 3H), 3.89 (dd, *J* = 12.0, 4.6 Hz, 1H), 3.80 (s, 3H), 3.69 (s, 3H), 3.23 (s, 6H); ^{13}C NMR (125 MHz, $CDCl_3$) δ 162.6, 159.7, 159.4, 158.2, 137.2, 133.3, 130.1, 129.5, 129.3, 127.90, 127.88, 125.2, 123.9, 117.8, 114.2, 113.8, 81.0, 76.2, 75.0, 70.0, 63.7, 62.9, 57.0, 55.5, 55.3, 37.4; LRMS (ESI) *m/z* calculated for $C_{33}H_{36}N_6O_5S$ $[M+H]^+$: 629.25; found: 629.40.

Compound **9n**: Prepared from compound **6c** and 1-bromo-2-butyne; White solid; Yield = 77%; $[\alpha]_D^{22}$ = –53.74 (c =0.25, $CHCl_3$); R_f = 0.56 (MeOH : $CHCl_3$ = 1 : 10); ^{1}H NMR (500 MHz, $CDCl_3$) δ 8.84 (s, 2H), 8.42 (d, *J* = 8.6 Hz, 2H), 7.48 (d, *J* = 8.6 Hz, 2H), 7.15 (d, *J* = 8.6 Hz, 2H), 6.87 (d, *J* = 8.6 Hz, 2H), 6.81 (d, *J* = 8.8 Hz, 2H), 6.64 (d, *J* = 8.6 Hz, 2H), 4.80–4.71 (m, 3H), 4.59 (dd, *J* = 7.0, 4.5 Hz, 1H), 4.52 (d, *J* = 7.1 Hz, 1H), 4.47 (d, *J* = 11.5 Hz, 1H), 4.16 (d, *J* = 11.5 Hz, 1H), 4.12 (d, *J* = 11.0 Hz, 1H), 4.08 (dd, *J* = 12.0, 6.1 Hz, 1H), 3.92 (d, *J* = 11.0 Hz, 1H), 3.83–3.79 (m, 4H), 3.66 (s, 3H), 2.27 (s, 3H); ^{13}C NMR (125 MHz, $CDCl_3$) δ 163.8, 159.9, 159.5, 157.7, 137.4,

137.3, 136.0, 130.2, 130.0, 129.8, 129.4, 129.1, 128.9, 128.8, 128.5, 114.2, 113.8, 80.1, 76.2, 74.8, 71.0, 63.7, 62.3, 56.3, 55.5, 55.3, 10.3; LRMS (ESI) *m/z* calculated for $C_{34}H_{34}ClN_5O_5$ $[M+H]^+$: 628.23; found: 628.55.

Compound **9o**: Prepared from compound **7a** and 1-bromo-2-butyne; White solid; Yield = 60%; $[\alpha]_D^{22}$ = –88.13 (c =0.44, $CHCl_3$); R_f = 0.12 (EtOAc : Hexane = 2 : 1); ^{1}H NMR (500 MHz, $CDCl_3$) δ 7.60 (s, 1H), 7.44 (s, 1H), 7.18 (d, *J* = 8.6 Hz, 2H), 6.91–6.85 (m, 4H), 6.75 (d, *J* = 8.6 Hz, 2H), 4.76 (d, *J* = 14.6 Hz, 1H), 4.70–4.65 (m, 2H), 4.57–4.54 (m, 2H), 4.48 (d, *J* = 11.5 Hz, 1H), 4.24–4.15 (m, 3H), 4.06 (dd, *J* = 12.0, 6.6 Hz, 1H), 3.91 (s, 3H), 3.86 (dd, *J* = 12.0, 4.4 Hz, 1H), 3.80 (s, 3H), 3.76 (s, 3H); ^{13}C NMR (125 MHz, $CDCl_3$) δ 159.44, 159.35, 139.7, 137.1, 130.2, 130.14, 130.05, 129.8, 129.7, 128.5, 119.0, 114.0, 113.7, 81.1, 74.9, 73.2, 70.1, 64.1, 62.3, 56.7, 55.5, 55.4, 39.3, 10.2; LRMS (ESI) *m/z* calculated for $C_{28}H_{33}N_5O_5$ $[M+H]^+$: 520.26; found: 520.38.

Compound **9p**: Prepared from compound **8a** and 1-bromo-2-butyne; White solid; Yield = 88%; $[\alpha]_D^{22}$ = –58.37 (c = 0.37, $CHCl_3$); R_f = 0. 18 (EtOAc : Hexane = 2 : 1); ^{1}H NMR (500 MHz, $CDCl_3$) δ 8.58 (s, 1H), 8.47 (s, 1H), 7.13 (d, *J* = 8.1 Hz, 2H), 6.84 (d, *J* = 8.3 Hz, 2H), 6.79 (d, *J* = 8.3 Hz, 2H), 6.56 (d, *J* = 8.1 Hz, 2H), 6.47 (s, 1H), 4.79–4.71 (m, 3H), 4.56–4.54 (m, 1H), 4.48–4.45 (m, 2H), 4.14 (d, *J* = 11.2 Hz, 2H), 4.05 (dd, *J* = 12.1, 6.0 Hz, 1H), 3.91 (d, *J* = 11 Hz, 1H), 3.78–3.74 (m, 4H), 3.69 (s, 3H), 2.52 (s, 3H), 2.25 (s, 3H); ^{13}C NMR (125 MHz, $CDCl_3$) δ 159.8, 159.4, 155.8, 149.9, 149.2, 137.3, 134.1, 130.1, 130.0, 128.8, 128.7, 128.5, 117.7, 114.1, 113.6, 96.3, 79.9, 76.0, 74.6, 70.7, 63.6, 62.3, 56.3, 55.4, 55.2, 14.8, 10.2; LRMS (ESI) *m/z* calculated for $C_{31}H_{34}N_6O_5$ $[M+H]^+$: 571.27; found: 571.46.

Synthesis of 2-morpholione-fused triazoles 10. The synthetic procedure is described at the Experimental section.

Compound **10a**: Prepared from compound **6a** and 2-butynoic acid; Yellow solid; Yield = 95%; $[\alpha]_D^{25}$ = –16.09 (c =0.61, $CHCl_3$); R_f = 0.19 (EtOAc :

Hexane = 1 : 1); ^{1}H NMR (300 MHz, $CDCl_3$) δ 8.42 (s, 2H), 7.14 (d, *J* = 8.7 Hz, 2H), 7.03 (d, *J* = 8.7 Hz, 2H), 6.85–6.76 (m, 4H), 4.68–4.64 (m, 1H), 4.54 (d, *J* = 5.8 Hz, 1H), 4.46–4.40 (m, 3H), 4.33 (d, *J* = 10.5 Hz, 1H), 4.23 (d, *J* = 10.5 Hz, 1H), 4.16 (d, *J* = 11.1 Hz, 1H), 3.92–3.89 (m, 1H), 3.79 (s, 3H), 3.78 (s, 3H), 3.22 (s, 6H), 2.54 (s, 3H); ^{13}C NMR (75 MHz, $CDCl_3$) δ 162.6, 159.8, 159.7, 158.1, 156.7, 148.9, 131.0, 130.1, 129.2, 128.4, 121.8, 117.0, 114.1, 114.0, 79.3, 77.4, 74.9, 70.6, 68.5, 55.7, 55.5, 55.4, 37.3, 11.4; HRMS (FAB+) *m/z* calculated for $C_{30}H_{34}N_6O_6$ $[M+H]^+$: 575.2618; found: 575.2622.

Compound **10b**: Prepared from compound **6b** and 2-butynoic acid; White solid; Yield = 72%; $[\alpha]_D^{20}$ = –45.84 (c =0.50, $CHCl_3$); R_f = 0.17 (EtOAc : Hexane = 1 : 1); ^{1}H NMR (500 MHz, $CDCl_3$) δ 8.35 (s, 2H), 7.15 (d, *J* = 8.1 Hz, 2H), 6.87 (d, *J* = 7.8 Hz, 2H), 6.76 (d, *J* = 8.1 Hz, 2H), 6.69 (d, *J* = 7.8 Hz, 2H), 5.06–5.04 (m, 1H), 4.54–4.47 (m, 2H), 4.40–4.35 (m, 2H), 4.23 (d, *J* = 7.6 Hz, 1H), 4.10 (d, *J* = 11.7 Hz, 1H), 3.89–3.84 (m, 2H), 3.80 (s, 3H), 3.74 (s, 3H), 3.23 (s, 6H), 2.56 (s, 3H); ^{13}C NMR (125 MHz, $CDCl_3$) δ 162.6, 159.9, 159.6, 158.1, 156.8, 149.2, 130.2, 130.1, 128.8, 128.5, 122.4, 117.0, 114.3, 113.9, 80.7, 75.7, 75.3, 69.9, 66.0, 56.0, 55.5, 55.4, 37.4, 11.4; LRMS (ESI) *m/z* calculated for $C_{30}H_{34}N_6O_6$ $[M+H]^+$: 575.26; found: 575.55.

Compound **10c**: Prepared from compound **6c** and 2-butynoic acid; Slightly yellow solid; Yield = 92%; $[\alpha]_D^{23}$ = –38.88 (c =0.59, $CHCl_3$); R_f = 0.38 (EtOAc : Hexane = 1 : 1); ^{1}H NMR (500 MHz, $CDCl_3$) δ 8.80 (s, 2H), 8.43 (d, *J* = 8.6 Hz, 2H), 7.49 (d, *J* = 8.6 Hz, 2H), 7.15 (d, *J* = 8.3 Hz, 2H), 6.89 (d, *J* = 8.3 Hz, 2H), 6.74 (d, *J* = 8.3 Hz, 2H), 6.64 (d, *J* = 8.6 Hz, 2H), 5.04 (m, 1H), 4.54 (d, *J* = 11.2 Hz, 2H), 4.45–4.40 (m, 3H), 4.14 (d, *J* = 11.5 Hz, 1H), 3.96 (d, *J* = 11.5 Hz, 1H), 3.82 (s, 3H), 3.74 (d, *J* = 10.8 Hz, 1H), 3.64 (s, 3H), 2.59 (s, 3H); ^{13}C NMR (125 MHz, $CDCl_3$) δ 164.2, 160.2, 159.8, 157.6, 156.6, 149.5, 137.6, 135.8, 130.31, 130.27, 129.8, 129.1, 128.6, 128.1, 127.8, 122.3, 114.5, 114.0, 80.1, 75.5, 75.3, 70.9, 65.9, 55.9, 55.5, 55.3, 29.9, 11.5; LRMS (ESI) *m/z* calculated for $C_{34}H_{32}ClN_5O_6$ $[M+H]^+$: 642.21; found: 642.55.

Compound **10d**: Prepared from compound **6c** and 2-pentynoic acid; Slightly yellow solid; Yield = 90%; $[\alpha]_D^{22}$ = –30.38 (c = 0.16, $CHCl_3$); R_f = 0.19 (EtOAc : Hexane = 1 : 2); ^{1}H NMR (400 MHz, $CDCl_3$) δ 8.79 (s, 2H), 8.45–8.41 (m, 2H), 7.51–7.48 (m, 2H), 7.17–7.14 (m, 2H), 6.91–6.87 (m, 2H), 6.75–6.71 (m, 2H), 6.64–6.61 (m, 2H), 5.05 (q, *J* = 3.8 Hz, 1H), 4.56–4.52 (m, 2H), 4.46–4.39 (m, 3H), 4.14 (d, *J* = 11.7 Hz, 1H), 3.97 (d, *J* = 11.0 Hz, 1H), 3.82 (s, 3H), 3.69 (d, *J* = 11.0 Hz, 1H), 3.64 (s, 3H), 3.04–2.98 (m, 2H), 1.34 (t, *J* = 7.4 Hz, 3H); ^{13}C NMR (100 MHz, $CDCl_3$) δ 164.5, 160.5, 160.1, 157.9, 155.4, 137.9, 136.1, 130.64, 130.58, 130.2, 129.5, 129.0, 128.5, 128.2, 122.1, 114.8, 114.3, 80.4, 75.9, 75.6, 71.2, 66.2, 56.2, 55.9, 55.6, 19.7, 13.6; LRMS (ESI) *m/z* calculated for $C_{28}H_{33}N_5O_5$ $[M+H]^+$: 656.23; found: 655.97.

Compound **10e**: Prepared from compound **7a** and 2-butynoic acid; Slightly yellow solid; Yield = 73%; $[\alpha]_D^{22}$ = –59.18 (c = 0.33, $CHCl_3$); R_f = 0.23 (EtOAc : Hexane = 1 : 1); ^{1}H NMR (300 MHz, $CDCl_3$) δ 7.60 (s, 1H), 7.43 (s, 1H), 7.17 (d, *J* = 8.5 Hz, 2H), 6.88–6.85 (m, 4H), 6.78–6.74 (m, 2H), 4.93 (q, *J* = 4.5 Hz, 1H), 4.63–4.58 (m, 1H), 4.53–4.36 (m, 4H), 4.20 (d, *J* = 11.5 Hz, 1H), 4.15 (d, *J* = 10.8 Hz, 1H), 4.03 (d, *J* = 10.6 Hz, 1H), 3.93 (s, 3H), 3.81 (s, 3H), 3.77 (s, 3H), 2.57 (s, 3H); ^{13}C NMR (125 MHz, $CDCl_3$) δ 159.74, 159.65, 156.9, 149.2, 139.4, 130.1, 129.99, 129.95, 129.5, 129.1, 122.2, 118.5, 114.2, 113.9, 80.7, 75.2, 72.4, 70.2, 66.5, 56.1, 55.51, 55.45, 39.4, 11.4; LRMS (ESI) *m/z* calculated for $C_{28}H_{31}N_5O_6$ $[M+H]^+$: 534.23; found: 534.02.

Compound **10f**: Prepared from compound **7a** and 3-phenyl-2-propynoic acid; White solid; Yield = 77%; $[\alpha]_D^{22}$ = –33.44 (c = 0.34, $CHCl_3$); R_f = 0.25 (EtOAc : Hexane = 1 : 1); ^{1}H NMR (400 MHz, $CDCl_3$) δ 8.27–8.24 (m, 2H), 7.64 (s, 1H), 7.51–7.44 (m, 4H), 7.18 (d, *J* = 8.6 Hz, 2H), 6.87–6.84 (m, 4H), 6.69 (d, *J* = 8.6 Hz, 2H), 5.05 (q, *J* = 4.3 Hz, 1H), 4.62 (dd, *J* = 12.3, 4.1 Hz, 1H), 4.55–4.52 (m, 2H), 4.48 (dd, *J* = 12.3, 4.1 Hz, 1H), 4.41 (dd, *J* = 6.5, 4.5 Hz, 1H), 4.23–4.16 (m, 2H), 4.01 (d, *J* = 10.6 Hz, 1H), 3.94 (s, 3H), 3.79 (s, 3H), 3.68 (s, 3H); ^{13}C NMR (100 MHz, $CDCl_3$) δ 159.7, 159.6, 156.5, 150.8, 139.4, 130.10, 130.07, 130.02, 129.4, 128.9, 128.8, 128.7, 121.2, 118.5, 114.2,

113.9, 80.9, 75.3, 72.4, 70.1, 66.0, 56.2, 55.5, 55.3, 39.4; LRMS (ESI) *m/z* calculated for $C_{33}H_{33}N_5O_6$ $[M+H]^+$: 596.25; found: 596.00.

Synthesis of piperazine-fused triazoles 11. The synthetic procedure is described at the Experimental section.

Compound **11a**: Prepared from compound **6a** and 4-methyl-*N*-(prop-2-yn-1-yl)benzenesulfonamide; White solid; Yield = 58%; $[\alpha]_D^{22}$ = –57.07 (c = 1.07, $CHCl_3$); R_f= 0.16 (EtOAc : Hexane = 2 : 1); ^{1}H NMR (400 MHz, $CDCl_3$) δ 8.40 (s, 2H), 7.54 (d, *J* = 8.2 Hz, 2H), 7.40 (s, 1H), 7.34 (d, *J* = 7.8 Hz, 2H), 7.08–7.03 (m, 4H), 6.80–6.76 (m, 4H), 4.70–4.66 (m, 2H), 4.46 (d, *J* = 11.7 Hz, 1H), 4.24–4.12 (m, 2H), 4.05–3.94 (m, 4H), 3.81 (s, 3H), 3.79 (s, 3H), 3.39 (dd, *J* = 13.3, 5.5 Hz, 1H), 3.24 (s, 6H), 3.12 (dd, *J* = 13.3, 3.9 Hz, 1H), 2.46 (s, 3H); ^{13}C NMR (100 MHz, $CDCl_3$) δ 162.5, 159.63, 159.61, 158.1, 144.9, 132.7, 130.8, 130.5, 130.3, 129.7, 129.4, 129.3, 129.0, 127.8, 117.6, 114.1, 114.0, 80.6, 75.1, 75.0, 69.9, 57.1, 55.0, 55.4, 45.2, 41.9, 37.4, 29.9, 21.8; LRMS (ESI) *m/z* calculated for $C_{36}H_{41}N_7O_6S$ $[M+H]^+$: 700.29; found: 700.00.

Compound **11b**: Prepared from compound **6a** and 4-methyl-*N*-(3-phenylprop-2-yn-1-yl)benzenesulfonamide (**S5**); White solid; Yield = 73%; $[\alpha]_D^{25}$ = –50.39 (c =0.46, $CHCl_3$); R_f= 0.20 (EtOAc : Hexane = 2 : 3); ^{1}H NMR (400 MHz, $CDCl_3$) δ 8.39 (s, 2H), 7.60–7.55 (m, 4H), 7.46–7.43 (m, 2H), 7.37–7.32 (m, 3H), 7.08–7.03 (m, 4H), 6.77–6.71 (m, 4H), 4.72–4.67 (m, 2H), 4.46 (d, *J* = 11.7 Hz, 1H), 4.34–4.19 (m, 3H), 4.15–4.09 (m, 2H), 4.02 (d, *J* = 11.7 Hz, 1H), 3.71 (s, 3H), 3.69 (s, 3H), 3.52 (dd, *J* = 13.1, 5.7 Hz, 1H), 3.17–3.13 (m, 7H), 2.46 (s, 3H); ^{13}C NMR (100 MHz, $CDCl_3$) δ 162.4, 159.59, 159.57, 157.9, 144.9, 141.9, 132.8, 130.8, 130.6, 130.4, 129.5, 129.1, 129.0, 128.2. 127.8, 126.3, 125.4, 117.5, 113.99, 113.98, 80.2, 75.1, 74.8, 69.8, 57.2, 55.4, 55.3, 44.4, 42.8, 37.3, 21.8; HRMS (FAB+) *m/z* calculated for $C_{42}H_{45}N_7O_6S$ $[M+H]^+$: 776.3230; found: 776.3234.

Compound **11c**: Prepared from compound **6a** and 4-methyl-*N*-(3-(*p*-tolyl)prop-2-yn-1-yl)benzenesulfonamide; Slightly yellow solid; Yield = 70%; $[\alpha]_D^{21}$ = –46.69 (c = 0.44, $CHCl_3$); R_f = 0.24 (EtOAc : Hexane = 1 : 1); ^1H NMR (400 MHz, $CDCl_3$) δ 8.39 (s, 2H), 7.58–7.56 (m, 2H), 7.46–7.44 (m, 2H), 7.35 (d, *J* = 7.8 Hz, 2H), 7.26 (d, *J* = 7.8 Hz, 2H), 7.08–7.03 (m, 4H), 6.77–6.72 (m, 4H), 4.70–4.67 (m, 2H), 4.46 (d, *J* = 11.7 Hz, 1H), 4.33–4.18 (m, 3H), 4.13–4.07 (m, 2H), 4.02 (d, *J* = 11.7 Hz, 1H), 3.72 (s, 3H), 3.70 (s, 3H), 3.50 (d, *J* = 13.3, 5.5 Hz, 1H), 3.18–3.12 (m, 7H), 2.46 (s, 3H), 2.40 (s, 3H); ^{13}C NMR (100 MHz, $CDCl_3$) δ 162.4, 159.6, 158.0, 144.9, 142.0, 138.1, 132.7, 130.8, 130.6, 130.3, 129.8, 129.5, 129.0, 127.74, 127.69, 126.2, 125.0, 117.6, 113.98, 113.96, 80.2, 77.4, 75.1, 74.6, 69.7, 57.2, 55.4, 55.3, 44.5, 42.8, 37.3, 21.9, 21.5; LRMS (ESI) *m/z* calculated for $C_{43}H_{47}N_7O_6S$ $[M+H]^+$: 790.34; found: 790.79.

Compound **11d**: Prepared from compound **6a** and *N*-(3-(4-cyanophenyl)prop-2-yn-1-yl)-4-methylbenzenesulfonamide; Slightly yellow solid; Yield = 71%; $[\alpha]_D^{22}$ = –46.12 (c = 0.25, $CHCl_3$); R_f = 0.12 (EtOAc : Hexane = 2 : 1); ^1H NMR (400 MHz, $CDCl_3$) δ 8.39 (s, 2H), 7.75–7.73 (m, 2H), 7.68–7.66 (m, 2H), 7.60 (d, *J* = 8.2 Hz, 2H), 7.38 (d, *J* = 7.8 Hz, 2H), 7.07–7.04 (m, 4H), 6.75–6.72 (m, 4H), 4.73–4.69 (m, 1H), 4.66 (d, *J* = 3.9 Hz, 1H), 4.47 (d, *J* = 11.7 Hz, 1H), 4.34–4.29 (m, 2H), 4.20–4.11 (m, 2H), 4.08 (d, *J* = 11.0 Hz, 1H), 4.03 (d, *J* = 11.7 Hz, 1H), 3.697 (s, 3H), 3.702 (s, 3H), 3.53 (dd, *J* = 13.1, 5.3 Hz, 1H), 3.17 (s, 6H), 3.12 (d, *J* = 13.1, 4.1 Hz, 1H), 2.47 (s, 3H); ^{13}C NMR (100 MHz, $CDCl_3$) δ 162.4, 159.62, 159.59, 158.0, 145.1, 135.0, 132.9, 123.7, 130.8, 130.6, 130.4, 129.5, 128.9, 127.8, 126.9, 126.5, 118.8, 117.4, 114.02, 113.99, 111.5, 110.2, 80.0, 75.2, 74.8, 69.8, 57.4, 55.4, 55.3, 44.3, 42.7, 37.3, 21.8; LRMS (ESI) *m/z* calculated for $C_{43}H_{44}N_8O_6S$ $[M+H]^+$: 801.32; found: 801.76.

Synthesis of vicinal diols 12. The synthetic procedure is described at the Experimental section.

Compound **12a**: Prepared from compound **9a**; White Solid; Yield = 99%; $[\alpha]_D^{23}$ = –4.84 (c = 0.52, $CHCl_3$: MeOH = 1 : 1); R_f= 0.09 (MeOH : $CHCl_3$ = 1 : 10); ^{1}H NMR (500 MHz, $CDCl_3$: CD_3OD = 25 : 2) δ 8.35 (s, 2H), 7.41 (s, 1H), 4.93–4.82 (m, 3H), 4.55 (q, *J* = 4.2 Hz, 1H), 4.33 (dd, *J* = 12.5, 4.4 Hz, 1H), 4.17 (dd, *J* = 6.2, 4.0 Hz, 1H), 4.02 (dd, *J* = 12.5, 4.4 Hz, 1H), 3.16 (s, 6H); ^{13}C NMR (125 MHz, $CDCl_3$: CD_3OD = 10 : 1) δ ; 161.7, 157.1, 131.9, 128.1, 120.4, 74.7, 69.9, 65.4, 62.3, 58.6, 37.3; LRMS (ESI) *m/z* calculated for $C_{13}H_{18}N_6O_3$ $[M+H]^+$: 307.15; found: 307.22.

Compound **12b**: Prepared from compound **9b**; White solid; Yield = 92%; $[\alpha]_D^{22}$ = –3.69 (c = 0.15, $CHCl_3$: MeOH = 1 : 1); R_f= 0.16 (MeOH : $CHCl_3$ = 1 : 10); ^{1}H NMR (500 MHz, $CDCl_3$: CD_3OD = 22 : 7) δ 7.99 (s, 2H), 4.54–4.41 (m, 3H), 4.26–4.22 (m, 3H), 4.17 (dd, *J* = 12.5, 3.7 Hz, 1H), 4.00 (dd, *J* = 7.3, 3.9 Hz, 1H), 3.71 (dd, *J* = 12.5, 4.4 Hz, 1H), 2.90 (s, 6H), 1.83 (s, 3H); ^{13}C NMR (125 MHz, $CDCl_3$: CD_3OD = 22 : 7) δ 161.1, 156.7, 136.4, 128.1, 120.3, 74.2, 69.7, 63.9, 61.5, 56.7, 36.9, 8.9; LRMS (ESI) *m/z* calculated for $C_{14}H_{20}N_6O_3$ $[M+H]^+$: 321.17; found: 320.97.

Compound **12c**: Prepared from compound **9c**; White solid; Yield = 92%; $[\alpha]_D^{23}$ = –5.10 (c = 0.39, $CHCl_3$: MeOH = 1 : 1); R_f= 0.28 (MeOH : DCM = 1 : 10); ^{1}H NMR (500 MHz, $CDCl_3$) δ 8.35 (s, 2H), 4.97 (d, *J* = 6.4 Hz, 1H), 4.78–4.71 (m, 2H), 4.55–4.52 (m, 2H), 4.28–4.21 (m, 3H), 4.00 (dd, *J* = 12.3, 4.5 Hz, 1H), 3.14 (s, 6H), 2.52 (q, *J* = 7.7 Hz, 2H), 1.17 (t, *J* = 7.7 Hz, 3H); ^{13}C NMR (125 MHz, $CDCl_3$) δ 162.0. 157.2, 142.8, 128.0, 120.6, 74.9, 70.4, 65.4, 62.4, 57.2, 37.4, 18.5, 13.2; LRMS (ESI) *m/z* calculated for $C_{15}H_{22}N_6O_3$ $[M+H]^+$: 335.18; found: 335.15.

Compound **12g**: Prepared from compound **9g**; Yellow solid; Yield = 99%; $[\alpha]_D^{22}$ = –27.56 (c = 0.42, $CHCl_3$: MeOH = 1 : 1); R_f= 0.24 (MeOH : EtOAc = 1 : 10); ^{1}H NMR (500 MHz, $CDCl_3$) δ 8.36 (s, 2H), 7.39 (s, 1H), 4.89–4.81 (m, 2H), 4.74–4.59 (m, 5H), 4.28–4.18 (m, 2H), 3.05 (s, 6H); ^{13}C NMR (125 MHz, $CDCl_3$) δ 161.8, 157.4, 132.3, 128.2, 120.8, 73.3, 71.0, 64.2, 62.4, 57.3,

37.4; LRMS (ESI) *m/z* calculated for $C_{13}H_{18}N_6O_3$ $[M+H]^+$: 307.15; found: 307.19.

Compound **12h**: Prepared from compound **9h**; White solid; Yield = 88%; $[\alpha]_D^{22}$ = –16.62 (c = 0.23, $CHCl_3$: MeOH = 1 : 1); R_f = 0.13 (MeOH : $CHCl_3$ = 1 : 10); ^{1}H NMR (500 MHz, $CDCl_3$: CD_3OD = 10 : 1) δ 8.33 (s, 2H), 4.74–4.67 (m, 2H), 4. 57 (m, 3H), 4.19–4.12 (m, 2H), 3.04 (s, 6H), 2.11 (s, 3H); ^{13}C NMR (125 MHz, $CDCl_3$: CD_3OD = 10 : 1) δ 161.5, 157.3, 136.9, 128.8, 121.3, 73.0, 70.4, 63.8, 62.0, 57.2, 37.3, 9.7; LRMS (ESI) *m/z* calculated for $C_{14}H_{20}N_6O_3$ $[M+H]^+$: 321.17; found: 321.23.

Compound **12i**: Prepared from compound **9i**; White solid; Yield = 99%; $[\alpha]_D^{23}$ = –14.61 (c = 0.54, $CHCl_3$: MeOH = 1 : 1); R_f = 0.35 (MeOH : $CHCl_3$ = 1 : 10); ^{1}H NMR (500 MHz, $CDCl_3$) δ 8.39 (s, 2H), 4.82–4.75 (m, 4H), 4.64 (bs, 1H), 4.46 (bs, 2H), 4.27–4.16 (m, 2H), 3.08 (s, 6H), 2.54 (q, *J* = 7.4 z, 2H), 1.16 (t, *J* = 7.5 Hz, 3H); ^{13}C NMR (125 MHz, $CDCl_3$) δ 161.9, 157.4 (t, *J* = 13.3 Hz), 142.8, 128.2, 120.8, 73.4, 71.1, 64.2, 62.4, 57.4, 37.4, 18.5, 13.3; LRMS (ESI) *m/z* calculated for $C_{15}H_{22}N_6O_3$ $[M+H]^+$: 335.18; found: 335.15.

Compound **12j**: Prepared from compound **9j**; White solid; Yield = 96%; $[\alpha]_D^{23}$ = +29.33 (c = 0.44, $CHCl_3$: MeOH = 1 : 1); R_f = 0.31 (MeOH : DCM = 1 : 10); ^{1}H NMR (500 MHz, $CDCl_3$) δ 8.44 (s, 2H), 7.40–7.31 (m, 5H), 5.15 (bs, 1H), 4.97–4.95 (m, 1H), 4.86–4.80 (m, 2H), 4.76–4.73 (m, 1H), 4.60 (d, *J* = 14.9 Hz, 1H), 4.30–4.22 (m, 2H), 4.07 (bs, 1H), 3.08 (s, 6H); ^{13}C NMR (125 MHz, $CDCl_3$) δ 162.0, 157.2, 141.2, 130.20, 130.19, 129.1, 128.9, 128.2, 126.2, 73.4, 71.2, 63.8, 63.1, 57.8, 37.4; LRMS (ESI) *m/z* calculated for $C_{19}H_{22}N_6O_3$ $[M+H]^+$: 383.18; found: 383.12.

Compound **12k**: Prepared from compound **9k**; White solid; Yield = 96%; $[\alpha]_D^{22}$ = +30.16 (c = 0.21, $CHCl_3$: MeOH = 1 : 1); R_f = 0.17 (MeOH : $CHCl_3$ = 1 : 10); ^{1}H NMR (500 MHz, $CDCl_3$: CD_3OD = 10 : 1) δ 8.46 (s, 2H), 7.51–7.48 (m, 2H), 7.15–7.12 (m, 2H), 5.03–4.96 (m, 2H), 4.80–4.77 (m, 1H), 4.74–4.68 (m, 2H), 4.35–4.27 (m, 2H), 3.15 (s, 6H); ^{13}C NMR (125 MHz, $CDCl_3$:

CD_3OD = 10 : 1) δ 162.5 (d, J = 248.4 Hz), 161.6, 157.2, 140.5, 128.6, 127.9 (d, J = 8.4 Hz), 126.6 (d, J = 3.3 Hz), 121.3, 116.1 (d, J = 21.8 Hz), 73.0, 70.4, 63.6, 63.0, 57.6, 37.3; LRMS (ESI) *m/z* calculated for $C_{19}H_{21}FN_6O_3$ $[M+H]^+$: 401.17; found: 401.30.

Compound **12l**: Prepared from compound **9l**; White solid; Yield = 89%; $[\alpha]_D^{22}$ = +42.38 (c = 0.34, $CHCl_3$: MeOH = 1 : 1); R_f = 0.23 (MeOH : $CHCl_3$ = 1 : 10); ^1H NMR (500 MHz, $CDCl_3$: CD_3OD = 10 : 1) δ 8.47 (s, 2H), 7.45 (d, J = 8.6 Hz, 2H), 6.98 (d, J = 8.6 Hz, 2H), 5.02–4.94 (m, 2H), 4.79–4.70 (m, 3H), 4.34–4.26 (m, 2H), 3.85 (s, 3H), 3.16 (s, 6H); ^{13}C NMR (125 MHz, $CDCl_3$: CD_3OD = 10 : 1) δ 161.7, 159.5, 157.3, 141.3, 128.0, 127.5, 123.0, 121.3, 114.5, 73.1, 70.5, 63.7, 63.2, 57.6, 55.4, 37.4; LRMS (ESI) *m/z* calculated for $C_{20}H_{24}N_6O_4$ $[M+H]^+$: 413.19; found: 413.30.

Compound **12m**: Prepared from compound **9m**; Yellow solid; Yield = 76%; $[\alpha]_D^{23}$ = +37.01 (c = 0.79, $CHCl_3$: MeOH = 1 : 1); R_f = 0.14 (MeOH : $CHCl_3$ = 1 : 10); ^1H NMR (300 MHz, $CDCl_3$) δ 8.40 (s, 2H), 7.28–7.27 (m, 1H), 7.05–7.02 (m, 1H), 6.97–6.96 (m, 1H), 5.04 (bs, 1H), 4.88–4.66 (m, 5H), 4.37–4.21 (m, 3H), 3.06 (s, 6H); ^{13}C NMR (75 MHz, $CDCl_3$) δ 161.9, 157.4, 136.7, 132.4, 128.0, 127.9, 125.3, 124.2, 120.7, 73.4, 71.1, 63.9, 62.7, 57.8, 37.4; LRMS (ESI) *m/z* calculated for $C_{17}H_{20}N_6O_3S$ $[M+H]^+$: 389.14; found: 389.27.

Compound **12n**: Prepared from compound **9n**; White solid; Yield = 94%; $[\alpha]_D^{23}$ = –0.60 (c = 0.59, $CHCl_3$: MeOH = 1 : 1); R_f = 0.16 (MeOH : $CHCl_3$ = 1 : 10); ^1H NMR (300 MHz, $CDCl_3$: CD_3OD = 10 : 1) δ 7.58 (s, 1H), 7.54 (s, 1H), 4.89 (d, J = 4.7 Hz, 1H), 4.80 (s, 2H), 4.55–4.48 (m, 2H), 4.32–4.26 (m, 1H), 4.13–4.07 (m, 1H), 3.87 (s, 3H), 2.22 (s, 3H); ^{13}C NMR (75 MHz, $CDCl_3$: CD_3OD = 10 : 1) δ 138.2. 137.0, 129.6, 128.7, 121.4, 73.1, 67.4, 64.1, 62.1, 57.2, 38.8, 9.8; LRMS (ESI) *m/z* calculated for $C_{18}H_{18}ClN_5O_3$ $[M+H]^+$: 388.12; found: 388.24.

Compound **12o**: Prepared from compound **9o**; White solid; Yield = 99%; $[\alpha]_D^{23}$ = –22.59 (c = 0.15, $CHCl_3$: MeOH = 1 : 1); R_f = 0.08 (MeOH : $CHCl_3$ = 1 : 10); ^{1}H NMR (500 MHz, $CDCl_3$) δ 8.96 (s, 2H), 8.32 (d, *J* = 8.6 Hz, 2H), 7.46 (d, *J* = 8.3 Hz, 2H), 4.87 (d, *J* = 6.6 Hz, 1H), 4.83–4.77 (m, 2H), 4.67–4.61 (m, 2H), 4.32–4.28 (m, 1H), 4.21 (dd, *J* = 12.1, 4.2 Hz, 1H), 2.21 (s, 3H); ^{13}C NMR (125 MHz, $CDCl_3$) δ 163.0, 156.8, 137.13, 137.08, 135.8, 132.6, 129.5. 129.0, 128.8, 72.9, 70.2, 63.8, 62.1, 57.2, 9.8; LRMS (ESI) *m/z* calculated for $C_{12}H_{17}N_5O_3$ $[M+H]^+$: 280.14; found: 280.23.

Synthesis of *p*-methoxyphenyl (PMP) acetal 13b and 13g by DDQ treatment. To a stirred solution of **9b** or **9g** (20 mg, 0.0357 mmol) in anhydrous DCM was added DDQ (2 equiv.) at 0 °C. The mixture was stirred at 0 °C for 1 h, then at room temperature for 9 h. The organic layer was washed with saturated $NaHCO_3$ solution and the aqueous layer was extracted twice with DCM. The combined organic layer was dried over anhydrous Na_2SO_4(s). The filtrate was concentrated under reduced pressure and purified by preparative thin layer chromatography (TLC) to yield **13b** or **13h** as a diastereomeric mixture.

Compound **13b**: Diastereomeric mixture (81 : 19); White solid; Yield = 59%; R_f = 0.35 (MeOH : $CHCl_3$ = 1 : 10); ^{1}H NMR (500 MHz, $CDCl_3$) δ [8.28 (s) : 8.23 (s) = 1.60 : 0.35, total 2H], [7.42 (d, *J* = 8.8 Hz) : 7.31 (d, *J* = 8.8 Hz) = 1.69 : 0.41, total 2H], 6.92–6.89 (m, 2H), [6.14 (s) : 5.92 (s) = 0.20 : 0.81, total 1H], [5.54 (d, *J* = 8.3 Hz) : 5.32 (d, *J* = 7.6 Hz) = 0.89: 0.26, total 1H], [4.90–4.72 (m), 4.47–4.37 (m), total 5H], 4.01–3.96 (m, 1H), 3.82 (s, 3H), 3.17 (s, 6H), 2.19 (s, 3H); LRMS (ESI) *m/z* calculated for $C_{22}H_{26}N_6O_4$ $[M+H]^+$: 439.21; found: 438.89.

Compound **13h**: Each diastereomer is indicated by **13h-1** and **13h-2.** They were separated by preparative TLC. Diastereomeric ratio of **13h-1** to **13h-2** is 66 to 34. Yield = 33% (total yield including both diastereomers).
13h-1: White solid; $[\alpha]_D^{23}$ = +20.74 (c = 0.44, $CHCl_3$); R_f = 0.44 (EtOAc : Hexane = 4 : 1); ^{1}H NMR (400 MHz, $CDCl_3$) δ 8.53 (s, 2H), 7.38 (d, *J* = 8.6

Hz, 2H), 6.90 (d, *J* = 8.6 Hz, 2H), 6.43 (s, 1H), 5.64 (d, *J* = 5.1 Hz, 1H), 4.79 (d, *J* = 14.9 Hz, 1H), 4.68 (d, *J* = 14.9 Hz, 1H), 4.37 (dd, *J* = 8.6, 5.5 Hz, 1H), 4.26–4.18 (m, 2H), 3.92–3.87 (m, 1H), 3.81 (s, 3H), 3.20 (s, 6H), 2.19 (s, 3H); ^{13}C NMR (100 MHz, $CDCl_3$) δ 162.2, 160.4, 158.1, 137.1, 131.3, 127.4, 127.2, 118.1, 114.0, 103.6, 78.4, 66.3, 62.4, 55.5, 55.1, 37.3, 29.9, 10.1; LRMS (ESI) *m/z* calculated for $C_{22}H_{26}N_6O_4$ $[M+H]^+$: 439.21; found: 438.95.

13h-2: White solid; $[\alpha]_D^{21}$ = +5.13 (c = 0.34, $CHCl_3$); R_f = 0.44 (EtOAc : Hexane = 4 : 1); ^{1}H NMR (400 MHz, $CDCl_3$) δ 8.48 (s, 2H), 7.50 (d, *J* = 8.6 Hz, 2H), 6.95 (d, *J* = 8.6 Hz, 2H), 5.91 (s, 1H), 5.57 (d, *J* = 6.3 Hz, 1H), 4.83–4.71 (m, 2H), 4.60 (dd, *J* = 7.8, 6.7 Hz, 1H), 4.29–4.20 (m, 2H), 3.94 (dd, *J* = 11.7, 7.4 Hz, 1H), 3.84 (s, 3H), 3.16 (s, 6H), 2.22 (s, 3H); ^{13}C NMR (75 MHz, $CDCl_3$) δ 162.3, 160.8, 158.6, 137.1, 128.2, 128.1, 127.1, 118.3, 114.2, 103.5, 80.0, 66.1, 62.4, 55.6, 55.0, 37.3, 31.2, 10.2; LRMS (ESI) *m/z* calculated for $C_{22}H_{26}N_6O_4$ $[M+H]^+$: 439.21; found: 438.95.

Synthesis of *p*-methoxyphenyl (PMP) acetal 13b by acetal exchange reaction. To a stirred solution of **12b** (5 mg, 0.0156 mmol) in DCM was added excess amount of *p*-anisaldehyde dimethyl acetal and catalytic amount of *p*-toluenesulfonic acid. The mixture was stirred for 15 min at room temperature. After removal of the solvent under reduced pressure, the residue was subjected to flash column chromatography to yield white solid **13b** as a diastereomeric mixture (71 : 29). Yield = 55%; R_f = 0.19 (EtOAc : Hexane = 4 : 1); ^{1}H NMR (500 MHz, $CDCl_3$) δ [8.28 (s) : 8.23 (s) = 1.37 : 0.55, total 2H], [7.42 (d, *J* = 8.8 Hz) : 7.31 (d, *J* = 8.8 Hz) = 1.46 : 0.60, total 2H], 6.91–6.89 (m, 2H), [6.14 (s) : 5.92 (s) = 0.29 : 0.71, total 1H], [5.54 (d, *J* = 8.3 Hz) : 5.32 (d, *J* = 7.3 Hz) = 0.73: 0.28, total 1H], [4.90–4.69 (m), 4.47–4.38 (m), total 5H], 4.01-3.96 (m, 1H), 3.81 (s, 3H), 3.17 (s, 6H), 2.19 (s, 3H); LRMS (ESI) *m/z* calculated for $C_{22}H_{26}N_6O_4$ $[M+H]^+$: 439.21; found: 438.99.

Synthesis of dimethyl acetal 14b. To a stirred solution of **12b** (3 mg, 0.0094 mmol) in acetone was added excess amount of 2,2-dimethoxypropane and catalytic amount of *p*-toluenesulfonic acid. The mixture was stirred overnight at room temperature. After removal of the solvent under reduced pressure, the

residue was subjected to preparative thin layer chromatography (TLC) to yield **14b** as a white solid. Yield = 85%; $[\alpha]_D^{24}$ = –3.51 (c = 0.10, $CHCl_3$); R_f= 0.27 (EtOAc : Hexane = 4 : 1); ^{1}H NMR (500 MHz, $CDCl_3$) δ 8.17 (s, 2H), 5.18 (d, *J* = 9.0 Hz, 1H), 4.88 (d, *J* = 14.9 Hz, 1H), 4.68–4.65 (m, 2H), 4.44–4.41 (m, 1H), 4.36 (dd, *J* = 9.2, 3.1 Hz, 1H), 3.91 (dd, *J* = 12.5, 4.2 Hz, 1H) 3.15 (s, 6H), 2.13 (s, 3H), 1.53 (s, 3H), 1.36 (s, 3H); ^{13}C NMR (125 MHz, $CDCl_3$) δ 157.1, 136.9, 127.7, 115.5, 109.5, 81.8, 75.9, 64.2, 62.1, 53.7, 37.4, 27.4, 26.8, 9.98, 9.97; LRMS (ESI) *m/z* calculated for $C_{17}H_{24}N_6O_3$ $[M+H]^+$: 361.20; found: 360.89.

Synthesis of diacetate 15b and 15h. To a stirred solution of **12b** or **12h** (5mg, 0.0156 mmol) in anhydrous DCM, triethylamine (5 equiv.), acetic anhydride (3 equiv.) and catalytic amount of 4-(dimethylamino)pyridine were added. The mixture was stirred for an hour and purified by preparative thin layer chromatography (TLC) to yield **15b** or **15h**.

Compound **15b**: White solid; Yield = 95%; $[\alpha]_D^{25}$ = –54.49 (c = 0.54, $CHCl_3$); R_f= 0.14 (EtOAc : Hexane = 4 : 1); ^{1}H NMR (500 MHz, $CDCl_3$) δ 8.35 (s, 2H), 6.10 (d, *J* = 6.8 Hz, 1H), 5.72 (dd, *J* = 6.8, 5.4 Hz, 1H), 4.84 (d, *J* = 15.2 Hz, 1H), 4.65 (d, *J* = 15.2 Hz, 1H), 4.53–4.51 (m, 1H), 4.36–4.33 (m, 1H), 3.82 (dd, *J* = 12.7, 3.9 Hz, 1H), 3.17 (s, 6H), 2.15 (s, 3H), 2.05 (s, 3H), 2.03 (s, 3H); ^{13}C NMR (125 MHz, $CDCl_3$) δ 169.8, 162.1, 157.7, 137.1, 127.4, 116.4, 73.0, 70.7, 64.9, 62.3, 54.8, 37.3, 21.1, 20.9, 10.1; LRMS (ESI) *m/z* calculated for $C_{18}H_{24}N_6O_5$ $[M+H]^+$: 405.19; found: 404.91.

Compound **15h**: White solid; Yield = 89%; $[\alpha]_D^{24}$ = –88.34 (c = 0.47, $CHCl_3$); R_f= 0.11 (EtOAc : Hexane = 4 : 1); ^{1}H NMR (400 MHz, $CDCl_3$) δ 8.50 (s, 2H), 6.12 (d, *J* = 3.9 Hz, 1H), 5.79 (dd, *J* = 6.8, 4.1 Hz, 1H), 4.87 (d, *J* = 15.3 Hz, 1H), 4.71 (d, *J* = 15.3 Hz, 1H), 4.51–4.47 (m, 1H), 4.10 (dd, *J* = 12.5, 3.1 Hz, 1H), 3.86 (dd, *J* = 12.5, 3.5 Hz, 1H), 3.19 (s, 6H), 2.20 (s, 3H), 2.14 (s, 3H), 1.99 (s, 3H); ^{13}C NMR (100 MHz, $CDCl_3$) δ 169.5, 169.4, 162.2, 158.5, 137.2, 127.3, 115.5, 72.0, 70.9, 64.2, 62.5, 54.9, 37.3, 21.1, 21.0, 10.1; LRMS (ESI) *m/z* calculated for $C_{18}H_{24}N_6O_5$ $[M+H]^+$: 405.19; found: 404.91.

Synthesis of carbonate 16b. To a stirred solution of **12b** (13 mg, 0.0406 mmol) in anhydrous DCM was added 1,1'-carbonyldiimidazole (1.5 equiv.). The reaction mixture was stirred at room temperature for 11 h and purified by preparative thin layer chromatography (TLC) to yield **16b** as a white solid. Yield = 79%; $[\alpha]_D^{23}$ = +84.60 (c =0.37, $CHCl_3$); R_f= 0.16 (EtOAc : Hexane = 4 : 1); ^{1}H NMR (400 MHz, $CDCl_3$) δ 8.18 (s, 2H), 5.95 (d, *J* = 8.6 Hz, 1H), 5.09 (dd, *J* = 8.6, 3.1 Hz, 1H), 4.95 (d, *J* = 14.9 Hz, 1H), 4.81 (q, *J* = 3.4 Hz, 1H), 4.76 (d, J = 15.3 Hz, 1H), 4.38 (dd, *J* = 12.9, 3.1 Hz, 1H), 4.06 (dd, *J* = 12.9, 4.3 Hz, 1H), 3.19 (s, 6H), 2.23 (s, 3H); ^{13}C NMR (75 MHz, $CDCl_3$) δ 162.8, 157.1, 152.9, 137.8, 182.1, 113.8, 81.3, 77.4, 64.0, 62.4, 53.5, 37.4, 10.1 ; LRMS (ESI) *m/z* calculated for $C_{15}H_{18}N_6O_4$ $[M+H]^+$: 347.15; found: 346.90.

Synthesis of monohydroxy azido compound 17b. To a stirred solution of **16b** (5 mg, 0.0144 mmol) in anhydrous DMF was added H_2O (1 equiv.) and NaN_3 (1.1 equiv.). The reaction mixture was stirred at 110 ^oC for 22 h. The solvent was removed under the reduced pressure and the residue was subjected to preparative thin layer chromatography (TLC) to yield **17b** as white solid. Yield = 49%; $[\alpha]_D^{25}$ = +43.09 (c = 0.19, $CHCl_3$); R_f= 0.17 (EtOAc : Hexane = 4 : 1); ^{1}H NMR (400 MHz, $CDCl_3$) δ 8.37 (s, 2H), 4.92 (d, *J* = 9.0 Hz, 1H), 4.89–4.86 (m, 1H), 4.84–4.78 (m, 2H), 4.20–4.09 (m, 2H), 4.00 (dd, *J* = 9.0, 2.7 Hz, 1H), 3.20 (s, 6H), 2.24 (s, 3H); ^{13}C NMR (100 MHz, $CDCl_3$) δ 162.5, 157.8, 137.2, 128.5, 116.7, 77.4, 75.1, 67.3, 62.64, 62.57, 56.0, 37.4, 10.2; LRMS (ESI) *m/z* calculated for $C_{14}H_{19}N_9O_2$ $[M+H]^+$: 346.17; found: 345.89.

Synthesis of alkynyl bromides (S1–S4)

Sonogashira couping: To a stirred solution of aryl iodide (100 mg, 1 equiv.) in anhydrous toluene (0.5 ml), $Pd(PPh_3)_2Cl_2$ (0.03 equiv.), CuI (0.06 equiv.) and piperidine (2 equiv.) was added. After stirring the mixture for 2 min at room temperature, propargyl alcohol (1.02 equiv.) was added slowly. The final reaction mixture was stirred for an hour and diluted with diethyl ether, then filtered through a short pad of silica. After removal of the solvent under the

reduced pressure, the residue was subjected to flash column chromatography to yield cross-coupling products. **Appel reaction:** To a stirred solution of cross-coupling products (1 equiv.) and CBr_4 (1.1 equiv.) in anhydrous DCM was added a solution of PPh_3 (1.1 equiv.) in anhydrous DCM dropwise at 0 ^oC. After stirring the mixture for 2 h at 0 ^oC, the solvent was removed under the reduced pressure. The residue was diluted with diethyl ether and filtered through a short pad of silica. The filtrate was condensed under the reduced pressure and purified by flash column chromatography to yield alkynyl bromides **S1**–**S4**.

3-bromo-1-(3-methoxyphenyl)-1-propyne (S1): Prepared from 1-iodo-3-methoxybenzene; Yellow liquid; Yield over two steps = 63%; R_f = 0.68 (EtOAc : Hexane = 1 : 8); ^{1}H NMR (500 MHz, $CDCl_3$) δ 7.26–7.21 (m, 1H), 7.04 (d, *J* = 7.8 Hz, 1H), 6.97 (d, *J* = 1.0 Hz, 1H), 6.90–6.88 (m, 1H), 4.16 (s, 2H), 3.79 (s, 3H).

3-bromo-1-(4-fluorophenyl)-1-propyne (S2): Prepared from 1-fluoro-4-iodobenzene; Yellow liquid; Yield over two steps = 85%; R_f= 0.78 (EtOAc : Hexane = 1 : 8); ^{1}H NMR (500 MHz, $CDCl_3$) δ 7.44–7.31 (m, 2H), 7.03–7.00 (m, 2H), 4.15 (s, 2H); ^{13}C NMR (125 MHz, $CDCl_3$) δ 163.0 (d, *J* = 250.3 Hz), 134.1 (d, *J* = 8.4 Hz), 118.4 (d, *J* = 3.3 Hz), 115.9 (d, *J* = 22.3 Hz), 85.9, 84.2, 15.4.

3-bromo-1-(4-methoxyphenyl)-1-propyne (S3): Prepared from 1-iodo-4-methoxybenzene; Yellow liquid; Yield over two steps = 73%; R_f = 0.62 (EtOAc : Hexane = 1 : 8); ^{1}H NMR (500 MHz, $CDCl_3$) δ 7.38 (d, *J* = 8.3 Hz, 2H), 6.84 (d, *J* = 8.3 Hz, 2H), 4.17 (s, 2H), 3.80 (s, 3H).

3-bromo-1-(2-thienyl)-1-propyne (S4): Prepared from 2-iodothiophene; Yellow liquid; Yield over two steps = 95%; R_f= 0.71 (EtOAc : Hexane = 1 : 8); ^{1}H NMR (500 MHz, $CDCl_3$) δ 7.28–7.27 (m, 1H), 7.23 (s, 1H), 6.97 (s, 1H), 4.17 (s, 2H).

Synthesis of 4-methyl-*N*-(3-phenylprop-2-yn-1-yl)benzenesulfonamide (S5). To a suspension of anhydrous K_2CO_3 (260.0 mg, 1 equiv.) in anhydrous acetonitrile, *p*-toluenesulfonamide (4 equiv.) and 3-chloro-1-phenyl-1-propyne (1 equiv.) was added. After stirring the mixture for 2 h at 80 ^oC, the solvent was removed under the reduced pressure and the residue was partitioned between diethyl ether and water. The aqueous layer was extracted with diethyl ether and the combined organic layer was dried over anhydrous Na_2SO_4. The filtrate was condensed under the reduced pressure and subjected to flash column chromatograph to yield **S5** as a slightly yellow solid. Yield = 37%; R_f = 0.27 (EtOAc : Hexane = 1 : 4); ^1H NMR (500 MHz, $CDCl_3$) δ 7.82 (d, J = 8.1 Hz, 2H), 7.28–7.23 (m, 5H), 7.13 (d, J = 7.1 Hz, 2H), 4.78 (bs, 1H), 4.07 (d, J = 5.9 Hz, 2H), 2.35 (s, 3H).

Chapter 2. Discovery of Small Molecule Inhibitors of Lin28–*let-7* Interactions Through the Development of a FRET-based High-Throughput Screening

2.1. Introduction

MicroRNAs (miRNAs) are small non-coding RNAs that regulate gene expression by functioning as guide molecules in RNA silencing.[1] They target most protein-coding transcript, thereby being involved in every biological phenomena in animals. miRNA biogenesis is tightly regulated temporally and spatially, and their dysregulation is associated with many human diseases including cancer.[1]

In the nucleus miRNA genes are transcribed by RNA polymerase II as a long primary trancript (pri-miRNA) containing a terminal loop structure and mature miRNA sequence in the stem region. Pri-miRNA is then processed by microprocessor comprising RNase III Drosha and DGCR8. The resulting precursor microRNA (pre-miRNA) is exported into the cytoplasm by exportin 5.[1,2] In the cytoplasm pre-miRNA is cleaved by RNase III Dicer near the terminal loop to release a mature miRNA duplex. The duplex is loaded onto an Ago protein to form RNA-induced silencing complex (RISC), and the passenger strand is removed.[1] The guide strand functions by base pairing with its target mRNAs usually at 3' untranslated region (UTR), and AGO proteins functions by recruiting factors that induce translational repression and mRNA decay.[1,2]

The miRNAs from the *let-7* family were among the first to be identified and were found to regulate development and proliferation. Mature *let-7* is absent or

present only in low amounts in stem cells but strongly induced upon differentiation, and its level is stably maintained in somatic cells.[3,4] In addition, *let-7* miRNAs are well known for its tumor suppressor function by targeting multiple oncoproteins such as Ras, c-Myc and HMGA2. Mature *let-7* is down-regulated in many cancer cells, and the growth of tumor was suppressed when *let-7* miRNAs were delivered into cancer cells *in vitro* and *in vivo*.[5,6] Interestingly, levels of pri- and/or pre-*let-7* are not affected even when mature *let-7* is down-regulated in stem cells and cancer cells, indicating the post-transcriptional regulation of *let-7* maturation.[3]

It was found that RNA binding protein Lin28 selectively blocks the *let-7* biogenesis at the post-transcriptional level.[7,8] Mammals have two Lin28 paralogs, Lin28A and Lin28B, with different physiological expression patterns but similar behavior *in vitro*. The effect of Lin28B on pri-*let-7* is more pronounced because of its nuclear localization signal.[9,10] Lin28 proteins bind terminal loop, or pre-element (preE) of pri-*let-7* in the nucleus and inhibit its processing by Drosha. In the cytoplasm Lin28 binds pre-*let-7* and block the processing by Dicer. Furthermore, Lin28 recruits terminal uridyl transferases (TUTs) that add uridines to the 3' end of pre-*let-7*. The uridylated RNA is degraded by a nuclease, Dis3l2.[11,12]

Cellular level of Lin28 is inversely related to the level of mature *let-7* miRNA. Lin28 is highly expressed in undifferentiated embryonic stem cells and represents part of a pluripotency network.[13] Lin28 is also overexpressed in a wide range of cancer cells resulting in *let-7* depletion. When siLin28 was introduced into those cancer cells, the *let-7* level was restored and tumor

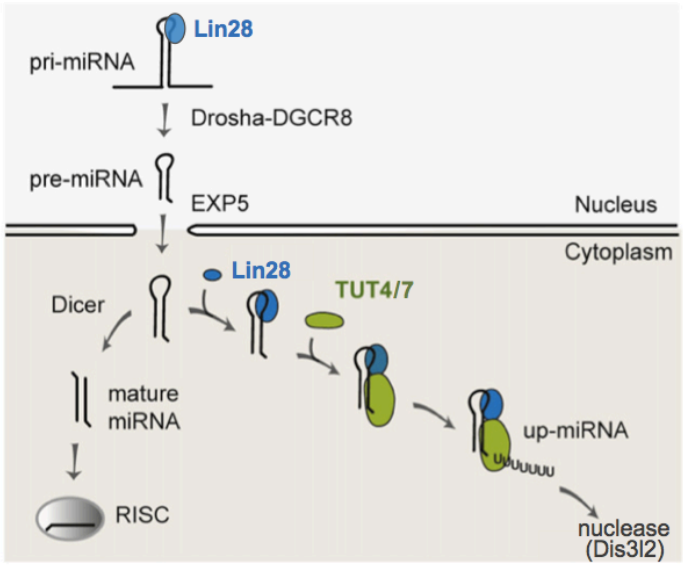

Figure 2.1. Regulation of *let-7* biogensis by Drosha, Dicer, and Lin28 proteins. Figure reproduced from [11].

growth was blocked *in vitro* and *in vivo*. Interestingly, a growing body of evidences suggests that Lin28 plays an important role in the formation of cancer stem cells, contributing to tumor resistance, recurrence, and metastasis of cancer.[14]

Small molecule inhibitors of the Lin28–*let-7* interactions would provide a promising approach to study miRNA biogenesis and stem cell development with temporal precision. Moreover, those inhibitors can be therapeutic agents against cancers with novel mode of actions. I aimed to identify cell permeable small molecule inhibitors of the protein–RNA interaction through the construction of a high-throughput screening system. Since the transcription levels of the *let-7* precursors do not change significantly,[3] antagonizing Lin28 action is the best way to restore mature *let-7* levels.

In this study, a simple assay based on Förster resonance energy transfer (FRET) was constructed to detect the Lin28–*let-7* interaction in a high-throughput manner. I sought to label Lin28 and *let-7* with FRET donor and acceptor at the predesigned position in order to increase the FRET efficiency, which resulted in the establishment of accurate and reliable assay. The assay was applied to high-throughput screening of small molecule library leading to the discovery of flavones as inhibitors of Lin28–*let-7* interactions.

2.2. Results and Discussion

2.2.1. A design strategy for FRET-based binding assay to detect Lin28–*let-7* interaction

Protein–RNA interactions are probed using various biochemical techniques, the most common of which is enzyme-linked immunosorbent assay (ELISA) and electrophoretic mobility shift assay (EMSA). These assays can be performed easily with common laboratory equipments. However, they are heterogeneous multiple-step assays requiring several addition-washing steps or time-consuming electrophoresis. Therefore, it is important to develop a new high-throughput assay to identify inhibitors of a protein–RNA interaction from the large number of small molecule libraries. The new assay should be simple, fast and accurate. Moreover, it should be a one-step homogenous process to prevent RNase contamination that may arise from multiple experimental steps.

I designed a FRET-based interaction assay to fulfill above requirements. FRET stands for energy transfer between two light-sensitive molecules. A fluorescent molecule (FRET donor) in its electronically excited state can

transfer energy to another chromophore (FRET acceptor) through a non-radiative mechanism when they are in close proximity (<100 Å). Because FRET efficiency is inversely proportional to the sixth power of the distance between donor and acceptor, FRET signal is sensitive to small changes in distance. As a result, FRET is a powerful tool to study biomolecular interactions.

Each interaction partners should be labeled with light-sensitive FRET donor–acceptor pairs to construct an interaction assay. Fluorescent proteins, organic fluorophores or quencher molecules are possible candidates for protein and nucleic acid labeling. In order to establish a precise assay with high signal-to-background ratio and maximized measurement window, it is highly desirable to label the biomolecules at specific positions without hampering their interactions to give high FRET efficiency. Current approaches in designing FRET assays largely rely on fluorescent proteins (e.g. CFP–YFP pair) which are labeled at the protein terminals only. Therefore, it is impossible to control the FRET efficiency and in some cases, FRET is even not observed. Assays based on fluorescently labeled anti-epitope tag antibodies suffer from similar problems. Alternatively, proteins can be directly labeled with organic fluorophores or quenchers using amine, acid or thiol functionalities. However, biomoleular interactions can be disrupted due to the random chemical labeling. To overcome these limitations, I adopted a site-specific chemical labeling strategy using unnatural amino acid mutagenesis and bioorthogonal chemistry to obtain precisely designed fluorescent Lin28A.

Labeling sites for protein and miRNA were selected based on the crystal structure of the Lin28A–*let-7* complex. Lin28A contains two folded regions,

the cold shock domain (CSD) and the tandem CCHC-type zinc finger domain, connected by a positively charged linker of ~15 amino acids.[10] Both domains bind the terminal loop (also termed pre-element, preE) of *let-7* miRNA at discrete sequences (Figure 2.2). The CSD insert into the loop of the preE structure at one end, while CCHCx2 zinc finger recognizes a GGAG motif at the other end of preE.[10] The linker between the CSD and CCHCx2 is flexible and lacks secondary structure. Deletion of up to 9 amino acids (127–135) in the linker region supports binding to let-7 miRNAs indicating that linker regions can be mutated without compromising binding affinity or specificity.[10] In the case of *let-7*, isolated preE segment, containing none of the mature-region nucleotides, is sufficient for selective high-affinity binding to Lin28.[10] *Let-7* family members bind Lin28 with the same binding mode through the interaction or key nucleobases, even though their preE sequences and predicted secondary structures are somewhat different. Therefore, it is reasonable that any member of the *let-7* miRNA family can be used and preE sequence only is sufficient for binding assay development.

I found from the crystal structure of the protein–miRNA complex that Lin28 linker region and *let-7* Dicer cleavage site, or terminus of the preE sequence, are located close to each other. Therefore, I planned to selectively label a Lin28A linker residue with Cy3 fluorophore as a FRET donor. Isolated preE sequence from *let-7a-1* will be used by labeling its 3' terminus with BHQ-2 quencher that serves as a FRET acceptor. Cy3–BHQ-2 is a highly efficient donor–acceptor pair with maximal spectral overlap between Cy3 fluorescence emission and BHQ-2 absorption. In fact, a double-strand oligonucleotide dual-labeled with Cy3 and BHQ-2 show the FRET efficiency

of 97%.[15] When the Lin28A-Cy3 and preE-*let-7a-1*-BHQ-2 bind, the fluorescence from Cy3 is quenched. In the presence of inhibitors that disrupt the protein–miRNA interaction, Cy3 fluorescence would be recovered, resulting in a turn-on binding assay. High FRET efficiency and large signal window is expected due to the site-specific chemical labeling strategy.

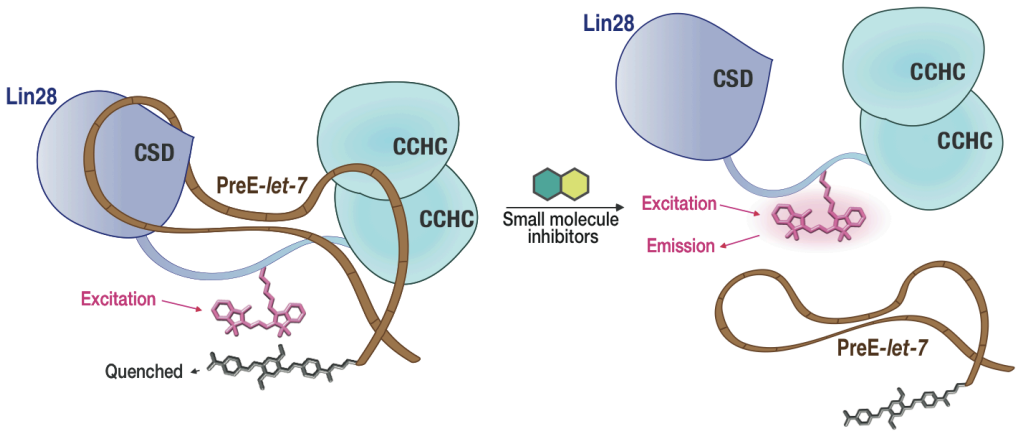

Figure 2.2. Schematic model of the Lin28–*let-7* binding and a design strategy to construct a FRET-based turn-on binding assay.

2.2.2. Site-specific fluorescent labeling of Lin28A through unnatural amino acid mutagenesis

I sought to label Lin28A and preE-*let-7a-1* at a pre-designed position. In the case of oligoribonucleotides, their synthetic methods including chemical labeling schemes are well established, and they are normally commercially available. PreE-*let-7a-1* sequence was selected to include both binding sites for Lin28 and to give the same predicted secondary loop structure (mfold web server[16]) as that of full-length pre-*let-7* to ensure efficient and selective binding toward the protein partner. The sequence of the RNA is presented at

the ‘Experimental Section’.

Next, Cy3 labeling of Lin28A linker residues was sought. Lin28A contains many lysine and cysteine residues, some of which have key roles in RNA binding or form important protein structural motif. As a result, conventional chemical labeling using *N*-hydroxysuccinimide or maleimide functionality is not appropriate. I therefore tried to introduce unnatural amino acids into Lin28A linker and label it with Cy3 using bioorthogonal chemistry. Among several bioorthognal chemistries, copper-free [3+2] cycloadditon between azide and cyclooctynes was selected due to its selectivity and high reaction rate in mild reaction conditions.

4-Azido-L-phenylalanine (AzF) can be incorporated into proteins in response to amber (UAG) stop codon.[17] A plasmid (pEVOL-AzF) encoding orthogonal $tRNA_{CUA}$ and aminoacyl tRNA synthetase (aaRS) for AzF[18] is cotransformed with a Lin28A vector containing amber mutation at the designated residue into *E. coli* to express a mutant protein. First, three different N-terminal 6xHis-tagged Lin28A linker mutants (K131AzF, R133AzF, K135AzF) were expressed and purified by Nickel affinity chromatography. However, only small amount of full length AzF mutant was obtained, while majority of the protein population was the truncated form of Lin28A by the action of amber codon as a stop signal (Figure S2.1). Competition between amber suppression and translational termination has been a major hurdle in unnatural amino acid mutagenesis. A simple solution to the problem is to attach the purification tag at the C-terminus of a protein. In the case of Lin28A, however, it was not possible to obtain C-terminal 6xHis-tagged functional protein despite several attempts. In order to produce Lin28A

AzF mutants in large amount through a single affinity chromatography step, I optimized cell culture conditions using Lin28A K135AzF as a model mutant.

Release factor 1 (RF1) is responsible for amber codon-mediate termination in *E. coli*. It is assumed that exogenously added orthogonal $tRNA_{CUA}$ and RF1 compete for binding to mRNA at the ribosome. In addition elongation factor Tu (EF-Tu) has a limited capability to incorporate bulky unnatural amino acid. There have been several attempts to increase the amber suppression efficiency such as RF1 knock-out or EF-Tu engineering.[19] However, there is not a general rule to increase the amber suppression compared to termination in normal protein expression strains such as BL21(DE3). Therefore, I tried protein expression in *E. coli* with various culture conditions for maximized read-through of an amber codon.

Temperature greatly affected the amber suppression. Higher temperature was advantageous for increased ratio of full length to truncated protein, mainly through the substantial decrease in the translation termination rather than increase in the read-through (Figure 2.3a). The culture temperature was set to 37 °C, and the effects of other components were investigated. The concentration of arabinose for aaRS induction and IPTG for Lin28A induction had minor effects at the ranges we tested (Figure S2.2a). It was somewhat beneficial to induce aaRS prior to Lin28A to ensure AzF-charged orthogonal $tRNA_{CUA}$ is present in the medium at the start of Lin28A expression (Figure S2.2b). By combining the optimized conditions, it was possible to produce Lin28A K135AzF mutant with substantially enhanced full length to truncated protein ratio (Figure S2.3a).

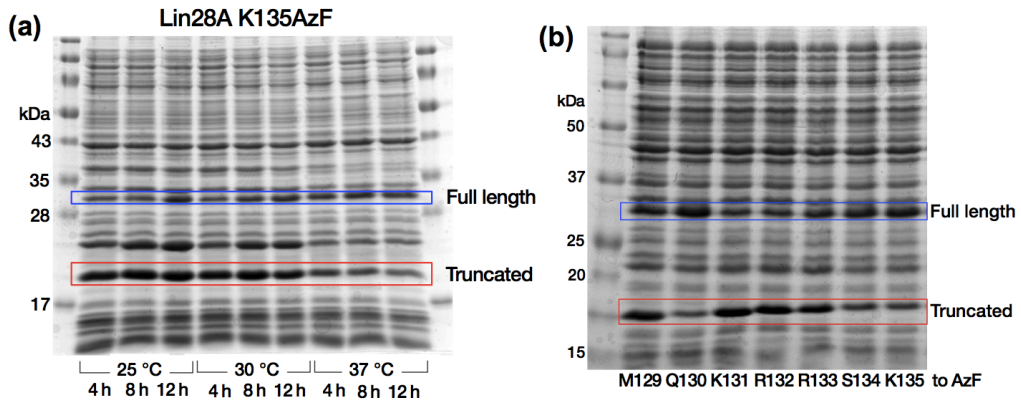

Figure 2.3. Optimization of the Lin28A AzF mutant expression. (a) The effect of protein induction temperature and time on the ratio of full length to truncated Lin28A K135AzF. (b) Expression of seven Lin28A AzF mutants with the optimized conditions.

I produced six additional Lin28A linker mutants using optimized conditions to find the best Cy3 labeling site for assay development (Figure 2.3b). However, only three of the mutants (Q130AzF, S134AzF, K135AzF) were produced in good full-length ratio, while the other mutants still yielded low amount of AzF-incorporated proteins. I further sought to increase the full-length protein yield by adjusting the mRNA context of the amber codon. In *E. coli* there exists a bias in the mRNA sequences several nucleotides before and after stop codons, indicating that termination efficiency is closely related to the mRNA context of the stop codon. Indeed, endogenous amber suppressor from *E. coli* CDJ64 exhibited substantially different read-through efficiency depending on mRNA context around the amber codon.[20] Accordingly it was expected that amber suppression efficiency would also be dependent on mRNA context when the exogenous orthogonal $tRNA_{CUA}$ was employed for unnatural amino acid insertion. However, there is no information about the preferred mRNA sequences before and after the amber codon. Therefore, part

of the information about the nucleotide preference was extracted from the above scanning mutation experiment. (Figure 2.3b, Figure S2.3b) I aimed to enhance the production of full-length Lin28A R133AzF mutant, and silently mutated two nucleotides before and after the amber codon based on the above information. As a result, it was possible to obtain the R133AzF mutant with improved full-length protein ratio. (Figure S2.3b)

I determined to use the protein mixture containing both the full-length AzF mutant and truncated form because it is easily obtained through a simple metal affinity chromatography. Truncated protein contains CSD only, the affinity of which toward preE-*let-7* is much weaker than the full-length protein.[10] Even when the binding event occurs between CSD-containing truncated form and miRNA, the unlabeled CSD would not contribute to the fluorescence signal.

I then proceeded to the fluorescent labeling of the four mutants (Q130AzF, R133AzF, S134AzF, K135AzF) using DIBO(dibenzocyclooctyne)-Alexa555 or BCN(bicyclononyne)-Cy3 (Scheme S2.1). Copper-free strain-promoted cycloaddition was used because it is quite an efficient and mild transformation for biomolecule labeling.[21] First, crude cell lysates from three mutants (Q130AzF, S134AzF, K135AzF) were labeled with the dyes. As shown in Figure 2.4, labeling with the BCN-Cy3 is much faster compared to DIBO-Alexa555, considering the fact that Alexa555 conjugates is generally more fluorescent than Cy3 conjugates. In addition, the reaction of BCN is highly selective, while that of DIBO yields nonspecific fluorescent signals of comparable intensity to the Lin28A signal. Moreover, BCN did not label the truncated protein while DIBO did. Finally, BCN-Cy3 was selected

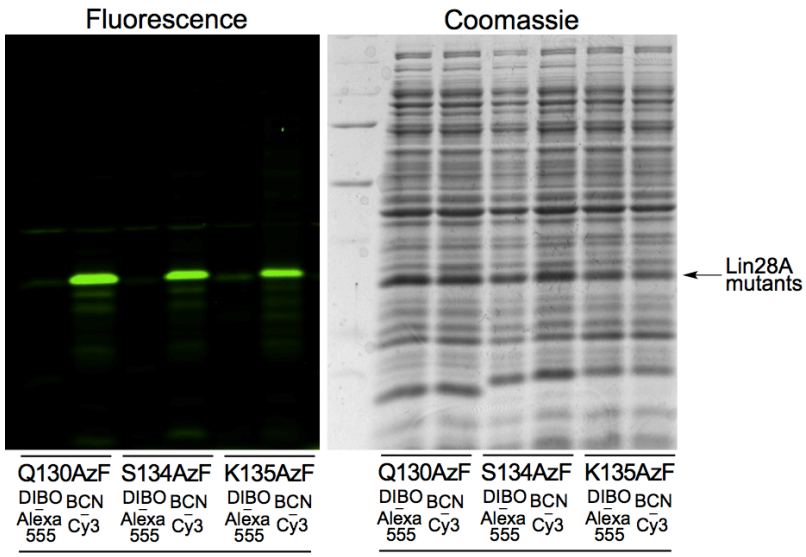

Figure 2.4. Labeling of crude lysates from three Lin28A AzF mutants using DIBO-Alexa555 or BCN-Cy3. Diluted lysates were incubated with 2.5 μM dyes in phosphate-buffered saline (PBS) for 1.5 h at room temperature. The reactions were stopped by adding excess AzF. The mixture was analyzed by SDS-PAGE followed by fluorescence gel scanning or coomassie staining.

for further Lin28A labeling.

Next, I labeled the purified proteins by on-bead labeling method, at which metal affinity bead-attached Lin28A mutants are incubate with BCN-Cy3 in a buffered solution. When the four mutant proteins were reacted at the same conditions, two of them (R133AzF, S134AzF) were labeled with higher efficiency than the other mutants (Q130AzF, K135AzF). In all cases, the reaction was selective leading to the single labeling of Lin28A at the azide functionality. Fluorescence purity of the product was high enough to be used for reliable binding assays. By modifying simple parameters such as BCN-Cy3 concentration, buffer species, reaction temperature and time, it was possible to label Lin28A S134AzF mutant with 80% yield (Figure 2.5b).

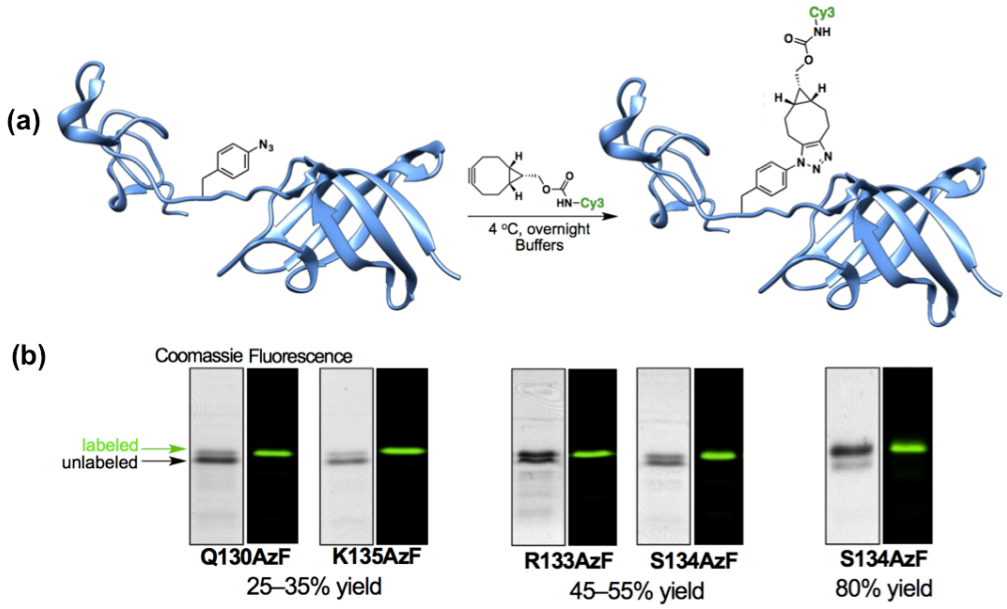

Figure 2.5. Site-specific labeling of Lin28A AzF mutants with BCN-Cy3. (a) Reaction scheme to produce Lin28A-Cy3. (b) Purified Lin28A-Cy3 was analyzed through SDS-PAGE. Labeling yields were determined by quantifying the band intensities of the coomassie-stained gels.

2.2.3. Validation of the binding assay and application to high-throughput screening of small molecule library

Binding event between Lin28A-Cy3 and preE-*let-7a-1*-BHQ-2 was detected by adding the RNA solution into the protein solutions pre-dispensed in the screening plate and measuring the Cy3 fluorescence. Simple mix-and-read format makes it possible to conduct the binding assay in a high-throughput manner. When Lin28A-Cy3 and preE-*let-7a-1*-BHQ-2 were bound fluorescence signal decreased sharply, but in the presence of excess unlabeled preE-*let-7a-1* as a competitor, the Cy3 signal was substantially recovered (Figure 2.6a). Quenching was dependent on the preE-*let-7a-1*-BHQ-2 concentration, and up to 85% of the Cy3 fluorescence was diminished at

higher miRNA concentrations (Figure 2.6b). High quenching efficiency arises from our rational design strategy to place the FRET donor and quencher in close proximity, which allows the precise determination of the protein–miRNA binding. Site-specific unnatural amino acid insertion and labeling might be superior alternatives to the use of fluorescent fusion proteins or fluorescent antibodies. Competition by unlabeled preE-*let-7a-1* was clearly observed in a dose-dependent manner, while yeast tRNA could not effectively compete out the preE-*let-7a-1*-BHQ-2 bound to Lin28A even at high concentrations (Figure 2.6c). These results indicate that the assay detects specific Lin28a–*let-7a-1* interaction.

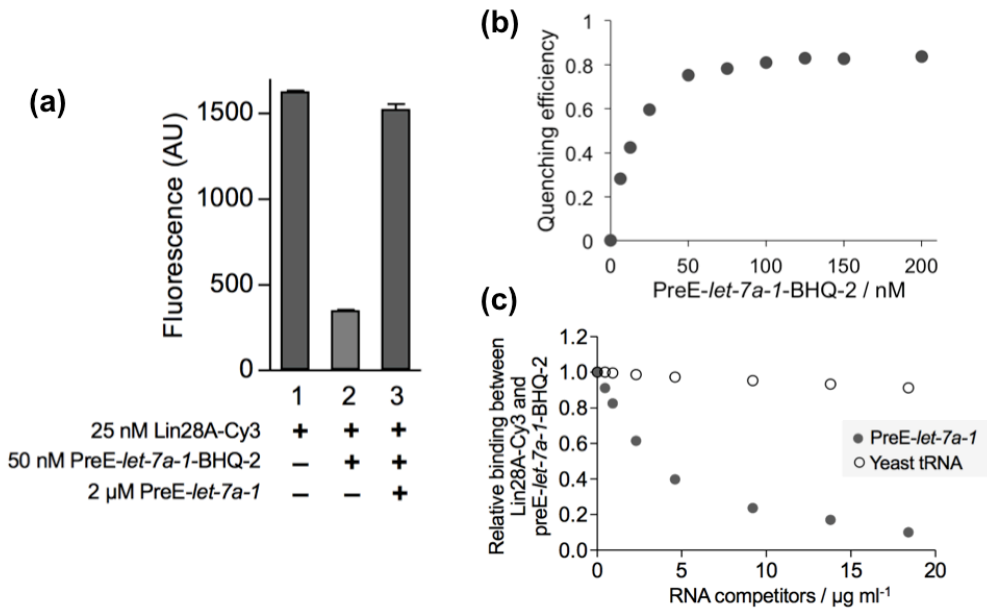

Figure 2.6. Validation of the binding assay. (a) Competition by excess unlabeled preE-*let-7a-1* restores the fluorescence signal. (b) Dependence of the quenching efficiency on the preE-*let-7a-1*-BHQ-2 concentration. 25 nM Lin28A-Cy3 was used. (c) Competition by unlabeled preE-*let-7a-1* or yeast tRNA to check the presence of nonspecific interactions. 25 nM Lin28A-Cy3 and 50 nM preE-*let-7a-1*-BHQ-2 were used.

The absorption spectra of Lin28A-Cy3, preE-*let-7a-1*-BHQ-2, and their mixture were measured. The spectrum of the mixture was the sum of the each spectrum, indicating that fluorescence turn-off in our assay is mediated through the FRET mechanism rather than contact quenching. FRET mechanism is preferred over contact quenching mechanism because in the latter case static interaction between dye and quencher results in enhancement of apparent binding affinity.[15]

The binding assay was conducted using a 96-well plate in a high-throughput setting. Z' factor was determined from forty positive controls and forty negative controls to access the quality of the screening system. Samples without preE-*let-7a-1*-BHQ-2 served as positive controls, and samples with preE-*let-7a-1*-BHQ-2 served as negative controls. Average Z' factor was calculated to be 0.94. Considering the fact that assays with Z' factors larger than 0.75 is regarded excellent, our assay is highly robust, reliable and close to an ideal screening system (Figure 2.7a).

The FRET-based high-throughput screening system was applied to identify inhibitors of the Lin28–*let-7* interaction from a small set of bioactive compounds. Several compounds showed recovery in the normalized fluorescence when added to the Lin28A-Cy3–preE-*let-7a-1*-BHQ-2 mixture, and they were validated through an independent assay, electrophoretic mobility shift assay (EMSA). EMSA is based on the difference in the electrophoretic mobility of RNA and RNA–Protein complex. Mobility of the RNA is greatly retarded when it is bound to a protein due to the increased mass to charge ratio. It is possible to directly detect the free RNA and protein-bound RNA after gel electrophoresis using the EMSA technique. Hit

compounds would increase the ratio of RNA band to protein–RNA complex band.

EMSA was conducted in the presence of increasing amount of recombinant native Lin28A (rLin28A) with preE-*let-7a-1* labeled with Cy5 at 5'-terminus (Cy5-preE-*let-7a-1*) for visualization. As shown in figure 2.7b, Lin28A and *let-7a-1* form a complex that is clearly differentiated by gel electrophoresis. Non-specific interaction between BSA and RNA was not observed (figure 2.7b, lane 1). rLin28A–Cy5-preE-*let-7a-1* interaction was clearly abolished in the presence of unlabeled preE-*let-7a-1* as an inhibitor (figure 2.7c). Hit compounds would behave the same way as unlabeled preE-*let-7a-1* in EMSA.

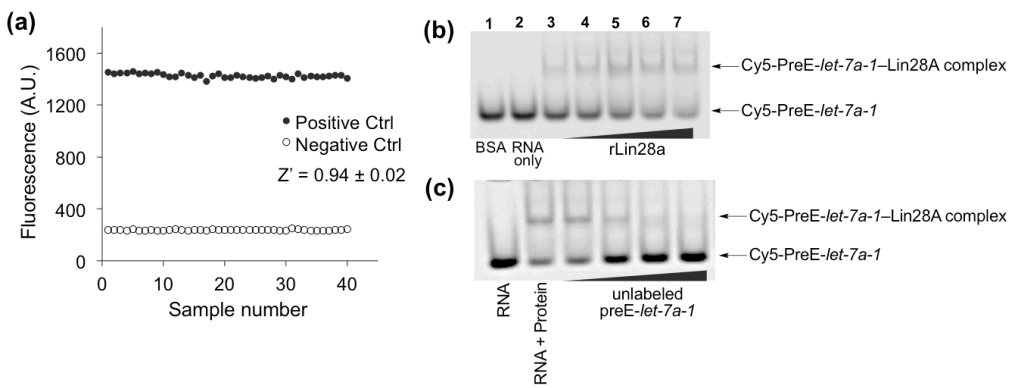

Figure 2.7. Application of the binding assay to high-throughput screening and EMSA for hit confirmation. (a) Determination of the Z' factor using 40 positive and negative controls. (b) Electrophoretic mobility shift assay to detect Lin28A–*let-7a-1* interaction. 25 nM RNA was incubated with 200 nM BSA (lane 1) or 0–200 nM rLin28A (lane 2–7). (c) Electrophoretic mobility shift assay in the presence of unlabeled preE-*let-7a-1*. 25 nM Cy5-preE-*let-7a-1*, 100 nM rLin28A and 0–2000 nM preE-*let-7a-1* were employed.

Two of the hits identified by the high-throughput assay were autrintricarboxylic aicd (ATA) and suramin, which are known as inhibitors of

several protein-nucleic acid interactions. These compounds were truly able to inhibit Lin28–*let-7* interaction as revealed by EMSA (Figure S2.4), highlighting the reliability of my screening system.

2.2.4. Discovery of flavones as inhibitors of Lin28–*let-7* interactions and their mode of action

Two flavones (luteolin and myricetin) were identified as another class of inhibitors through the high-throughput screening. They showed clear antagonistic effect against the protein–RNA interaction with IC_{50} of low micromolar ranges in EMSA (Figure 2.8). A variety of flavones are found in nature, and they are well known for various biological activities. With the purpose of finding new compounds with enhanced activity and selectivity, I performed structure-activity relationship studies of the natural flavones against Lin28A–*let-7a-1* interaction using EMSA (Figure S2.5). The results are summarized in table 2.1. Clear structure-activity relationship pattern was observed from the compounds tested. For example, hydroxyl group at R^1 was indispensible for inhibitory activity (myricetin vs. rhamnetin). R^2 position

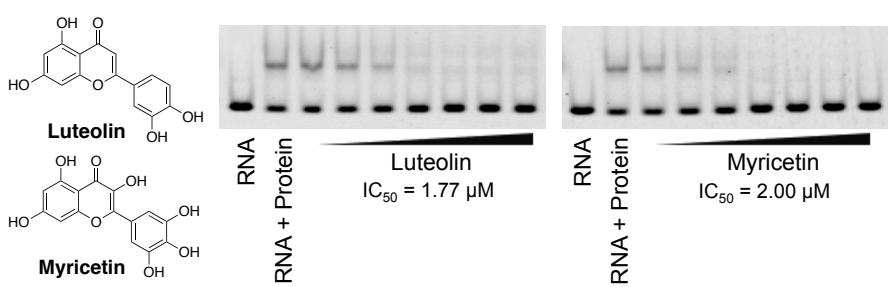

Figure 2.8. Luteolin and myricetin as inhibitors of the Lin28A–*let-7a-1* interactions. EMSA was performed as described in the 'Experimental Section' with 0–20 μM of compounds.

Table 2.1. Structure-activity relationship of selected flavones against Lin28A–*let-7a-1* and Lin28B–*let-7a-1* interaction determined by EMSA.

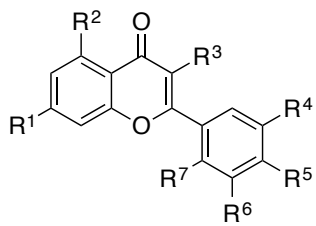

Compound	R^1	R^2	R^3	R^4	R^5	R^6	R^7	$IC_{50\ Lin28A}$ (μM)	$IC_{50\ Lin28B}$ (μM)
Myricetin	OH	OH	OH	OH	OH	OH	H	2.00	4.14
Quercetin	OH	OH	OH	OH	OH	H	H	1.96	2.53
Isorhamnetin	OH	OH	OH	OMe	OH	H	H	Not Active	N.D.
Morin	OH	OH	OH	H	OH	H	OH	>100	>100
Luteolin	OH	OH	H	OH	OH	H	H	1.67	2.97
Diosmetin	OH	OH	H	OMe	OH	H	H	Not Active	N.D.
Apigenin	OH	OH	H	H	OH	H	H	Not Active	N.D.
Fisetin	OH	H	OH	OH	OH	H	H	1.40	N.D.
Rhamnetin	OMe	OH	OH	OH	OH	OH	H	Not Active	N.D.

Not Active (>80% binding at all conc. tested)
N.D. (not determined)

may be further modified because fisetin was active in the absence of R^2 hydroxyl group (fisetin vs. quercetin). The same applies to R^3 hydroxyl group. R^3 position may be changed to other functionalities (luteolin vs. quercetin). Presence of vicinal diols at the *para*- and *meta*-position of the phenyl ring seems to be important for inhibitory effect of flavones (quercetin vs. isorhamnetin; quercetin vs. morin; luteolin vs. diosmetin; luteolin vs. apigenin). On the basis of these relationships, compounds with improved activity, selectivity and physical properties could be designed and synthesized.

Given the high sequence homology and structural similarity between Lin28A and Lin28B, the inhibitory effect of the flavones against Lin28B–*let-7* interaction was also assessed through EMSA using rLin28B and Cy5-preE-*let-*

7a-1 as a probe. It is interesting that inhibitors of the Lin28A–*let-7* interaction are also inhibitors of the Lin28B–*let-7* interaction with similar inhibitory activities (table 2.1 and figure 2.9). Many cancer cells appear to predominantly express either Lin28A or Lin28B. Therefore, inhibitors against both Lin28A–*let-7* and Lin28B–*let-7* interactions are highly desirable to cover wide array of cancers.[13]

There are twelve human *let-7* family members and they all bind Lin28 with almost identical mode.[10] The ideal inhibitors should disrupt interactions of Lin28 with all *let-7* family members for fast and substantial increase in the cellular mature *let-7* levels. I found that luteolin inhibits the interaction between Lin28A and *let-7g* with similar inhibitory activity to *let-7a-1*. Therefore, hydroxyflavone cores might be a good starting point for designing inhibitors of the important therapeutic target, Lin28–*let-7* interaction.

Biophysical studies were conducted to elucidate the inhibitory mechanism of the flavones. Biacore analysis indicated that inhibitors clearly bind to the

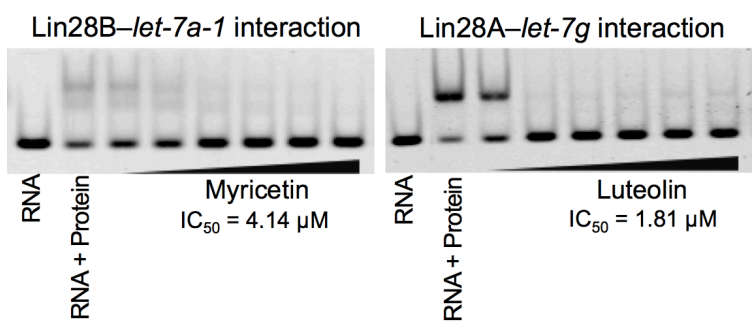

Figure 2.9. Inhibitory activity of flavones against Lin28B–*let-7a-1* interaction and Lin28A–*let-7g* interaction.

Lin28A protein, while compounds without inhibitory effect did not show any specific binding to the protein. Slow-on and slow-off binding event was observed for all inhibitors investigated (luteolin, fisetin, quercetin and myricetin) (Figure S2.6). From these data I concluded that flavones exert their inhibitory effect primarily through the specific binding to Lin28 proteins.

2.3. Conclusion

RNA is emerging as a viable target for small molecules drugs beyond the conventional antibiotics-targeted bacterial rRNA, as the understating of RNA tertiary structures is improved and the number of RNA-binding chemical entities is increased. At the same time protein–RNA interactions, which were regarded undruggable, is increasingly recognized as an important class of potential drug targets. However, there have been only a few reports regarding small molecule modulators of protein–RNA interactions, the majority of which are targeting HIV tat protein.

In this study I constructed a FRET-based high throughput assay to identify inhibitors of Lin28–*let-7* interaction, a type of protein–miRNA interaction. The assay was highly robust and reliable through the novel design strategy employing site-specific protein labeling by unnatural amino acid mutagenesis. I identified four natural flavones as inhibitors of the oncogenic Lin28–*let-7* interaction. The inhibition was mediated by the specific binding between Lin28 and inhibitors. Based on the structure-inhibitory activity relationship study, it would be possible to design novel inhibitors of Lin28–*let-7* interaction with enhanced activity and selectivity. In addition, our robust screening platform may be applied to the high-throughput screening of large

number of small molecule libraries to identify inhibitors with different core structures. Finally, assays development strategy employed here might be applied to construct other kinds of FRET-based high-throughput protein–nucleic acid binding screening systems.

2.4. Experimental section

Protein expression and purification. N-terminal 6xHis-tagged native human Lin28A and Lin28B were overexpressed in *E. coli* Rosetta2 (DE3) pLysS. The cells were grown to optical density at 600 nm of 0.6–0.8. Protein expression was induced with 0.5 mM IPTG overnight at 18 °C. Cell pellets were resuspended in cold lysis buffer (20 mM Tris·HCl [pH 8.0], 500 mM NaCl, 10 mM imidazole, 1x protease inhibitor cocktail, 1 mM PMSF, 1 mM DTT, 50 μM $ZnCl_2$, 10 % glycerol) and sonicated. The lysate was cleared through centrifugation followed by filtering. The filtrate was incubated with Ni-NTA agarose bead (Qiagen) for 1.5 hr at 4 °C. The bead was washed with 80 bead volumes of wash buffer A (20 mM Tris·HCl [pH 8.0], 500 mM NaCl, 20 mM imidazole, 50 μM $ZnCl_2$, 10 % glycerol), then 30 bead volumes of wash buffer B (20 mM Tris·HCl [pH 8.0], 500 mM NaCl, 50 mM imidazole, 50 μM $ZnCl_2$, 10 % glycerol). The proteins were eluted with 8 bead volumes of elution buffer (20 mM HEPES [pH 7.5], 500 mM NaCl, 100–300 mM imidazole, 10 % glycerol). Imdazole was removed using a PD-10 column (GE Healthcare) to give the protein solution in dialysis buffer (20 mM HEPES, pH 7.5, 500 mM NaCl, 10 % glycerol). The protein was aliquoted in small fractions, snap-frozen in liquid nitrogen and stored at –80 °C. Protein expression was verified through mass spectrometry and western blot analysis.

Unnatural amino acid mutagenesis. Mutant human Lin28A with unnatural amino acid was expressed in *E. coli* BL21(DE3) after codon optimization at 4 residues (R122, R133, R138, L145) for efficient protein expression. Site-directed mutagenesis was performed to introduce amber codon at the linker positions of Lin28A. *E. coli* BL21(DE3) was co-transformed with the amber mutant plasmid and pEVOL-AzF[18]. The cells were grown to optical density at 600 nm of 0.6. 1 mM or 1.5 mM azidophenylalanine (AzF) and 0.06% arabinose was added to produce AzF-charged orthogonal tRNA. After incubation for an hour at 37 °C, Lin28A expression was induced with 0.25 mM IPTG for 6 h at 37 °C. Protein purification procedure was the same as that of native Lin28.

Fluorescent labeling of Lin28A. Cleared lysate from 50 mL of AzF mutant culture was incubated with 120 μL Ni-NTA agarose bead and washed as described above. Next, The bead was washed with reaction buffer (PBS, 10% glycerol) and resuspended in 500 μL buffer. 5 nmole BCN-Cy3 was added and the mixture was incubated overnight at 4 °C. After the reaction, excess dye was removed and the bead was washed with wash buffer C (PBS, 0.05% Tween20) and wash buffer B. The protein was stored at –80 °C after elution and buffer exchange as described above.

RNA sequence. RNAs were synthesized by Bioneer. Sequences used for FRET-based binding assay, high-throughput screening, and electrophoretic mobility shift assay are as follows. PreE-*let-7a-1*: 5'-UUA GGG UCA CAC CCA CCA CUG GGA GAU AA-3'; PreE-*let-7a-1*-BHQ2: 5'-UUA GGG UCA CAC CCA CCA CUG GGA GAU AA-3'-(BHQ2); Cy5-PreE-*let-7a-1*: (Cy5)-5'-UUA GGG UCA CAC CCA CCA CUG GGA GAU AA-3'; Cy5-

PreE-*let-7g*: (Cy5)-5'-UGA GGG UCU AUG AUA CCA CCC GGU ACA GGA GAU AA-3'

FRET-based binding assays and high-throughput screening. 25 nM Cy3-Lin28A was mixed with 50 nM PreE-*let-7a-1*-BHQ2 in a binding buffer (50 mM Tris·HCl [pH 7.5], 100 mM NaCl, 10 mM β-mercaptoethanol, 1.5 % DMSO, 0.01% Tween 20, 2.6 U recombinant RNase inhibitor) in 50 μL volume. 96-well half area non-binding black plate with clear bottom (Corning #3881) was used for binding reaction and high-throughput screening. The mixture was incubated for 30–60 min at room temperature with mild shaking. Cy3 fluorescence was recorded with Synergy HT micro plate reader (BioTek) with excitation at 530/25 nm and emission at 590/35 nm. High-throughput screening was conducted at the same conditions. Reactions in the presence of 2 μM unlabeled PreE-*let-7a-1* or reactions in the absence of any RNA served as positive controls. Reactions with PreE-*let-7a-1*-BHQ-2 and DMSO served as a negative control. Fluorescence changes induced by compounds in the absence of RNA were normalized to evaluate the correct inhibitory effects.

Electrophoretic mobility shift assay (EMSA). EMSA was performed to confirm the activities of primary hit compounds and to determine IC_{50} values. Cy5-preE-*let-7a-1* and Cy5-preE-*let-7g* was used as a probe. 10 nM native rLin28A or rLin28B was incubated with 5 nM *let-7* probes and hit compounds at various concentrations in a binding buffer (50 mM Tris·HCl [pH 7.5], 100 mM NaCl, 10 mM β-mercaptoethanol, 2% DMSO, 0.01% Tween 20, 12% glycerol, 5 U recombinant RNase inhibitor). The mixture was resolved by native acrylamide gel electrophoresis and Cy5 signal was visualized using Typhoon Trio (GE healthcare).

Surface plasmon resonance analysis. The binding of hit compounds toward rLin28A was determined by surface plasmon resonance spectroscopy using a Biacore 3000 instrument (GE Healthcare). The surface carboxyl group of CM5 sensor chip was activated with a mixture of 1-ethyl-3-(3-dimethylaminopropyl)-carbodiimide and *N*-hydroxysuccinimide in flow cells 1 and 2 to generate the reactive succinimide ester on the surface of sensor chip. Human rLin28A (30 μg/ml in 10 mM sodium phosphate buffer, pH 6.5) was immobilized on the flow cell (4500 RU) via amide bond formation. The remaining succinimide ester on flow cells 1 and 2 was quenched by injecting 1 M ethanolamine·HCl (pH 8.0). 20 mM HEPES·NaOH (pH 7.4) buffer with 100 mM NaCl and 0.005% P20 was used as the running buffer throughout the immobilization process. After immobilization, various ligands were injected for 90 s at a flow rate of 30 μL/min, and dissociation from the sensor surface was monitored for 480 s at the same flow rate. 50 mM Tris·HCl (pH 8.0) containing 100 mM NaCl, 1 mM DTT, 0.005% P20 and 2% DMSO was used as the running buffer. The binding events were measured at 25 °C. Data were analyzed using the Biacore 3000 Evaluation software (GE Healthcare). Final sensorgrams were obtained by eliminating responses from flow cell 1 and the buffer-only control.

Synthesis of bicyclononyne-Cy3 (BCN-Cy3). Bicyclononyne **S1** was synthesized as previously described.[21] **S1** (1 equiv.) was dissolved in anhydrous CH_2Cl_2, then pyridine (2.5 equiv.) and 4-nitrophenyl chloroformate (1.25 equiv.) was added. After stirring overnight at room temperature, the mixture was partitioned between CH_2Cl_2 and saturated aqueous ammonium chloride solution. The organic layer was washed with brine and subjected to

flash column chromatography to give **S2**. **S2** was dissolved in *N*,*N*-dimetylformamide, then triethylamine (3 equiv.) and 2,2'-(Ethylenedioxy)bis(ethylamine) (6 equiv.) was added. The mixture was stirred at room temperature for 30 min, and partitioned between CH_2Cl_2 and 1 N NaOH. The organic layer was condensed and subjected to flash column chromatography to give **S3**. To a stirred solution of Cy3-NHS ester (1 equiv.) in acetonitrile, **S3** (1 equiv.) and diisopropylethylamine (2 equiv.) was added. The mixture was stirred for 9 h the solvent was evaporated. The crude mixture was purified by flash column chromatography to give BCN-Cy3. LRMS (ESI+) m/z calculated for $C_{46}H_{61}N_4O_5$ $[M]^+$, 749.46; Found, 749.51; Purity: 92 %.

3.5. References

[1] Ha, M.; Kim, V.N. Regulation of microRNA biogenesis. *Nat. Rev. Mol. Cell Bio.* **2014**, 15, 509–524.

[2] Huntzinger, E.; Izaurralde, E. Gene silencing by microRNAs: contributions of translational repression and mRNA decay. *Nat. Rev. Genet.* **2011**, 12, 99–110.

[3] Mayr, F.; Schutz, A.; Doge, N.; Heinemann, U. The Lin28 cold-shock domain remodels pre-let-7 microRNA. *Nucleic Acids Res.* **2012**, 40, 7492–7506.

[4] Desjardins, A.; Bouvette, J.; Legault, P. Stepwise assembly of multiple Lin28 proteins on the terminal loop of let-7 miRNA precursors. *Nucleic Acids Res.* **2014**, 42, 4615–4628.

[5] Buechner, J.; Tomte E.; Haug, B. H.; Henriksen, J. R.; Lokke, C.; Flægstad, T.; Einvik, C. Tumour-suppressor microRNAs let-7 and mir-101 target the

proto-oncogene MYCN and inhibit cell proliferation in MYCN-amplified neuroblastoma. *Brit. J. Cancer* **2011**, 105, 296–303.

[6] Trang, P.; Medina P. P.; Wiggins J.F.; Ruffino L.; Kelnar K.; Omotola, M.; Homer, R.; Brown, D.; Badaer, A.G.; Weidhaas, J.B.; Slack, F. J. Regression of murine lung tumors by the let-7 microRNA. *Oncogene* **2010**,29: 1580–1587.

[7] Viswanathan, S. R.; Daley G. Q.; Gregory, R. I. Selective blockade of MicroRNA processing by Lin28. *Science* **2008**, 320, 97–100.

[8] Piskounova, E.; Viswanathan, S. R.; Janas, M.; LaPierre, R.J.; Daley, G.Q.; Sliz, P.; Gregory, R. I. (2008) Determinants of microRNA processing inhibition by the developmentally regulated RNA-binding protein Lin28. *J. Biol. Chem.* **2008**, 283, 21310–21314.

[9] Piskounova, E.; Polytarchou, C.; Thornton, J. E.; LaPierre, R. J.; Pothoulakis, C.; Hagan, J. P.; Illiopoulos, D.; Gregory, R. I. (2011) Lin28A and Lin28B inhibit let-7 microRNA biogenesis by distinct mechanisms. *Cell* **2011**, 147, 1066–1079.

[10] Nam, Y.; Chen, C.; Gregory, R. I.; Chou, J. J.; Sliz, P. Molecular basis for interaction of let-7 microRNAs with Lin28. *Cell* **2011**, 147, 1080–1091.

[11] Heo, I.; Joo, C.; Kim, Y.-K.; Ha, M.; Yoon, M.-J.; Cho, J.; Yeom, K.-H.; Han, J.; Kim, V. N. TUT4 in concert with Lin28 suppresses microRNA biogenesis through pre-microRNA uridylation. *Cell* **2009**, 138, 696–708.

[12] Chang, H. M.; Triboulet, R.; Thornton, J. E.; Gregory, R. I. A role for the Perlman syndrome exonuclease Dis3l2 in the Lin28-let-7 pathway. *Nature* **2013**, 497, 244–248.

[13] Thornton J. E.; Gregory, R.I. How does Lin28 let-7 control development and disease? *Trends Cell Biol.* **2012**, 22, 474–482.

[14] Zhou, J. B.; Ng, S. B.; Chng, W. J. LIN28/LIN28B: An emerging oncogenic driver in cancer stem cells. *Int. J. Biochem. Cell B.* **2013**, 45, 973–978.

[15] Marras S. A. E.; Kramer, F. R.; Tyagi, S. Efficiencies of fluorescence resonance energy transfer and contact-mediated quenching in oligonucleotide probes. *Nucleic Acids Res.* **2002**, 30, e122.

[16] Zuker, M. Mfold web server for nucleic acid folding and hybridization prediction. *Nucleic Acids Res.* **2003**, 31, 3406–3415.

[17] Liu, C. C.; Schultz, P. G. Adding new chemistries to the genetic code. *Annu. Rev. of Biochem.* **2010**, 79, 413–444.

[18] Young, T. S.; Ahmad, I.; Yin, J. A.; Schultz, P. G. An enhanced system for unnatural amino acid mutagenesis in *E. coli. J. Mol. Biol.* **2010**, 395, 361–374.

[19] O'Donoghue, P.; Ling, J. Q.; Wang, Y.S.; Soll, D. Upgrading protein synthesis for synthetic biology. *Nat. Chem. Biol.* **2013**, 9, 594–598.

[20] Cridge, A.G.; Major, L. L.; Mahagaonkar, A. A.; Poole, E. S.; Isaksson, L. A.; Tate, W.P. Comparison of characteristics and function of translation termination signals between and within prokaryotic and eukaryotic organisms. *Nucleic Acids Res.* **2006**, 34, 1959–1973.

[21] Dommerholt, J.; Schmidt, S.; Temming, R.; Hendriks, L. J. A.; Rutjes, F. P. J. T; van Hest, J. C. M.; Lefeber, D. J.; Friedl, P.; van Delft, F. L. Readily accessible bicyclononynes for bioorthogonal labeling and three-dimensional imaging of living cells. *Angew. Chem. Int. Ed.* **2010**, 49, 9422–9425.

[22] Velagapudi S. P.; Gallo S. M.; Disney M. D. Sequence-based design of bioactive small molecules that target precursor microRNAs. *Nat. Chem. Biol.* **2014**, 10, 291–297.

2.6 Acknowledgement

This work was supported by the Creative Research Initiative Grant (2014R1A3A2030423) and the Bio & Medical Technology Development Program (2012M3A9C4048780) funded by the National Research Foundation of Korea (NRF). I thank Dr. Kyoung Hoon Kim for providing me with the gene for Lin28 and technical supports.

2.7. Supporting Information

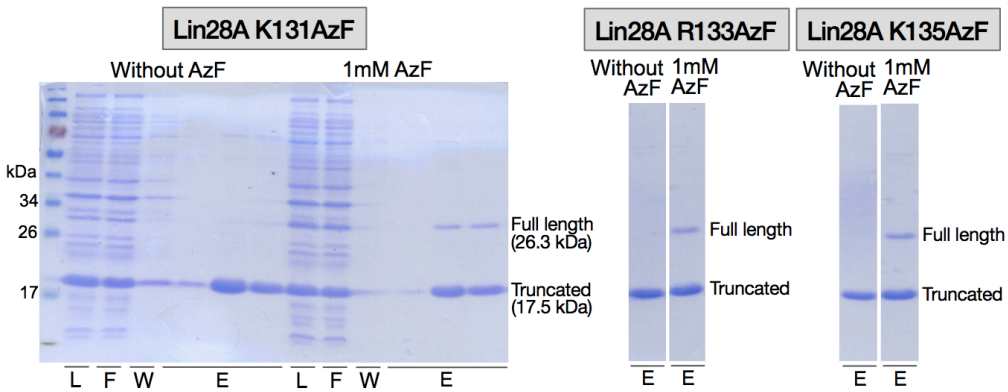

Figure S2.1. Expression of Lin28A AzF mutants in BL21(DE3). Cells were grown to $OD_{600\ nm}$ of 0.6, then 1 mM AzF (or DMSO), 0.02% Arabionse and 0.5 mM IPTG was added. They were incubated overnight at 18 °C and purified by Nickel affinity chromatography.

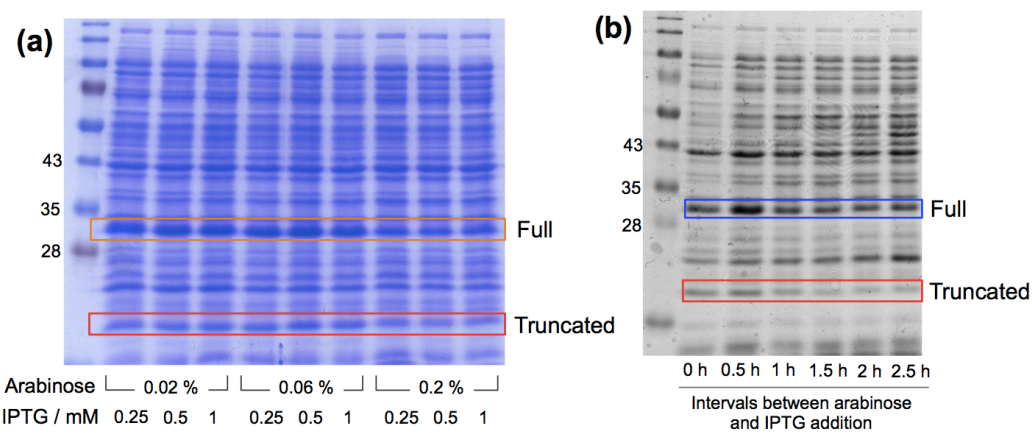

Figure S2.2. Optimization of Lin28A K135AzF production BL21(DE3). (a) Effect of inducer concentrations. Indicated amount of arabinose and 1 mM AzF were added when the culture reached $OD_{600\ nm}$ of 0.6. IPTG was added 30 min later. Cells were grown for total 8 h at 37 °C. (b) Effect of induction order. 0.02% of arabinose and 1 mM AzF were added when the culture reached $OD_{600\ nm}$ of 0.6. After indicated time inteverals, 0.5 mM IPTG were added and cells were further grown for 4 h.

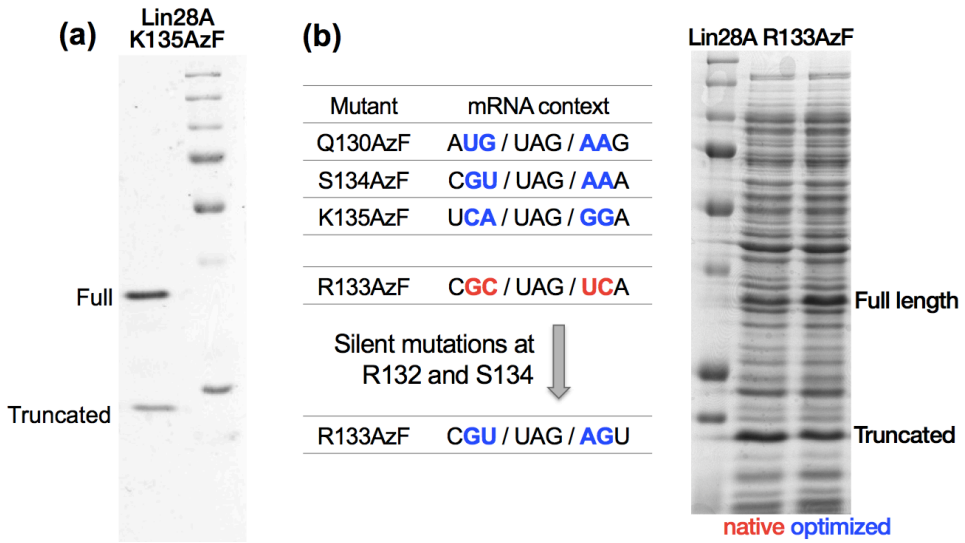

Figure S2.3. (a) Optimized production of Lin28A K135AzF mutant in BL21(DE3). (b) mRNA context optimization to enhance the production of full-length R133AzF mutant. First two bases before and after the amber codon was silently mutated on the basis of the information about the preferred nucleotide sequences for high read-through over termination.

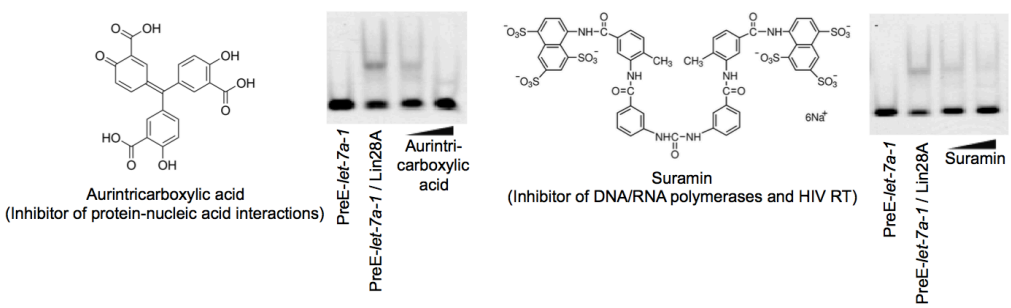

Figure S2.4. Identification of aurintricarboxylic acid and suramin as inhibitors of the Lin28–*let-7* interaction.

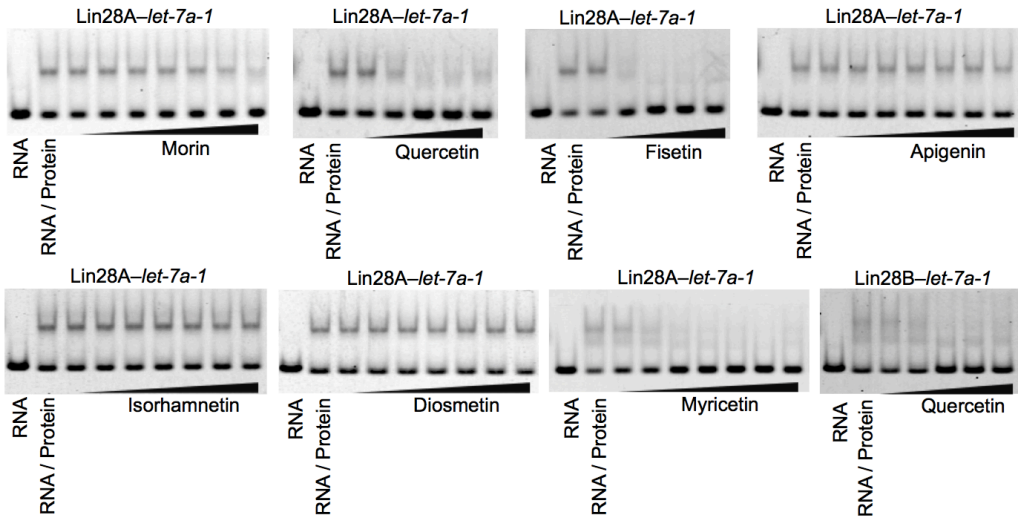

Figure S2.5. EMSA images showing inhibitory effects of several flavones against Lin28A–*let7a-1* or Lin28B–*let-7a-1* interaction.

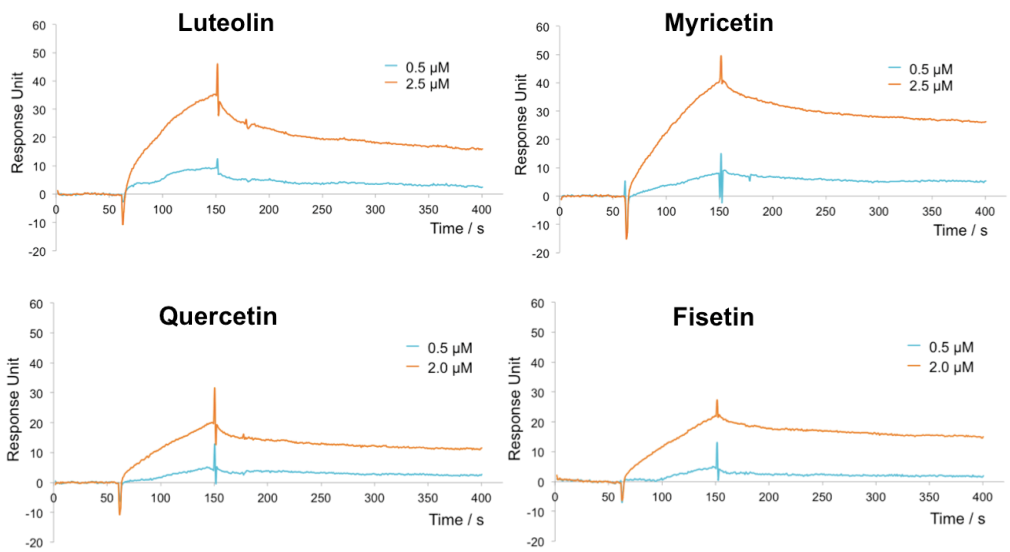

Figure S2.6. Biacore analysis of the Lin28A–Flavone interactions. Inhibitory compounds (luteolin, myricetin, quercetin, and fisetin) displayed strong binding. Weakly active morin (IC_{50} >100 μM) showed very weak binding, and an inactive compound (rhamnetin) exhibited no specific binding. Continued at the next page.

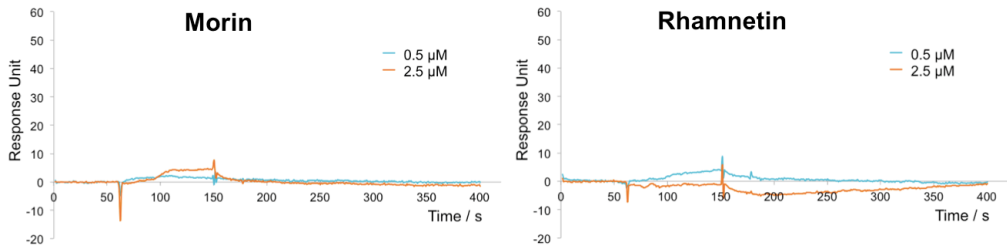

Figure S2.6. Continued.

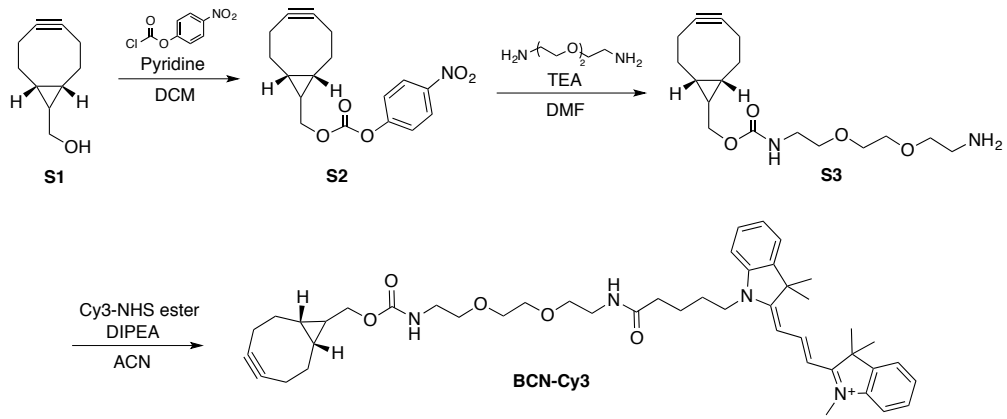

Scheme S2.1. Synthesis of BCN-Cy3. Detailed synthetic methods are described at 'Experimental Section'.

Chapter 3. Discovery of Carbohybrid-Based 2-Aminopyrimidine Analogues As a New Class of Rapid-Acting Antimalarial Agents Using Image-Based Cytological Profiling Assay

J. Med. Chem. **2014**, 57, 7425−7434.

3.1. Introduction

With nearly a million deaths annually and over 219 million hospital cases each year, malaria remains a serious public health problem, particularly in the high transmission areas of Sub-Sahara Africa, Southeast Asia, and Latin America.[1−3] The disease is caused by mosquito-borne protozoan parasites of the genus *Plasmodium*, five species of which are known to infect humans (*Plasmodium falciparum*, *Plasmodium vivax*, *Plasmodium ovale*, *Plasmodium malariae*, and *Plasmodium knowlesi*).[4,5] In the absence of vaccines with operational utilities against the disease, accurate diagnosis and treatment with available antimalarial regimens alongside effective vector control measures remain the best hope of controlling the disease globally.[6−8]

Plasmodium parasites, however, exhibit a high propensity to rapidly developed resistance against newly introduced medicines, necessitating as such a continuous search and development of new antimalarial agents to combat emerging resistant strains.[9,10] To stop the spread of multidrug resistance worldwide, the World Health Organization recommends the use of artemisinin-based combination treatments for all uncomplicated malaria cases globally. A key inclusion benefit of artemisinin in the current combinations lies in its rapid-acting multistage activities against most drug-resistant strains of *Plasmodium* parasites.[11] Unfortunately, parasite resistance to artemisinin has been inevitable, as revealed by the recent emergence and spread of drug-

tolerant parasites along the Thai−Cambodian borders in South East Asia.[12,13]

This dire situation calls for the immediate development, preferably, of nonartemisinin-based compounds with fast-acting, long-lasting, and multistage activities capable of reducing treatment durations while also improving patient compliances.[11] Indeed, compared to slow-acting single-target drugs such as pyrimethamine (antifolate), sulfadoxine (antifolate), and atovaquone (cytochrome bc1 complex inhibitor), anti-malarial compounds that exhibit fast-acting and pleiotropic activities similar to that of artemisinin and chloroquine are expected to display shorter parasite clearance times (PCTs), increased useful therapeutic lives (UTLs), and high parasitaemia reduction ratios (PRR), with net effects being increased cure rates and mitigation of resistance development.[10,14,15] Discovering new therapeutic agents in malaria requires a combination of new chemical libraries and innovative screening technologies. Indeed, plausible efforts by both pharmaceutical industries and academic research institutions recently had led to the identification of several structurally diverse antimalarial compounds, some of which are under scrutiny by partnerships such as the Medicine for Malaria Ventures (MMV) for inclusion into the lead discovery chain.

Recently, a group in Institut Pasteur Korea reported the development of an automated image-based screening system for the quantitative detection and classification of *P. falciparum* life cycle stages in a 384-culture well format.[16] In parallel, a small-molecule library of over 4000 drug-like compounds containing 60 distinct core structures was constructed using a privileged-substructure-based diversity-oriented synthetic (pDOS) approach.[17] By using the above image-based system first as a growth inhibition screening assay and then as a cytological profiling tool, carbohybrid-based 2-aminopyrimidines

were identified from the pDOS library as a new class of antimalarial compounds with potent activities against three laboratory strains of multiple drug-resistant *P. falciparum*. In chapter 1, I reported the synthesis of stereochemically enriched acyclic polyols fused with various privileged heterocycles from naturally abundant carbohydrates and named them as "carbohybrids".[18] On the basis of structure−activity relationship studies of the carbohybrids, 2-aminopyrimidine analogues (**8aA** and **11aA**) of the initial hit compounds were identified as the most promising candidates given their high *in vitro* potency and excellent *in vivo* PK properties and efficacy in a mouse malaria model.

3.2. Results and Discussion

3.2.1. A novel image-based cytological profiling assay

Plasmodium parasites exhibit a complex life cycle that involves multiple parasite stages and forms, which display variable degrees of sensitivity to most antimalarial compounds.[14,19,20] To facilitate the discovery and development of new therapies that target existing strains of drug-resistant *P. falciparum*, a cytological profiling method was developed using a previously reported image-based screening system.[16] This assay relies on the quantitative detection of each major blood form (early rings, late rings, trophozoites, and schizonts) of *P. falciparum* parasites in a 384-well format based on the numbers and sizes of detectable nuclear condensation spots in infected erythrocytes. In this assay, all host cells are stained with wheat germ agglutinin−AlexaFluor-488 conjugate whereas individual parasites in infected

erythrocytes are identified using the nuclear stain DAPI. The assay also employs the fluorescent dye Mitotracker red CMXRos to stain and discriminate functional mitochondria in live parasites and disrupted mitochondria in dead parasites. A major advantage of this image-based system is in its ability to quantify drug activities on the basis of total culture parasitaemia and to determine each parasite stage proportion in an automated fashion. The cytological profiling approach as developed in this study involves parasite treatment at well-defined time-points in the parasite's intraerythrocytic life cycle and comparison of the resulting stage accumulation indices following 36 or 24 h of drug pressure. Institut Pasteur Korea confirmed the reliability of this approach by profiling the stage specificities of four mechanistically known antimalarial agents using three different drug-resistant lines of *P. falciparum* (Figure 3.1). Consistent with their known modes of actions,[14,19,21−27] the data show that artemisinin (ART) and chloroquine (CQ) are fast-acting in inhibiting early and late ring development to the midtrophozoite stage, but that these compounds are only weakly active against trophozoite development to the schizont stages (Figure 3.1a). Indeed, at clinically relevant concentrations (peak plasma concentrations of ∼2 μM for ART and 1−10 μM for CQ),[28−30] both chloroquine and artemisinin are known to rapidly inhibit cell cycle development in malaria parasites, resulting in parasite clearance times of <24 h for both drugs.

trans-Epoxysuccinyl-L-leucylamido-(4-guanidino)butane (E64) on its part inhibited early ring development and schizont maturation, whereas *N*-acetylglucosamine (GlcNAc) was only weakly effective at inhibiting early ring development in all three parasite lines (Figure 3.1a). As shown in Figure 3.1b, ART, E64, and GlcNAc also produced significant decreases in culture

(a)

HB3

6 hpi	ER	LR	T	S	18 hpi	LR	T	S	30 hpi	T	S
ART	1.74	3.53	0.37	0.11	ART	4.40	1.06	0.47	ART	1.21	1.66
CQ	1.82	3.05	0.53	0.20	CQ	2.17	1.85	0.82	CQ	1.09	1.83
E64	3.15	1.15	1.32	0.45	E64	0.80	1.33	2.05	E64	1.06	3.85
GlcNAc	1.40	2.14	0.78	0.29	GlcNAc	1.00	1.06	0.51	GlcNAc	0.87	0.70

W2

6 hpi	ER	LR	T	S	18 hpi	LR	T	S	30 hpi	T	S
ART	2.06	1.33	0.81	0.47	ART	2.01	1.06	1.22	ART	1.51	1.05
CQ	1.78	1.51	0.65	0.53	CQ	1.82	1.12	1.64	CQ	1.26	1.13
E64	1.78	0.91	1.40	1.20	E64	0.76	1.22	2.10	E64	1.44	3.00
GlcNAc	1.52	0.88	0.92	0.54	GlcNAc	0.83	1.12	1.08	GlcNAc	0.34	1.40

K1

6 hpi	ER	LR	T	S	18 hpi	LR	T	S	30 hpi	T	S
ART	1.96	1.28	0.51	0.17	ART	2.52	0.70	0.26	ART	1.09	0.31
CQ	1.72	1.62	1.11	0.25	CQ	1.38	1.22	0.37	CQ	0.75	0.56
E64	1.69	0.67	1.25	0.55	E64	0.39	1.45	2.11	E64	0.50	2.07
GlcNAc	1.33	1.32	0.80	0.66	GlcNAc	0.86	1.18	0.64	GlcNAc	0.96	1.04

(b)

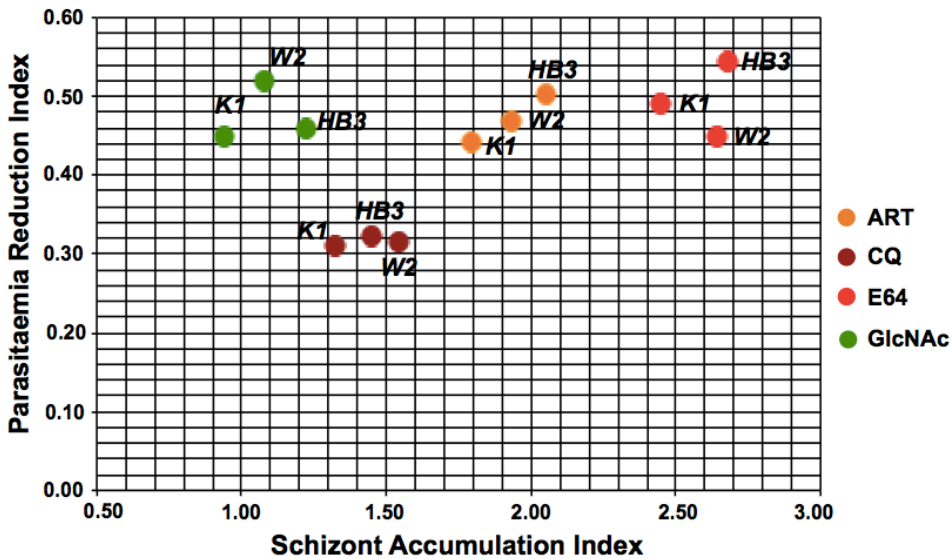

Figure 3.1. Stage-specific activities of selected antimalarial agents as determined using a novel image-based cytological profiling method. Tightly synchronized *P. falciparum* (HB3, W2, or K1 strains) were treated with 10 μM final concentration of each antimalarial agent at (a) the 6 hpi (hour postinvasion, early ring), 18 hpi (late ring), or 30 hpi (midtrophozoite) time-points for a continuous duration of 36 h, or (b) at the 42 hpi time-point (midschizont) for 24 h. The parasite nuclei, mitochondria, and host erythrocytes were then stained with DAPI, Mitotracker Red CMXRos, and wheat germ agglutinin−AlexaFluor-488, respectively, and the proportion of infected and viable parasitaemia determined by automated image mining. (a) Heat-map and

parasite stage accumulation index at each treatment time-point. ER, early rings; LR, late rings; T, trophozoites; S, schizonts. (b) A plot of parasitaemia reduction index (PRI) against schizont accumulation index (SAI) indicating the rapid-acting effects of E64 and artemisinin (ART) on schizonts and the invasion-specific effect (high PRI and low SAI) of *N*-acetylglucosamine (GlcNAc) against all three parasite strains. Accumulation or reduction indices greater than the control's mean plus three standard deviations (n = 3) were considered significant.

parasitaemia when added at the 42 h time-point for 24 h. Indeed, both ART and E64 gave significantly high schizont accumulation indices, indicating rapid inhibition of schizont maturation and/or merozoite egress, whereas GlcNAc reduced culture parasitaemia without a significant retention of schizonts. This later indicates that GlcNAc predominantly acts on extracellular merozoites, inhibiting host cell entry as reported previously.[21] Taken together, the above results demonstrated the ability of the novel cytological profiling approach to quantify the stage specificities of antimalarial agents at different time-points during the parasite's asexual developmental cycle with high reliability and in a high-throughput screening format.

3.2.2. Discovery of carbohybrid-based aminopyrimidines as a new antimalarial drug class

To identify antimalarial compounds with novel modes of action, 3980-membered in house small-molecule library was screened using the image-based parasitological assay system and the chloroquine/pyrimethamine-resistant *P. falciparum* K1 strain. This initial screen resulted in 89 hit compounds (hit rate of 2.4%) that inhibited parasite growth by >90% when used at 5 μM final concentrations and exhibited EC_{50} values less than 2 μM. Counter-screening of these initial hits against two other drug-resistant parasite strains (W2 and HB3) identified the carbohybrid frameworks containing 2-

aminopyrimidine moiety **1** (SNU3701) and **2** (SNU3662)[31] that displayed similar EC_{50} values (less than 1 μM) against all three *P. falciparum* strains (Table 3.1).

Dose-responsive cytotoxicity analyses of the above compounds using three different human cell lines (HepG2, THP-1, and U2OS) gave high selectivity indices in all three cell lines (Table 3.1), indicating *in vitro* safety toward the these cell lines. Cytological profiling of the compounds using drug-resistant *P. falciparum* K1 parasites revealed that carbohybrid-based 2-aminopyrimidine analogues (**1** and **2**) exhibit fast-acting antimalarial activities by inhibiting further development of early rings, late rings, and midtrophozoite stage parasites when treated at the 6, 18, or 30 h postinvasion (Figure 3.2). These two compounds, however, did not significantly affect parasite mitochondrial integrity as assessed by using the mitochondrial membrane potential indicator, Mitotracker Red CMXRos.

Table 3.1. Antimalarial and cytotoxicity profiles of 2-aminopyrimidine-based hit compounds.

	EC_{50} (μM)[a]			
compds	K1	HB3	W2	selectivity index[b]
CQ	0.208 ± 0.015	0.033 ± 0.005	0.221 ± 0.012	>450
ART	0.003 ± 0.001	0.018 ± 0.004	0.011 ± 0.001	>5550
1	0.251 ± 0.042	0.442 ± 0.080	0.320 ± 0.038	>226
2	0.535 ± 0.048	0.448 ± 0.061	0.406 ± 0.066	>187

[a]EC_{50} values are means ± SD of two independent experiments each done in duplicate. [b]Selectivity indices are calculated as the ratio of 50% cytotoxicity (CC_{50}) values against HepG2 cells to the highest parasitological EC_{50} values of the three *P. falciparum* strains. The CC_{50} of amphotericin B (positive cytotoxicity control) was 40 ± 3.2 μM using the resazurin-based assay as described in the 'Experimental Section'.

(a)

6 hpi	ER	LR	T	S	18 hpi	LR	T	S	30 hpi	T	S
ART	2.30	1.20	0.58	0.28	ART	2.87	0.80	0.60	ART	1.60	1.28
E64	1.64	0.61	1.30	1.06	E64	0.87	1.40	2.30	E64	1.42	3.00
GlcNAc	1.40	1.70	0.87	0.40	GlcNAc	0.54	1.12	0.98	GlcNAc	0.86	1.20
1	1.90	2.41	0.88	1.01	1	3.03	1.33	0.67	1	1.71	0.95
2	1.60	1.80	0.60	0.90	2	2.10	1.40	1.10	2	1.70	1.10

(b)

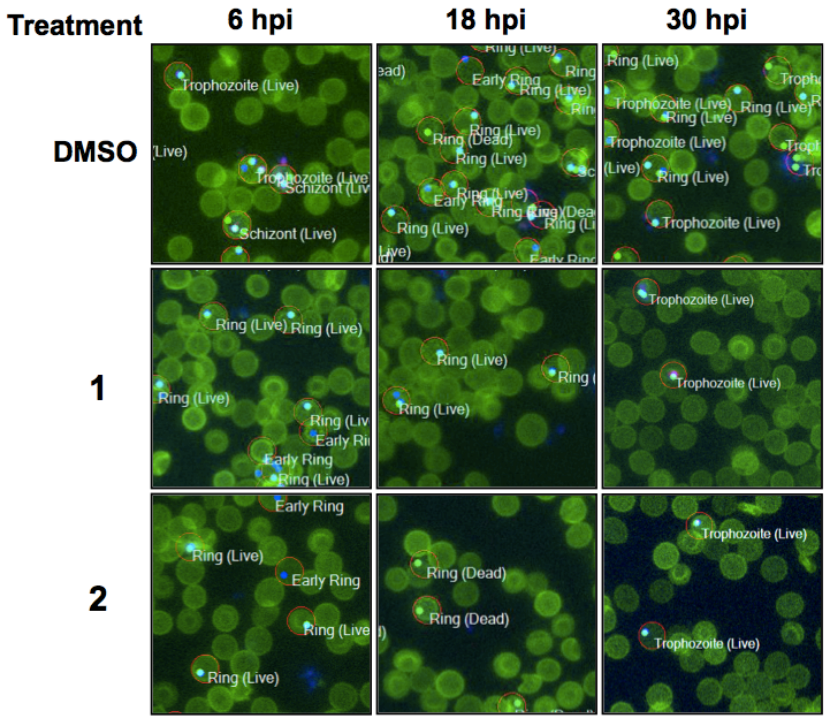

Figure 3.2. Cellular modes of action of 2-aminopyrimidine-based carbohybrid compounds. Tightly synchronized *P. falciparum* (K1 strain) were treated at the 6 hpi (early ring), 18 hpi (late ring), or 30 hpi (midtrophozoite) time-points with 10 µM final concentration **1** or **2** for a continuous duration of 36 h. Parasite nuclei, parasite mitochondrial, and the host erythrocytes were then stained with DAPI, Mitotracker Red CMXRos, and wheat germ agglutinin−AlexaFluor-488, respectively, and the proportion of infected and viable parasitaemia determined by automated image analysis. (a) Heat-map and parasite stage accumulation index at each treatment time-point. ER, early rings; LR, late rings; T, trophozoites; S, schizonts. (b) Representative images of parasitized cultures showing blockage of further development of "early ring", late ring ("Ring"), or "Trophozoite" stage parasites in **1**- or **2**-treated cultures compared to the DMSO-treated control. The mitotracker-positive parasitized erythrocytes are indicated as "Live", whereas mitotracker-negative cells are labeled as "Dead".

Treatment of the parasites at the 42 hpi time-point resulted in a parasitaemia reduction index of 0.52 for **1** and 0.46 for **2** and schizont accumulation index of approximately 2.4 for each compound. These results indicate that both compounds are fast acting in inhibiting schizont maturation and/or merozoite egress from the infected erythrocytes, leading to accumulation of schizonts in culture. Collectively, I concluded that carbohybrid-based 2-aminopyrimidine analogues are a novel class of fast acting blood-stage antimalarial compounds on the basis of their ability to block cell cycle progression from the treated parasite stages.

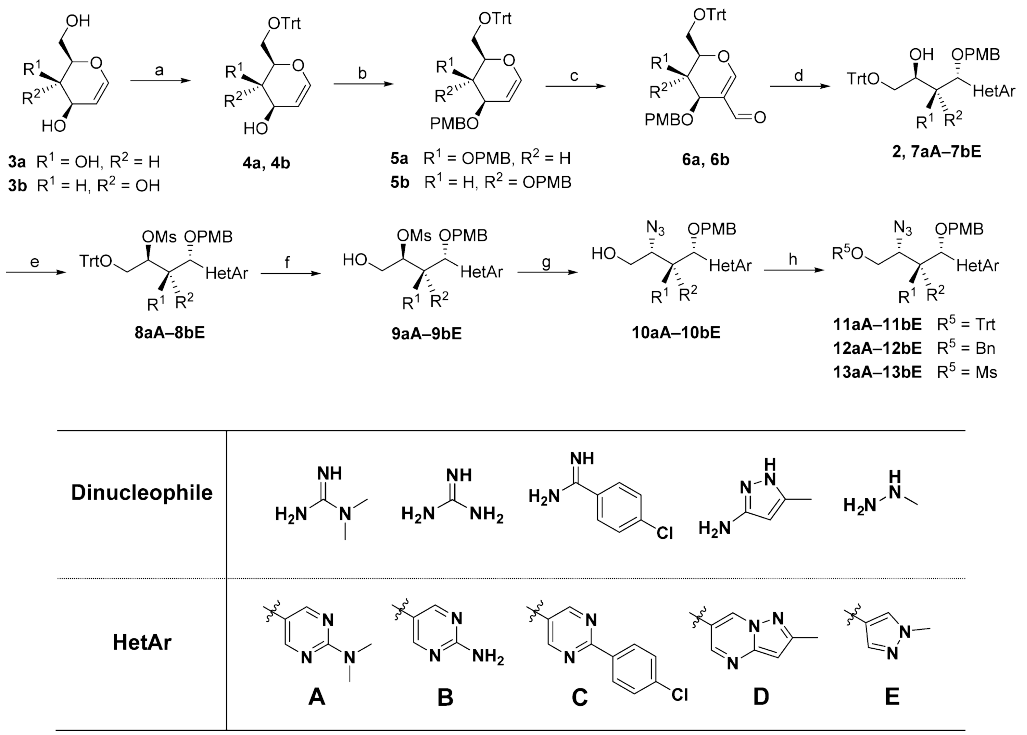

Scheme 3.1. Synthesis of carbohybrid-based molecular frameworks. Reagents and conditions: (a) TrtCl, DIPEA, DMAP, DCM, RT; (b) PMBCl, NaH, DMF, 0 °C–RT; (c) $POCl_3$, DMF, 0 °C–RT; (d) dinucleophiles, K_2CO_3, EtOH/THF, RT; (e) MsCl, TEA, DCM, 0 °C–RT; (f) *p*-TsOH, MeOH, RT; (g) NaN_3, DMF, 120 °C; (h) TrtCl, DIPEA, DCM, RT/BnBr, NaH, DMF, RT/MsCl, TEA, DCM, 0 °C–RT.

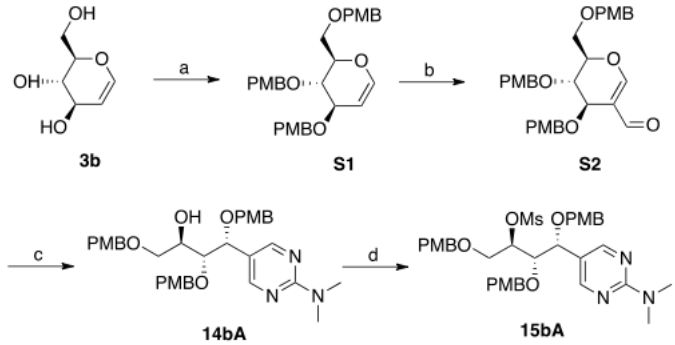

Scheme 3.2. Synthesis of compound **14bA** and **15bA**. Reagents and conditions: (a) PMBCl, NaH, DMF, 0 °C–RT; (b) $POCl_3$, DMF, 0 °C–RT; (c) 1,1-Dimethylguanidine sulfate, K_2CO_3, EtOH/THF, RT; (d) MsCl, TEA, DCM, 0 °C–RT.

Encouraged by these findings, I constructed a focused library of 2-aminopyrimidine-based carbohybrids using a divergent synthetic strategy.[18] As shown in Scheme 3.1, 6-hydroxyl groups in D-galactal (**3a**, R^1 = OH, R^2 = H) and D-glucal (**3b**, R^1 = H, R^2 = OH) were selectively protected with trityl group to afford **4a** and **4b**. *p*-Methoxybenzyl (PMB) protection of secondary hydroxyl groups, followed by Vilsmeier−Haack formylation, resulted in the 2-*C*-formyl glycals, **6a** and **6b**. The condensation of these intermediates (**6a** and **6b**) with dinucleophiles and the subsequent ring opening yielded the carbohybrid scaffolds **7** consisting of diverse heterocyclic moieties (pyrimidine, pyrazolopyrimidine, and pyrazole). Sequential modifications of functional groups through mesylation, trityl deprotection, and azide substitution allowed the formation of carbohybrids **8**, **9**, and **10**, respectively, with different appendices. Finally, the primary hydroxyl group in **10** was transformed via tritylation, benzylation, and mesylation to afford analogues **11**, **12**, and **13**, respectively. The modification of **7bA** with PMB group, instead of trityl group at the R^5 position, and the subsequent *O*-mesylation yield analogues **14bA** and **15bA**, respectively

Table 3.2. Antimalarial and cytotoxicity profiles of 2-aminopyrimidine-based hit compounds.

Cpds.	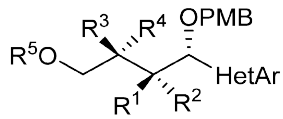						EC_{50} (μM) (K1 strain)
	HetAr	R^1	R^2	R^3	R^4	R^5	
2	B	OPMB	H	OH	H	Trt	0.351
7aA	A	OPMB	H	OH	H	Trt	0.200
7aC	C	OPMB	H	OH	H	Trt	0.578
7aD	D	OPMB	H	OH	H	Trt	0.352
7aE	E	OPMB	H	OH	H	Trt	0.396
7bA	A	H	OPMB	OH	H	Trt	0.559
7bE	E	H	OPMB	OH	H	Trt	0.478
8aA	A	OPMB	H	OMs	H	Trt	0.116
8aC	C	OPMB	H	OMs	H	Trt	0.225
8aD	D	OPMB	H	OMs	H	Trt	0.160
8aE	E	OPMB	H	OMs	H	Trt	0.158
8bA	A	H	OPMB	OMs	H	Trt	0.198
8bE	A	H	OPMB	OMs	H	Trt	0.237
9aA	A	OPMB	H	OMs	H	H	5.032
10aA	A	OPMB	H	H	N_3	H	5.447
10aD	D	OPMB	H	H	N_3	H	18.01
11aA	A	OPMB	H	H	N_3	Trt	0.092
11aE	E	OPMB	H	H	N_3	Trt	0.371
11bA	A	H	OPMB	H	N_3	Trt	0.167
11bE	E	H	OPMB	H	N_3	Trt	0.281
12aA	A	OPMB	H	H	N_3	Bn	1.424
12aE	E	OPMB	H	H	N_3	Bn	1.534
12bA	A	H	OPMB	H	N_3	Bn	1.197
13aA	A	OPMB	H	H	N_3	Ms	6.665
13bA	A	H	OPMB	H	N_3	Ms	11.72
14bA	A	H	OPMB	OH	H	PMB	2.897
15bA	A	H	OPMB	OMs	H	PMB	1.043

Given the occurrence of 2-aminopyrimidine heterocycles in carbohybrid-based hit compounds, I investigated the antimalarial activities of carbohybrids that contained pyrimidine (**2**, **7aA**, **7aC**), pyrazolopyrimidine (**7aD**), and pyrazole (**7aE**) in their substructures. As shown in Table 3.2, carbohybrid analogues containing all three heterocycles exhibited antimalarial activities (EC_{50} <1 μM) against chloroquine/pyrimethamine-resistant *P. falciparum* strain K1. Stereochemical modifications at the R^1 and R^2 positions, which were achieved by using different glycals (**3a** or **3b**) as starting material, minimally affected their inhibitory activities. However, the galactal-derived compounds (**7aA**, **7aE**, **8aA**, **8aE**, and **11aA**) exhibited slightly higher antimalarial activities compared with those of the glucal-based derivatives (**7bA**, **7bE**, **8bA**, **8bE**, and **11bA**). The modification at the primary hydroxyl group (R^5) appeared critical for the antimalarial activity. For example, the introduction of bulky hydrophobic moieties such as the trityl group in **8aA** and **11aA** allowed a more than 50-fold enhancement in antimalarial activities compared with those of unmodified hydroxyl version in carbohybrid analogues **9aA** and **10aA**. Consistent with this observation, the introduction of benzyl group (**12aA**) enhanced their antimalarial activities, albeit not as much as those in trityl-containing carbohybrid derivatives. Importantly, *O*-mesylation as examplified in derivative **8aA** and azide substitution at the R^4 position of the carbohybrid chain (e.g., **11aA**) enhanced the class antimalarial activities. On the basis of their potent *in vitro* activities (EC_{50}: 104−147 and 80−96 nM, respectively, against all three drug-resistant parasite strains), fast-acting activities against ring, trophozoite, and schizont development (Figure 3.3), and high selectivity indices (SI >680 for **8aA** and >1000 for **11aA**),

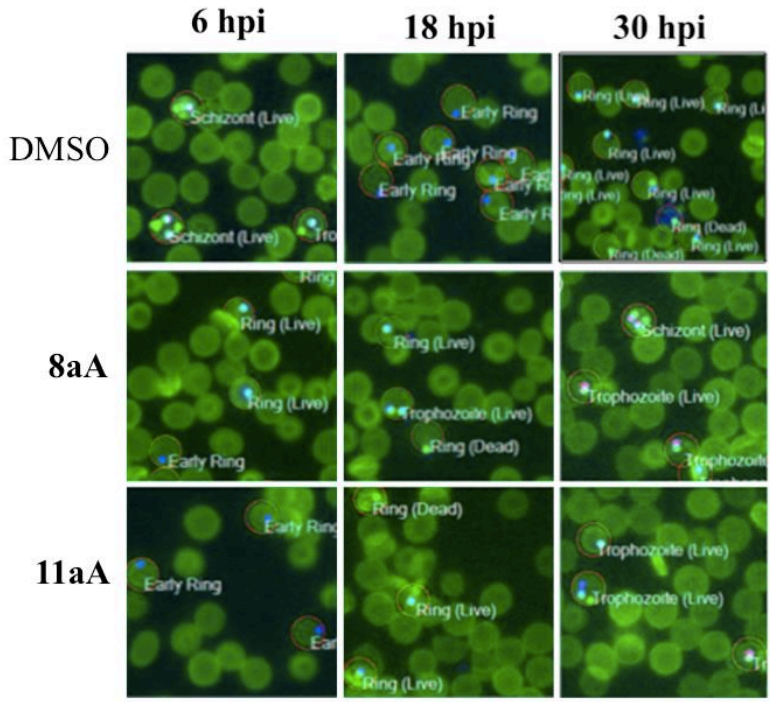

Figure 3.3. Speed of action and stage-specificity of derivatives **8aA** and **11aA**. Representative images showing rapid arrest of parasite development from the early ring, ring, and trophozoite stages following treatment at the 6, 18, and 30 hpi time points with 10 μM of each test compound. Representative images were cropped from one of five image fields per well of drug-treated cultures in a 384-well plate.

the above two carbohybrid-based 2-aminopyrimidine derivatives were selected for further pharmacokinetics analyses.

Candidate compounds **8aA** and **11aA** were examined for their microsomal stability (n = 3). As shown in Table 3, both compounds showed excellent *in vitro* metabolic stability, with greater than 80% compound remaining after 30 min in human and mouse liver microsomes. In addition, carbohybrid-based 2-aminopyrimidine derivative **8aA** at the dose of 1 and 5 mg/kg showed excellent pharmacokinetic behavior after intraperitoneal (IP) injection in SD male rats (n = 5), with rapid absorption (time to peak concentration [T_{max}]

Table 3.3. Microsomal stability and *in vivo* pharmacokinetic properties of candidate compounds **8aA** and **11aA**. Data represent mean ± SD.

	microsomal stability (% remaining after 30 min, n = 3)		PK study (n = 5)				
compd	human	mouse	dose (mg/kg)	T_{max} (h)	C_{max} (μg/mL)	AUC (μg/mL × h)	$T_{1/2}$ (h)
8aA	88.1 ± 8.01	88.6 ± 5.43	1	1.00 ± 0.00	1.80 ± 0.40	9.79 ± 1.47	10.3 ± 4.62
			5	1.00 ± 0.00	12.9 ± 9.30	41.3 ± 26.1	10.6 ± 12.1
11aA	89.0 ± 7.46	81.6 ± 7.48	1	3.40 ± 1.34	1.03 ± 0.30	8.20 ± 1.62	6.36 ± 0.70
			5	4.00 ± 0.00	3.07 ± 1.03	26.6 ± 8.37	5.78 ± 1.32

of 1 h and maximum concentration [C_{max}] of 1.80 ± 0.40 and 12.9 ± 9.30 g/mL, respectively) and stable plasma concentration of more than 0.10 and 0.15 μg/mL over 24 h. The area under the curve (AUC) of **8aA** and **11aA** confirmed the excellent pharmacokinetic property, which assures their pharmacological activities *in vivo* (Figure S3.1).

3.2.3. Novel *in vivo* antimalarial activity of 8aA and 11aA in a mouse malaria model

To assess the *in vivo* efficacy of carbohybrid-based antimalarial candidates (**8aA** and **11aA**), groups of *P. chabaudi*-infected mice were treated by IP injection on day 1 (trophozoite-stage parasites) to day 3 postinfection using fixed doses of 0.03, 0.3, 3, 10, or 30 mg/kg for each compound. Percent inhibitions of parasite growth in treated groups relative to the control parasitaemia on day 4 were then used in probit analyses of compounds' effects. As shown in Figure 4, both candidate compounds (**8aA** and **11aA**) displayed significant *in vivo* antimalarial activities in a dose-dependent manner. On the basis of the probit 5-response point, the compound's ED_{50} against *P. chabaudi* infection were estimated to be 0.32 mg/kg for **8aA** and 0.12 mg/kg for **11aA**.

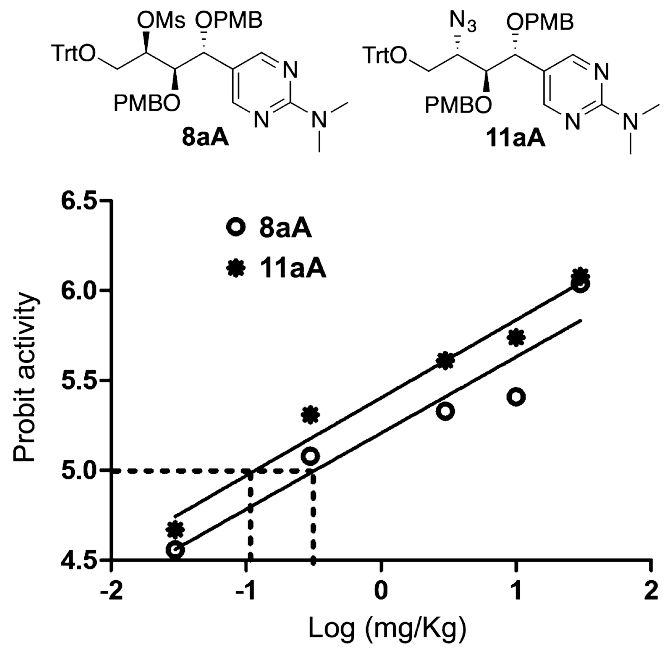

Figure 3.4. Chemical structures and probit analyses of *in vivo* parasitaemia reduction effects of carbohybrid-based 2-aminopyrimidine **8aA** and **11aA** derivatives. Mice (n = 5 per group) were infected with 2×10^7 parasitized erythrocytes per mouse followed by a 3 day treatment from day 1 post-infection with variable doses (0.03, 0.3, 3.0, 10.0, or 30.0 mg/kg body weight) of compound **8aA** or **11aA**. Day 4 parasitaemia were then quantified by light microscopy examination of thin smears and used in probit plots to analyze the dose-response effects.

As observed by light microscopy examination of thin smears, mice treatment with either **8aA** or **11aA** at doses greater than 3 mg/kg resulted in a significant reduction in blood parasitaemia and accumulation of ring-stage parasites in the infected mice unlike trophozoite stage parasites in untreated controls (Figure 3.5). These findings are consistent with the 24 h life cycle of synchronously developing *P. chabaudi* in mice and indicate a fast acting (approximately 12 h post-IP drug administration) *in vivo* antimalarial activity of the compounds. Collectively, the above data demonstrate clearly the therapeutic potential of the carbohybrid-based 2-aminopyrimidine **8aA** and **11aA** in a mouse malaria model.

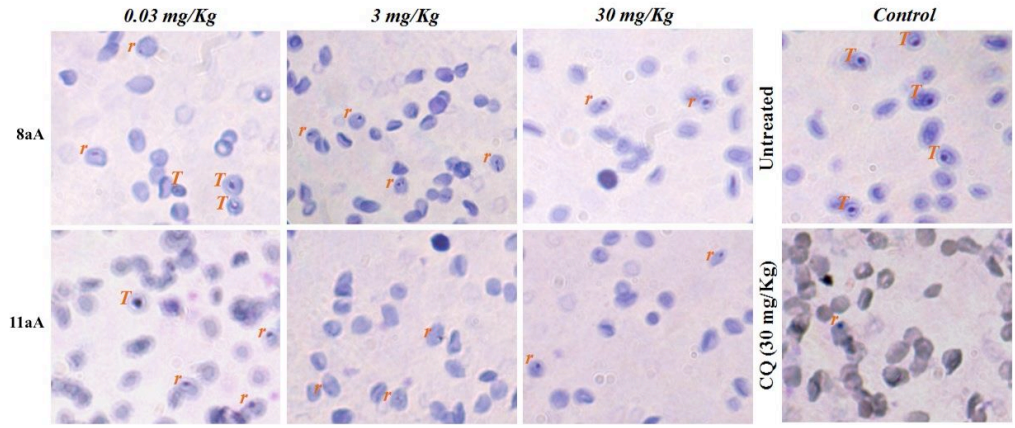

Figure 3.5. Light microscopy images of Day 4 blood smears from *P. chabaudi*-infected mice showing *in vivo* antimalarial activity of derivative **8aA** and **11aA**. Compared to the untreated control group in which trophozoite stage (T) parasites were detected, predominantly ring-stage parasites (r) were found in the **8aA** and **11aA**-treated mice groups particularly at doses > 3 mg/kg body weight.

3.3. Conclusion

Herein, the development and application of a novel image-based cytological profiling assay for the discovery of novel antimalarial agents is reported. Using this screening system, carbohybrid-based 2-aminopyrimidines were identified from 3980-membered in-house pDOS small-molecule library as a new class of blood-stage antimalarial agents. On the basis of the *in vitro* biological evaluation of their synthetic analogues, I optimized our initial hit compound to **8aA** and **11aA** as antimalarial candidates with excellent potency, high selectivity indices, and rapid acting activities against all major asexual parasite forms. Finally, these lead compounds exhibited favorable pharmacokinetic properties and fast-acting *in vivo* efficacy. I conclude that these carbohybrid-based 2-aminopyrimidine analogues **8aA** and **11aA** can be a promising class of antimalarial agents with potentials for clinical use against

uncomplicated and/or severe malaria case.

3.4. Experimental Section

Chemistry. All commercially available reagents and solvents were used without further purification unless noted otherwise. ^{1}H and ^{13}C NMR spectra were recorded on Varian Inova-500 (Varian Associates) or Agilent 400-MR DD2 (Agilent) instruments. Chemical shifts were reported in ppm relative to tetramethylsilane (TMS) as an internal standard or residual solvent peak ($CDCl_3$; ^{1}H, δ = 7.26 ppm; ^{13}C, δ = 77.23 ppm). Multiplicity is indicated as follows: s (singlet), d (doublet), t (triplet), q (quartet), m (multiplet), dd (doublet of doublet), dt (doublet of triplet), td (triplet of doublet), brs (broad singlet). Coupling constants are reported in hertz. HRMS analyses were conducted at the National Center for Inter-University Research Facilities in Seoul National University by fast atom bombardment (FAB) method. Routine mass spectrometric analysis was performed on a Finnigan Surveyor MSQ Plus LC/MS (Thermo) by electrospray ionization (ESI) method. Purity of the compounds was determined using the Finnigan Surveyor MSQ Plus LC/MS (Thermo) equipped with a Hypersil Gold column and photodiode array detector, or a Shimadzu SCL-10AVP HPLC (Shimadzu) equipped with a VP-ODS column and 254 nm detector. All the final compounds were >95% pure. The conversion of starting materials was monitored by thin-layer chromatography (TLC) using precoated glass-backed plates (silica gel 60; F_{254} = 0.25 mm), and the reaction components were visualized by observation under UV light (254 and 365 nm) or by treatment of TLC plates with visualizing agents such as $KMnO_4$, phosphomolybdic acid, and ceric sulfate

followed by heating. Products were purified by flash column chromatography on silica gel (230−400 mesh) using a mixture of EtOAc/hexane or MeOH/CH_2Cl_2 as eluents. Synthetic methods and spectroscopic data for **2**, **6a**, **6b**, **7aA−7bA**, and **10aA−10aD** are reported in Chapter 1.[18]

Synthesis of a glucal-derived pyrazole-containing carbohybrid 7bE. A solution of **6b** (100 mg) in tetrahydrofuran (3 mL) was added to a stirred solution of methylhydrazine sulfate (2 equiv.) and K_2CO_3 (5 equiv.) in ethanol (3 mL). The reaction mixture was stirred at room temperature for 15 h. The solvent was removed under reduced pressure, and the residue was partitioned between ethyl acetate and water. The aqueous layer was extracted with ethyl acetate twice, and the combined organic layer was dried over anhydrous Na_2SO_4(s). The filtrate was condensed under reduced pressure and subjected to flash column chromatography; white solid; yield 56%. ^{1}H NMR (400 MHz, $CDCl_3$) δ 7.43−7.40 (m, 7H), 7.29−7.21 (m, 10H), 7.13 (d, *J* = 8.6Hz, 2H), 6.98 (d, *J* = 8.6 Hz, 2H), 6.80 (d, *J* = 8.6 Hz, 2H), 6.76 (d, *J* = 8.6 Hz, 2H), 4.52 (d, *J* = 3.9Hz, 1H), 4.43 (d, *J* = 11.7 Hz, 1H), 4.31 (s, 2H), 4.11 (d, *J* = 11.7 Hz, 1H), 3.94−3.90 (m, 1H), 3.85 (s, 3H), 3.783 (s, 3H), 3.778 (s, 3H), 3.69 (dd, J = 6.5, 3.7 Hz, 1H), 3.26−3.23 (m, 1H), 3.19−3.15 (m, 2H). ^{13}C NMR (100 MHz, $CDCl_3$) δ 159.4, 159.3, 144.1, 139.3, 130.3, 130.1, 129.9, 129.84, 129.80, 128.9, 128.0, 127.2, 118.9, 114.0, 113.7, 86.6, 80.5, 73.7, 73.2, 70.8, 70.2, 64.8, 55.43, 55.42, 39.2. HRMS (FAB+) m/z calculated for $C_{43}H_{44}N_2O_6$ $[M + H]^+$, 685.3278; found, 685.3282.

General synthetic procedure for *O*-mesylated carbohybrids 8. Triethylamine (3 equiv.) and methanesulfonyl chloride (2 equiv.) were added to a stirred solution of **7** (100 mg) in anhydrous CH_2Cl_2 at 0 °C. The mixture was stirred at 0 °C for 2 h, diluted with CH_2Cl_2, and washed with brine. The

aqueous layer was extracted with CH_2Cl_2, and the combined organic layer was dried over anhydrous Na_2SO_4(s). The filtrate was condensed under reduced pressure and subjected to flash column chromatography. **8aA**: Prepared from **7aA** as a white solid; yield 99%. ^{1}H NMR (400 MHz, $CDCl_3$) δ 8.18 (s, 2H), 7.39− 7.37 (m, 6H), 7.31−7.22 (m, 11H), 6.90 (d, J = 8.6 Hz, 2H), 6.80 (d, J = 8.6 Hz, 2H), 6.71 (d, J = 8.6 Hz, 2H), 4.99 (dt, J = 6.7, 3.5, 1H), 4.32−4.22 (m, 4H), 4.10 (d, J = 10.6 Hz, 1H), 3.91 (dd, J = 6.7, 4.3 Hz, 1H), 3.76 (s, 3H), 3.75 (s, 3H), 3.35 (dd, J = 10.8, 3.3 Hz, 1H), 3.20 (s, 6H), 3.18−3.16 (m, 1H), 2.92 (s, 3H). ^{13}C NMR (100 MHz, $CDCl_3$) δ 162.4, 159.5, 158.2, 143.4, 130.4, 130.1, 129.8, 129.3, 128.7, 128.2, 127.5, 118.0, 114.0, 113.8, 87.4, 81.5, 80.4, 76.0, 75.3, 70.0, 63.5, 55.5, 55.4, 38.9, 37.4, 31.7. HRMS (FAB+) m/z calculated for $C_{46}H_{49}N_3O_8S$ $[M + H]^+$, 804.3319; found, 804.3315.

General synthetic procedure for detritylated carbohyrids 9. To a stirred solution of **8** (100 mg) in methanol, *p*-toluenesulfonic acid (1.5 equiv.) was added. The mixture was stirred at room temperature for 8 h, and the solvent was removed under the reduced pressure. The residue was partitioned between ethyl acetate and saturated $NaHCO_3$ solution. The aqueous layer was extracted with ethyl acetate twice, and the combined organic layer was dried over anhydrous Na_2SO_4(s). The filtrate was condensed under reduced pressure and subjected to flash column chromatography. **9aA**: prepared from **8aA** as a white solid; yield 94%. ^{1}H NMR (400 MHz, $CDCl_3$) δ 8.36 (s, 2H), 7.26 (d, *J* = 8.6 Hz, 2H), 7.00 (d, *J* = 8.6 Hz, 2H), 6.85 (d, *J* = 8.6 Hz, 2H), 6.78 (d, *J* = 8.6Hz, 2H), 5.08 (dt, *J* = 6.7, 3.7 Hz, 1H), 4.37−4.27 (m, 3H), 4.14 (s, 2H), 3.85−3.80 (m, 1H), 3.78 (s, 3H), 3.77 (s, 3H), 3.74 (dd, *J* = 8.2, 3.1 Hz, 1H), 3.71−3.68 (m, 1H), 3.23 (s, 6H), 3.04 (s, 3H), 2.35 (brs, 1H). ^{13}C NMR (100 MHz, $CDCl_3$) δ 162.5, 159.7, 159.6, 158.0, 130.4, 130.3, 129.6, 129.0, 118.3,

114.03, 113.99, 82.4, 80.0, 76.5, 75.0, 70.5, 62.7, 55.44, 55.40, 39.0, 37.4. HRMS (FAB+) m/z calculated for $C_{27}H_{35}N_3O_8S$ $[M + H]^+$, 562.2223; found, 562.2222.

General synthetic procedure for *O*-tritylated azide-containing carbohybrids 11. To a stirred solution of **10** (150 mg) and trityl chloride (1.2 equiv) in anhydrous CH_2Cl_2, diisopropylethylamine (1.5 equiv) and 4-dimethylaminopyridine (0.1 equiv) were added. After stirring at room temperature for 24 h, the mixture was diluted with CH_2Cl_2 and washed with brine. The organic layer was dried over anhydrous Na_2SO_4(s), and the filtrate was condensed under reduced pressure followed by flash column chromatography. **11aA**: prepared from **10aA** as a white solid; yield 88%. ^{1}H NMR (400 MHz, $CDCl_3$) δ 8.23 (s, 2H), 7.42−7.40 (m, 6H), 7.29−7.20 (m, 9H), 7.07 (d, *J* = 8.6Hz, 2H), 6.86 (d, *J* = 8.6Hz, 2H), 6.81(d, *J* = 8.6Hz, 2H), 6.69 (d, *J* = 8.6 Hz, 2H), 4.42−4.33 (m, 2H), 4.28 (dd, J = 8.0, 2.9 Hz, 2H), 4.06 (d, *J* = 11.0 Hz, 1H), 3.78 (s, 3H), 3.77 (s, 3H), 3.62 (dd, *J* = 6.7, 5.5 Hz, 1H), 3.50−3.46 (m, 1H), 3.42−3.39 (m, 1H), 3.33−3.28 (m, 1H), 3.20 (s, 6H). ^{13}C NMR (100 MHz, $CDCl_3$) δ 162.4, 159.34, 159.29, 158.1, 143.8, 130.1, 129.9, 129.8, 129.5, 128.9, 128.0, 127.2, 117.7, 113.9, 113.7, 87.4, 80.1, 77.8, 74.2, 70.4, 64.1, 63.2, 55.44, 55.38, 37.4. HRMS (FAB+) m/z calculated for $C_{45}H_{46}N_6O_5$ $[M + H]^+$, 751.3608; found, 751.3604.

General synthetic procedure for *O*-benzylated azide-containing carbohybrids 12. To a stirred solution of **10** (40 mg) in anhydrous dimethylformamide, NaH (2 equiv) was added slowly at 0 °C. After stirring the mixture for 10 min, benzyl bromide (2 equiv) was added. The reaction mixture was stirred for 5 h at room temperature and partitioned between ethyl acetate and water. The aqueous layer was extracted with ethyl acetate, and the

combined organic layer was dried over anhydrous Na_2SO_4. The filtrate was condensed under reduced pressure and subjected to flash column chromatography. **12aA**: prepared from **10aA** as a white solid; yield 71%. ^{1}H NMR (400 MHz, $CDCl_3$) δ 8.27 (s, 2H), 7.37−7.29 (m, 5H), 7.16 (d, *J* = 8.6 Hz, 2H), 7.02 (d, *J* = 8.6Hz, 2H), 6.85 (d, *J* = 8.6 Hz, 2H), 6.77 (d, *J* = 8.6 Hz, 2H), 4.49−4.37 (m, 5H), 4.29 (d, *J* = 5.9 Hz, 1H), 4.15 (d, *J* = 11.3 Hz, 1H), 3.80 (s, 3H), 3.78 (s, 3H), 3.75−3.74 (m, 1H), 3.66−3.58 (m, 3H), 3.21 (s, 6H). ^{13}C NMR (100 MHz, $CDCl_3$) δ 162.5, 159.50, 159.45, 158.1, 138.1, 130.2, 129.9, 129.83, 129.75, 128.6, 127.9, 127.8, 117.9, 114.0, 113.9, 80.5, 77.3, 74.5, 73.5, 70.3, 69.7, 62.1, 55.5, 55.4, 37.4. HRMS (FAB+) m/z calculated for $C_{33}H_{38}N_6O_5$ $[M + H]^+$, 599.2982; found, 599.2979.

General synthetic procedure for *O*-mesylated azide-containing carbohybrids 13. Triethylamine (3 equiv.) and methanesulfonyl chloride (2 equiv.) were added to a stirred solution of **10** (38 mg) in anhydrous CH_2Cl_2 at 0 °C. The mixture was stirred at room temperature for 3 h, diluted with CH_2Cl_2, and washed with brine. The aqueous layer was extracted with CH_2Cl_2, and the combined organic layer was dried over anhydrous Na_2SO_4(s). The filtrate was condensed under reduced pressure and subjected to flash column chromatography. **13aA**: prepared from **10aA** as a clear syrup; yield 88%. ^{1}H NMR (400 MHz, $CDCl_3$) δ 8.24 (s, 2H), 7.18 (d, *J* = 8.6 Hz, 2H), 7.01 (d, *J* = 8.6 Hz, 2H), 6.87 (d, *J* = 9.0 Hz, 2H), 6.77 (d, *J* = 9.0Hz, 2H), 4.46 (d, *J* = 11.0Hz, 1H), 4.41 (d, *J*=11.0Hz, 1H), 4.35−4.25 (m, 3H), 4.23 (d, *J* = 7.0 Hz, 1H), 4.16 (d, *J* = 11.0 Hz, 1H), 3.88 (dt, *J* = 8.0, 3.8 Hz 1H), 3.79 (s, 3H), 3.78 (s, 3H), 3.68 (dd, J = 7.0, 4.3 Hz, 1H), 3.23 (s, 6H), 2.97 (s, 3H). ^{13}C NMR (100 MHz, $CDCl_3$) δ 162.5, 159.7, 159.6, 157.9, 130.2, 130.0, 129.2, 129.1, 117.6, 114.2, 114.0, 80.5, 76.4, 74.2, 70.3, 69.0, 61.7, 55.44, 55.38, 37.6, 37.4.

HRMS (FAB+) m/z calculated for $C^{27}H^{34}N^{6}O^{7}S$ $[M + H]^{+}$, 587.2288; found, 587.2289.

Biological materials. HepG2 (human hepatocellular carcinoma), THP-1 (human monocytic leukemia), and U2OS (human osteosarcoma) cells were obtained from American Type Culture Collection (ATCC) and cultured in Dulbecco's Modified Eagle Medium (DMEM) (Gibco) containing 10% fetal bovine serum (FBS) (Gibco) and 1% antibiotic−antimycotic solution at 37 °C in an atmosphere of 5% CO_2. BALB/c mice were obtained from The Jackson Laboratory (Bar Harbor, ME). All mice were bred and maintained in specific pathogen-free conditions at the animal facility of the Institute of Pasteur Korea. All animal experiments were performed with the approval of the Institutional Animal Care and Use Committee (IACUC) at IPK (authorization no. IPK05050203IPK-12009). The following materials were purchased from companies in the parentheses: hypoxanthine (Sigma-Aldrich), gentamycin (Life Technologies), Albumax (Life Technologies), Resazurin (Sigma-Aldrich), Mitotracker Red CMXRos (Life Technologies), and wheat germ agglutinin−AlexaFluor-488 conjugate (Life Technologies).

Parasite lines and culture conditions. *P. falciparum* strain HB3 (Pyr^{R}), K1 (CQ^{R}, Pyr^{R}), and W2 (CQ^{R}, Pyr^{R}, SDX^{R}) were obtained from the Biodefense and Emerging Infections (BEI) Research Resources (Manassas, VA) and maintained at <10% parasitaemia in human red blood cells at 3% hematocrit (blood type O+, Gyeonggi Blood Center, Korean Red Cross). The culture media consisted of RPMI1640, 25 mM HEPES buffer (pH 7.4), 0.1 mM hypoxanthine, 0.016 mM thymidine, 0.5% Albumax, and 20 μg/mL gentamycin. Cultures were maintained at 37 °C in gassed chambers following injection with a mixture of 5% CO_2, 1% O_2, and 94% N_2. When needed,

parasites were synchronized at the ring stage by two sorbitol treatments (8 h intervals) and further cultivated through one complete cycle prior to the drug activity studies.

Compound library and image-based parasitological screening. An in-house drug-like compound library of 3980 small molecules that had previously been constructed using a privileged substructure-based diversity-oriented synthesis (pDOS) approach was subjected to automated high-throughput screening using our novel image-based parasitaemia detection method.[16,17,27] Briefly, DMSO-solubilized test compounds were diluted in complete media and cocultured with *P. falciparum* (K1)-parasitized erythrocytes at a parasitaemia of 1% and hematocrit 1.5%. The final drug concentrations were 5 μM in a final DMSO amount of 0.5% per well of 50 μL sample. All liquid-handling procedures were completed using a Biomek's NX robotic station (compound dilution) or a CyBi liquid handler (compound transfer) or a Well-Mate dispenser (dispensation of parasitized cultures into drugged wells). The cultures were then placed in gassed chambers (5% CO_2, 1% O_2, and 94% N_2) and grown for 72 h at 37 °C. 5 μL of each well content was transferred into a staining solution comprising wheat germ agglutinin−AlexaFluor-488 conjugate (RBC membrane stain) and Mitotracker Red CMXRos (mitochondrial membrane potential indicator) and maintained at 37 °C for 20 min to allow for complete incorporation of the dyes. The resulting cultures were again diluted in fixing solution comprising 5 μg/mL DAPI and 4% (w/v) paraformaldehyde to a final hematocrit of 0.02% in a 384-well imaging plate (black glass-bottom plate, Matrical). Following a 10 min incubation period at room temperature, the plates were gently vortexed (1700 rpm for 30 s) and spun at 1000 rpm for 1 min to layer the suspended cells onto the well bottom.

Five image fields were then acquired from each well using an Operetta 2.0 microscopy system that was equipped with a robotic arm and a 40× objective lens. The acquired images were then submitted for automated image analysis using our previously developed image mining algorithms for malaria.[16] Raw data were further exported onto an Excel spreadsheet and normalized using the DMSO-only wells as positive growth controls and RBC-only wells as image-mining background.

Hit selection and confirmation. Primary screening hits were defined as reducing the final culture parasitaemia by more than 90% when compared to the mean culture parasitaemia in DMSO control wells. These primary hits were subjected to dose-response studies against all three drug-resistant parasite strains to identify those with novel activities. Compounds exhibiting complete dose-response curves within the analyzed drug range of 0−40 μM and an EC_{50} less than 2 μM were selected for cluster analyses and *in silico* activity searches. Further hit confirmation analysis involved compound resynthesis and antimalarial activity testing in dose-response assays.

***In vitro* cytotoxicity studies.** Compounds were evaluated for cytotoxicity using three human cell lines HepG2, THP-1, and U2OS. Cells were seeded at a density of 2500 cells/well (total volume 50 μL) in 384-well plates and incubated for 24 h prior to drug treatment. Two-fold serial dilutions of the compounds (starting at 100 μM) were added to the plates and incubated under humidified conditions at 37 °C for an additional 48 h. Resazurin (7-hydroxy-3H-phenoxazin-3-one-10-oxide) was added to a final concentration of 10 μM, and the plates were further incubated for 12 h at 37 °C. Fluorescence due to the metabolic product of resazurin, resorufin, was measured at excitation/ emission of 531/572 nm using Victor3 V spectrophotometer (PerkinElmer).

The percent cell viability in each triplicate well was quantified by normalizing against the solvent-treated cells using the formula: % viability = ($uF_{compound}/uF_{solvent}$) × 100, where $uF_{compound}$ is the mean resorufin fluorescence in compound-treated wells and $uF_{solvent}$ is the mean fluorescence in the solvent-treated wells. Compound concentrations resulting in a 50% (CC_{50}) reduction in cell viability was determined by nonlinear regression curve fitting using GraphPad Prism 5.04. The cytotoxic control wells consisted of serial dilutions of amphotericin B, starting from a final concentration of 100 μM and 0.5% final DMSO concentration.

Cytological profiling of antimalarial drug effects. The effects of each selected antimalarial compound on trophic and schizont development, egress, and merozoite invasion, and on the parasite mitochondrial membrane potential were determined by high content imaging using a four-time point experimental setup. Synchronized *P. falciparum* (strain HB3)-infected cultures at 1.5% hematocrit and 5% parasitaemia were treated for 36 h starting at either the early ring stage (6 hpi), late ring stage (18 hpi), or at the late trophozoite (30 hpi) stage with either test or reference compounds at a single maximum effect concentrations of 10 μM (i.e., the concentration at which no further increase in culture parasitaemia is observed following drug treatment). Drug effects on egress and invasion were determined following a 24 h treatment, with each compound added at the midschizont stage (42 hpi). Cultures were sequentially diluted in staining and fixing solutions as described above and imaged using an Operetta 2.0 microscopy system. Following parasite stage quantification using our customized image-mining algorithms, stage accumulation index (stage proportion in test wells relative to same stage proportion in solvent control wells) were calculated and used to assess the rapid acting effects of

each compound on trophozoite and schizont development in vitro. Meanwhile, following the 24 h drug treatment at the 42 hpi, the resulting schizont accumulation index was compared against the total parasitaemia reduction index (decrease in well parasitaemia relative to control parasitaemia) to distinguish between egress inhibition (high schizont accumulation and parasitaemia reduction indices) and drug effects on extracellular merozoites (low schizont accumulation index and high parasitaemia reduction index). The drug effects on parasite mitochondrial activities were also assessed by comparing the proportion of viable (Mitotracker-positive) parasitaemias in drug-treated wells relative to that in the solvent controls following a 36 h treatment allowing for early ring development into the schizont stage.

Phase I metabolic stability study. Liver metabolic stability was determined in human and mouse liver microsomes. The compound (1 μM) was mixed with human or rat liver microsomes (0.5 mg/mL) (Gentest, BD Biosciences) in 100 mM potassium phosphate buffer (pH 7.4) and incubated at 37 °C for 5 min. The reaction was initiated by NADPH regeneration solution (BD Biosciences) and terminated by three times volume of ice-cold acetonitrile with imipramine (80 ng/ mL) as internal standard at single time-point 30 min. After pretreatment of biological samples with vortex and centrifuge, the samples were analyzed by LC/MS/MS system.

Pharmacokinetic study. The carbohybrid-based antimalarial candidates (**8aA** and **11aA**) were administered by intraperitonial injection (1 and 5 mg/kg) in SD male rats (n = 5). Our candidate compounds were prepared as a solution (DMSO, PEG400, Tween 80, and hydroxylpropyl-β-cyclodextrin (HPβCD) solution in PBS (final 10% HPβCD) at 10:10:2.5:77.5, v:v:v:v %). Blood samples were taken at 10 and 30 min and at 1, 4, 8, and 24 h postinjection.

After the purification of plasma by centrifugation, the concentration of carbohybrid-based antimalarial candidates was analyzed using Agilent 6460 LC/MS/MS system (Agilent) using electron spray ionization and a reverse-phase column (Hypersil GOLD C18, 50 mm × 2.1 mm, Thermo Scientific). Pharmacokinetic parameters were obtained after the analysis of plasma concentration-time plot with WinNonlin software (Pharsight).

***In vivo* efficacy assessment of antimalarial drug candidates 8aA and 11aA.** Compounds **8aA** and **11aA** that exhibited potent in vitro multistage antiplasmodial activities, selectivity indices >600, good metabolic stability, and intraperitoneal PK properties were selected for *in vivo* efficacy assessment in *Plasmodium chabaudi*-infected BALB/c mice. Each group of five mice was infected by IP injection of 2×10^7 parasitized erythrocytes per mouse. Twenty-four hours later (day 1), thin smears were prepared from tail blood and used to determine the pretreatment parasitaemias. This was immediately followed by IP injection of the compounds to final doses of 0.03, 0.3, 3, 10, or 30 mg/kg body weights per group. These treatments were repeated for two additional days, followed by parasitaemia assessment by light microscopy examination of Giemsa-stained thin smears on day 4 post-infection. Probit analyses of the drug effects were then undertaken as previously described.[32−34]

3.5. References

[1] Burchard, G. D. [Malaria - update 2013]. *MMW–Fortschr. Med.* **2013**, 155, 42−44.

[2] Lopez Del Prado, G. R.; Hernan Garcia, C.; Moreno Cea, L.; Fernandez Espinilla, V.; Munoz Moreno, M. F.; Delgado Marquez, A.; Polo Polo, M. J.;

Andres Garcia, I. Malaria in developing countries. *J. Infect. Dev. Countries* **2014**, 8, 1−4.

[3] Murray, C. J.; Rosenfeld, L. C.; Lim, S. S.; Andrews, K. G.; Foreman, K. J.; Haring, D.; Fullman, N.; Naghavi, M.; Lozano, R.; Lopez, A. D. Global malaria mortality between 1980 and 2010: a systematic analysis. *Lancet* **2012**, 379, 413−431.

[4] Greenwood, B. M.; Fidock, D. A.; Kyle, D. E.; Kappe, S. H.; Alonso, P. L.; Collins, F. H.; Duffy, P. E. Malaria: progress, perils, and prospects for eradication. *J. Clin. Invest.* **2008**, 118, 1266−1276.

[5] Chang, H. H.; Moss, E. L.; Park, D. J.; Ndiaye, D.; Mboup, S.; Volkman, S. K.; Sabeti, P. C.; Wirth, D. F.; Neafsey, D. E.; Hartl, D. L. Malaria life cycle intensifies both natural selection and random genetic drift. *Proc. Natl. Acad. Sci. USA*. **2013**, 110, 20129−20134.

[6] Wells, T. N.; Alonso, P. L.; Gutteridge, W. E. New medicines to improve control and contribute to the eradication of malaria. *Nature Rev. Drug Discovery* **2009**, 8, 879−891.

[7] Dondorp, A. M.; Yeung, S.; White, L.; Nguon, C.; Day, N. P.; Socheat, D.; von Seidlein, L. Artemisinin resistance: current status and scenarios for containment. *Nature Rev. Microbiol.* **2010**, 8, 272−280.

[8] Verma, R.; Khanna, P.; Chawla, S. Malaria vaccine can prevent millions of deaths in the world. *Hum. Vaccines Immunother.* **2013**, 9, 1268−1271.

[9] Olliaro, P.; Wells, T. N. The global portfolio of new antimalarial medicines under development. *Clin. Pharmacol. Ther.* **2009**, 85, 584−595.

[10] Muregi, F. W.; Wamakima, H. N.; Kimani, F. T. Novel drug targets in malaria parasite with potential to yield antimalarial drugs with long useful therapeutic lives. *Curr. Pharm. Des.* **2012**, 18, 3505−3521.

[11] Enserink, M. If artemisinin drugs fail, what's plan B? *Science* **2010**, 328, 846.

[12] Dondorp, A. M.; Nosten, F.; Yi, P.; Das, D.; Phyo, A. P.; Tarning, J.; Lwin, K. M.; Ariey, F.; Hanpithakpong, W.; Lee, S. J.; Ringwald, P.; Silamut, K.; Imwong, M.; Chotivanich, K.; Lim, P.; Herdman, T.; An, S. S.; Yeung, S.; Singhasivanon, P.; Day, N. P.; Lindegardh, N.; Socheat, D.; White, N. J. Artemisinin resistance in Plasmodium falciparum malaria. *N. Engl. J. Med.* **2009**, 361, 455−467.

[13] Noedl, H.; Se, Y.; Schaecher, K.; Smith, B. L.; Socheat, D.; Fukuda, M. M. Evidence of artemisinin-resistant malaria in western Cambodia. *N. Engl. J. Med.* **2008**, 359, 2619−2620.

[14] Sanz, L. M.; Crespo, B.; De-Cozar, C.; Ding, X. C.; Llergo, J. L.; Burrows, J. N.; Garcia-Bustos, J. F.; Gamo, F. J. P. falciparum in vitro killing rates allow to discriminate between different antimalarial mode-of-action. *PLoS One* **2012**, 7, e30949.

[15] Grimberg, B. T.; Mehlotra, R. K. Expanding the antimalarial drug arsenal–now, but how? *Pharmaceuticals (Basel)* **2011**, 4, 681−712.

[16] Moon, S.; Lee, S.; Kim, H.; Freitas-Junior, L. H.; Kang, M.; Ayong, L.; Hansen, M. A. An image analysis algorithm for malaria parasite stage classification and viability quantification. *PLoS One* **2013**, 8, e61812.

[17] Oh, S.; Park, S. B. A design strategy for drug-like polyhetero- cycles with privileged substructures for discovery of specific small- molecule modulators. *Chem. Commun.* **2011**, 47, 12754−12761.

[18] Lim, D.; Park, S. B. Synthesis of molecular frameworks containing two distinct heterocycles connected in a single molecule with enhanced three-dimensional shape diversity. *Chem. Eur. J.* **2013**, 19, 7100−7108.

[19] Zhang, Y.; Asante, K. S.; Jung, A. Stage-dependent inhibition of chloroquine on Plasmodium falciparum in vitro. *J. Parasitol.* **1986**, 72, 830−836.

[20] Delves, M. J.; Ruecker, A.; Straschil, U.; Lelievre, J.; Marques, S.; Lopez-Barragan, M. J.; Herreros, E.; Sinden, R. E. Male and female Plasmodium falciparum mature gametocytes show different responses to antimalarial drugs. *Antimicrob. Agents Chemother.* **2013**, 57, 3268− 3274.

[21] Naik, R. S.; Krishnegowda, G.; Gowda, D. C. Glucosamine inhibits inositol acylation of the glycosylphosphatidylinositol anchors in intraerythrocytic Plasmodium falciparum. *J. Biol. Chem.* **2003**, 278, 2036−2042.

[22] Salmon, B. L.; Oksman, A.; Goldberg, D. E. Malaria parasite exit from the host erythrocyte: a two-step process requiring extraerythrocytic proteolysis. *Proc. Natl. Acad. Sci. USA* **2001**, 98, 271−276.

[23] Soni, S.; Dhawan, S.; Rosen, K. M.; Chafel, M.; Chishti, A. H.; Hanspal, M. Characterization of events preceding the release of malaria parasite from the host red blood cell. *Blood Cells, Mol., Dis.* **2005**, 35, 201−211.

[24] Klonis, N.; Crespo-Ortiz, M. P.; Bottova, I.; Abu-Bakar, N.; Kenny, S.; Rosenthal, P. J.; Tilley, L. Artemisinin activity against Plasmodium falciparum requires hemoglobin uptake and digestion. *Proc. Natl. Acad. Sci. USA* **2011**, 108, 11405−11410.

[25] Gligorijevic, B.; Purdy, K.; Elliot, D.; Cooper, R. A.; Roepe, P. D. Stage independent chloroquine resistance and chloroquine toxicity revealed via spinning disk confocal microscopy. *Mol. Biochem. Parasitol.* **2008**, 159, 7−23.

[26] Klonis, N.; Creek, D. J.; Tilley, L. Iron and heme metabolism in Plasmodium falciparum and the mechanism of action of artemisinins. *Curr.*

Opin. Microbiol. **2013**, 16, 722−727.

[27] Singh, K.; Kaur, H.; Smith, P.; de Kock, C.; Chibale, K.; Balza- rini, J. Quinoline−pyrimidine hybrids: synthesis, antiplasmodial activity, SAR, and mode of action studies. *J. Med. Chem.* **2014**, 57, 435−448.

[28] Zhao, S. High-performance liquid chromatographic determi- nation of artemisinine (qinghaosu) in human plasma and saliva. *Analyst* **1987**, 112, 661−664.

[29] White, N. J. Clinical pharmacokinetics and pharmacodynamics of artemisinin and derivatives. *Trans. R. Soc. Trop. Med. Hyg.* **1994**, 88, 41−43.

[30] Krishna, S.; White, N. J. Pharmacokinetics of quinine, chloroquine and amodiaquine. Clinical implications. *Clin. Pharmacokinet.* **1996**, 30, 263−299.

[31] SNU3701 and SNU3662 are identical to compound **11b** and **3d**, respectively, in ref 18.

[32] Berres, M. An effective method for the estimation and comparison of the ED50 with small sample sizes. *J. Exp. Anim. Sci.* **1991**, 34, 21−29.

[33] Kelly, G. E.; Lindsey, J. K. Robust estimation of the median lethal dose. *J. Biopharm. Stat.* **2002**, 12, 137−147.

[34] Loshadkin, N. A.; Gladkikh, V. D.; Kolosova, N. A.; Sinitsyn, A. N.; Goldenkov, V. A. The use of probit-method for an estimation of toxic effects of combined toxicants at low concentration levels. *Radiats. Biol., Radioekol.* **2003**, 43, 337−340.

3.6. Acknowledgements

This work was supported by the Creative Research Initiative Grant (2014R1A3A2030423), the Bio & Medical Technology Development Program

(2012M3A9C4048780), the Basic Research Laboratory (2010-0019766) funded by the National Research Foundation of Korea (NRF), the National Research Foundation of Korea (NRF) grant funded by the Korea Government (MSIP, no. 2007-00559), Gyeonggi-do, and KISTI. I thank Institut Pasteur Korea for working on biological assays, and Korea Research Institute of Chemical Technology for working on pharmacokinetics studies in this project. I am grateful for a WCU-BK21 scholarship.

3.7. Supporting Information

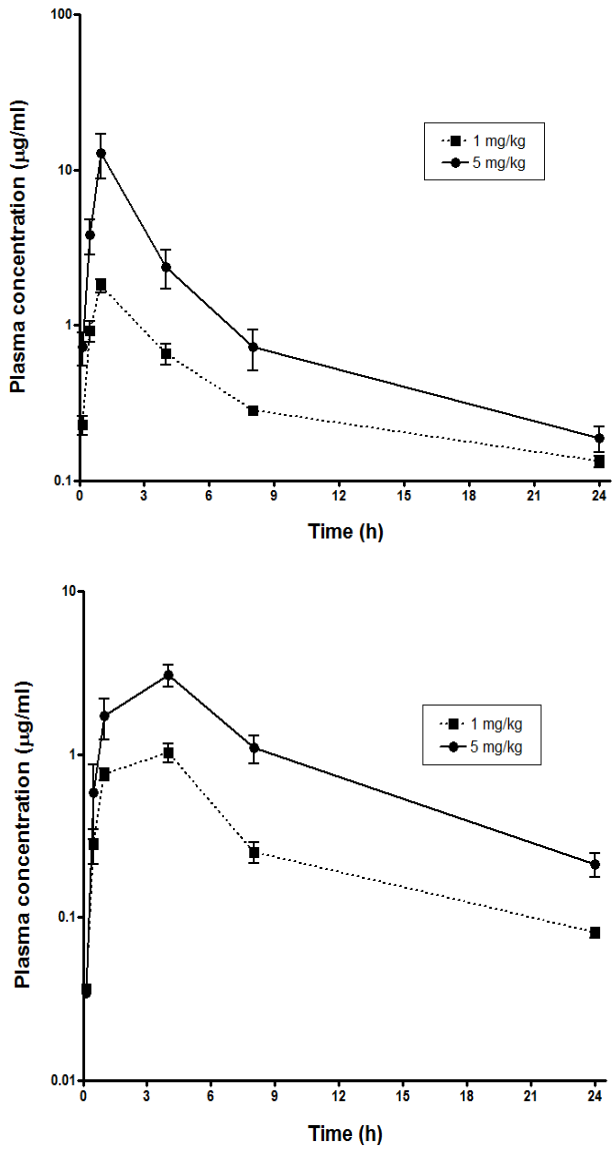

Figure S3.1. Pharmacokinetics of **8aA** (A) and **11aA** (B) after intraperitoneal injection in mice. The data shown are the means ± S.D. (n = 5).

Table S3.1. Purities of all final compounds. The purities were determined using the Finnigan Surveyor MSQ Plus LC/MS [Thermo] equipped with a Hypersil Gold HPLC column (100 x 4.6 mm) and photodiode array detector, or a Shimadzu SCL-10AVP HPLC [Shimadzu] equipped with a VP-ODS column (150 x 4.6 mm) and 254 nm detector.

Compound	Purity (Area %)	**Compound**	Purity (Area %)
7bE	95.5	**11bA**	97.7
8aA	99.1	**11bE**	96.1
8aC	96.1	**12aA**	96.4
8aD	97.4	**12aE**	95.0
8aE	97.3	**12bA**	95.6
8bA	98.5	**13aA**	99.4
8bE	96.4	**13bA**	98.8
9aA	95.1	**14bA**	98.7
11aA	98.8	**15bA**	96.0
11aE	95.9		

Spectroscopic Data of final compounds

Compound **8aC**: Prepared from **7aC** as a yellow syrup; Yield = 88%; ^{1}H NMR (400 MHz, $CDCl_3$) δ 8.55 (s, 2H), 8.40 (d, *J* = 9.0 Hz, 2H), 7.48 (d, *J* = 9.0 Hz, 2H), 7.41–7.39 (m, 6H), 7.33–7.24 (m, 11H), 6.84 (d, *J* = 8.6 Hz, 2H), 6.73 (d, *J* = 9.0 Hz, 2H), 6.61 (d, *J* = 8.6 Hz, 2H), 5.21–5.17 (m, 1H), 4.49–4.43 (m, 2H), 4.25 (d, *J* = 10.2 Hz, 1H), 4.04–3.97 (m, 2H), 3.87 (dd, *J* = 7.8, 3.1 Hz, 1H), 3.79 (s, 3H), 3.67 (s, 3H), 3.40–3.31 (m, 2H), 3.01 (s, 3H); ^{13}C NMR (100 MHz, $CDCl_3$) δ 163.8, 159.8, 159.7, 157.5, 143.3, 137.4, 136.0, 130.5, 130.4, 130.0, 129.8, 129.3, 129.1, 128.8, 128.5, 128.3, 127.6, 114.2, 113.9, 87.8, 80.7, 80.1, 76.1, 75.2, 71.2, 63.4, 55.5, 55.3, 39.2; LRMS (ESI) *m/z* calculated for $C_{50}H_{47}ClN_2O_8S$ $[M+H]^+$: 871.28; found: 871.28.

Compound **8aD**: Prepared from **7aD** as a clear syrup; Yield = 85%; ^{1}H NMR (400 MHz, $CDCl_3$) δ 8.38 (d, *J* = 2.0 Hz, 1H), 8.25 (d, *J* = 2.3 Hz, 1H), 7.42–7.39 (m, 6H), 7.33–7.22 (m, 11H), 6.83 (d, *J* = 9.0 Hz, 2H), 6.73 (d, *J* = 8.6 Hz, 2H), 6.56 (d, *J* = 8.6 Hz, 2H), 6.48 (s, 1H), 5.18–5.15 (m, 1H), 4.44–4.41 (m, 2H), 4.27 (d, *J* = 10.6 Hz, 1H), 4.11–4.03 (m, 2H), 3.88 (dd, *J* = 7.8, 3.1 Hz, 1H), 3.78 (s, 3H), 3.72 (s, 3H), 3.42–3.32 (m, 2H), 3.00 (s, 3H), 2.53 (s, 3H); ^{13}C NMR (100 MHz, $CDCl_3$) δ 159.7, 159.6, 155.9, 149.9, 149.3, 143.3, 133.7, 130.4, 130.3, 129.2, 128.7, 128.5, 128.3, 127.6, 118.5, 114.1, 113.8, 96.4, 87.8, 80.7, 80.0, 75.8, 75.1, 71.0, 63.3, 55.5, 55.3, 39.2, 14.8; LRMS (ESI) m/z calculated for $C_{47}H_{47}N_3O_8S$ $[M+H]^+$: 814.32; found: 814.27.

Compound **8aE**: Prepared from **7aE** as a white solid; Yield = 99%; ^{1}H NMR (400 MHz, $CDCl_3$) δ 7.38–7.35 (m, 6H), 7.31–7.23 (m, 9H), 7.16–7.10 (m, 6H), 6.80 (d, *J* = 8.6 Hz, 2H), 6.73 (d, *J* = 8.6 Hz, 2H), 4.69 (d, *J* = 10.6 Hz, 1H), 4.59–4.56 (m, 1H), 4.41–4.36 (m, 2H), 4.32 (d, *J* = 5.1 Hz, 1H), 4.24–4.17 (m, 2H), 3.81 (s, 3H), 3.78 (s, 3H), 3.73 (s, 3H), 3.40 (dd, *J* = 11.3, 2.3 Hz, 1H), 2.91–2.87 (m, 4H); ^{13}C NMR (100 MHz, $CDCl_3$) δ 159.4, 159.3, 143.4, 139.8, 130.4, 130.3, 130.2, 130.1, 129.4, 128.7, 128.2, 127.4, 118.0, 114.0, 113.8, 87.0, 82.8, 80.4, 75.4, 71.9, 69.3, 63.5, 55.43, 55.40, 39.2, 38.6; LRMS (ESI) *m/z* calculated for $C_{44}H_{46}N_2O_8S$ $[M+H]^+$: 763.30; found: 763.22.

Compound **8bA**: Prepared from **7bA** as a white solid; Yield = 75%; ^{1}H NMR (500 MHz, $CDCl_3$) δ 8.21 (s, 2H), 7.39–7.37 (m, 6H), 7.30–7.22 (m, 9H), 7.14 (d, *J* = 8.8 Hz, 2H), 6.88 (d, *J* = 8.3 Hz, 2H), 6.80 (d, *J* = 8.8 Hz, 2H), 6.68 (d, *J* = 8.8 Hz, 2H), 5.10–5.07 (m, 1H), 4.34 (d, *J* = 4.4 Hz, 1H), 4.27–4.18 (m, 4H), 3.78–3.77 (m, 4H), 3.765 (s, 3H), 3.50 (dd, *J* = 11.0, 2.7 Hz, 1H), 3.28 (dd, *J* = 11.2, 7.3 Hz, 1H), 3.22 (s, 6H), 2.98 (s, 3H); ^{13}C NMR (125 MHz, $CDCl_3$) δ 162.5, 159.4, 157.7, 143.5, 130.3, 130.0, 129.9, 129.5, 128.9, 128.1, 127.4, 117.8, 113.9, 113.8, 87.5, 82.1, 81.5, 76.7, 74.8, 70.5, 63.1, 55.43, 55.38, 39.0, 37.3; LRMS (ESI) *m/z* calculated for $C_{46}H_{49}N_3O_8S$ $[M+H]^+$: 804.33; found: 804.10.

Compound **8bE**: Prepared from **7bE** as a white solid; Yield = 79%; ^{1}H NMR (400 MHz, $CDCl_3$) δ 7.38–7.34 (m, 7H), 7.30–7.18 (m, 10H), 7.13 (d, *J* = 8.6 Hz, 2H), 7.00 (d, *J* = 8.6 Hz, 2H), 6.80 (d, *J* = 8.6 Hz, 2H), 6.75 (d, *J* = 8.6 Hz, 2H), 4.97–4.94 (m, 1H), 4.46–4.38 (m, 3H), 4.33 (d, *J* = 11.0 Hz, 1H), 4.21 (d, *J* = 11.0 Hz, 1H), 3.91 (dd, *J* = 5.5, 3.9 Hz, 1H), 3.82 (s, 3H), 3.78 (s, 3H), 3.77 (s, 3H), 3.42–3.39 (m, 1H), 3.34–3.29 (m, 1H), 2.96 (s, 3H); ^{13}C NMR (100 MHz, $CDCl_3$) δ 159.32, 159.26, 143.5, 139.0, 130.3, 130.1, 130.0, 129.7, 129.6, 128.9, 128.1, 127.3, 118.8, 113.8, 113.7, 87.4, 82.9, 82.4, 77.4, 74.9, 73.2, 70.3, 62.7, 55.4, 39.2, 38.8; LRMS (ESI) *m/z* calculated for $C_{44}H_{46}N_2O_8S$ $[M+H]^+$: 763.30; found: 763.58.

Compound **11aE**: Prepared from **10aE** as a white solid; Recovery yield = 88% (Conversion = 0.75); ^{1}H NMR (400 MHz, $CDCl_3$) δ 7.44–7.40 (m, 7H), 7.29–7.20 (m, 10H), 7.11 (d, *J* = 8.6 Hz, 2H), 6.89 (d, *J* = 8.6 Hz, 2H), 6.82 (d, *J* = 8.6 Hz, 2H), 6.72 (d, *J* = 8.6 Hz, 2H), 4.51–4.47 (m, 2H), 4.35 (dd, *J* = 11.0, 5.5 Hz, 2H), 4.13 (d, *J* = 11.0 Hz, 1H), 3.85 (s, 3H), 3.79 (s, 3H), 3.78 (s, 3H), 3.67 (dd, *J* = 7.0, 4.7 Hz, 1H), 3.47–3.40 (m, 2H), 3.31–3.26 (m, 1H); ^{13}C NMR (100 MHz, $CDCl_3$) δ 159.30, 159.25, 143.9, 139.8, 130.5, 130.3, 130.2, 130.0, 129.3, 128.9, 128.0, 127.2, 118.3, 113.9, 113.7, 87.3, 80.2, 74.5, 74.3, 70.2, 64.0, 63.4, 55.47, 55.45, 39.2; LRMS (ESI) *m/z* calculated for $C_{43}H_{43}N_5O_5$ $[M+H]^+$: 710.33; found: 710.43.

Compound **11bA**: Prepared from **10bA** as a white solid; ^{1}H NMR (400 MHz, $CDCl_3$) δ 8.21 (s, 2H), 7.39–7.37 (m, 6H), 7.29–7.19 (m, 9H), 7.06–7.03 (m, 4H), 6.79–6.74 (m, 4H), 4.58–4.49 (m, 2H), 4.25 (d, *J* = 6.3 Hz, 1H), 4.22 (d, *J* = 11.0 Hz, 1H), 3.93 (d, *J* = 11.0 Hz, 1H), 3.77 (s, 3H), 3.76 (s, 3H), 3.61 (dd, *J* = 6.3, 4.3 Hz, 1H), 3.34–3.29 (m, 2H), 3.24 (s, 6H), 3.20–3.16 (m, 1H); ^{13}C NMR (100 MHz, $CDCl_3$) δ 162.4, 159.3, 157.5, 143.6, 130.2, 130.0, 129.9, 129.7, 128.7, 128.1, 127.9, 127.3, 118.2, 113.9, 113.8, 87.3, 80.9, 79.1, 75.0, 70.8, 63.6, 62.5, 55.40, 55.36, 37.4; LRMS (ESI) *m/z* calculated for $C_{45}H_{46}N_6O_5$ $[M+H]^+$: 751.36; found: 751.32.

Compound **11bE**: Prepared from **10bE** as a yellow solid; ^{1}H NMR (400 MHz, $CDCl_3$) δ 7.43 (s, 1H), 7.36–7.34 (m, 6H), 7.29–7.20 (m, 10H), 7.10 (d, *J* = 8.2 Hz, 2H), 7.03 (d, *J* = 8.6 Hz, 2H), 6.80 (d, *J* = 8.6 Hz, 2H), 6.75 (d, *J* = 8.6 Hz, 2H), 4.66 (d, *J* = 11.0 Hz, 1H), 4.53 (d, *J* = 7.0 Hz, 1H), 4.47 (d, *J* = 11.0 Hz, 1H), 4.33 (d, *J* = 11.3 Hz, 1H), 4.12 (d, *J* = 11.0 Hz, 1H), 3.91 (s, 3H), 3.79 (s, 3H), 3.78 (s, 3H), 3.59 (dd, *J* = 7.0, 3.1 Hz, 1H), 3.37–3.33 (m, 1H), 3.23–3.16 (m, 2H); ^{13}C NMR (100 MHz, $CDCl_3$) δ 159.3, 143.7, 138.6, 130.5, 130.4, 130.0, 129.6, 129.5, 128.8, 128.1, 127.3, 119.5, 113.9, 113.8, 87.4, 81.2, 77.4, 75.9, 74.9, 70.8, 63.8, 62.7, 55.47, 55.45, 39.3; LRMS (ESI) *m/z* calculated for $C_{43}H_{43}N_5O_5$ $[M+H]^+$: 710.33; found: 710.23.

Compound **12aE**: Prepared from **10aE** as a slightly yellow syrup; Yield = 99%; ^{1}H NMR (400 MHz, $CDCl_3$) δ 7.49 (s, 1H), 7.35–7.29 (m, 6H), 7.19 (d, *J* = 8.6 Hz, 2H), 7.08 (d, *J* = 8.6 Hz, 2H), 6.85 (d, *J* = 9.0 Hz, 2H), 6.81 (d, *J* = 8.6 Hz, 2H), 4.56–4.51 (m, 3H), 4.49 (s, 2H), 4.44 (d, *J* = 11.3 Hz, 1H), 4.22 (d, *J* = 11.3 Hz, 1H), 3.88 (s, 3H), 3.80-3.78 (m, 7H), 3.66–3.64 (m, 2H), 3.52 (td, *J* = 6.2, 4.1 Hz, 1H); ^{13}C NMR (100 MHz, $CDCl_3$) δ 159.5, 159.4, 139.8, 138.1, 130.42, 130.37, 130.1, 129.5, 129.0, 128.6, 127.9, 127.8, 118.6, 114.0, 113.9, 80.5, 74.6, 73.9, 73.5, 70.1, 69.8, 62.2, 55.5, 39.3, 38.9; LRMS (ESI) *m/z* calculated for $C_{31}H_{35}N_5O_5$ $[M+H]^+$: 558.27; found: 558.17.

Compound **12bA**: Prepared from **10bA** as a slightly yellow syrup; Yield = 92%; ^{1}H NMR (400 MHz, $CDCl_3$) δ 8.28 (s, 2H), 7.35–7.24 (m, 5H), 7.18–7.14 (m, 4H), 6.84–

6.81 (m, 4H), 4.66–4.55 (m, 2H), 4.42–4.37 (m, 4H), 4.16 (d, *J* = 11.3 Hz, 1H), 3.79 (s, 6H), 3.63 (dd, *J* = 6.5, 4.1 Hz, 1H), 3.52–3.42 (m, 2H), 3.37–3.33 (m, 1H), 3.22 (s, 6H); ^{13}C NMR (100 MHz, $CDCl_3$) δ 162.5, 159.50, 159.45, 157.7, 137.7, 130.24, 130.22, 129.92, 129.89, 128.7, 128.1, 128.0, 118.1, 114.0, 113.9, 81.1, 78.8, 75.2, 73.6, 70.6, 69.9, 61.8, 55.48, 55.46, 37.4; LRMS (ESI) *m/z* calculated for $C_{33}H_{38}N_6O_5$ $[M+H]^+$: 599.30; found: 599.17.

Compound **13bA**: Prepared from **10bA** as a yellow syrup; Yield = 94%; ^{1}H NMR (400 MHz, $CDCl_3$) δ 8.29 (s, 2H), 7.19–7.17 (m, 4H), 6.87–6.83 (m, 4H), 4.62–4.54 (m, 2H), 4.45–4.42 (m, 2H), 4.21–4.15 (m, 3H), 3.800 (s, 3H), 3.798 (s, 3H), 3.59–3.57 (m, 1H), 3.54–3.50 (m, 1H), 3.23 (s, 6H), 2.94 (s, 3H); ^{13}C NMR (100 MHz, $CDCl_3$) δ 162.5, 159.71, 159.66, 157.7, 130.4, 130.1, 129.44, 129.41, 117.4, 114.2, 114.1, 80.4, 77.6, 75.0, 70.6, 68.8, 61.0, 55.49, 55.46, 37.6, 37.4; LRMS (ESI) *m/z* calculated for $C_{27}H_{34}N_6O_7S$ $[M+H]^+$: 587.23; found: 587.38.

Compounds **14bA**: White solid. ^{1}H NMR (400 MHz, $CDCl_3$) δ 8.29 (s, 2H), 7.22 (d, *J* = 8.6 Hz, 2H), 7.17 (d, *J* = 8.6 Hz, 2H), 7.02 (d, *J* = 8.6 Hz, 2H), 6.86 (d, *J* = 8.6 Hz, 2H), 6.83 (d, *J* = 8.6 Hz, 2H), 6.75 (d, *J* = 9.0 Hz, 2H), 4.49–4.42 (m, 4H), 4.30–4.27 (m, 1H), 4.21–4.14 (m, 2H), 3.97–3.92 (m, 1H), 3.782 (s, 3H), 3.777 (s, 3H), 3.77 (s, 3H), 3.54 (d, *J* = 4.3 Hz, 2H), 3.51 (dd, *J* = 7.4, 3.1 Hz, 1H), 3.22 (s, 6H), 2.68 (d, *J* = 5.5 Hz, 1H); ^{13}C NMR (100 MHz, $CDCl_3$) δ 162.3, 159.53, 159.46, 159.4, 157.7, 130.3, 130.1, 130.0, 129.9, 129.8, 129.6, 118.2, 113.99, 113.97, 113.8, 81.2, 76.1, 74.2, 73.2, 70.7, 70.4, 70.2, 55.40, 55.39, 55.3, 37.4; LRMS (ESI) m/z calculated for $C_{34}H_{41}N_3O_7$ $[M+H]^+$: 604.30; found: 604.04.

Compounds **15bA**: Clear Syrup. ^{1}H NMR (500 MHz, $CDCl_3$) δ 8.26 (s, 2H), 7.21 (d, *J* = 8.3 Hz, 2H), 7.18 (d, *J* = 8.3 Hz, 2H), 7.06 (d, *J* = 8.3 Hz, 2H), 6.86 (d, *J* = 8.8 Hz, 2H), 6.81 (d, *J* = 8.3 Hz, 2H), 6.76 (d, *J* = 8.8 Hz, 2H), 4.96–4.93 (m, 1H), 4.46 (d, *J* = 11.2 Hz, 1H), 4.41–4.39 (m, 3H), 4.36–4.29 (m, 2H), 4.23 (d, *J* = 10.8 Hz, 1H), 3.84–3.81 (m, 2H), 3.78 (s, 3H), 3.763 (s, 3H), 3.756 (s, 3H), 3.70 (dd, *J* = 11.2, 6.8

Hz, 1H), 3.22 (s, 6H), 2.93 (s, 3H); ^{13}C NMR (100 MHz, $CDCl_3$) δ 162.4, 159.51, 159.45, 159.4, 157.7, 130.3, 130.0, 129.70, 129.67, 129.65, 129.4, 117.7, 114.0, 113.9, 113.8, 82.3, 81.4, 76.8, 74.9, 73.1, 70.6, 68.7, 55.39, 55.36, 55.3, 38.7, 37.3; LRMS (ESI) m/z calculated for $C_{35}H_{43}N_3O_9S$ $[M+H]^+$: 682.28; found: 682.15.

국문초록

화학생물학의 주된 과제 중의 하나는 생리활성이 있는 새로운 저분자 화합물을 발굴하는 것이다. 이 화합물들은 복잡한 생명현상을 이해하기 위한 도구로, 더 나아가 다양한 질병의 치료를 위한 의약품으로 개발될 수 있다. 생리활성 저분자 화합물을 찾는 과정은 크게 두 가지로 나누어볼 수 있다.

표적 기반 스크리닝 방법에서는 특정 질병에 중요한 역할을 한다고 밝혀진 표적을 설정하고, 저분자 화합물들이 그 표적의 기능에 어떠한 영향을 미치는지 살펴보는 생화학적 분석을 통해 유효화합물들을 발굴하게 된다. 그리고 이 화합물들이 실제로 세포, 혹은 개체 수준에서 원하는 표현형의 변화를 일으키는지 판별하는 과정을 거치게 된다. 이와는 반대로 표현형 기반 스크리닝 방법에서는 특정 질병 모델과 관련된 표현형을 먼저 선정하고, 이 표현형의 변화를 일으키는 화합물들을 선별하는 스크리닝을 거치게 된다. 이어서 유효화합물들의 표적 단백질을 찾아내면 화합물의 작용 메커니즘을 파악하고 효능이 개선된 화합물을 설계할 수 있게 된다.

위의 두 가지 스크리닝 방법이 가지는 장점을 상황에 맞게 조합함으로써 원하는 생리활성이 있는 화합물을 효율적으로 찾을 수 있다. 그런데 어떠한 방법을 사용하더라도 생리활성 화합물 도출을 위해 가장 먼저 확보되어야 하는 것은 적절한 화학적 공간을 점유하는 저분자 화합물 라이브러리이다. 따라서 본 논문의 Chapter 1 에서는 새로운 구조의 저분자 화합물 라이브러리를 확보하기 위한 전략을 제시하였다.

단백질–단백질 상호작용을 비롯해 새롭게 제시되는 질병관련 타겟을 조절하기 위해서는 기존의 전형적인 라이브러리 설계 전략을 뛰어넘는 새로운 접근법이 필요하다. 이에 따라 본 연구에서는 한 분자 안에 두

가지의 독점적 구조가 독립적으로 존재하는 융합분자의 개념을 제시하였다. 구체적으로는 분자의 한 쪽 부분에 pyrimidine, pyrazole 혹은 pyrazolopyrimidine 이, 반대쪽 부분에는 fused-triazole 이 각각 별개로 존재하는 융합분자 화합물 라이브러리를 확보하였다. 먼저 2-*C*-formyl glycal 과 여러가지 dinucleophie 사이의 축합반응을 통해 pyrimidine, pyrazole 및 pyrazolopyrimidine 이 포함된 carbohybrid 를 합성하였다. 이후 carbohybrid 에 존재하는 polyol 작용기의 반응을 이용하여 azide 와 alkyne 작용기가 포함된 중간체를 다양하게 확보하였다. 그리고 분자내 1,3-dipolar cycloaddition 반응을 거쳐 fused-triazole 을 형성함으로써 최종적으로 하나의 분자 안에 두 가지의 독립된 중심골격이 존재하는 융합분자를 만들어 내었다. 다음으로 각 중심골격을 연결하는 linker 에 존재하는 stereodivergent diol 작용기의 반응을 통해 중심골격의 배향을 다양하게 만들어 주어 3 차원적 분자 모양의 다양성을 확보하였다. 마지막으로 계산화학적 방법을 통해 분자들의 3 차원적 다양성을 검증하여 본 연구에서 제시한 라이브러리 구축 전략이 유효함을 확인하였다.

Chapter 2 에서는 표적 기반 스크리닝 방법을 통해 항암 물질을 발굴하기 위한 시도를 진행하였다. 구체적으로, 단백질–miRNA 상호작용의 일종인 Lin28–*let-7* 상호작용을 관찰하는 새로운 방법를 개발하고, 이를 이용해 flavone 기반 Lin28–*let-7* 상호작용 저해제를 발굴한 연구를 서술하였다.

miRNA 는 세포 내에서 유전자 발현을 조절하는 매우 중요한 역할을 담당하며, miRNA 의 생성 및 작용이 제대로 제어되지 않을 경우 다양한 질병이 발생한다. *Let-7* miRNA family 는 암 억제 기능을 가진 것으로 알려져 있는데, Lin28 단백질은 *let-7* miRNA 의 전구체에 결합하여 mature *let-7* 이 생성되는 것을 방해한다. 따라서 Lin28–*let-7* 상호작용을

저해하는 것은 새로운 항암 전략이 될 수 있다. 본 연구에서는 FRET 메커니즘에 기반하여 Lin28–*let-7* 상호작용을 관찰할 수 있는 고효율 스크리닝 방법을 개발하였다. 비천연 아미노산의 도입 및 위치선택적인 단백질 형광표지를 통해 높은 FRET 효율 및 정확도를 보이는 스크리닝 시스템을 구축할 수 있었다. 이를 바탕으로 Lin28–*let-7* 상호작용을 저해하는 플라본 구조의 천연물을 발굴해 내었고, 이 화합물들이 Lin28 과 결합함으로써 활성을 띄게 된다는 사실을 밝혀내었다.

Chapter 3 에서는 표현형 기반 고집적, 고효율 스크리닝 시스템을 통해 발굴한 2-aminopyrimidine 기반 항 말라리아 물질에 대해 서술하였다.

약물 저항성 말라리아를 치료할 수 있는 차세대 항말라리아 물질을 개발하기 위해서는 말라리아 원충의 무성 적혈구 생활상의 여러단계에 걸쳐 활성을 보이는 화합물을 확보하는 것이 중요하다. 이를 위해 먼저 원충의 적혈구 생활상의 각 단계를 관찰할 수 있는 이미지 기반 고효율, 고집적 스크리닝 방법을 개발하였고, 다음으로 저분자 화합물 라이브러리에 대한 스크리닝을 진행하였다. 그 결과 2-aminopyrimidine 기반 carbohybrid 화합물들이 빠른 작용을 통해 약물저항성 말라리아 원충의 증식을 효과적으로 억제한다는 것을 밝혀내었다. 구조–활성 상관관계 연구를 통해 활성이 좋고 인간 세포 대비 말라리에 원충에 대한 선택성이 높으며, 말라리아에 감염된 쥐에서도 효과를 보이는 화합물 두 가지 (**8aA**, **11aA**)를 최종적으로 발굴해 내었다. 이 화합물들은 말라리아 원충의 무성 적혈구 생활상의 모든 단계에 활성을 가짐으로써 빠른 작용을 보인다는 것을 알 수 있었다.

Appendix

NMR spectra of new compounds in Chapter 1

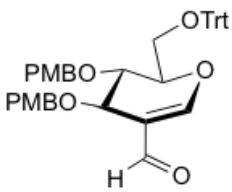

1

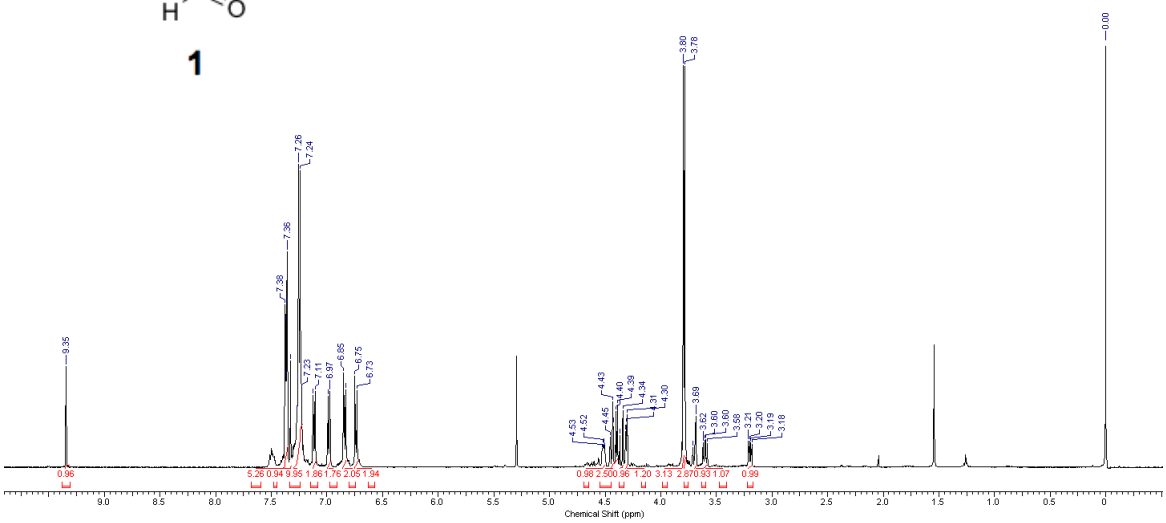

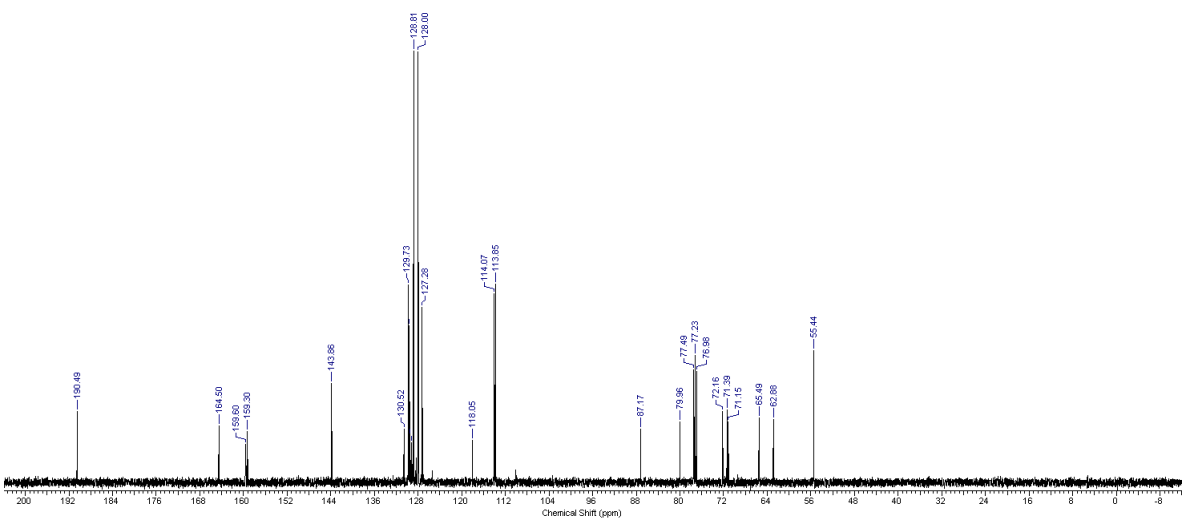

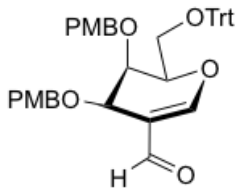
PMBO
OTrt
O
PMBO
H
O

2

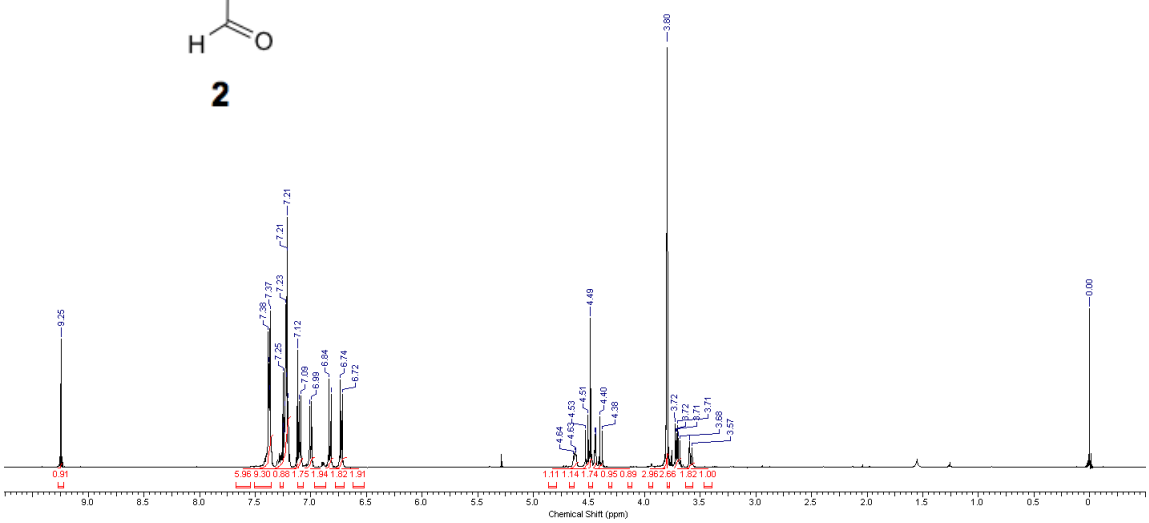
9.25
7.38
7.37
7.23
7.21
7.21
7.12
7.09
6.99
6.84
6.74
6.72
4.64
4.63
4.53
4.51
4.49
4.40
4.38
3.80
3.72
3.72
3.71
3.71
3.68
3.57
0.00
0.91
5.96
9.30
0.88
1.75
1.94
1.82
1.91
1.11
1.14
1.74
0.95
0.89
2.96
2.66
1.82
1.00
Chemical Shift (ppm)

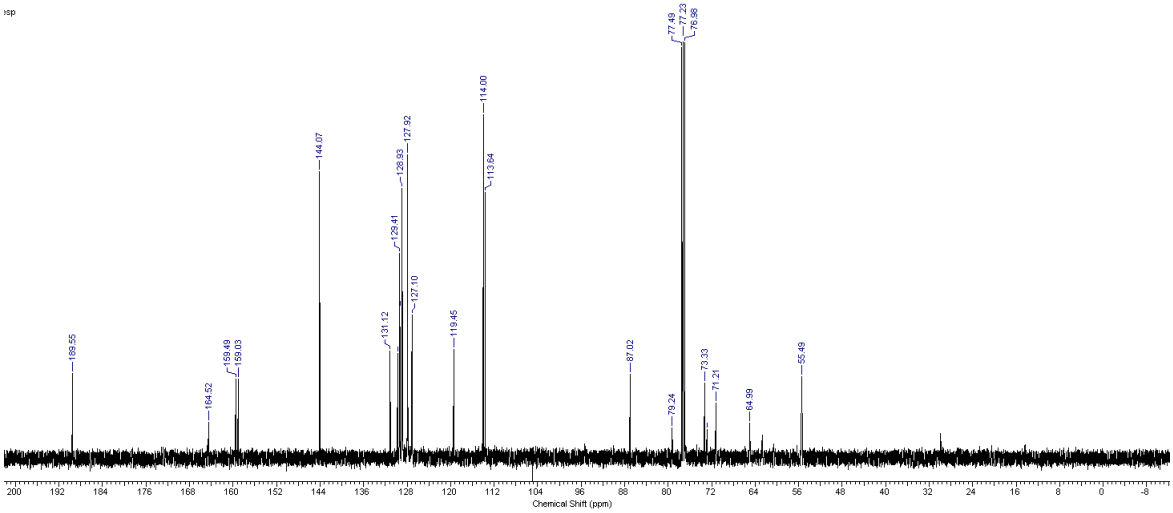
169.55
164.52
159.49
159.03
144.07
131.12
129.41
128.93
127.92
127.10
119.45
114.00
113.64
87.02
79.24
77.49
77.23
76.98
73.33
71.21
64.99
55.49
Chemical Shift (ppm)

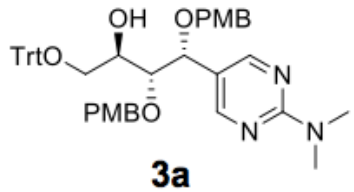
OH
OPMB
TrtO
PMBO
N
N
N

3a

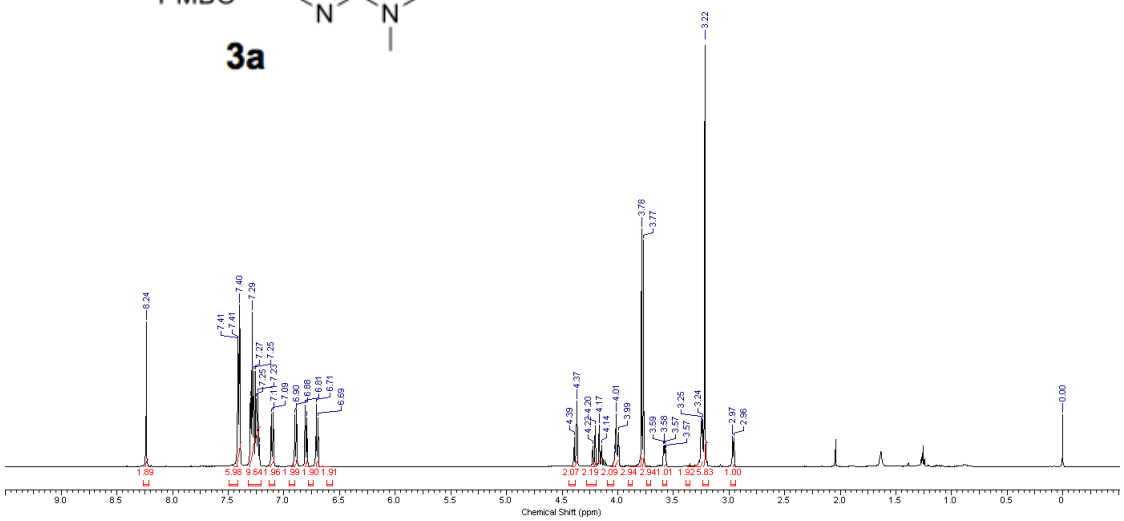
8.24
7.41
7.41
7.40
7.29
7.27
7.25
7.25
7.23
7.10
7.09
6.90
6.88
6.81
6.71
6.69
4.39
4.37
4.22
4.20
4.17
4.14
4.01
3.99
3.78
3.77
3.59
3.58
3.57
3.57
3.25
3.24
3.22
2.97
2.96
0.00
1.89
5.98
9.64
1.96
1.99
1.90
1.91
2.07
2.19
2.09
2.94
2.94
1.01
1.92
5.83
1.00
Chemical Shift (ppm)

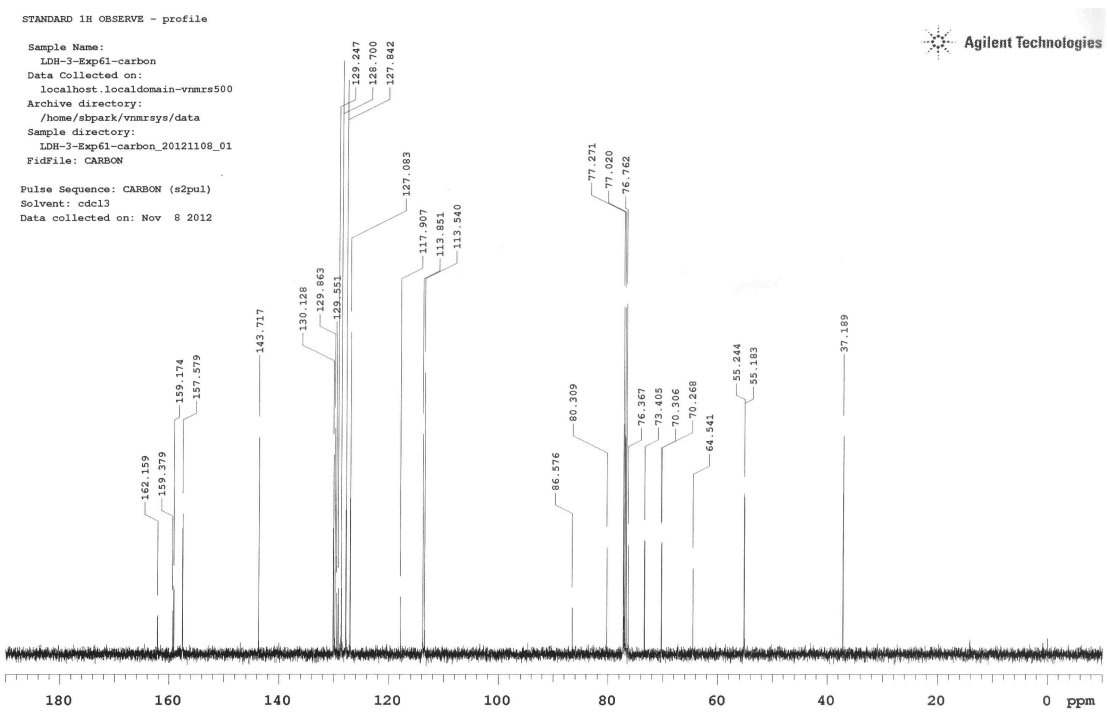
STANDARD 1H OBSERVE - profile
Sample Name:
LDH-3-Exp61-carbon
Data Collected on:
localhost.localdomain-vnmrs500
Archive directory:
/home/sbpark/vnmrsys/data
Sample directory:
LDH-3-Exp61-carbon_20121108_01
FidFile: CARBON
Pulse Sequence: CARBON (s2pul)
Solvent: cdcl3
Data collected on: Nov 8 2012
Agilent Technologies
162.159
159.379
159.174
157.579
143.717
130.128
129.863
129.551
129.247
128.700
127.842
127.083
117.907
113.851
113.540
86.576
80.309
77.271
77.020
76.762
76.367
73.405
70.306
70.268
64.541
55.244
55.183
37.189
ppm

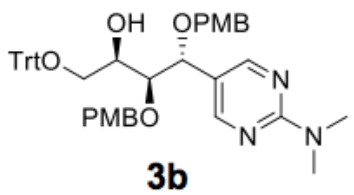

3b

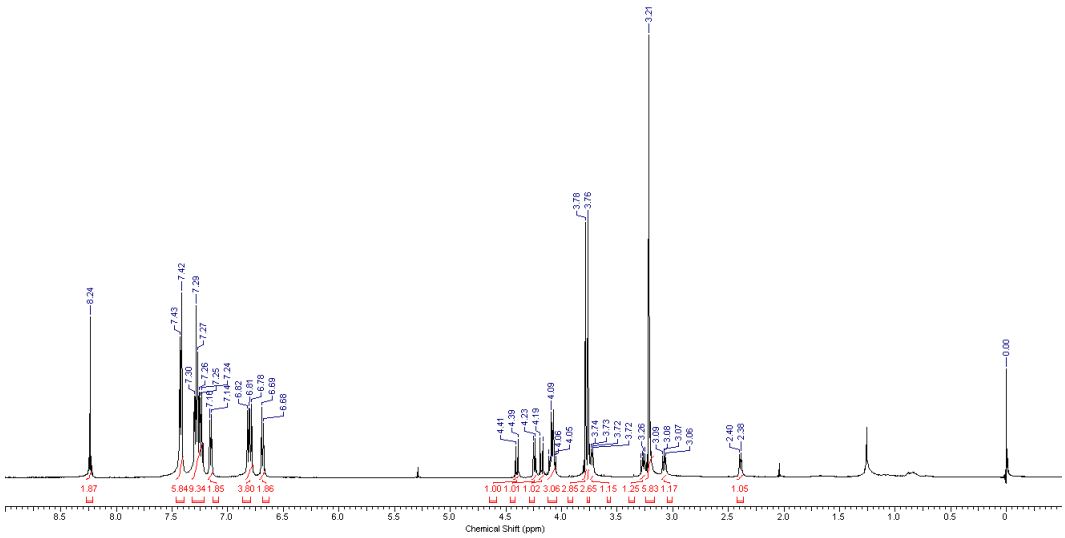

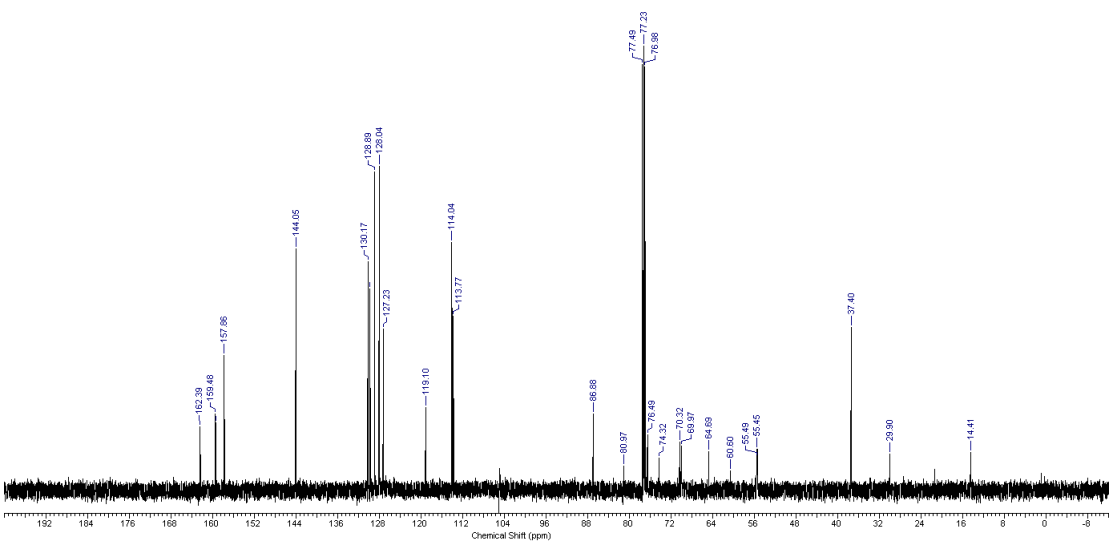

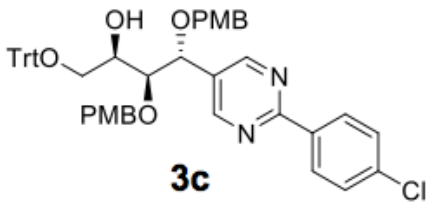
OH
OPMB
TrtO
PMBO
N
N
Cl

3c

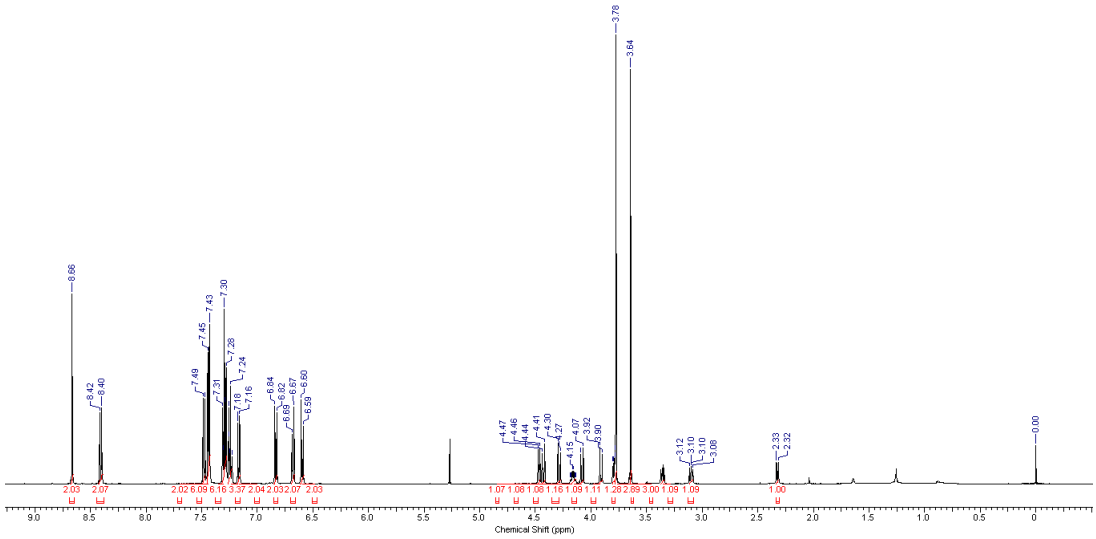
Chemical Shift (ppm)

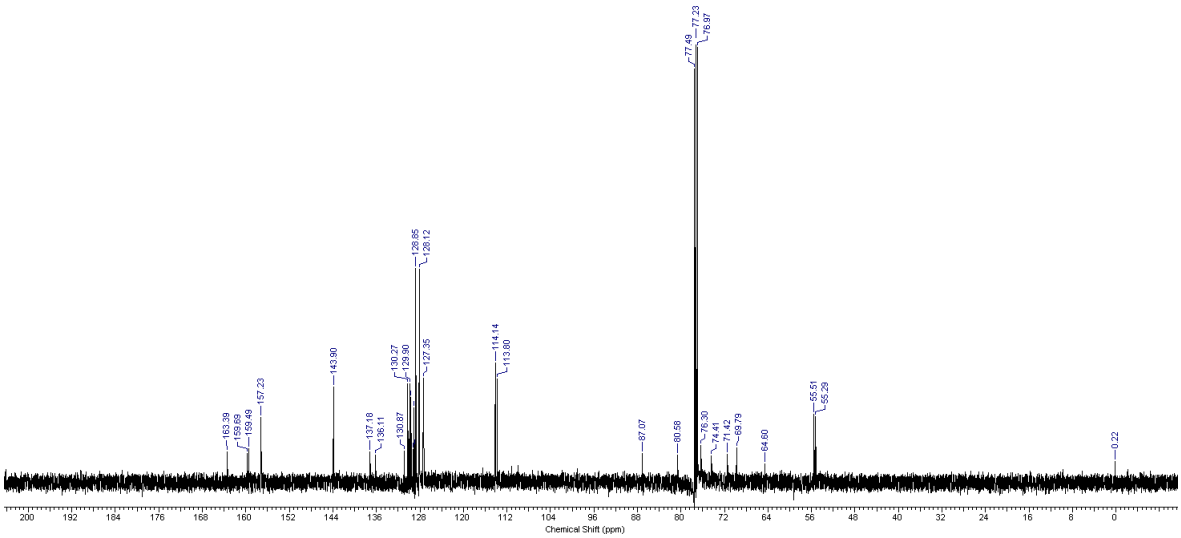
Chemical Shift (ppm)

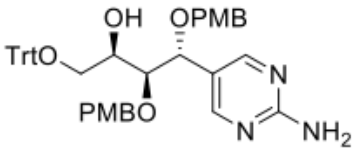
OH
OPMB
TrtO
PMBO
N
N
NH2

3d

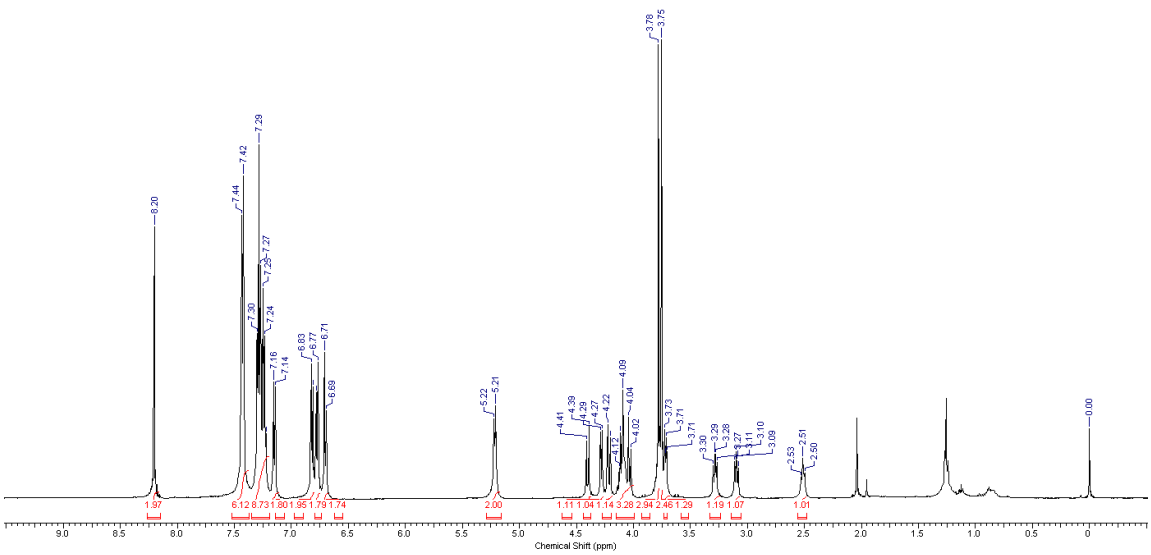
Chemical Shift (ppm)

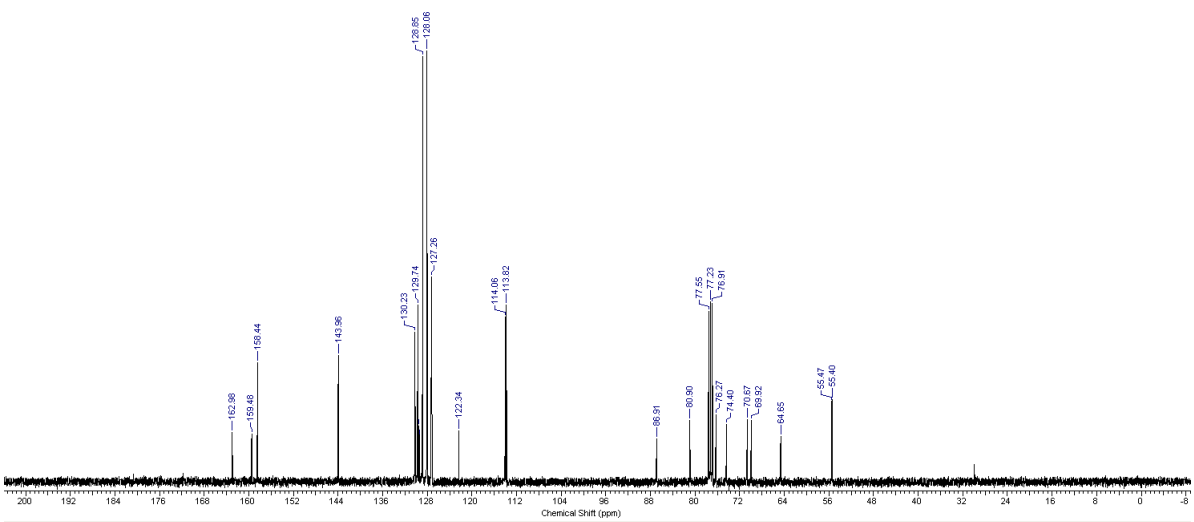
Chemical Shift (ppm)

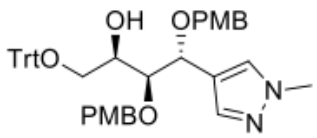

4a

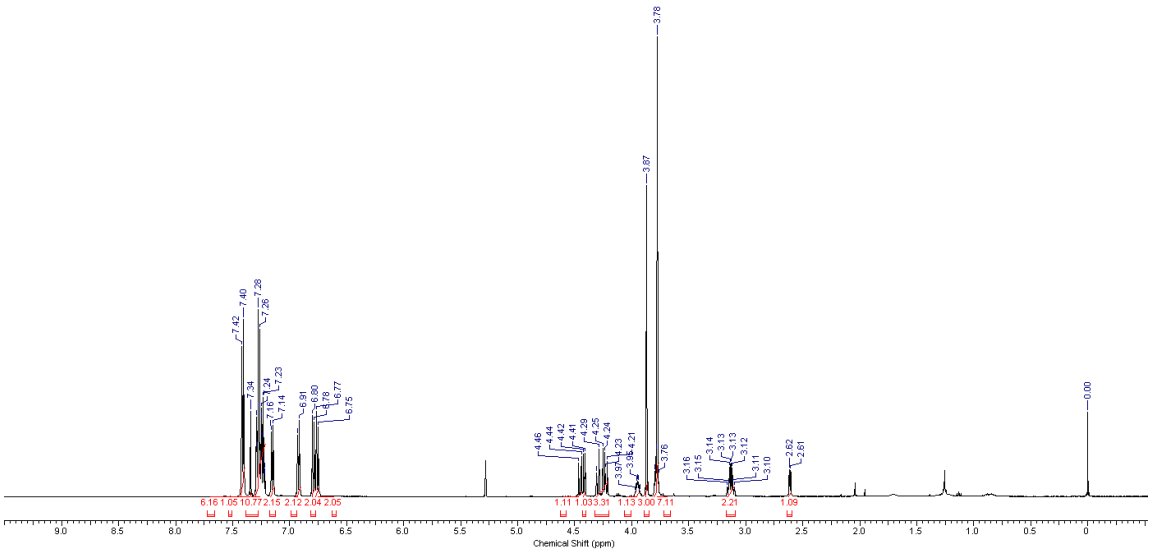

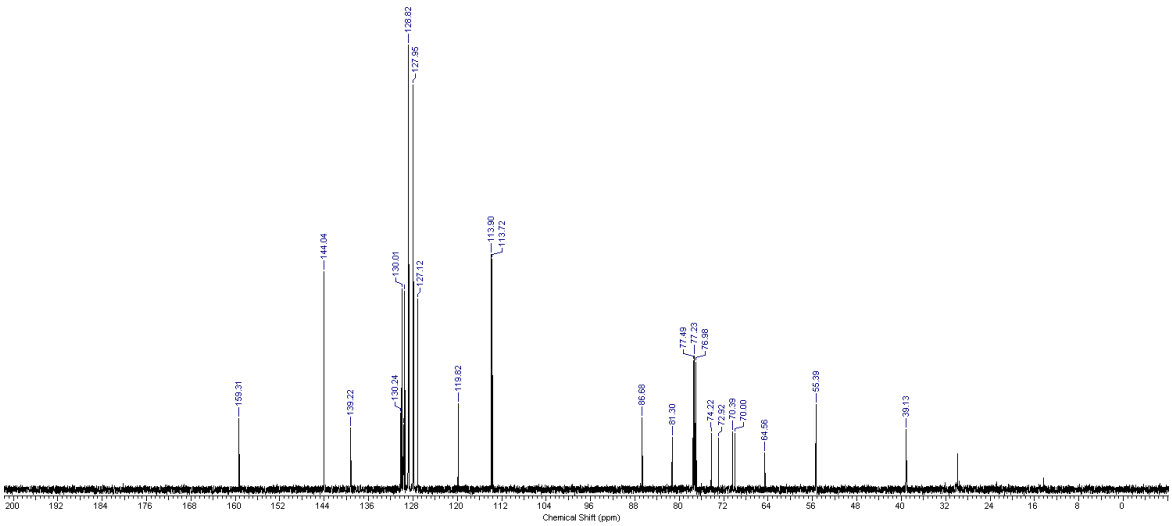

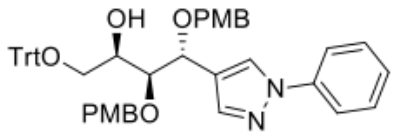

4b

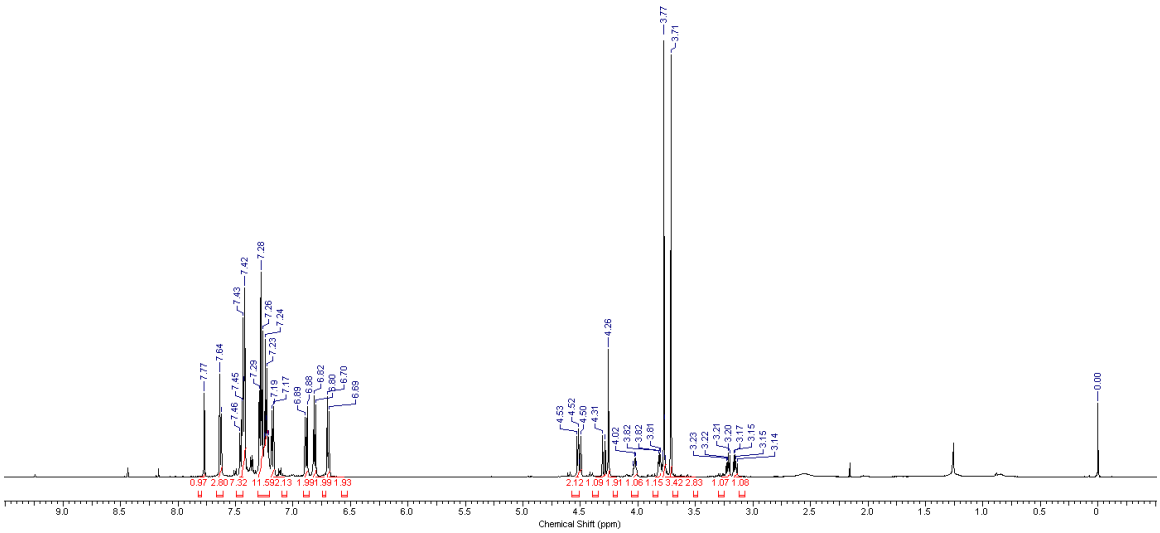

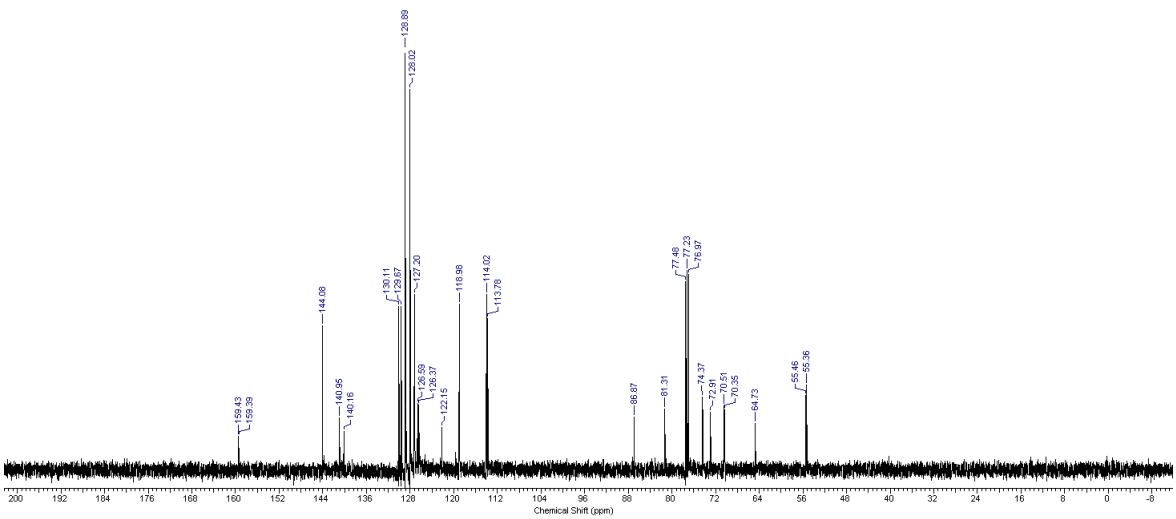

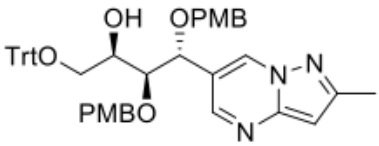

5a

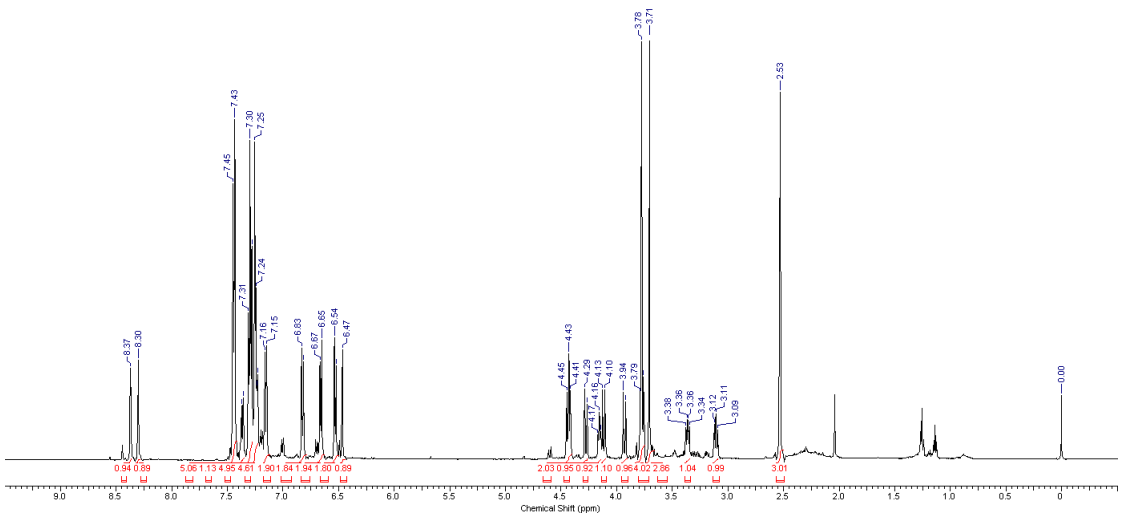

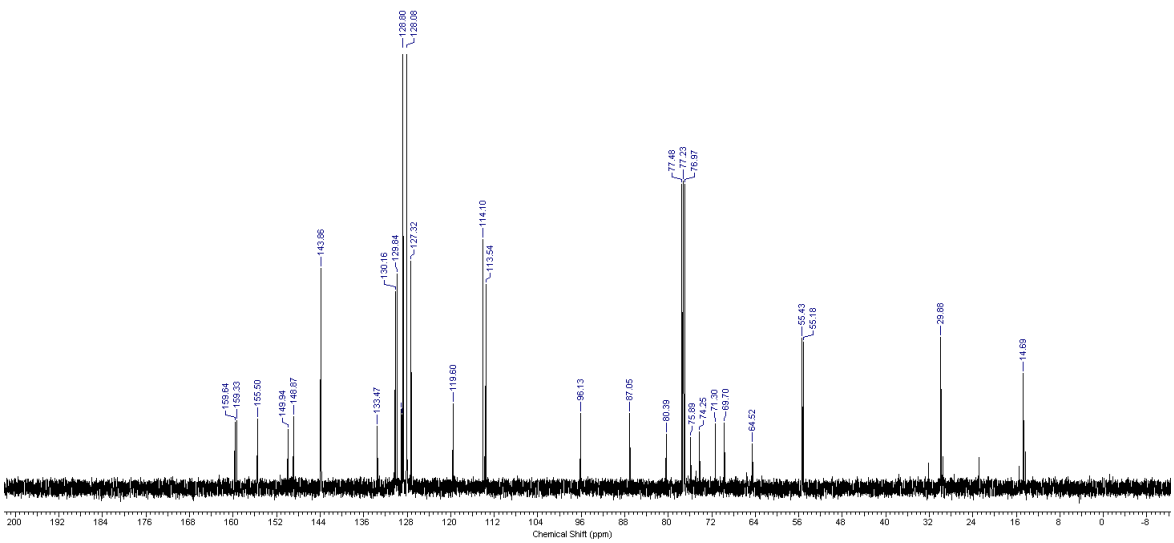

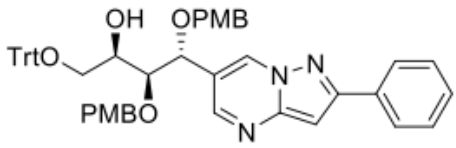

5b

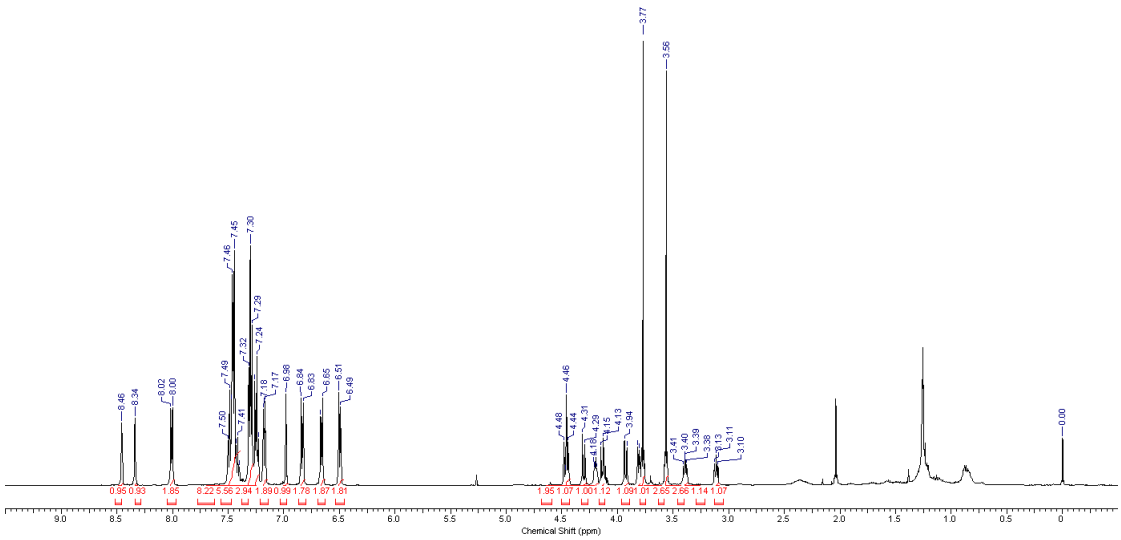

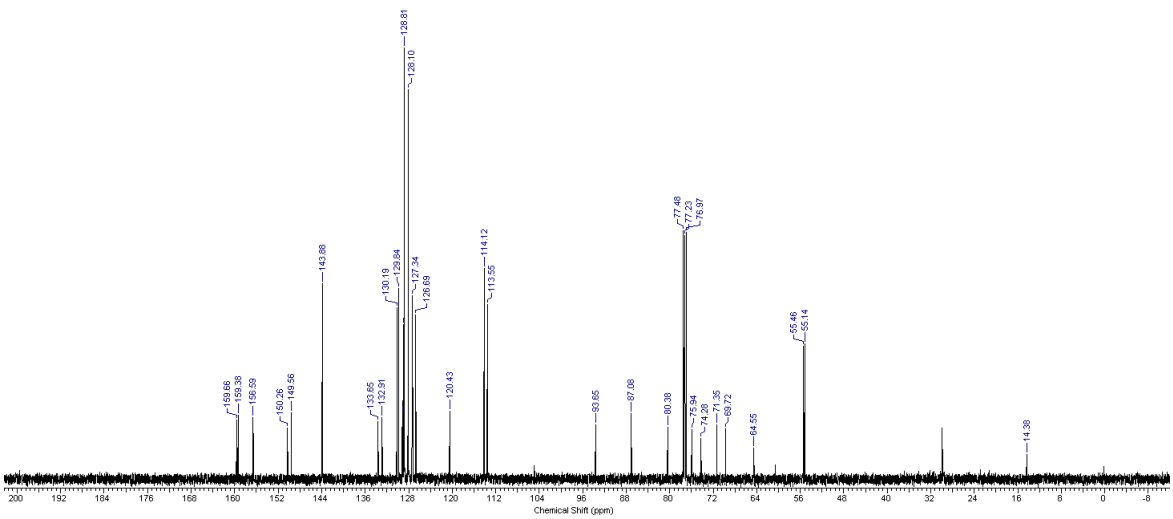

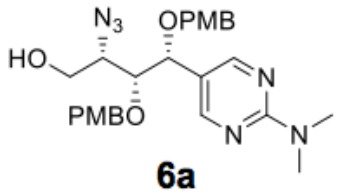
N3
OPMB
HO
PMBO
N
N
N

6a

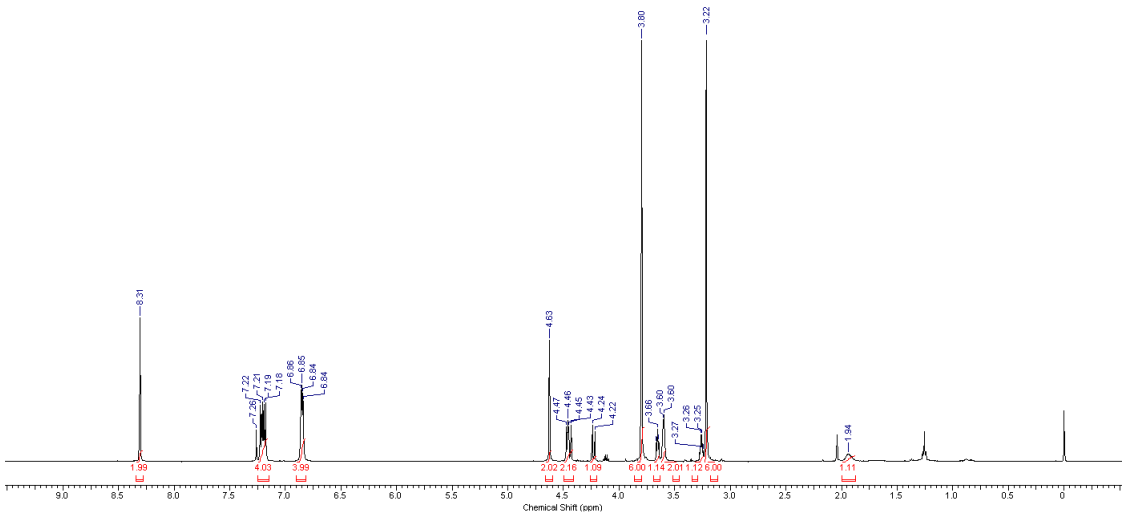
8.31
7.22
7.21
7.19
7.18
6.86
6.85
6.84
6.84
4.63
4.47
4.46
4.45
4.43
4.24
4.22
3.80
3.66
3.60
3.60
3.27
3.26
3.25
3.22
1.94
1.99
4.03
3.99
2.02
2.16
1.09
6.00
1.14
2.01
1.12
6.00
1.11
Chemical Shift (ppm)

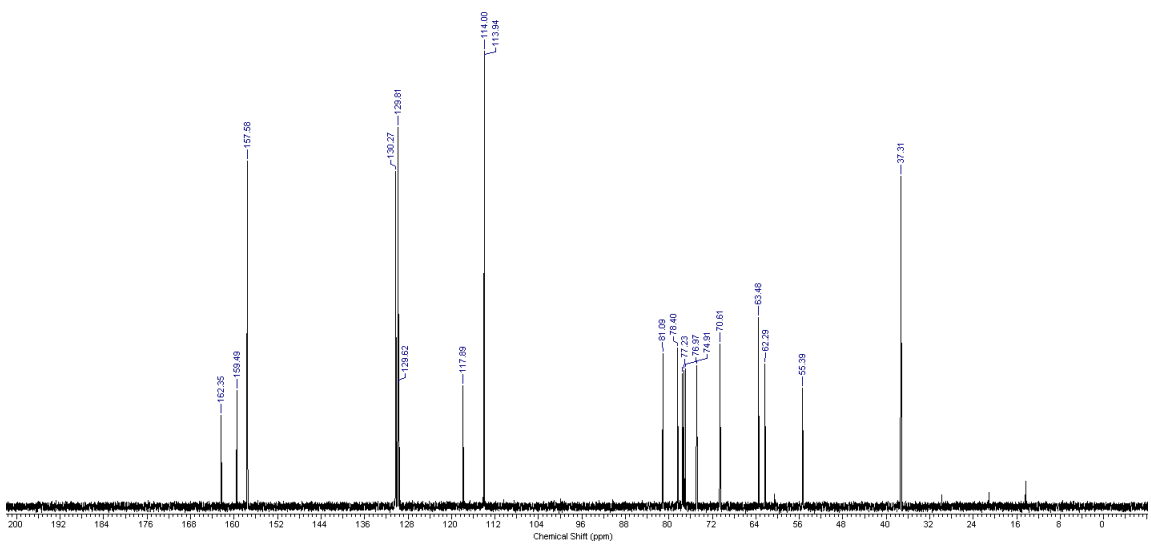
162.35
159.49
157.58
130.27
129.81
129.62
117.89
114.00
113.94
81.09
78.40
77.23
76.97
74.91
70.61
63.48
62.29
55.39
37.31
Chemical Shift (ppm)

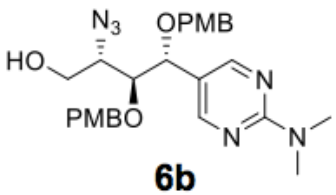
N3
OPMB
HO
PMBO
N
N
N

6b

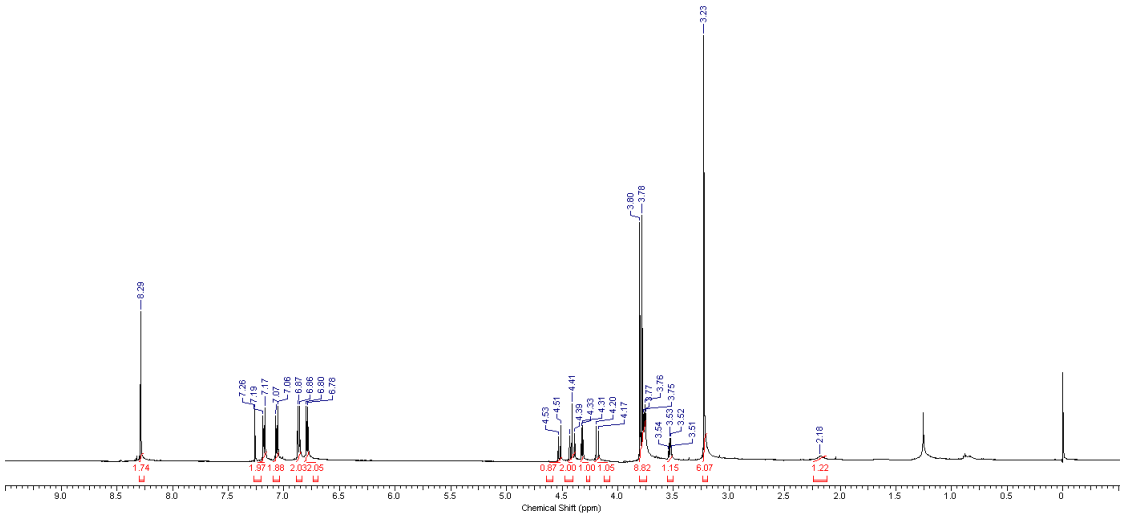
8.29
7.26
7.19
7.17
7.07
7.06
6.87
6.86
6.80
6.78
4.53
4.51
4.41
4.39
4.33
4.31
4.20
4.17
3.80
3.77
3.76
3.75
3.63
3.62
3.54
3.51
3.23
2.16
1.74
1.97
1.88
2.03
2.05
0.87
2.00
1.00
1.05
8.82
1.15
6.07
1.22
Chemical Shift (ppm)

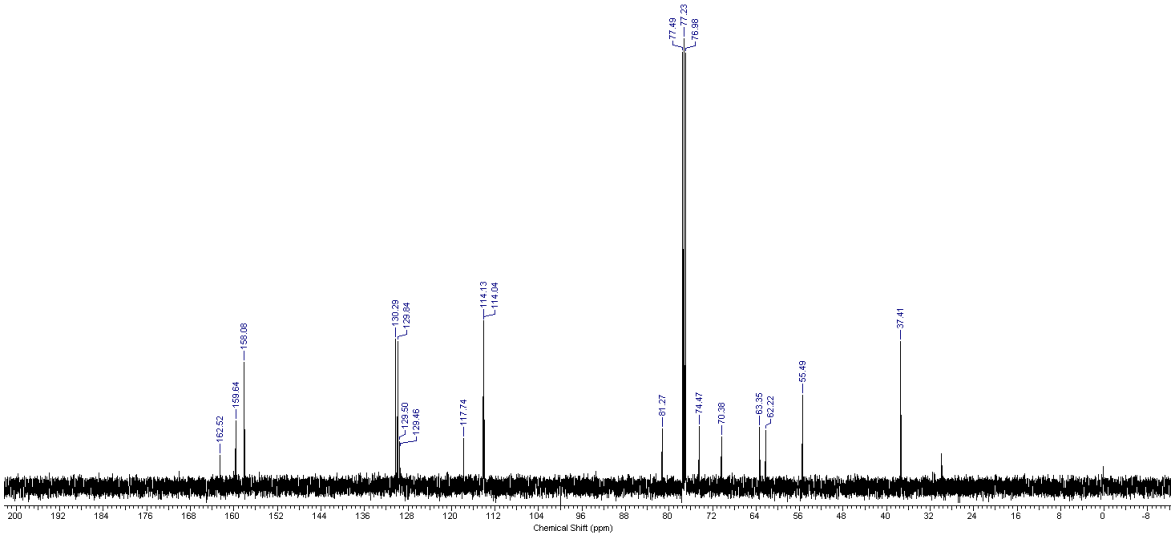
77.49
77.23
76.98
162.52
159.64
158.08
130.29
129.84
129.50
129.46
117.74
114.13
114.04
81.27
74.47
70.38
63.35
62.22
55.49
37.41
Chemical Shift (ppm)

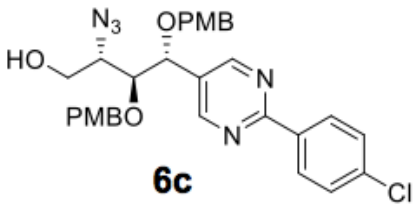
N3
OPMB
HO
PMBO
N
N
Cl

6c

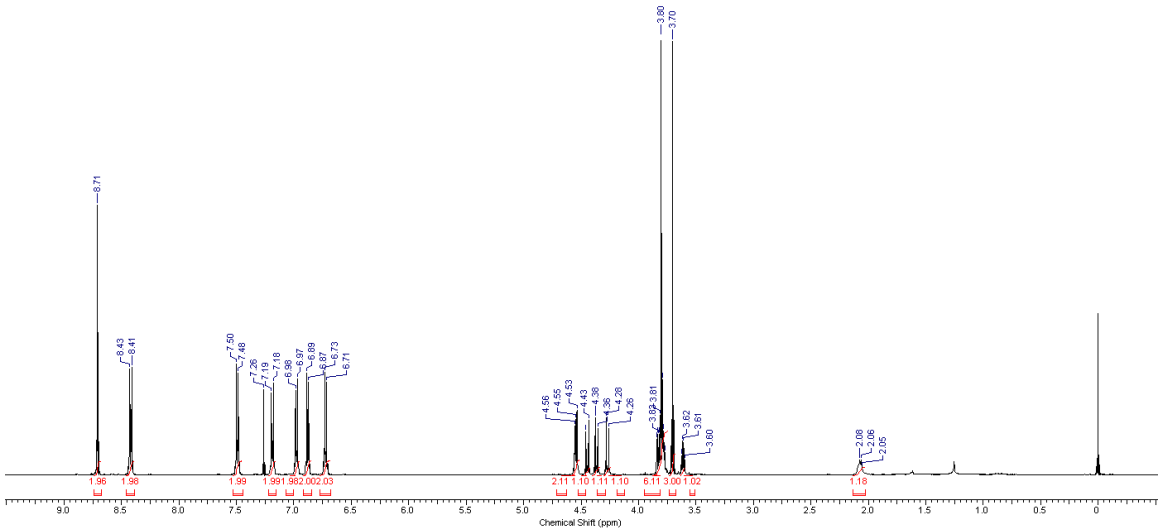
8.71
8.43
8.41
7.60
7.48
7.26
7.19
7.18
6.98
6.97
6.89
6.87
6.73
6.71
4.56
4.55
4.53
4.43
4.38
4.36
4.26
3.81
3.80
3.70
3.62
3.61
3.60
2.08
2.06
2.05
1.96
1.98
1.99
1.99
1.98
2.00
2.03
2.11
1.10
1.11
1.10
6.11
3.00
1.02
1.18
Chemical Shift (ppm)

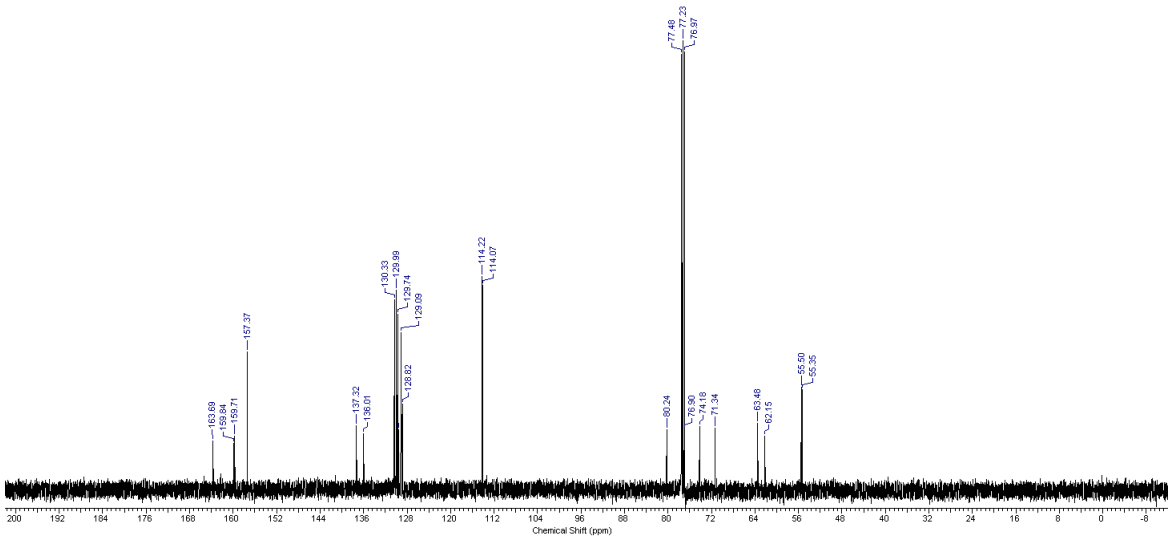
77.46
77.23
76.97
163.69
159.84
159.71
157.37
137.32
136.01
130.33
129.99
129.74
129.09
128.62
114.22
114.07
80.24
76.90
74.18
71.34
63.48
62.15
55.50
55.35
Chemical Shift (ppm)

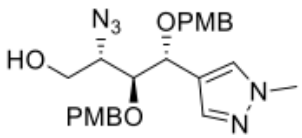
N3
OPMB
HO
PMBO
N
N

7a

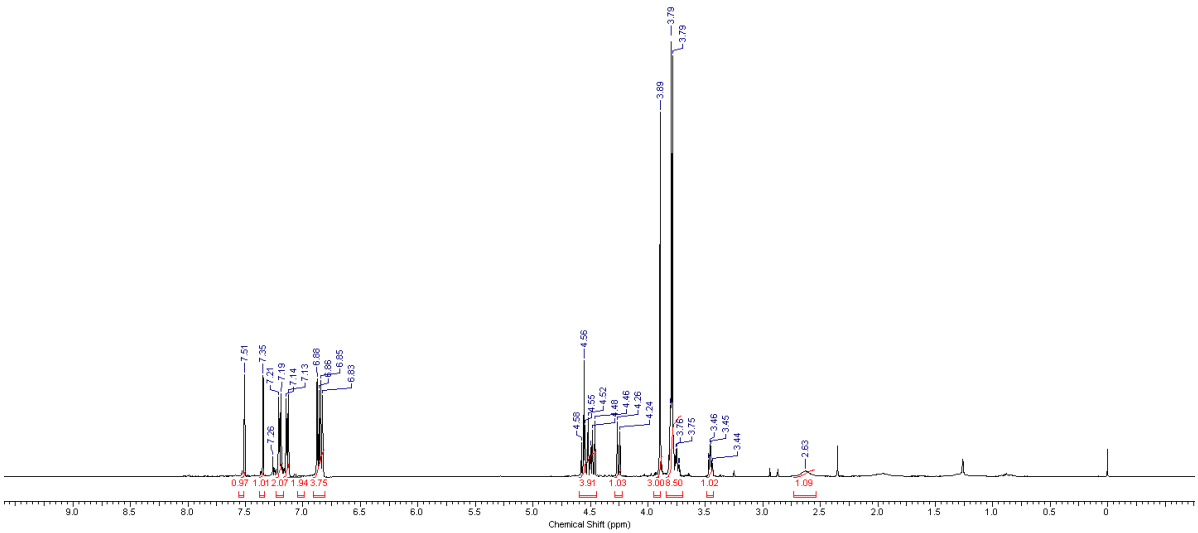
7.51
7.35
7.21
7.19
7.14
7.13
6.88
6.86
6.85
6.83
7.26
4.56
4.55
4.52
4.49
4.46
4.26
4.24
3.79
3.79
3.69
3.76
3.75
3.46
3.45
3.44
2.63
0.97
1.01
2.07
1.94
3.75
3.91
1.03
3.00
8.50
1.02
1.09
Chemical Shift (ppm)

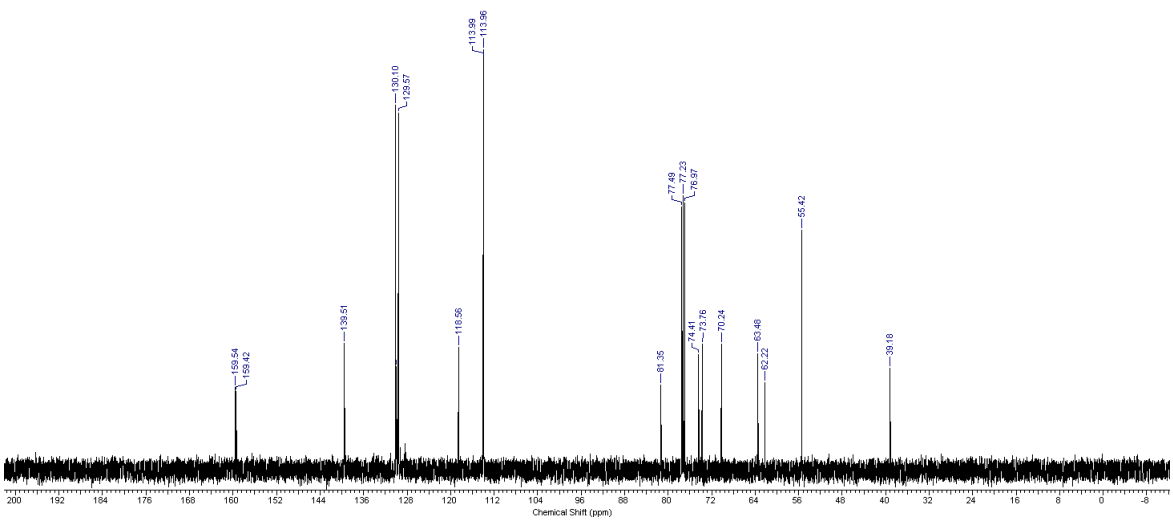
159.54
159.42
139.51
130.10
129.57
118.56
113.99
113.96
77.49
77.23
76.97
74.41
73.16
70.24
63.48
62.22
61.35
55.42
39.18
Chemical Shift (ppm)

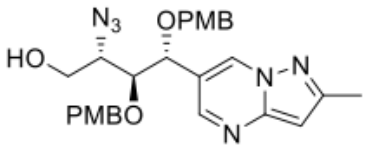
N3
OPMB
HO
PMBO
N
N
N

8a

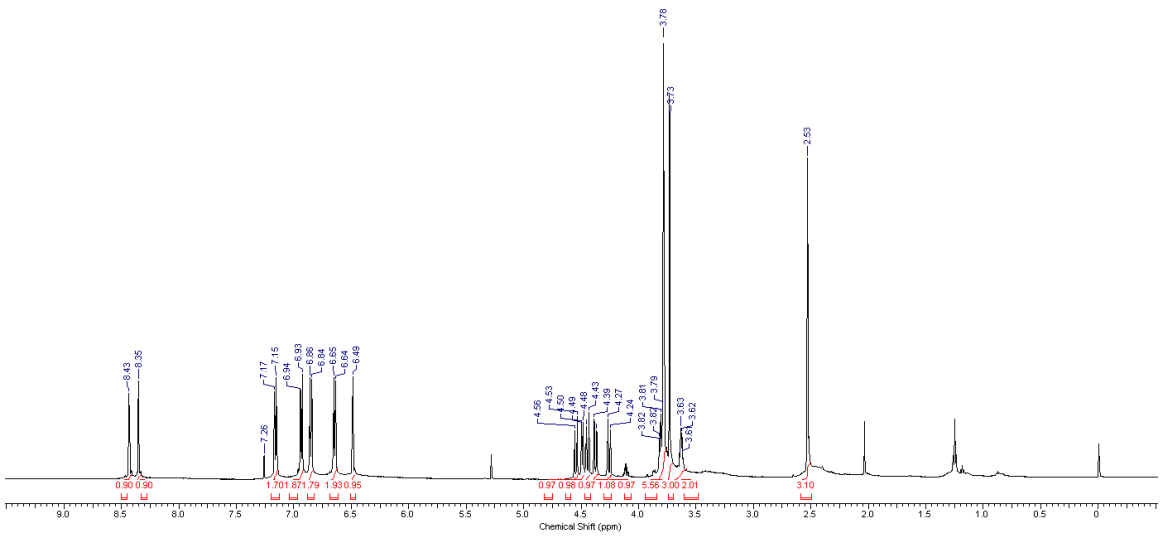
8.43
8.35
7.26
7.17
7.15
6.94
6.93
6.86
6.84
6.65
6.64
6.49
4.56
4.53
4.50
4.49
4.48
4.43
4.39
4.27
4.24
3.82
3.81
3.79
3.78
3.73
3.63
3.62
2.53
0.90 0.90
1.70 1.87 1.79
1.93 0.95
0.97 0.98 0.97 1.08 0.97
5.56 3.00 2.01
3.10
Chemical Shift (ppm)

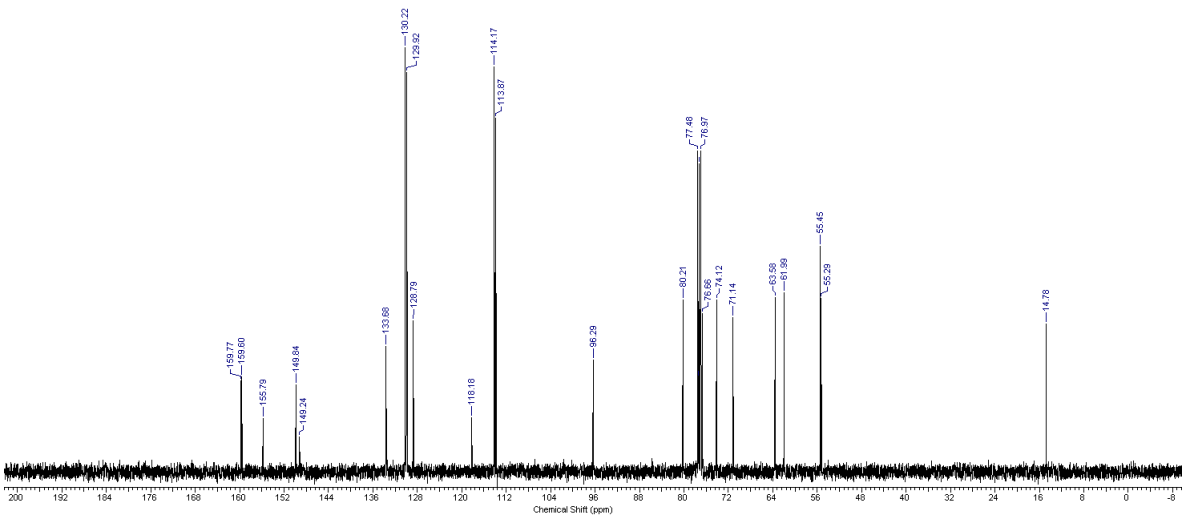
159.77
159.60
155.79
149.84
149.24
133.88
130.22
128.92
128.79
118.18
114.17
113.87
96.29
80.21
77.48
76.97
76.86
74.12
71.14
63.58
61.99
55.45
55.29
14.78
Chemical Shift (ppm)

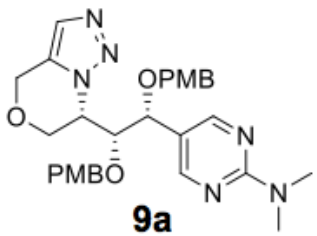
N
N
N
OPMB
O
N
PMBO
N
N

9a

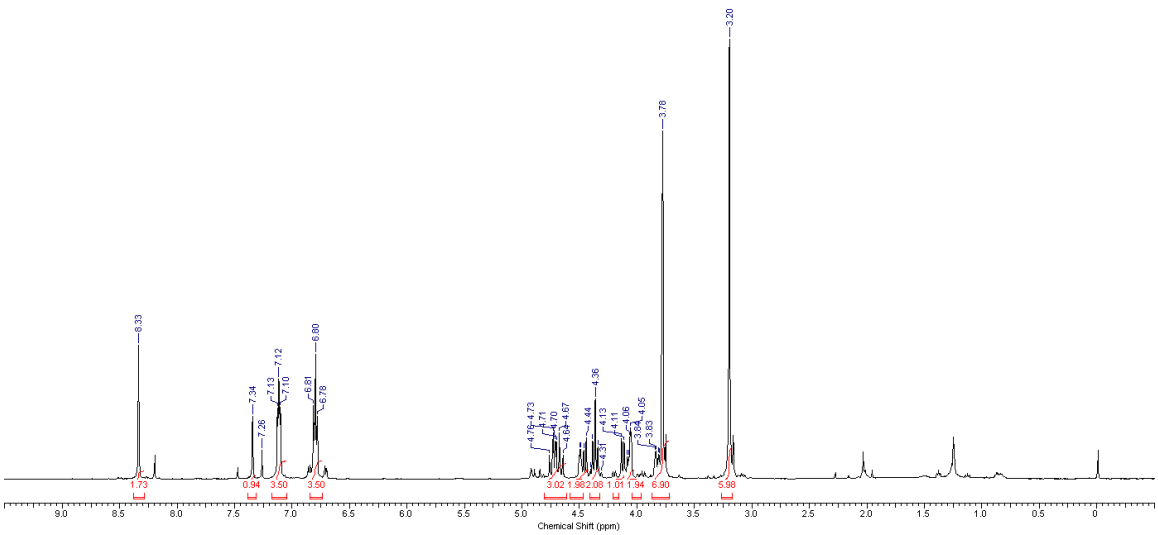
8.33
7.34
7.28
7.13
7.12
7.10
6.81
6.80
6.78
4.76-4.73
4.71
4.70
4.68-4.67
4.44
4.36
4.13
4.11
4.06
4.05
3.84
3.83
3.78
3.20
1.73
0.94
3.50
3.50
3.02
1.95
2.09
1.01
1.94
6.90
5.98
Chemical Shift (ppm)

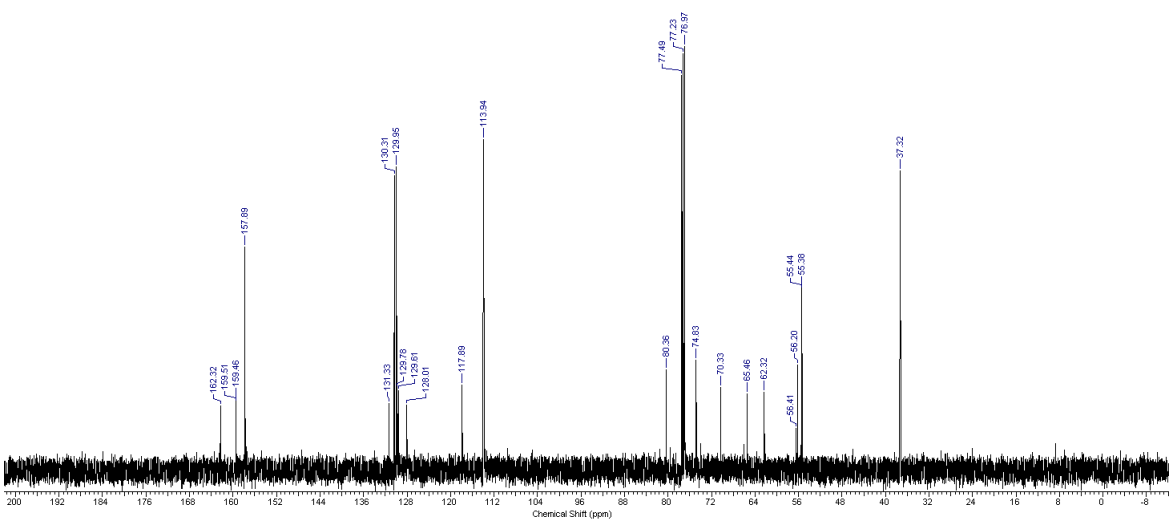
157.89
152.32
150.91
159.46
130.31
129.95
131.33
129.78
129.61
128.01
117.89
113.94
77.49
77.23
76.97
80.36
74.83
70.33
65.46
62.32
56.41
56.20
55.44
55.38
37.32
Chemical Shift (ppm)

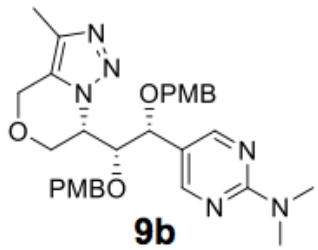
N
N
N
OPMB
O
N
PMBO
N
N

9b

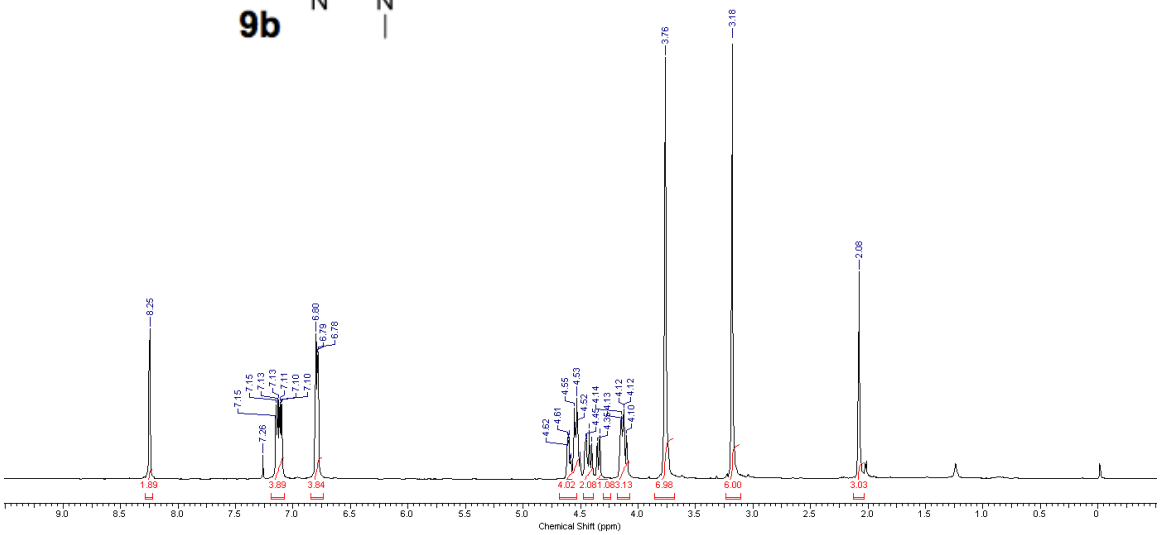
8.25
7.36
7.15
7.15
7.13
7.13
7.11
7.10
7.10
6.80
6.79
6.78
4.62
4.61
4.55
4.53
4.52
4.46
4.45
4.14
4.13
4.12
4.12
4.10
3.76
3.18
2.08
1.89
3.89
3.84
4.02
2.06
1.06
3.13
6.98
6.00
3.03
Chemical Shift (ppm)

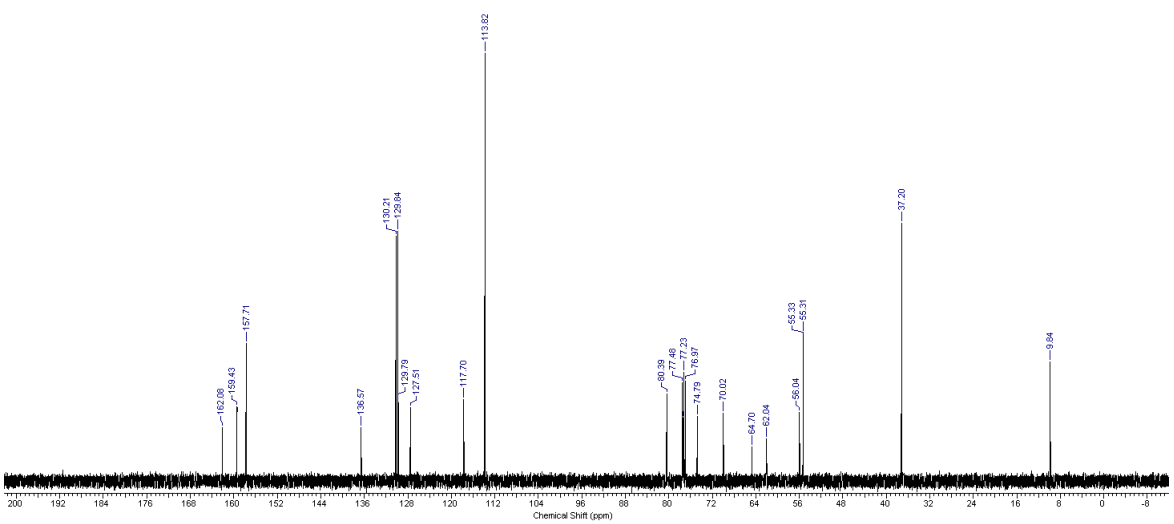
162.08
159.43
157.71
136.57
130.21
129.84
129.79
127.51
117.70
113.62
80.39
77.48
77.23
76.97
74.78
70.02
64.70
62.04
56.04
55.33
55.31
37.20
9.84
Chemical Shift (ppm)

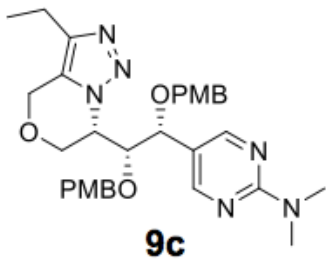
N
N
N
OPMB
O
N
PMBO
N
N

9c

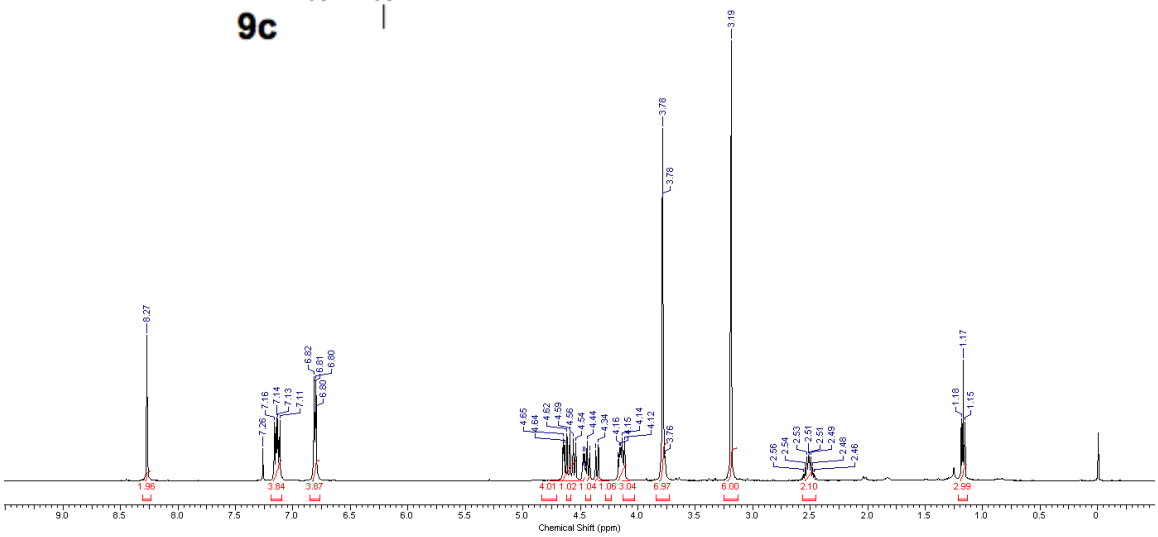
8.27
7.26
7.16
7.14
7.13
7.11
6.82
6.81
6.80
6.80
4.65
4.64
4.62
4.59
4.56
4.54
4.44
4.34
4.15
4.15
4.14
4.12
3.76
3.78
3.19
2.56
2.54
2.53
2.51
2.51
2.49
2.48
2.46
1.18
1.17
1.15
1.96
3.84
3.87
4.01
1.02
1.04
1.06
3.04
6.97
6.00
2.10
2.99
Chemical Shift (ppm)

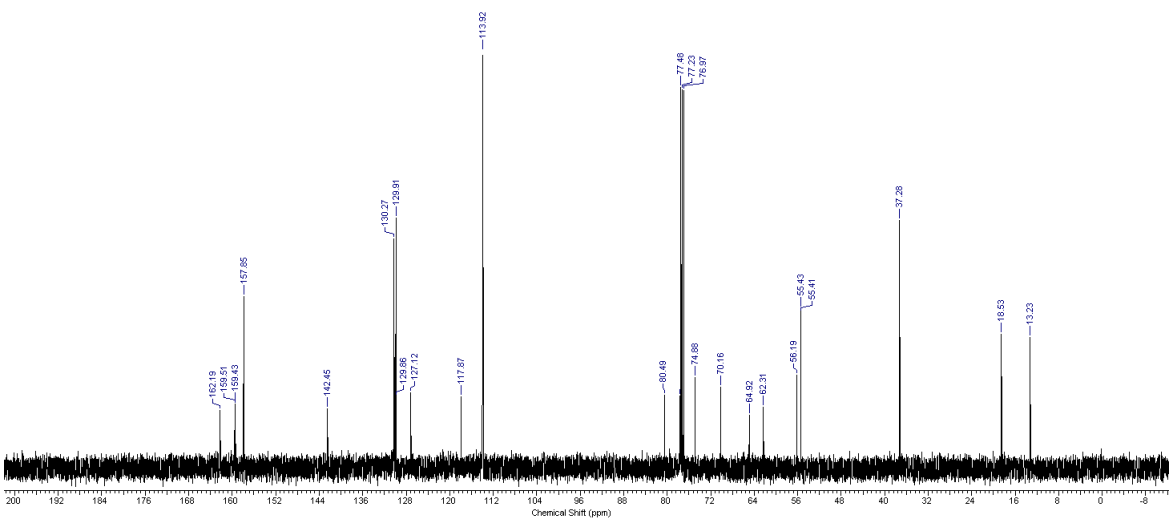
162.19
159.81
159.43
157.86
142.45
130.27
129.91
129.86
127.12
117.87
113.92
80.49
77.48
77.23
76.97
74.88
70.16
64.92
62.31
56.19
55.43
55.41
37.28
18.53
13.23
Chemical Shift (ppm)

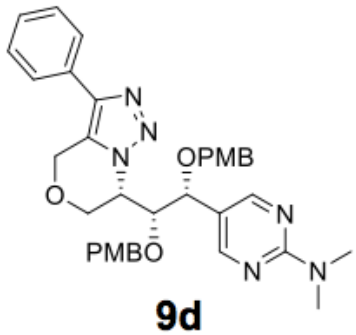
N
N
N
OPMB
O
PMBO
N
N
N

9d

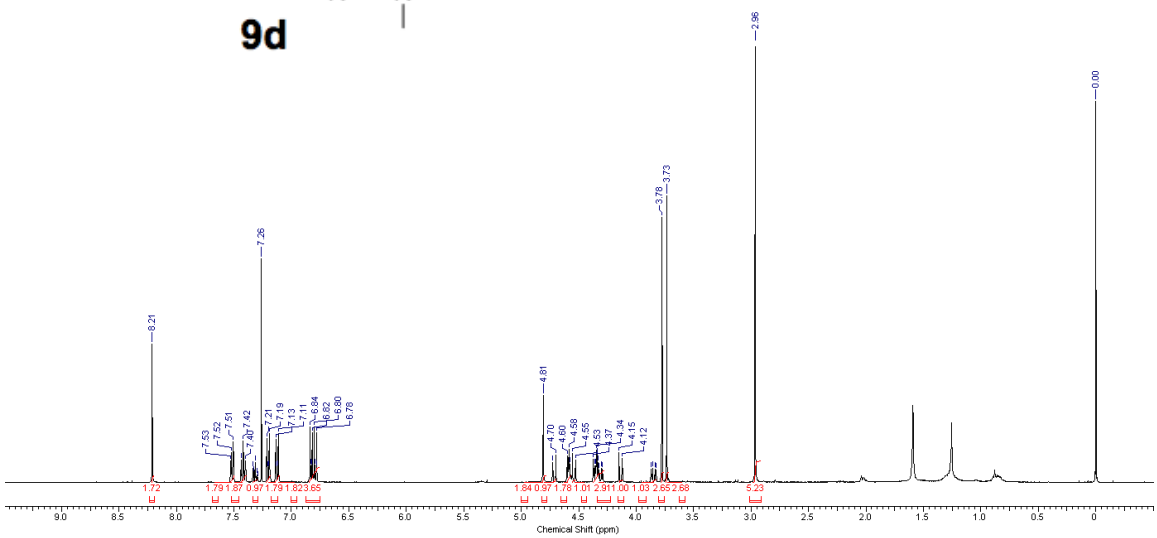
8.21
7.53
7.52
7.51
7.42
7.26
7.21
7.19
7.13
7.11
6.84
6.82
6.80
6.78
4.81
4.70
4.60
4.58
4.55
4.53
4.37
4.34
4.15
4.12
3.78
3.73
2.96
0.00
1.72
1.79 1.87 0.97 1.79 1.82 3.65
1.84 0.97 1.78 1.01 2.91 1.00 1.03 2.65 2.68
5.23
Chemical Shift (ppm)

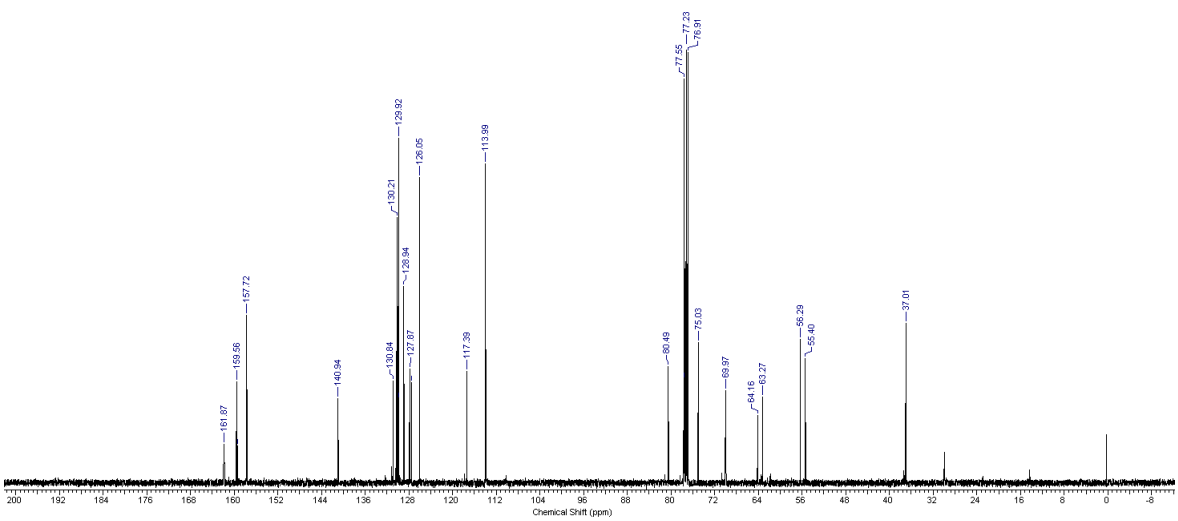
161.87
159.56
157.72
140.94
130.84
130.21
129.92
128.94
127.87
126.05
117.39
113.99
80.49
77.55
77.23
76.91
75.03
69.97
64.16
63.27
56.29
55.40
37.01
Chemical Shift (ppm)

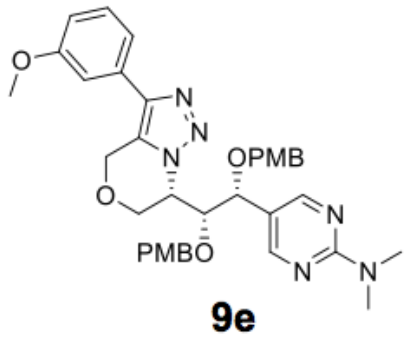
O
N
N
N
OPMB
O
PMBO
N
N
N

9e

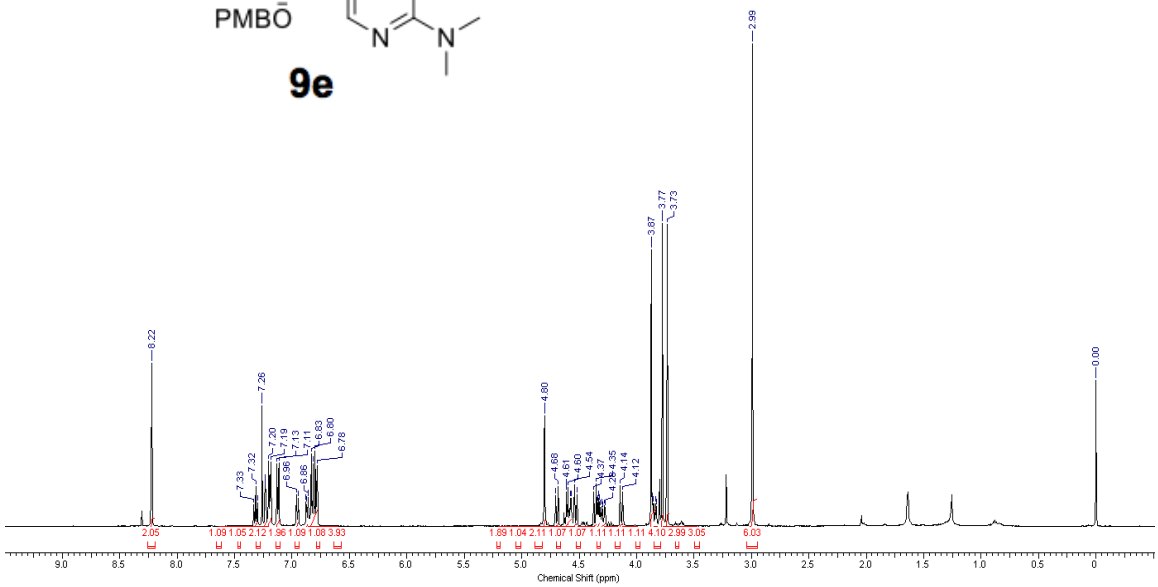
8.22
7.26
7.33
7.32
7.20
7.19
7.13
7.11
6.96
6.86
6.83
6.80
6.78
4.80
4.66
4.61
4.60
4.54
4.37
4.35
4.14
4.12
3.87
3.77
3.73
2.99
0.00
2.05
1.09 1.05 2.12 1.96 1.09 1.08 3.93
1.89 1.04 2.11 1.07 1.07 1.11 1.11 1.11 4.10 2.99 3.05
6.03
Chemical Shift (ppm)

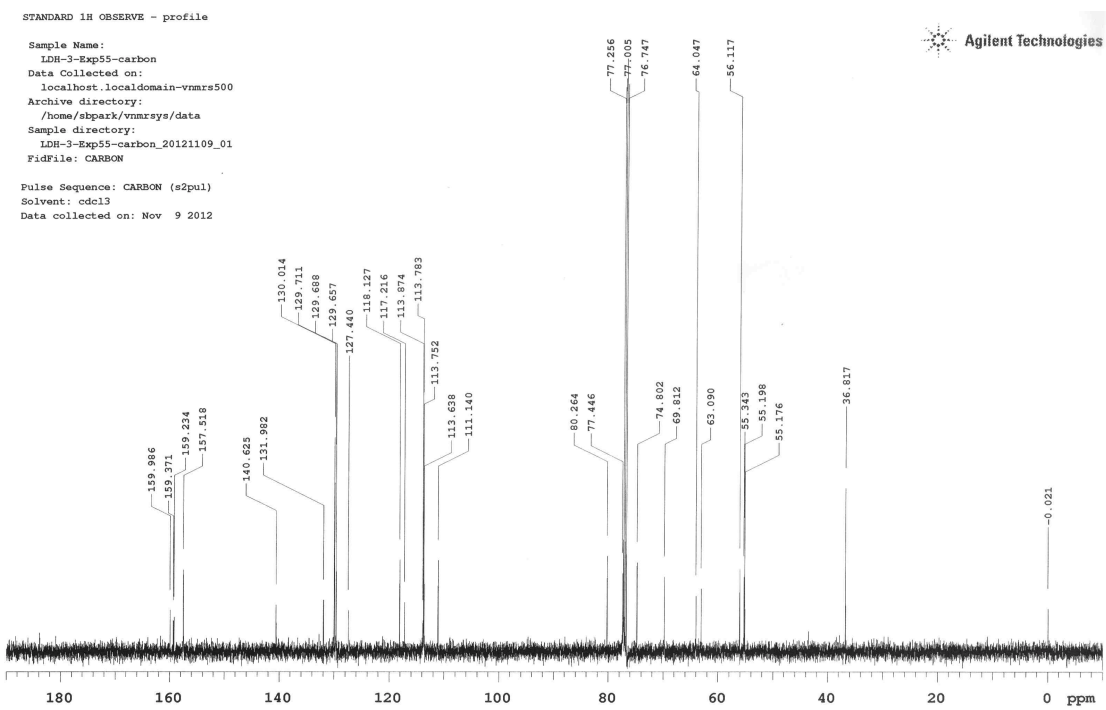
STANDARD 1H OBSERVE - profile
Sample Name:
LDH-3-Exp55-carbon
Data Collected on:
localhost.localdomain-vnmrs500
Archive directory:
/home/sbpark/vnmrsys/data
Sample directory:
LDH-3-Exp55-carbon_20121109_01
FidFile: CARBON
Pulse Sequence: CARBON (s2pul)
Solvent: cdcl3
Data collected on: Nov 9 2012
Agilent Technologies
77.256
77.005
76.747
64.047
56.117
130.014
129.711
129.608
129.657
127.440
118.127
117.216
113.874
113.783
113.752
113.638
111.140
159.986
159.371
159.234
157.518
140.625
131.982
80.264
77.446
74.802
69.812
63.090
55.343
55.198
55.176
36.817
0.021
ppm

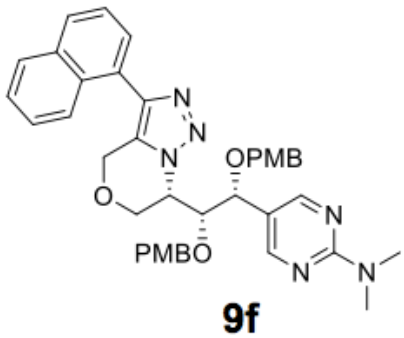

9f

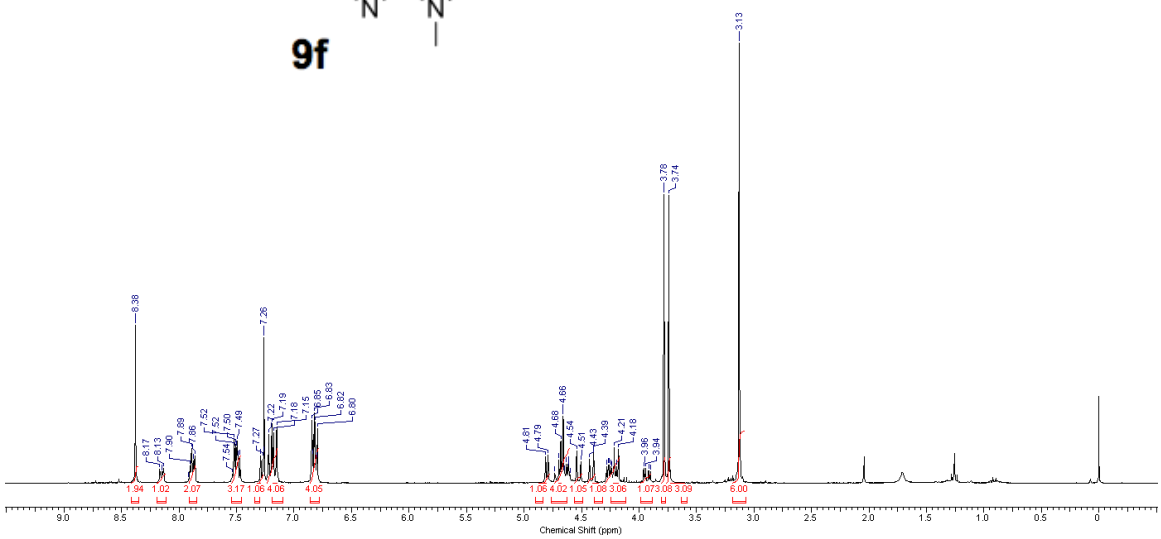

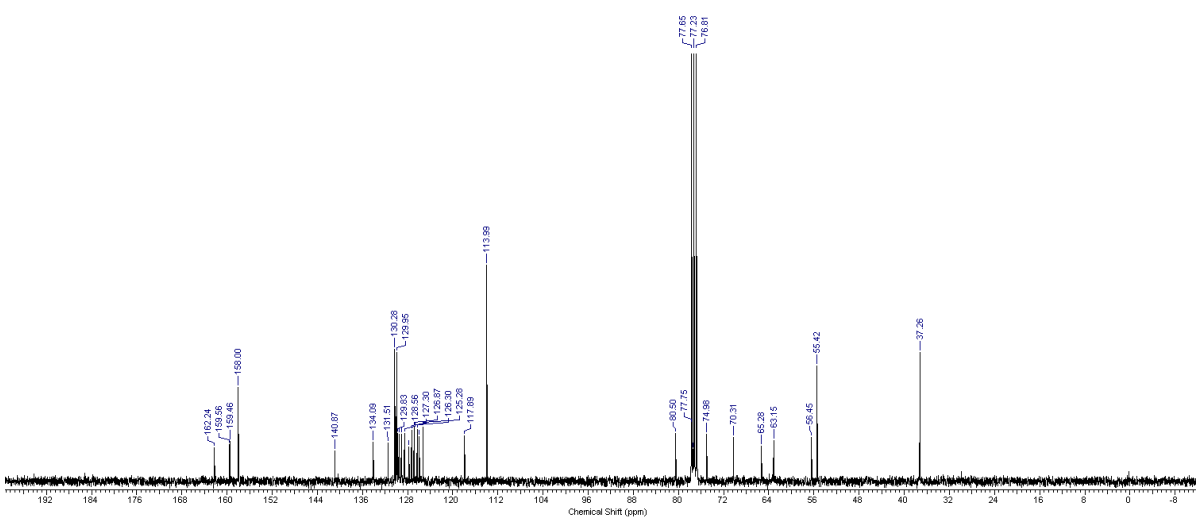

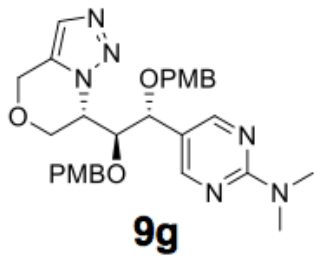
N
N
N
OPMB
O
PMBO
N
N
N

9g

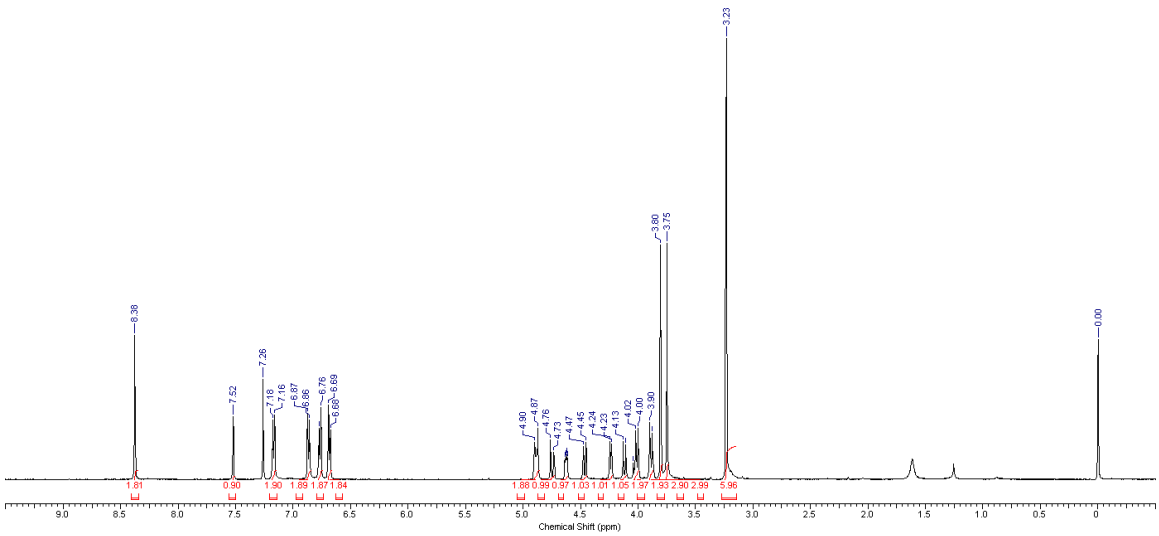
8.38
7.52
7.26
7.18
7.16
6.87
6.86
6.76
6.69
6.68
4.90
4.87
4.76
4.73
4.47
4.45
4.34
4.23
4.13
4.02
4.00
3.90
3.80
3.75
3.23
0.00
1.61
0.90
1.90
1.89
1.87
1.84
1.88
0.99
0.97
1.03
1.01
1.05
1.97
1.93
2.90
2.99
5.96
Chemical Shift (ppm)

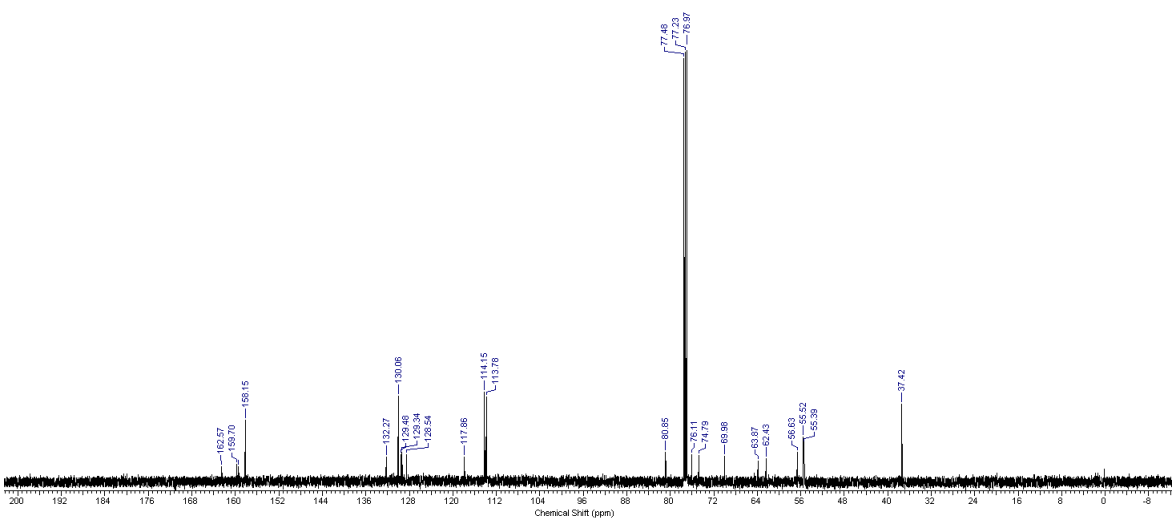
162.57
159.70
158.15
132.27
130.06
129.48
129.34
128.54
117.86
114.15
113.76
80.85
77.48
77.23
76.97
76.11
74.79
69.98
63.87
62.43
56.63
55.52
55.39
37.42
Chemical Shift (ppm)

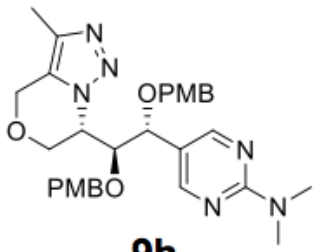
N
N
N
OPMB
O
N
PMBO
N
N

9h

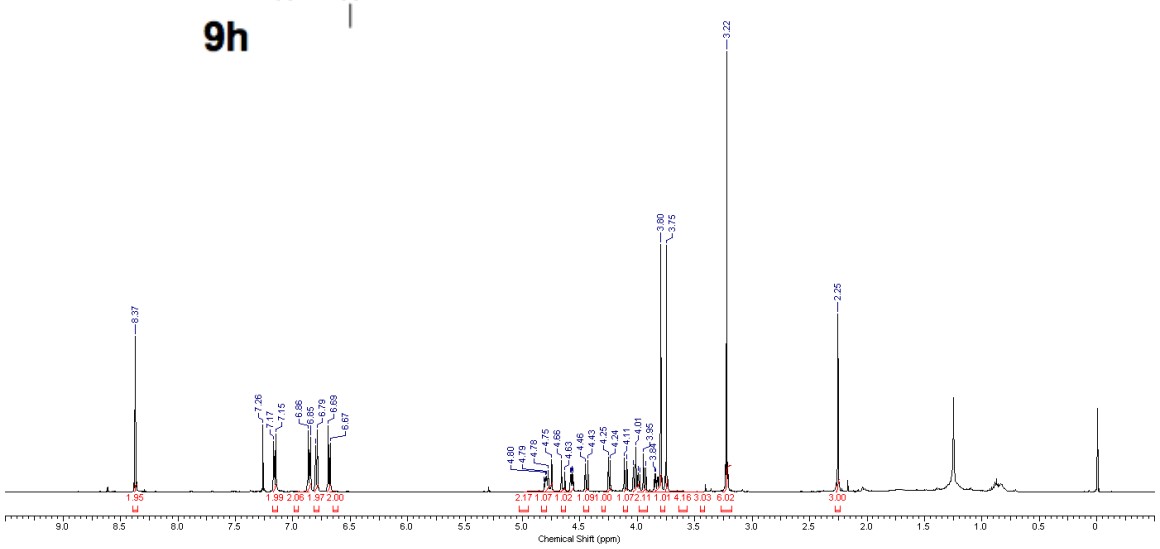
8.37
7.26
7.17
7.15
6.86
6.85
6.79
6.69
6.67
4.80
4.79
4.78
4.75
4.66
4.63
4.46
4.43
4.25
4.24
4.11
4.01
3.95
3.84
3.80
3.75
3.22
2.25
1.95
1.99
2.06
1.97
2.00
2.17
1.07
1.02
1.09
1.00
1.07
2.11
1.01
4.16
3.03
6.02
3.00
Chemical Shift (ppm)

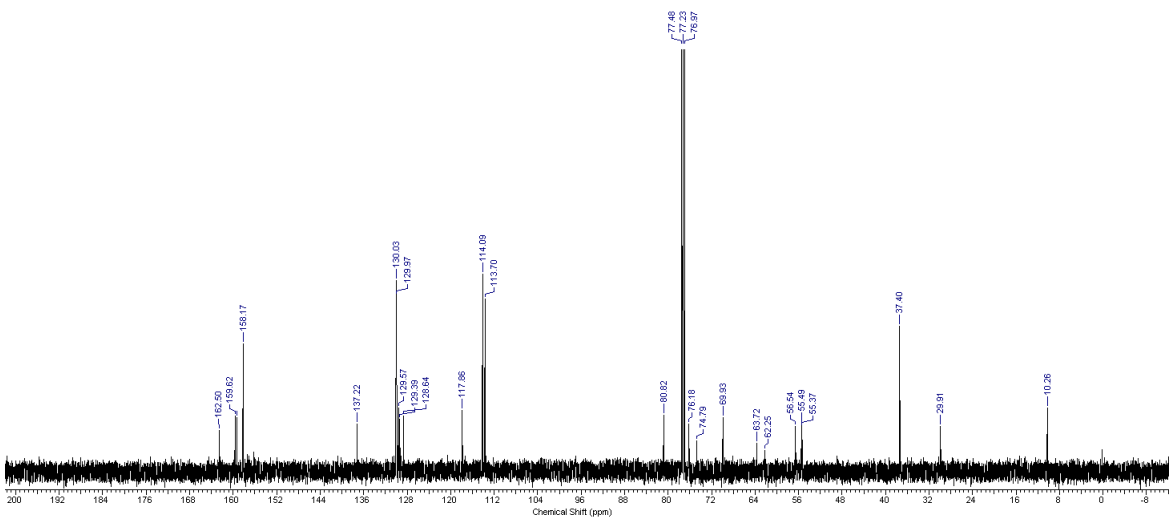
77.48
77.23
76.97
130.03
129.97
114.09
113.70
158.17
162.50
159.62
137.22
129.57
129.39
126.84
117.86
80.82
76.18
74.79
69.93
63.72
62.25
55.64
55.49
55.37
37.40
29.91
10.26
Chemical Shift (ppm)

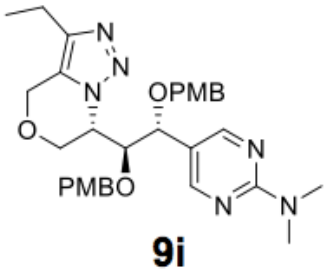
N
N
N
OPMB
O
N
PMBO
N
N

9i

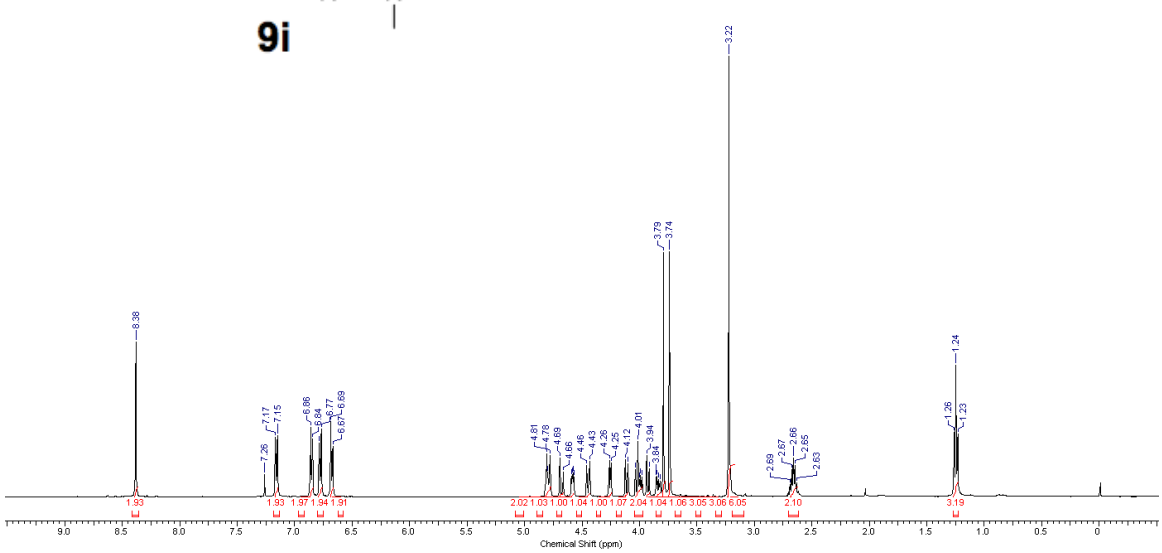
8.38
7.26
7.17
7.15
6.86
6.84
6.77
6.67
6.69
4.81
4.78
4.69
4.66
4.46
4.43
4.25
4.12
4.01
3.94
3.84
3.79
3.74
3.22
2.69
2.67
2.66
2.65
2.63
1.26
1.24
1.23
1.93
1.93
1.97
1.94
1.91
2.02
1.03
1.00
1.04
1.00
1.07
2.04
1.04
1.06
3.05
3.06
6.05
2.10
3.19
Chemical Shift (ppm)

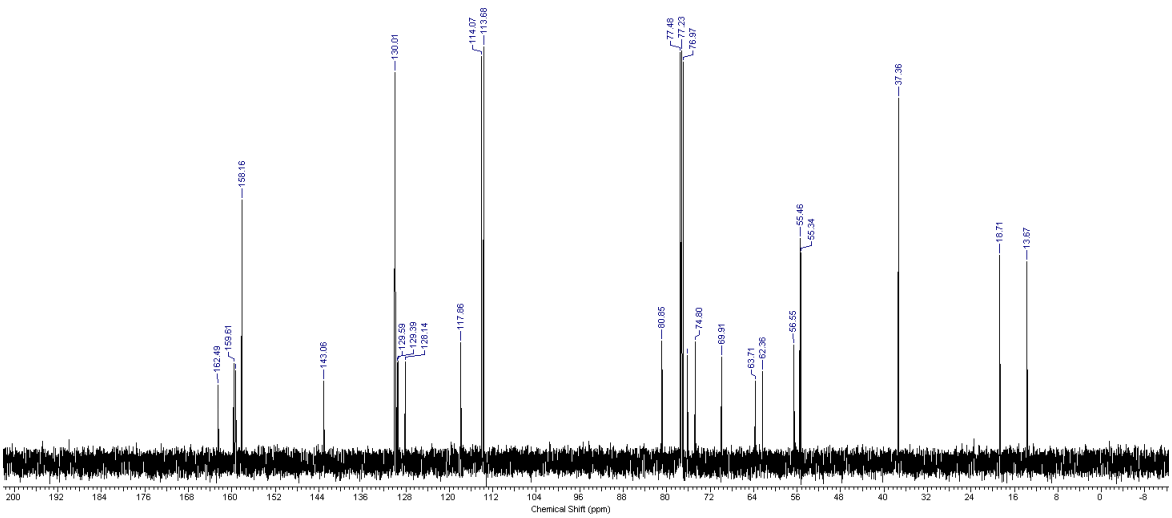
162.49
159.61
158.16
143.06
130.01
129.59
129.39
128.14
117.86
114.07
113.68
80.05
77.48
77.23
76.97
74.80
69.91
63.71
62.36
56.55
55.46
55.34
37.36
18.71
13.67
Chemical Shift (ppm)

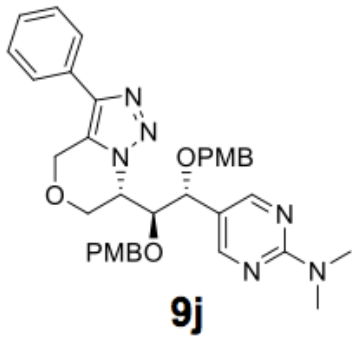
N
N
N
OPMB
O
N
PMBO
N
N

9j

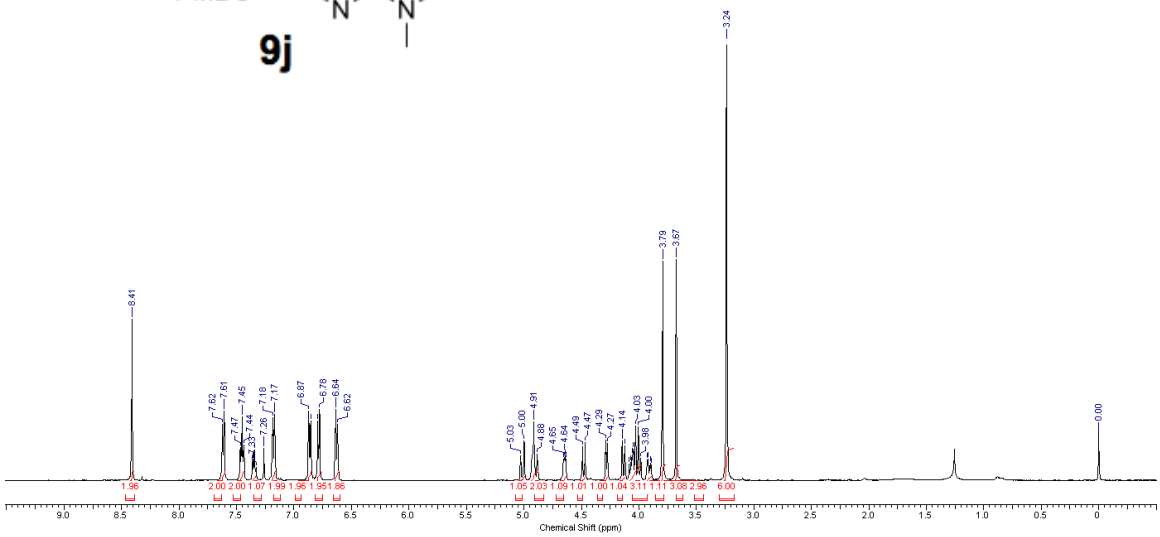
8.41
7.62
7.61
7.45
7.47
7.44
7.33
7.26
7.18
7.17
6.87
6.78
6.64
6.62
5.03
5.00
4.91
4.88
4.85
4.84
4.49
4.47
4.29
4.27
4.14
4.03
4.00
3.98
3.79
3.67
3.24
0.00
1.96
2.00
2.00
1.07
1.99
1.96
1.95
1.86
1.05
2.03
1.09
1.01
1.00
1.04
3.11
1.11
3.06
2.96
6.00
Chemical Shift (ppm)

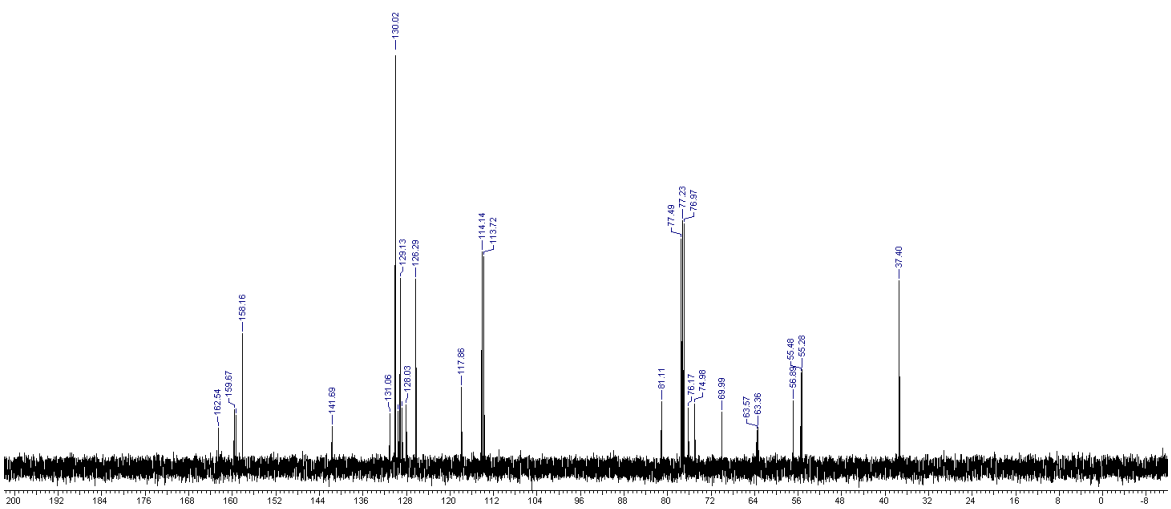
130.02
129.13
126.29
114.14
113.72
77.49
77.23
76.97
37.40
158.16
162.64
159.67
141.69
131.06
120.03
117.86
81.11
76.17
74.98
69.99
63.57
63.36
56.89
55.49
55.28
Chemical Shift (ppm)

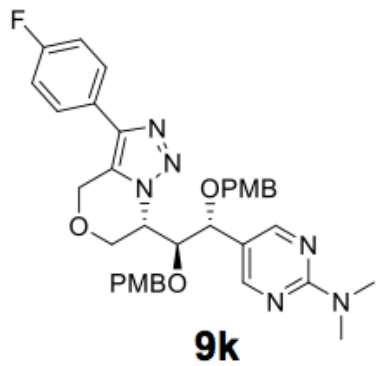
F
N
N
N
O
OPMB
PMBO
N
N
N

9k

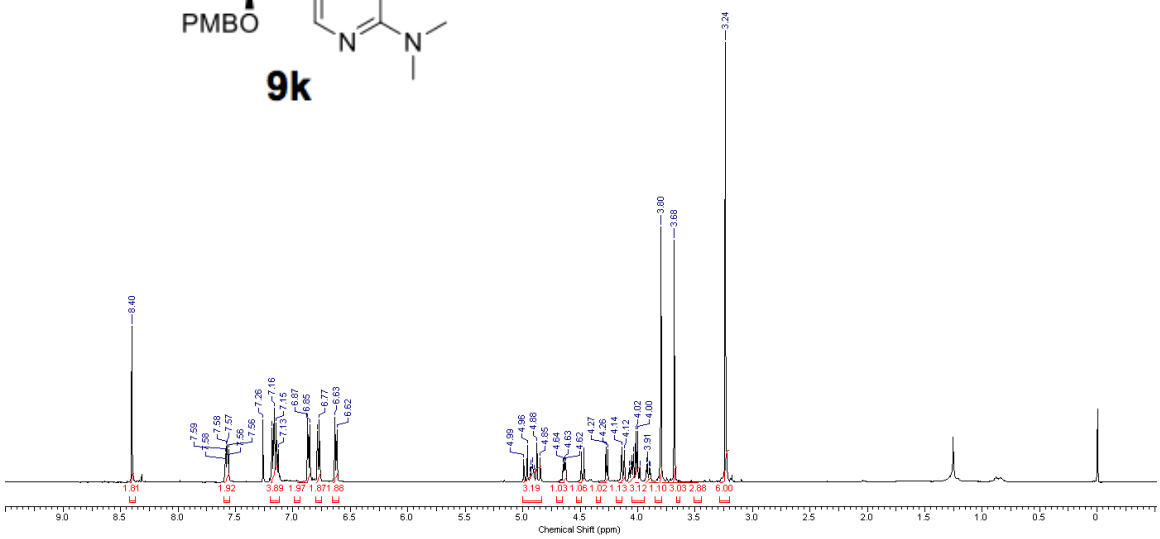
8.40
7.59
7.58
7.58
7.57
7.56
7.56
7.26
7.16
7.15
7.13
6.87
6.85
6.77
6.63
6.62
4.99
4.96
4.88
4.65
4.64
4.63
4.62
4.27
4.26
4.14
4.12
4.02
4.00
3.91
3.80
3.68
3.24
1.81
1.92
3.89
1.97
1.87
1.88
3.19
1.00
1.06
1.06
1.02
1.13
3.12
1.10
3.03
2.88
6.00
Chemical Shift (ppm)

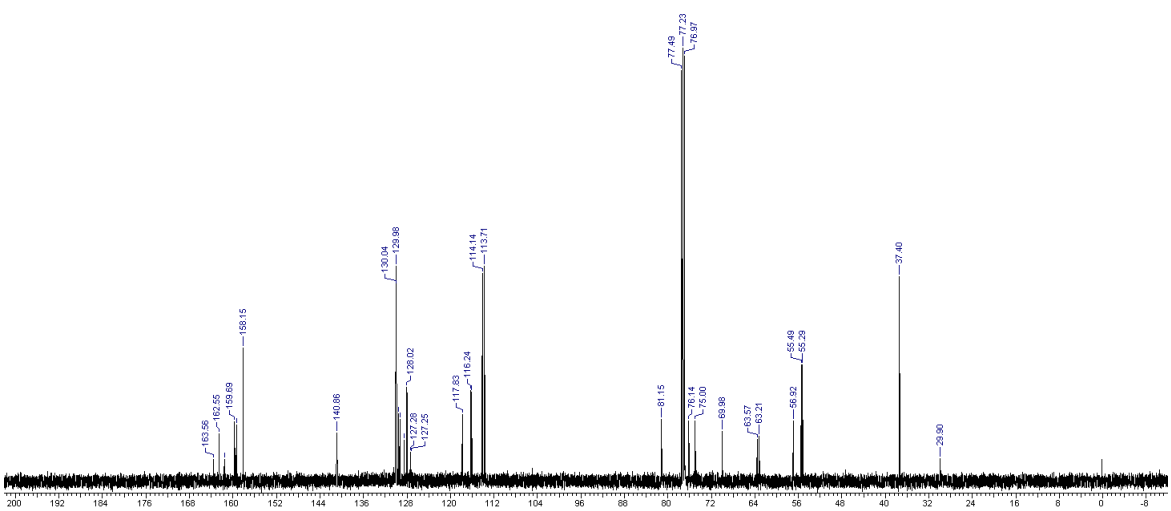
77.49
77.23
76.97
130.04
129.98
114.14
113.71
158.15
128.02
116.24
117.83
140.86
163.56
162.55
159.69
127.28
127.25
81.15
76.14
75.00
69.98
63.57
63.21
55.49
55.29
56.92
37.40
29.90
Chemical Shift (ppm)

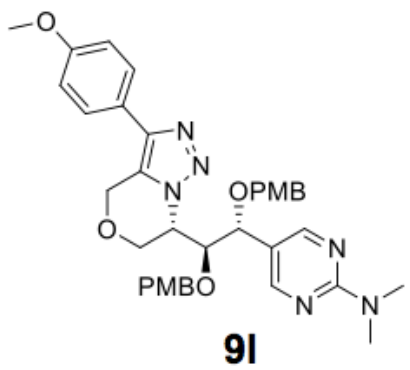
O
N
N
N
OPMB
O
PMBO
N
N
N

9l

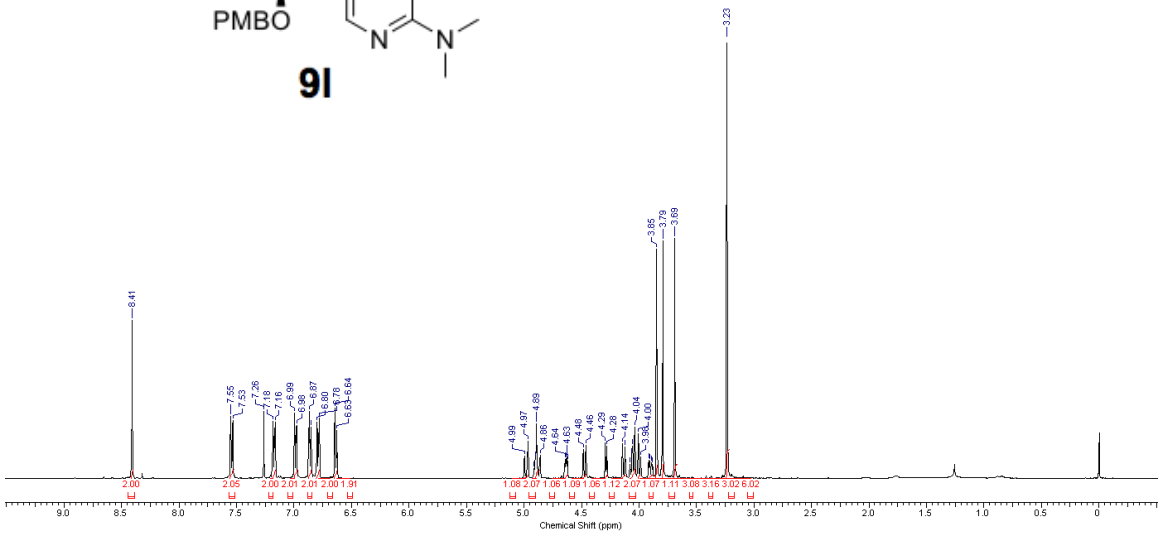
8.41
7.55
7.53
7.26
7.18
7.16
6.99
6.98
6.97
6.80
6.78
6.63-6.64
4.99
4.97
4.89
4.86
4.64
4.63
4.48
4.46
4.29
4.28
4.14
4.04
4.00
3.98
3.85
3.79
3.69
3.23
2.00
2.05
2.00
2.01
2.01
2.00
1.91
1.08
2.07
1.06
1.09
1.05
1.12
2.07
1.07
1.11
3.08
3.16
5.02
6.02
Chemical Shift (ppm)

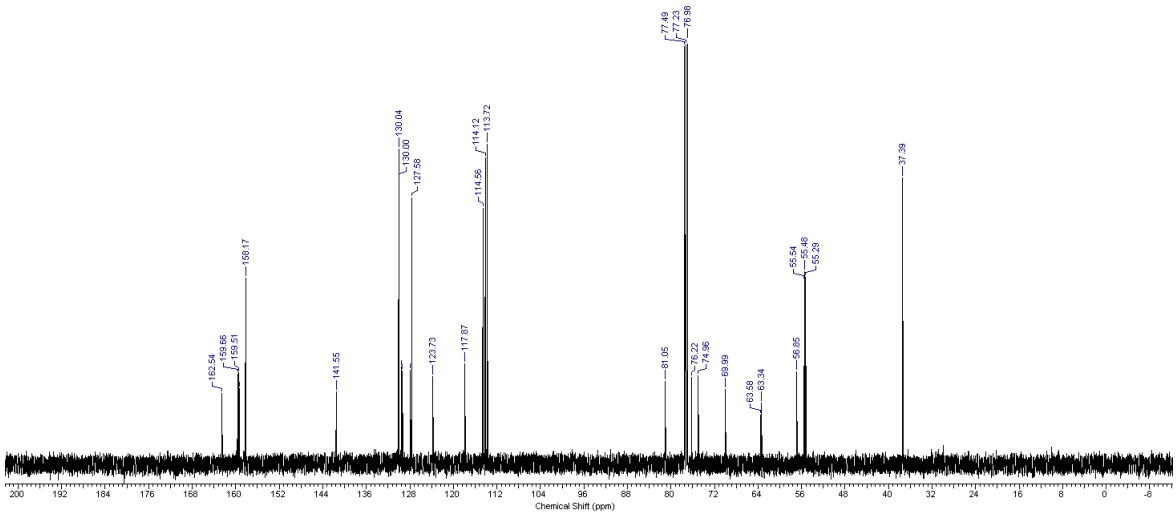
77.49
77.23
76.98
130.04
130.00
127.58
114.12
113.72
114.56
162.54
159.66
159.51
158.17
141.55
123.73
117.67
81.05
76.22
74.96
69.99
63.58
63.34
56.85
55.54
55.46
55.29
37.39
Chemical Shift (ppm)

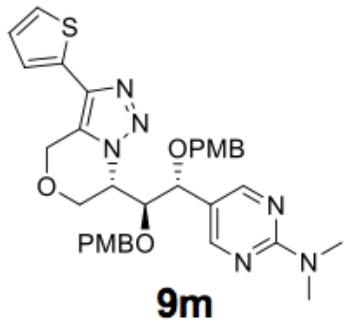
S
N
N
N
O
OPMB
PMBO
N
N
N

9m

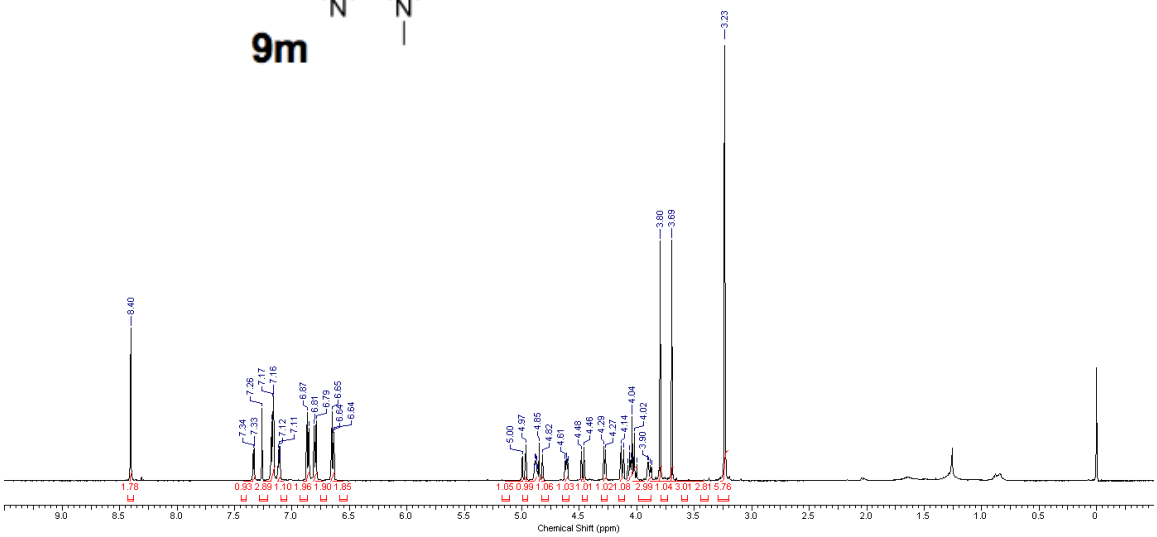
8.40
7.34
7.33
7.26
7.17
7.16
7.12
7.11
6.87
6.81
6.79
6.64
6.65
6.64
5.00
4.97
4.85
4.82
4.61
4.48
4.46
4.29
4.27
4.14
4.04
4.02
3.90
3.80
3.69
3.23
1.76
0.93 2.89 1.10 1.96 1.90 1.85
1.05 0.99 1.06 1.03 1.01 1.02 1.08 2.99 1.04 3.01 2.81 5.76
Chemical Shift (ppm)

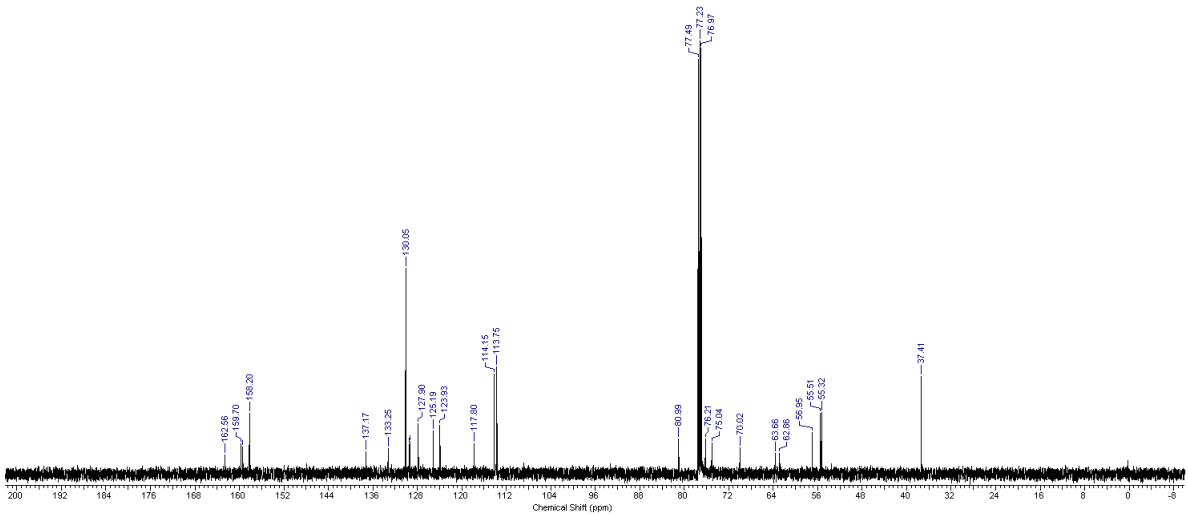
77.49
77.23
76.97
130.05
114.15
113.75
162.56
159.70
159.20
137.17
133.25
127.90
125.19
123.93
117.80
80.99
76.21
75.04
70.02
63.86
62.88
56.95
55.51
55.32
37.41
Chemical Shift (ppm)

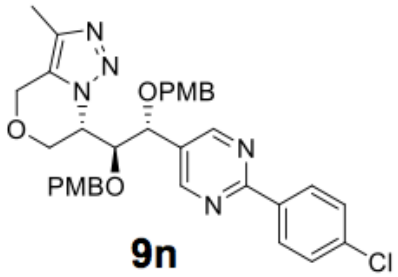

9n

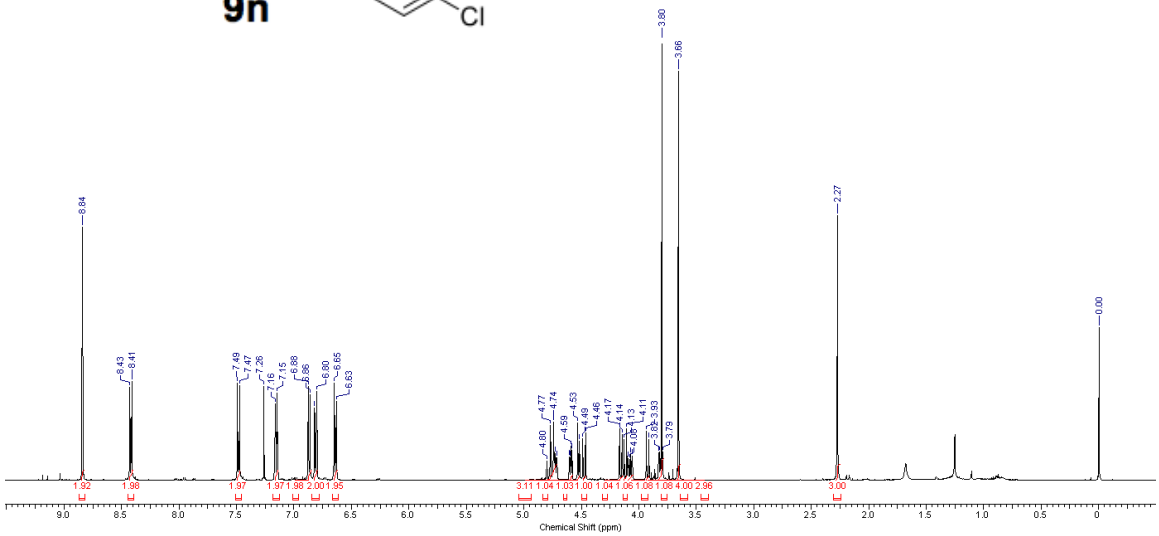

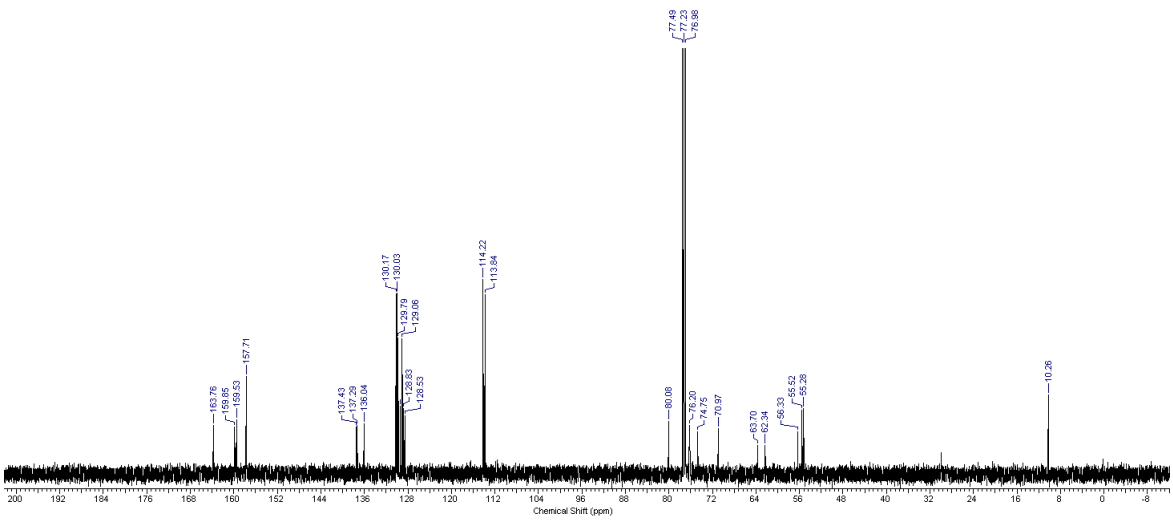

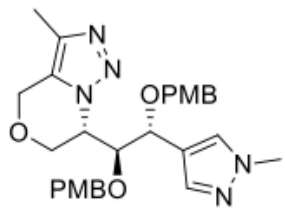
N
N
N
OPMB
O
N
PMBO
N

9o

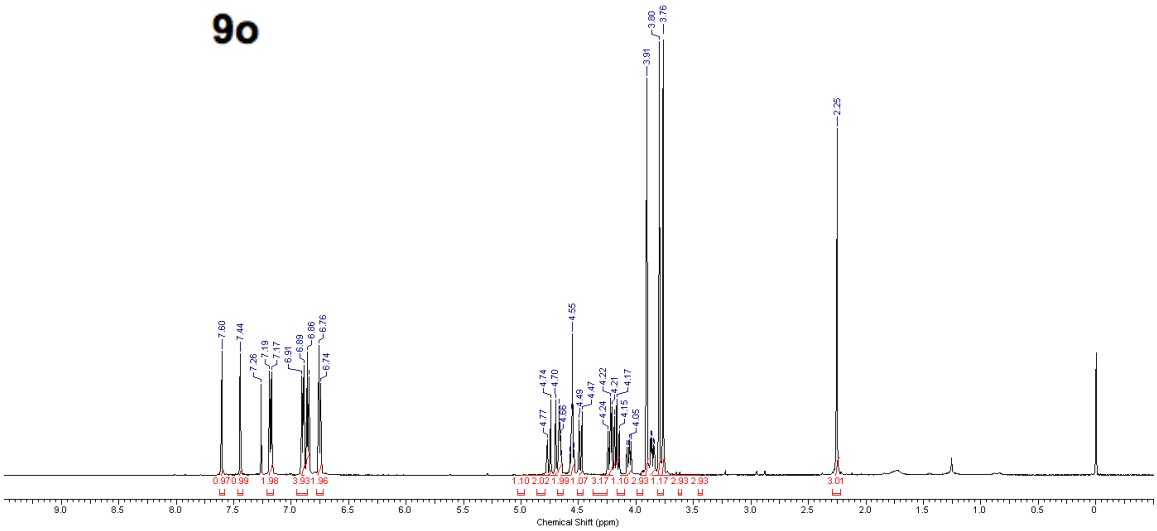
7.80
7.44
7.26
7.19
7.17
6.91
6.89
6.86
6.76
6.74
4.55
4.74
4.70
4.49
4.47
4.24
4.22
4.21
4.17
4.15
4.05
4.77
4.68
3.90
3.76
3.91
2.25
0.97 0.99 1.98 3.93 1.96
1.10 2.02 1.99 1.07 3.17 1.10 2.93 1.17 2.93 2.93
3.01
Chemical Shift (ppm)

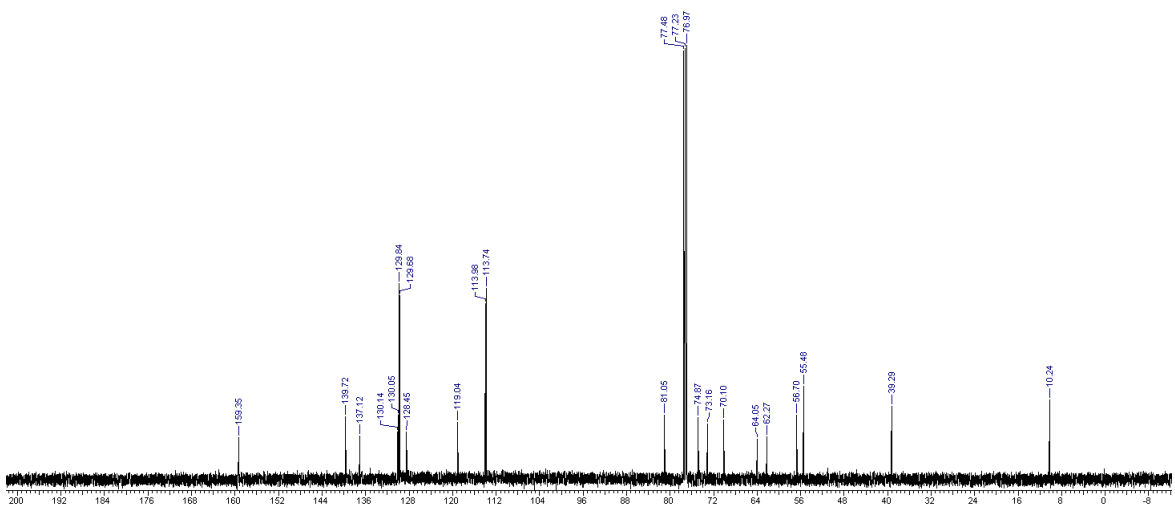
77.48
77.23
76.97
129.84
129.68
113.98
113.74
159.35
139.72
137.12
130.14
130.05
128.45
119.04
81.05
74.87
73.16
70.10
64.05
62.27
56.70
55.46
39.29
10.24
Chemical Shift (ppm)

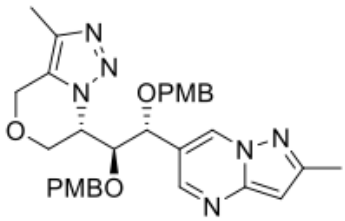
N
N
N
OPMB
O
N
N
PMBO
N

9p

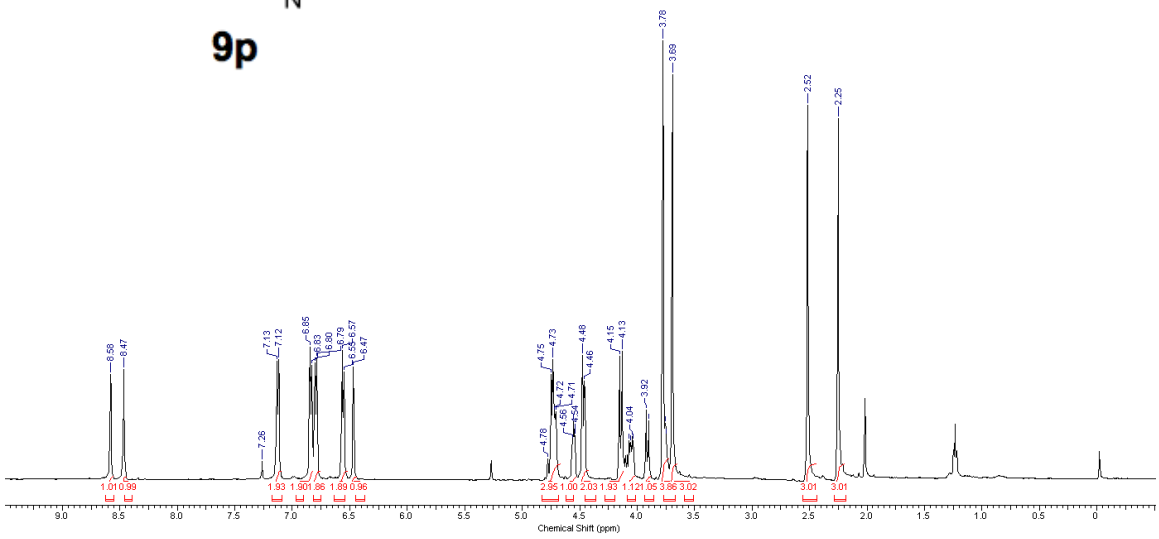
8.58
8.47
7.26
7.13
7.12
6.85
6.83
6.80
6.79
6.59
6.57
6.47
4.75
4.73
4.72
4.71
4.56
4.54
4.48
4.46
4.15
4.13
4.04
3.92
3.78
3.69
2.52
2.25
1.01 0.99
1.93 1.90 1.86
1.89 0.96
2.95 1.00 2.03 1.93
1.12 1.05 3.86 3.02
3.01
3.01
Chemical Shift (ppm)

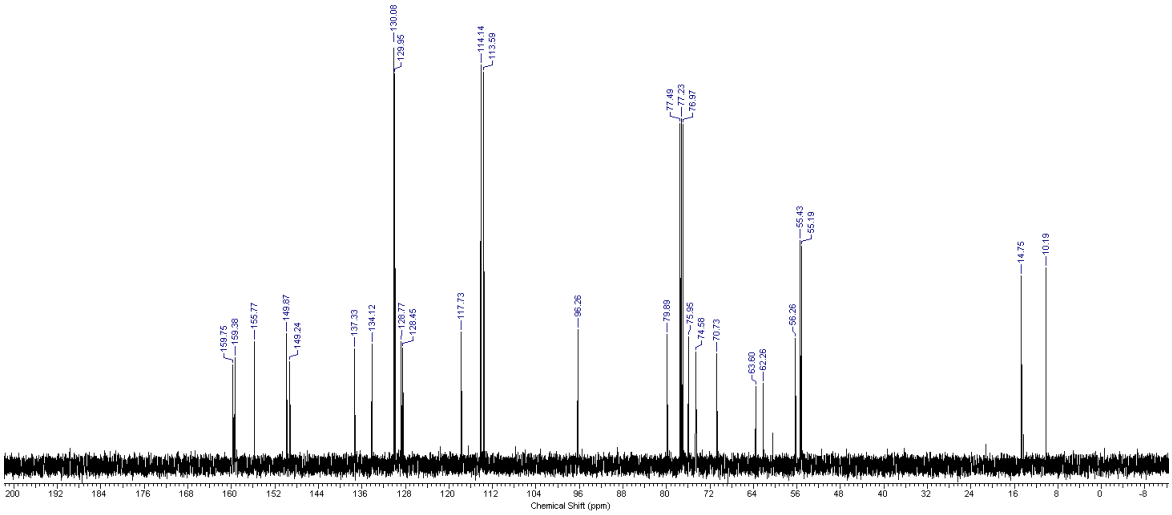
159.75
159.38
155.77
149.67
149.24
137.33
134.12
130.08
129.95
128.77
128.45
117.73
114.14
113.59
96.26
79.89
77.49
77.23
76.97
75.95
74.56
70.73
63.80
62.26
56.26
55.43
55.19
14.75
10.19
Chemical Shift (ppm)

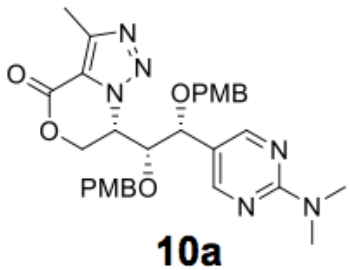
N
N
N
O
O
OPMB
PMBO
N
N
N

10a

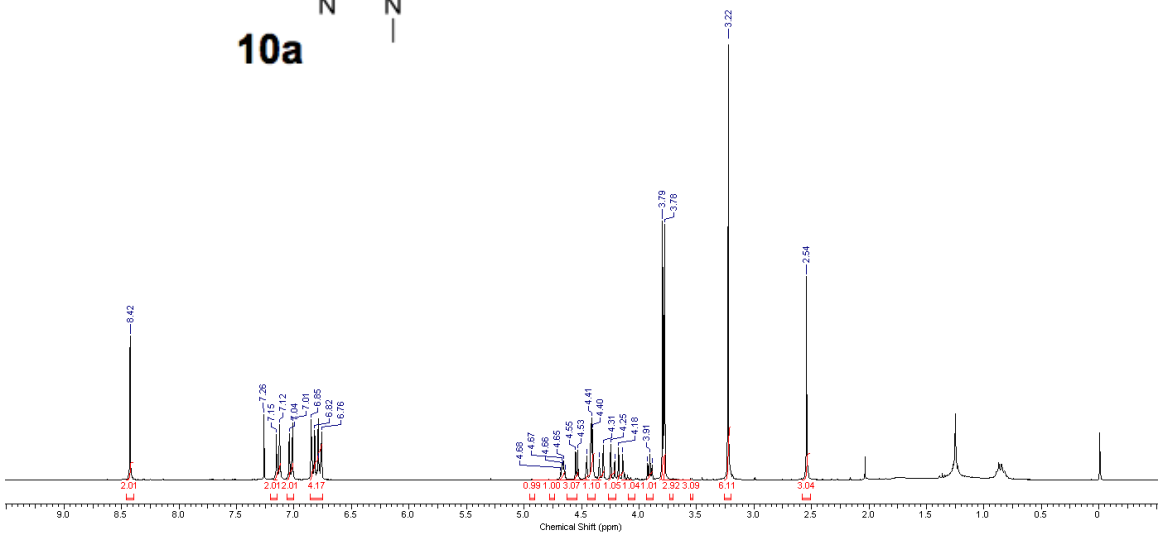
8.42
7.26
7.15
7.12
7.04
7.01
6.85
6.82
6.76
4.68
4.67
4.66
4.65
4.55
4.53
4.41
4.40
4.31
4.25
4.16
3.91
3.79
3.78
3.22
2.54
2.01
2.01
2.01
4.17
0.99
1.00
3.07
1.10
1.05
1.04
1.01
2.92
3.09
6.11
3.04
Chemical Shift (ppm)

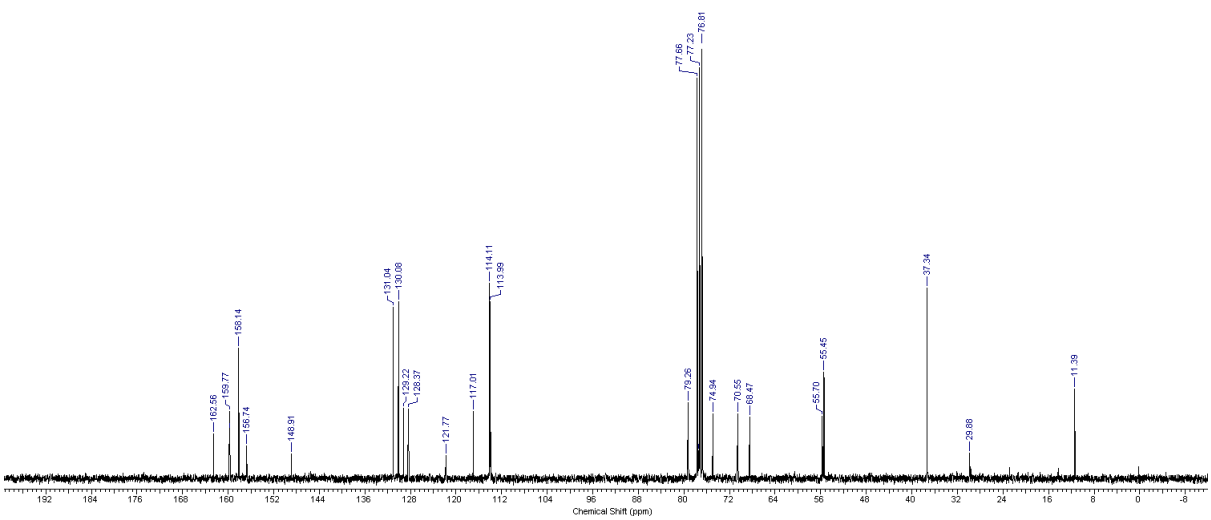
162.56
159.77
158.14
156.74
148.91
131.04
130.08
129.22
126.37
121.77
117.01
114.11
113.99
77.66
77.23
76.81
79.26
74.94
70.55
68.47
55.70
55.45
37.34
29.88
11.39
Chemical Shift (ppm)

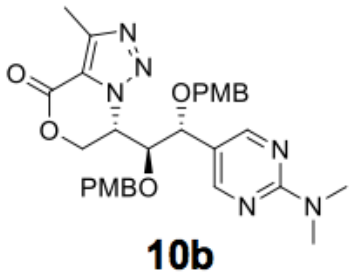
O
N
N
N
O
OPMB
PMBO
N
N
N

10b

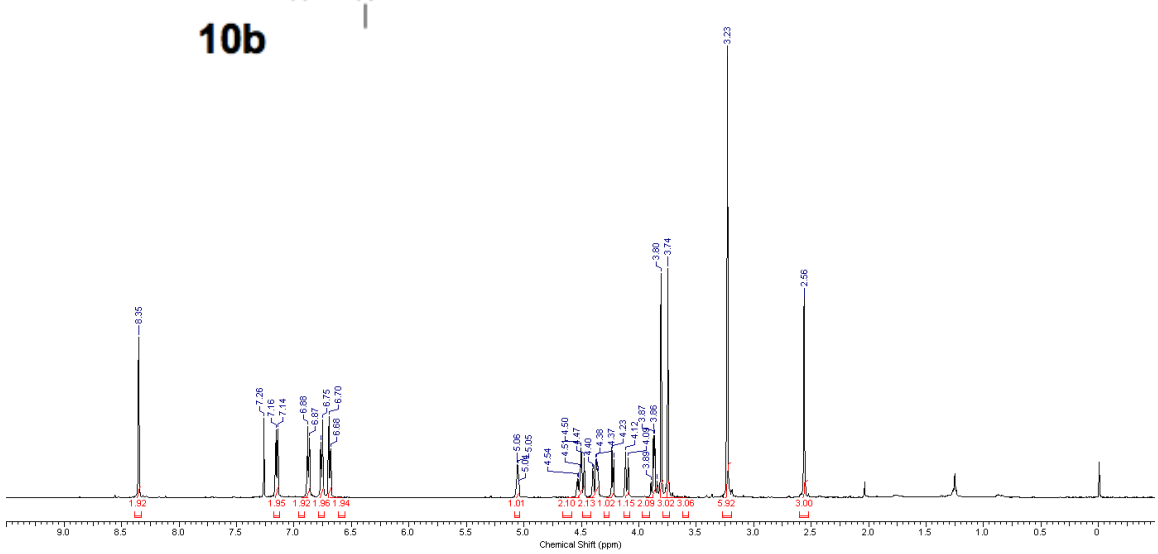
8.35
7.26
7.16
7.14
6.88
6.87
6.75
6.70
6.68
5.06
5.05
4.54
4.51
4.50
4.47
4.40
4.38
4.37
4.23
4.12
4.07
3.89
3.87
3.85
3.80
3.74
3.23
2.56
1.92
1.95
1.92
1.95
1.04
1.94
1.01
2.10
2.13
1.02
1.15
2.09
3.02
3.06
6.92
3.00
Chemical Shift (ppm)

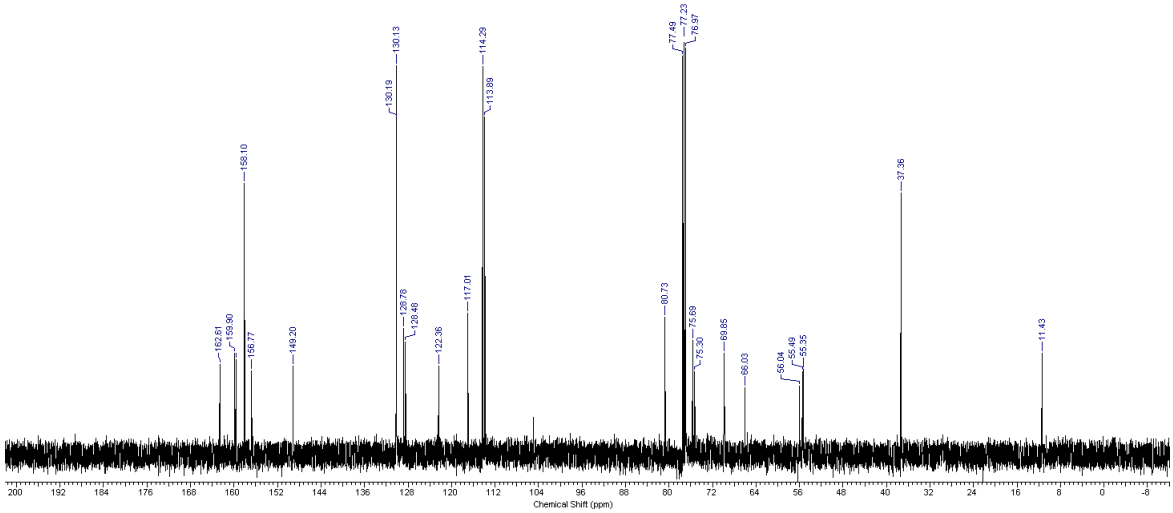
162.61
159.90
158.10
156.77
149.20
130.19
130.13
128.76
128.48
122.36
117.01
114.29
113.89
80.73
77.49
77.23
76.97
75.69
75.30
69.85
66.03
56.04
55.49
55.35
37.36
11.43
Chemical Shift (ppm)

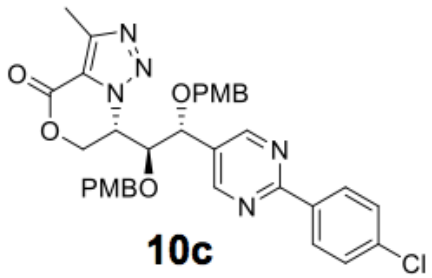
N
N
N
O
O
OPMB
PMBO
N
N
Cl

10c

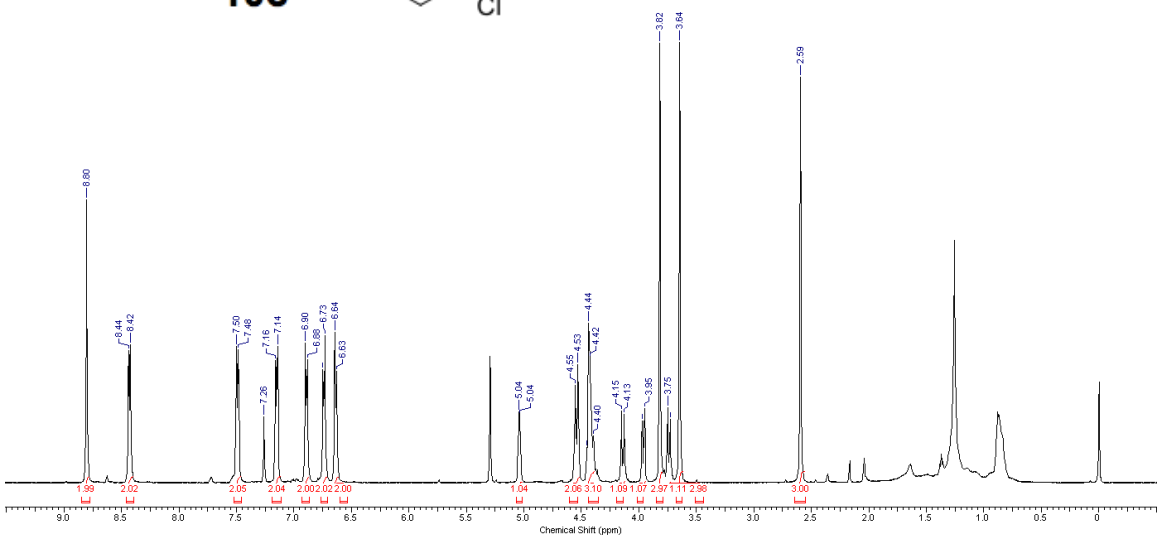
8.80
8.44
8.42
7.50
7.48
7.26
7.16
7.14
6.90
6.88
6.73
6.64
6.63
5.04
5.04
4.55
4.53
4.44
4.42
4.40
4.15
4.13
3.95
3.82
3.75
3.64
2.59
1.99
2.02
2.05
2.04
2.00
2.02
2.02
2.00
1.04
2.06
3.10
1.09
1.07
2.97
1.11
2.98
3.00
Chemical Shift (ppm)

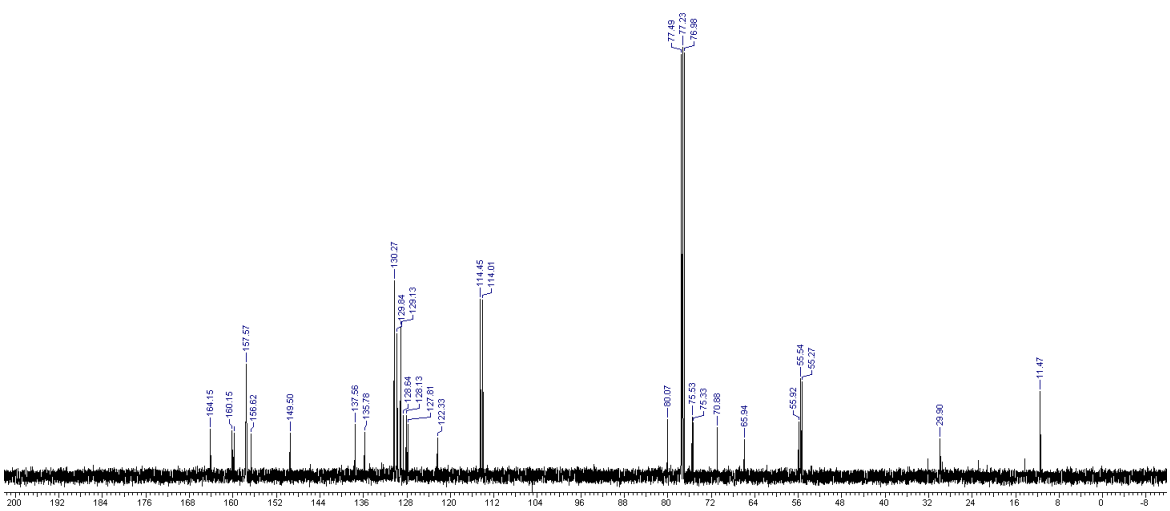
164.15
160.15
157.57
155.62
149.50
137.56
135.76
130.27
129.84
129.13
128.84
128.13
127.81
122.33
114.45
114.01
77.49
77.23
76.98
80.07
75.53
75.33
70.88
65.94
55.92
55.54
55.27
29.90
11.47
Chemical Shift (ppm)

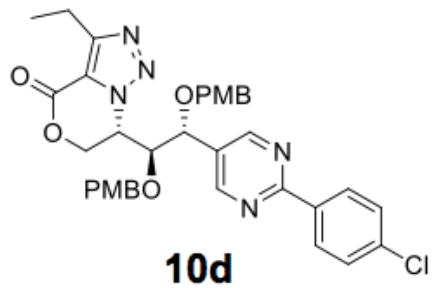
O
N
N
N
O
OPMB
PMBO
N
N
Cl

10d

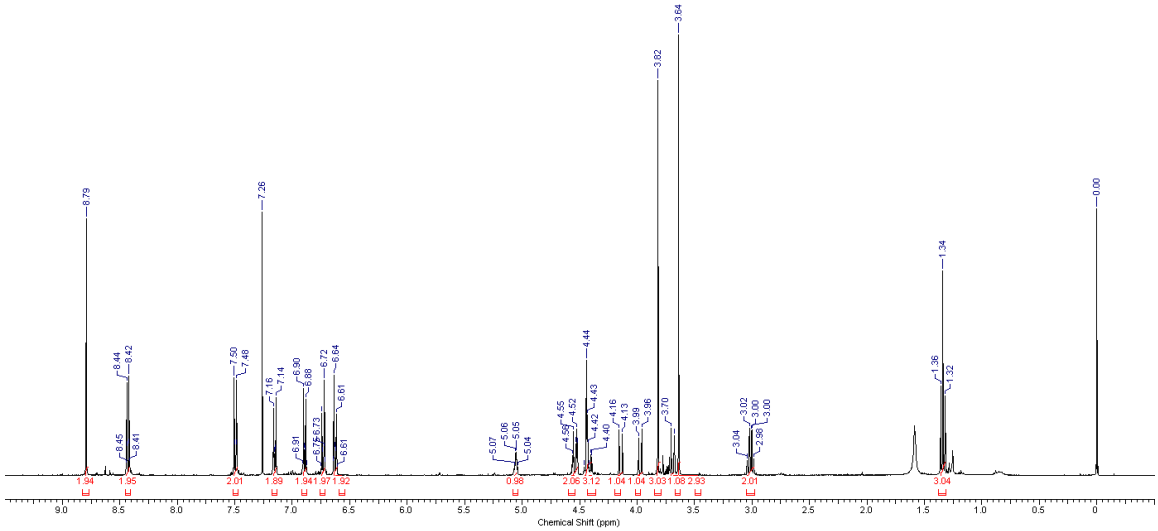
8.79
8.44
8.42
8.41
7.50
7.48
7.26
7.16
7.14
6.90
6.88
6.72
6.64
6.61
5.07
5.06
5.05
5.04
4.55
4.52
4.44
4.43
4.42
4.40
4.16
4.13
3.96
3.82
3.70
3.64
3.04
3.02
3.00
3.00
2.98
1.36
1.34
1.32
0.00
Chemical Shift (ppm)

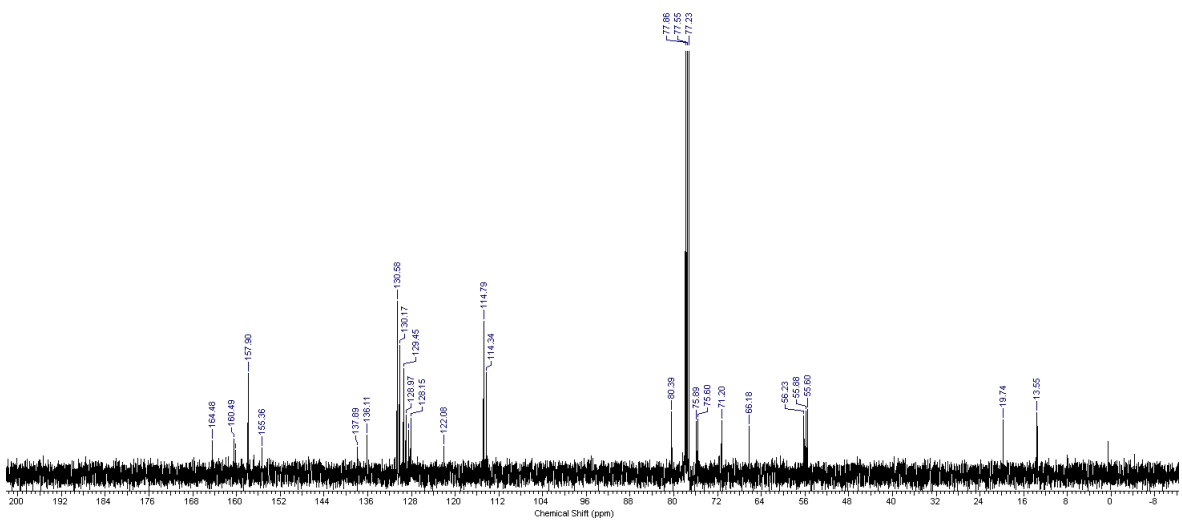
77.86
77.55
77.23
164.48
160.49
157.90
155.36
137.69
136.11
130.58
130.17
129.45
128.97
128.15
122.08
114.79
114.34
80.39
75.89
75.60
71.20
66.18
55.33
55.28
55.00
19.74
13.55
Chemical Shift (ppm)

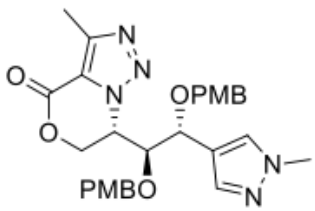
O
N
N
N
O
OPMB
PMBO
N
N

10e

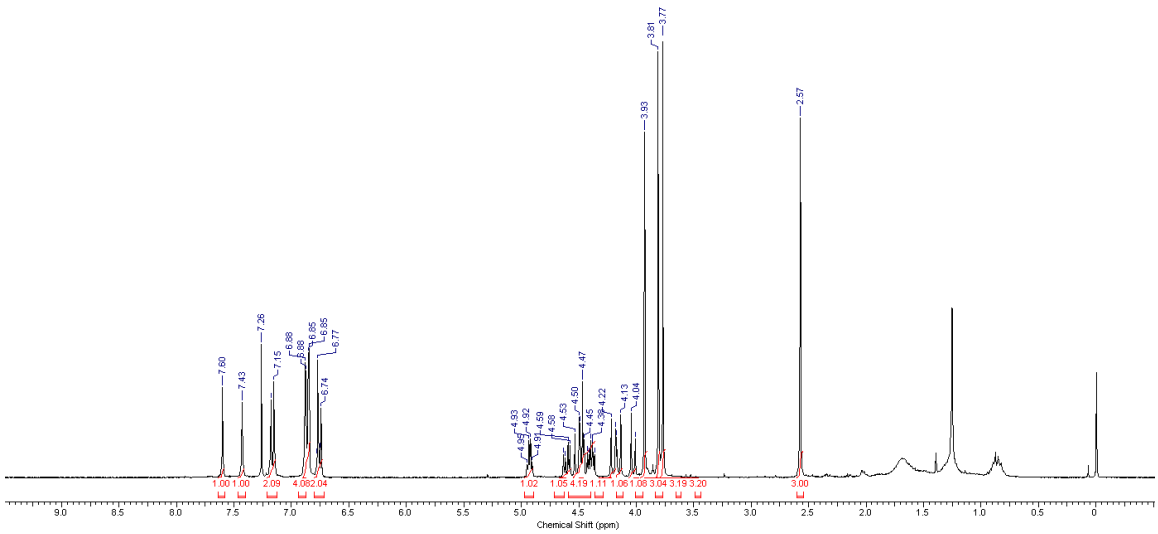
7.60
7.43
7.26
7.15
6.88
6.86
6.85
6.77
6.74
4.93
4.92
4.59
4.53
4.50
4.47
4.45
4.22
4.13
4.04
3.93
3.81
3.77
2.57
Chemical Shift (ppm)

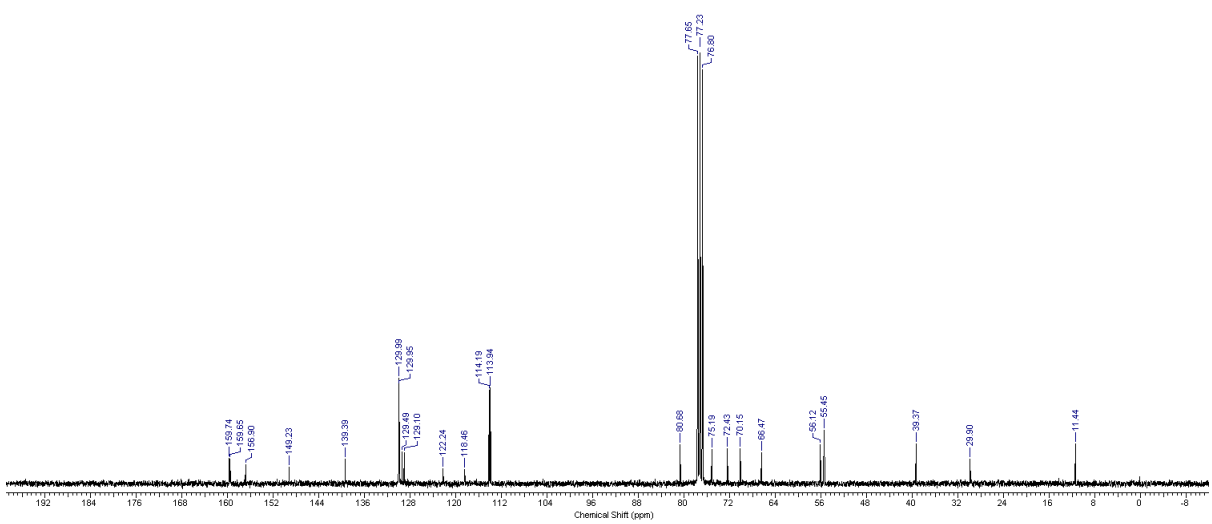
159.74
158.65
158.90
149.23
139.39
129.99
129.95
129.49
129.10
122.24
118.46
114.19
113.94
80.88
77.65
77.23
76.80
75.19
72.43
70.15
66.47
56.12
55.45
39.37
29.90
11.44
Chemical Shift (ppm)

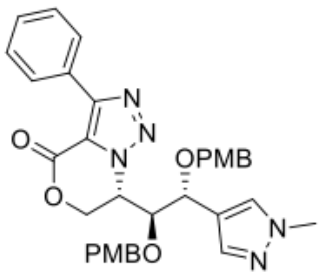
N
N
N
O
O
OPMB
PMBO
N
N

10f

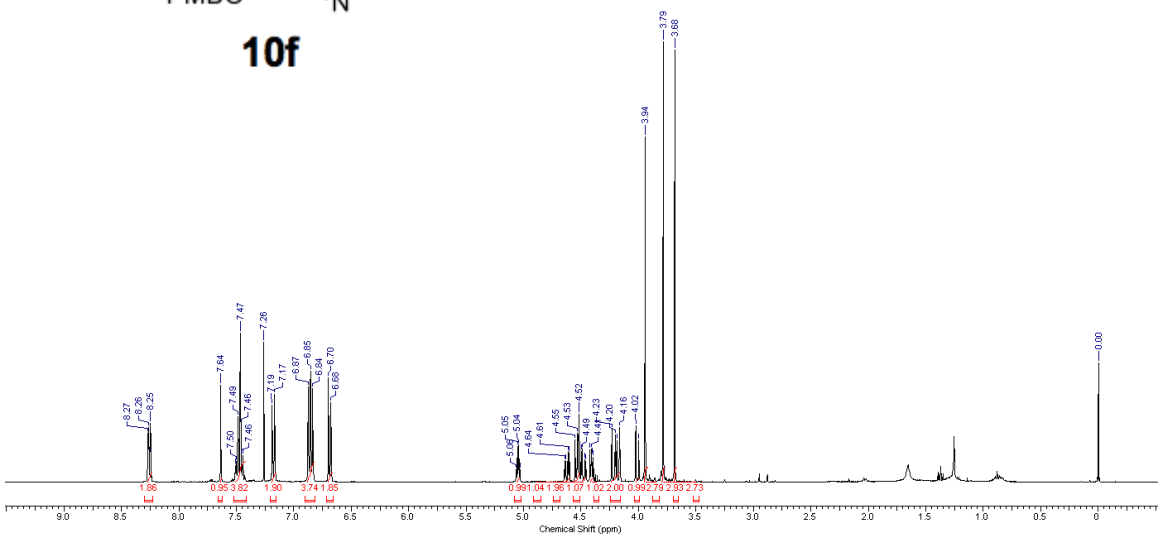
8.27
8.26
8.25
7.64
7.50
7.49
7.47
7.46
7.26
7.19
7.17
6.87
6.85
6.84
6.70
6.68
5.05
5.04
4.64
4.61
4.55
4.53
4.52
4.49
4.23
4.20
4.16
4.02
3.94
3.79
3.68
0.00
1.86
0.95
3.82
1.90
3.74
1.85
0.99
1.04
1.96
1.07
1.02
2.00
0.99
2.79
2.93
2.73
Chemical Shift (ppm)

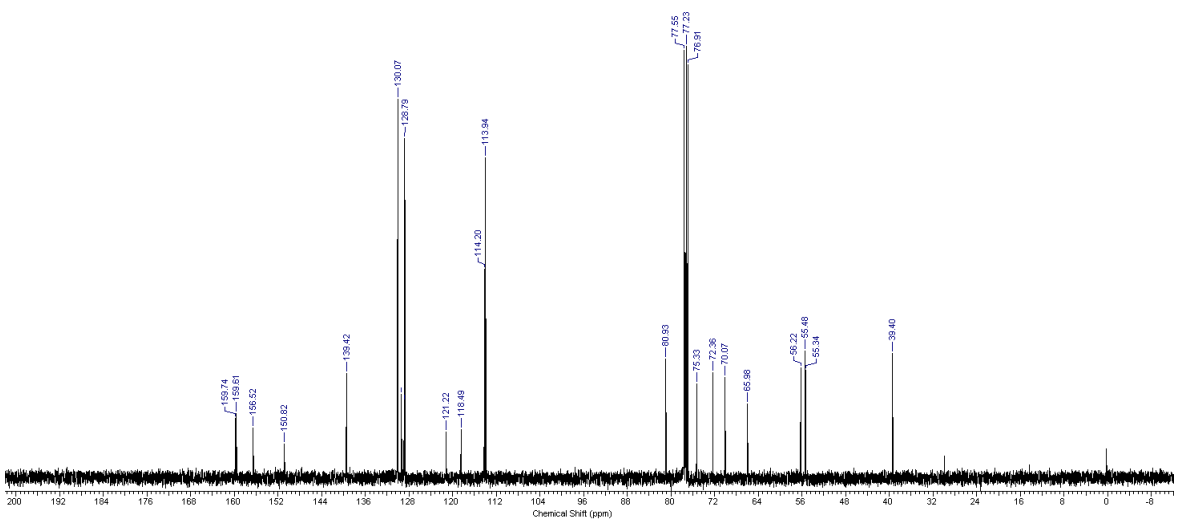
159.74
159.61
156.52
150.82
139.42
130.07
128.79
121.22
118.49
114.20
113.94
77.55
77.23
76.91
80.93
75.33
72.36
70.07
65.98
56.22
55.48
55.34
39.40
Chemical Shift (ppm)

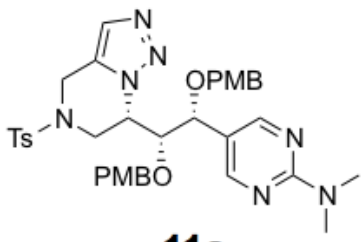
N
N
N
OPMB
Ts
N
N
PMBO
N
N

11a

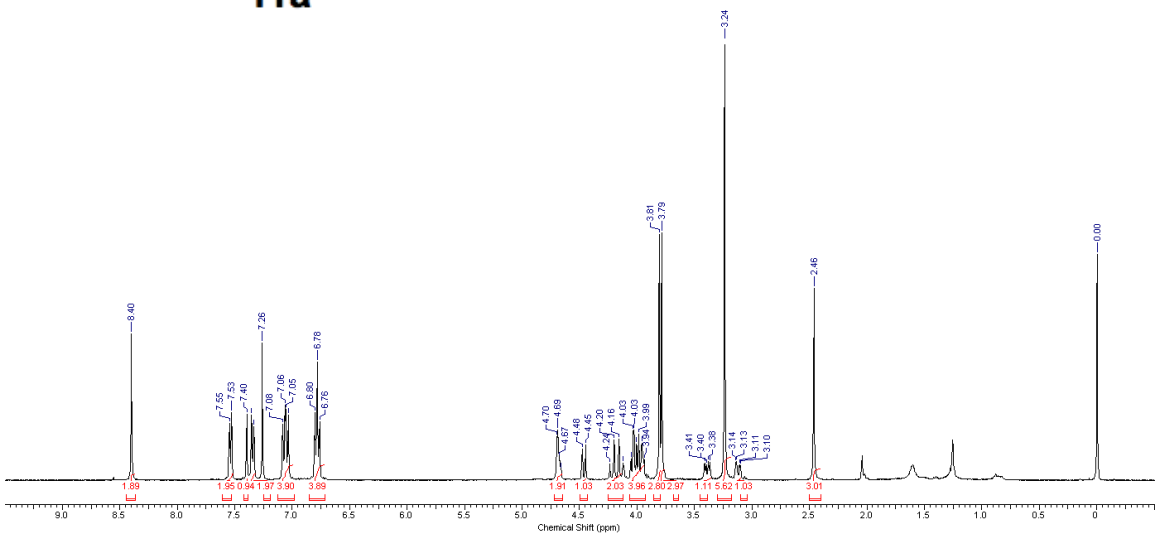
8.40
7.55
7.53
7.40
7.26
7.08
7.06
7.05
6.80
6.78
6.76
4.70
4.69
4.67
4.46
4.45
4.20
4.16
4.03
4.03
3.99
3.94
3.41
3.40
3.38
3.24
3.14
3.13
3.11
3.10
3.81
3.79
2.46
0.00
1.89
1.95
0.94
1.97
3.90
3.89
1.91
1.03
2.03
3.96
2.80
2.97
1.11
5.62
1.03
3.01
Chemical Shift (ppm)

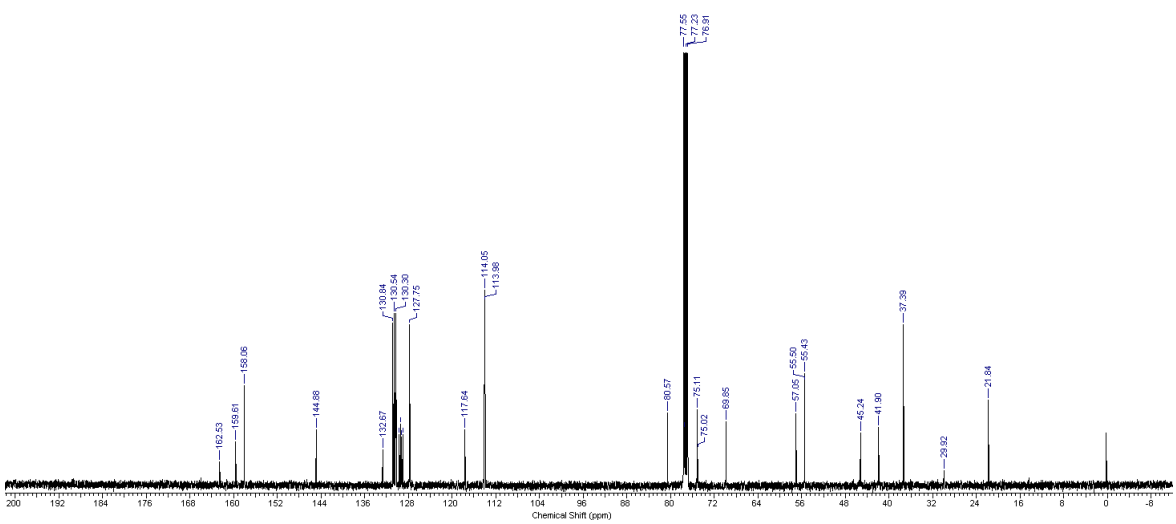
77.55
77.23
76.91
130.84
130.54
130.30
127.75
114.05
113.98
162.53
159.61
158.06
144.88
132.67
117.64
80.57
75.11
75.02
69.85
57.05
55.50
55.43
45.24
41.90
37.39
29.92
21.84
Chemical Shift (ppm)

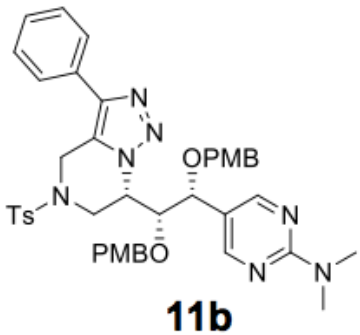

11b

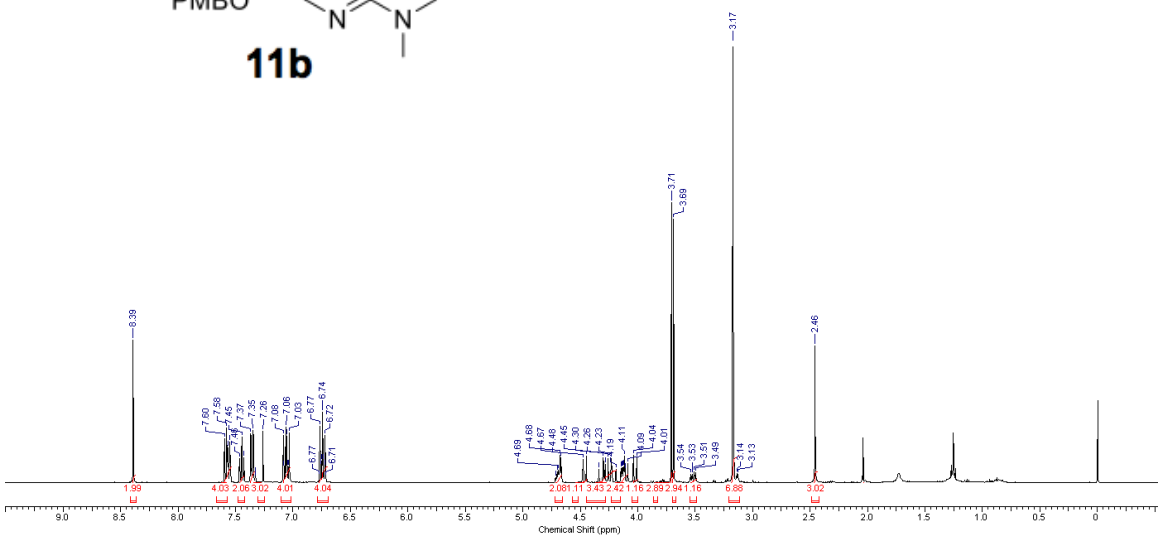

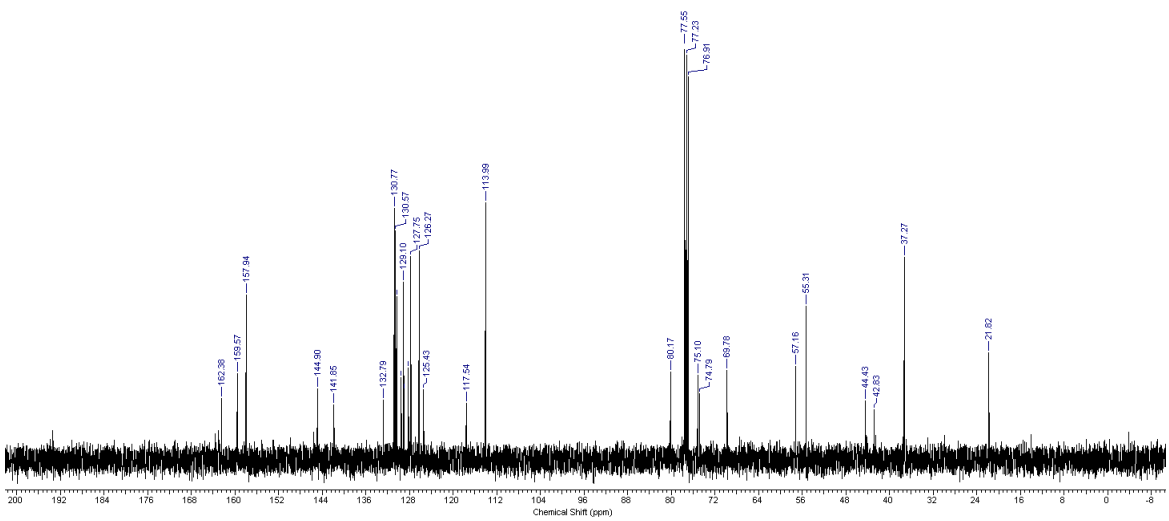

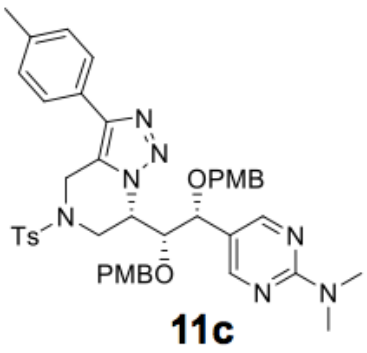
N
N
N
OPMB
Ts
N
PMBO
N
N
N

11c

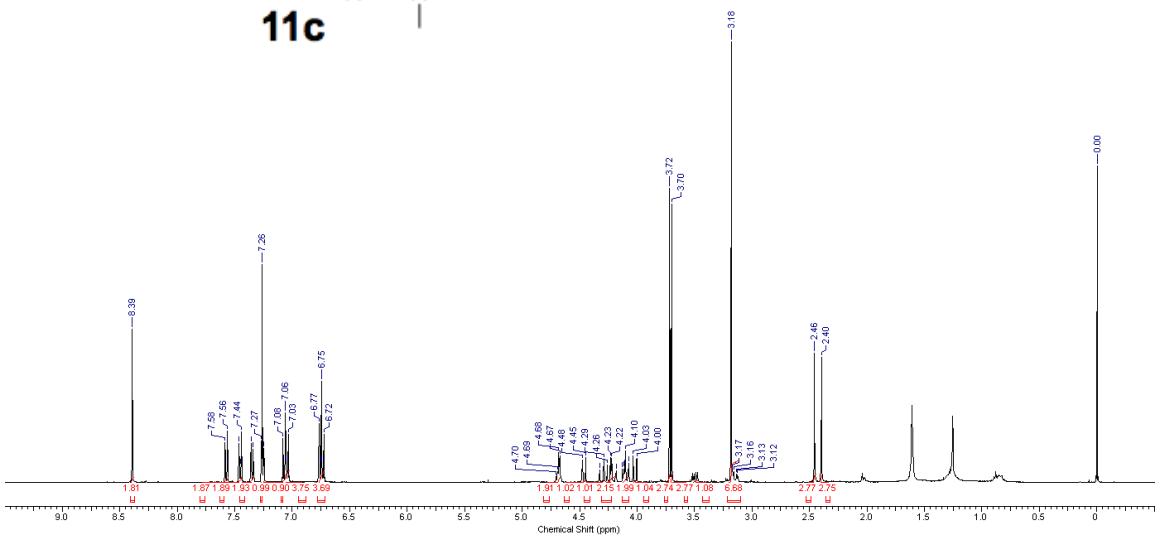
8.39
7.58
7.56
7.44
7.27
7.26
7.08
7.06
7.03
6.77
6.75
6.72
4.70
4.69
4.68
4.67
4.48
4.45
4.39
4.26
4.23
4.22
4.10
4.03
4.00
3.72
3.70
3.18
3.17
3.16
3.13
3.12
2.46
2.40
0.00
1.81
1.87 1.89 1.93 0.99 0.90 3.75 3.69
1.91 1.02 1.01 2.15 1.99 1.04 2.74 2.77 1.08
6.68
2.77 2.75
Chemical Shift (ppm)

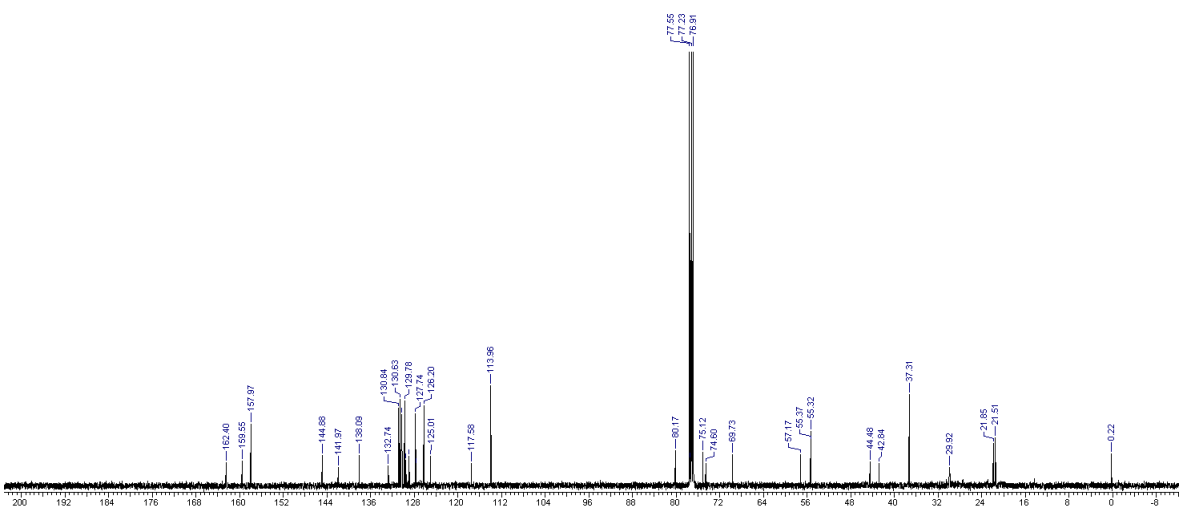
162.40
159.55
157.97
144.88
141.97
138.09
132.74
130.84
130.63
129.76
127.74
126.20
125.01
117.58
113.96
80.17
77.55
77.23
76.91
75.12
74.69
69.73
57.17
55.57
55.32
44.48
42.84
37.31
29.92
21.85
21.51
0.22
Chemical Shift (ppm)

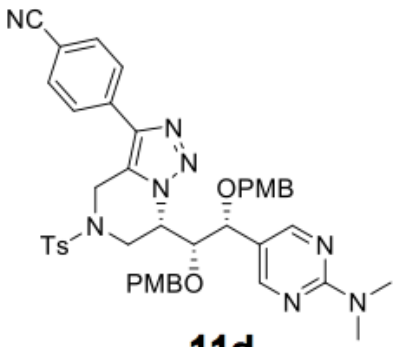
NC
N
N
N
OPMB
Ts
N
PMBO
N
N
N

11d

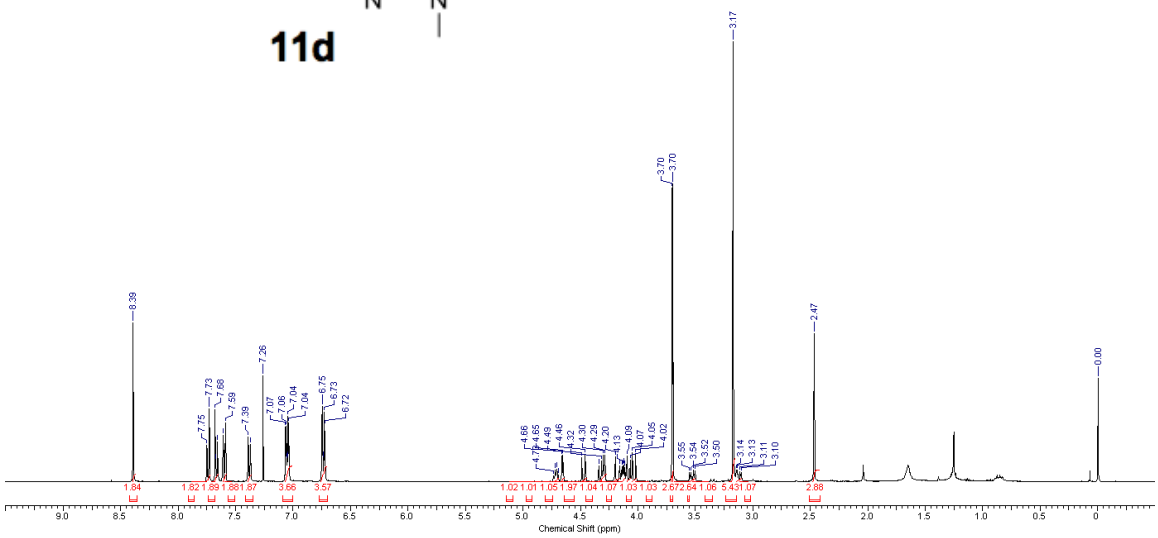
Chemical Shift (ppm)

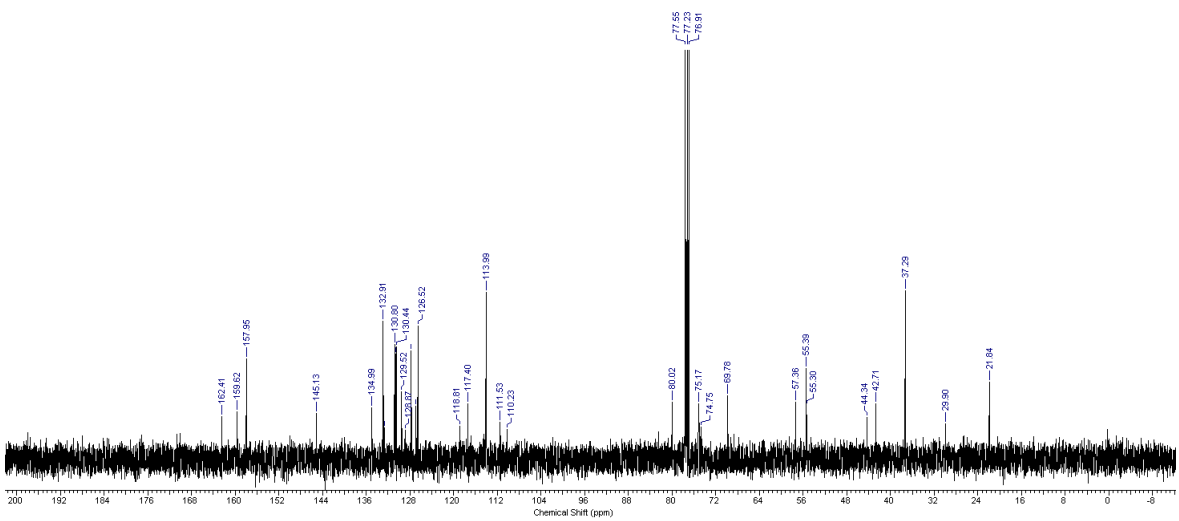
Chemical Shift (ppm)

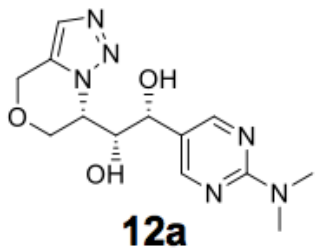
N
N
N
OH
O
OH
N
N
N

12a

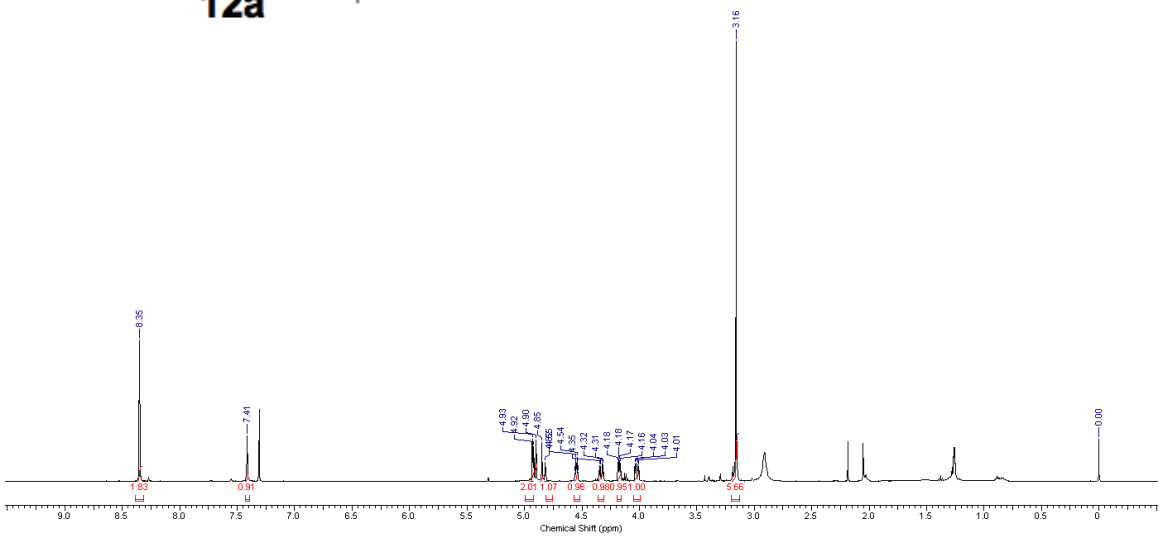
8.35
7.41
4.93
4.92
4.90
4.85
4.54
4.35
4.32
4.31
4.18
4.18
4.17
4.16
4.04
4.03
4.01
3.16
0.00
1.83
0.91
2.01
1.07
0.96
0.98
0.95
1.00
5.66
Chemical Shift (ppm)

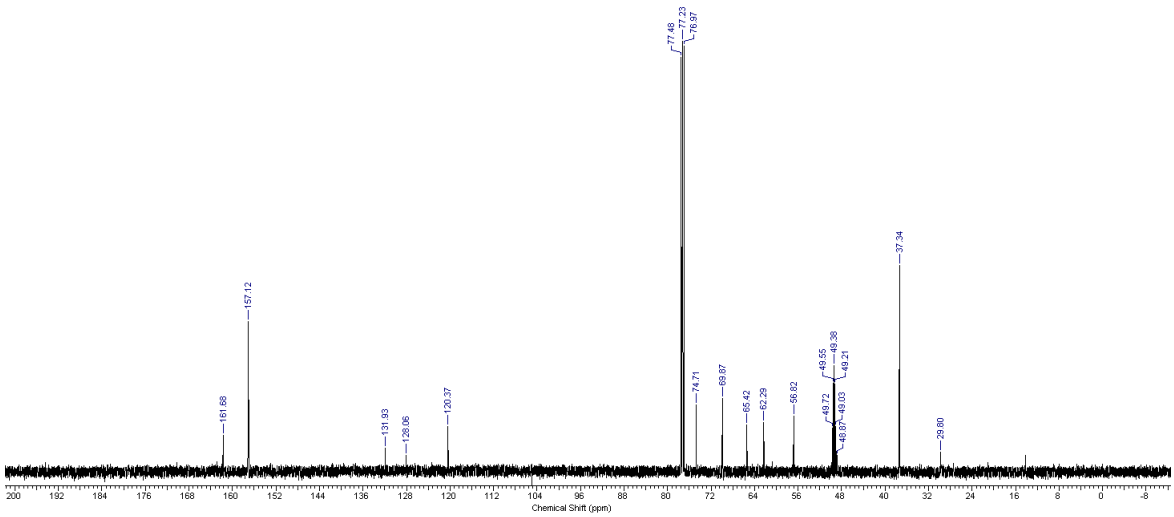
161.68
157.12
131.93
128.06
120.37
77.48
77.23
76.97
74.71
69.87
65.42
62.29
56.82
49.72
49.55
49.38
49.21
49.03
48.87
37.34
29.80
Chemical Shift (ppm)

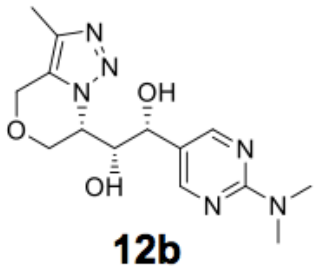
N
N
N
OH
O
OH
N
N
N

12b

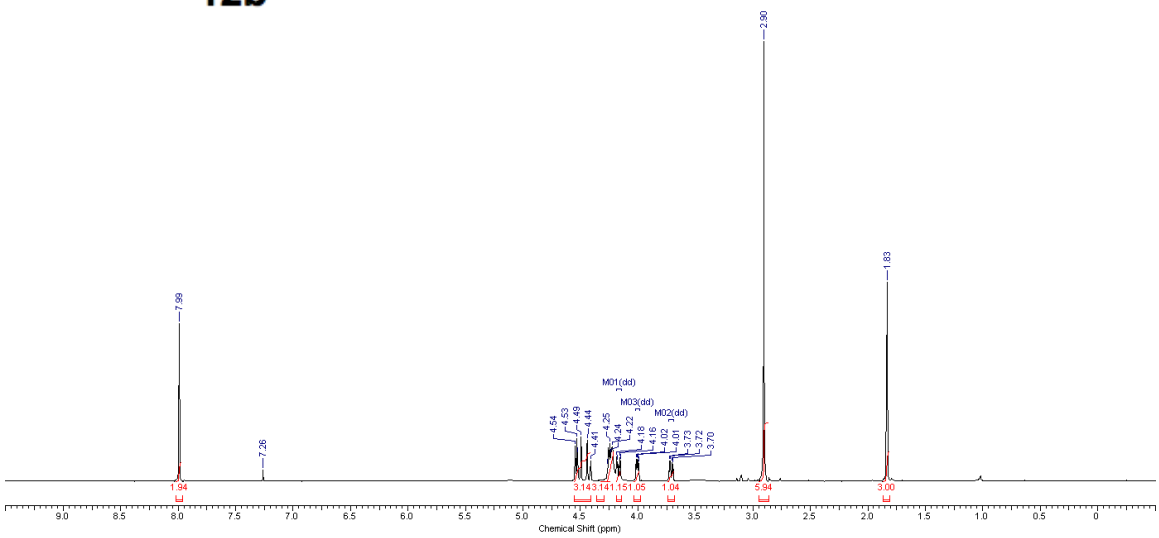
7.99
7.26
M01(dd)
M03(dd)
M02(dd)
4.54
4.53
4.49
4.44
4.41
4.25
4.24
4.22
4.18
4.16
4.07
4.01
3.73
3.72
3.70
2.90
1.83
1.94
3.14
3.14
1.41
1.51
1.05
1.04
5.94
3.00
Chemical Shift (ppm)

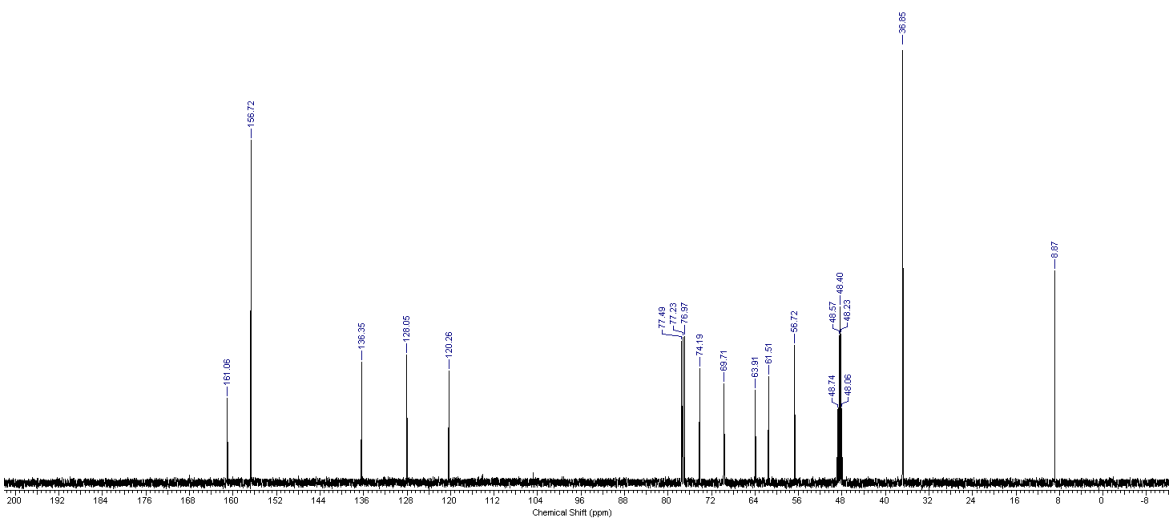
161.06
156.72
136.35
128.05
120.26
77.49
77.23
76.97
74.19
69.71
63.91
61.51
56.72
48.74
48.57
48.40
48.23
48.06
36.85
8.87
Chemical Shift (ppm)

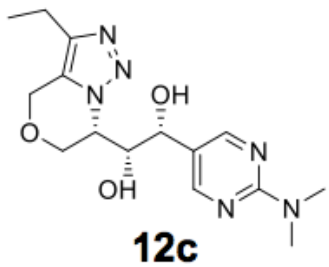
N
N
N
OH
O
OH
N
N
N

12c

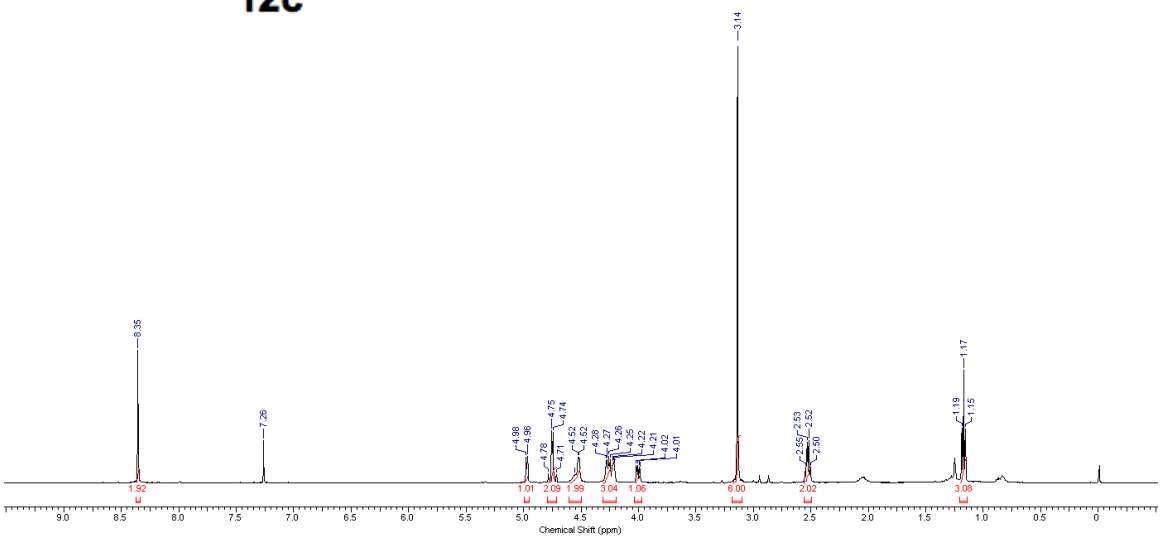
8.35
7.26
4.88
4.86
4.78
4.75
4.74
4.71
4.52
4.52
4.28
4.27
4.26
4.25
4.22
4.21
4.02
4.01
3.14
2.55
2.53
2.52
2.50
1.19
1.17
1.15
1.92
1.01
2.09
1.99
3.04
1.06
6.00
2.02
3.08
Chemical Shift (ppm)

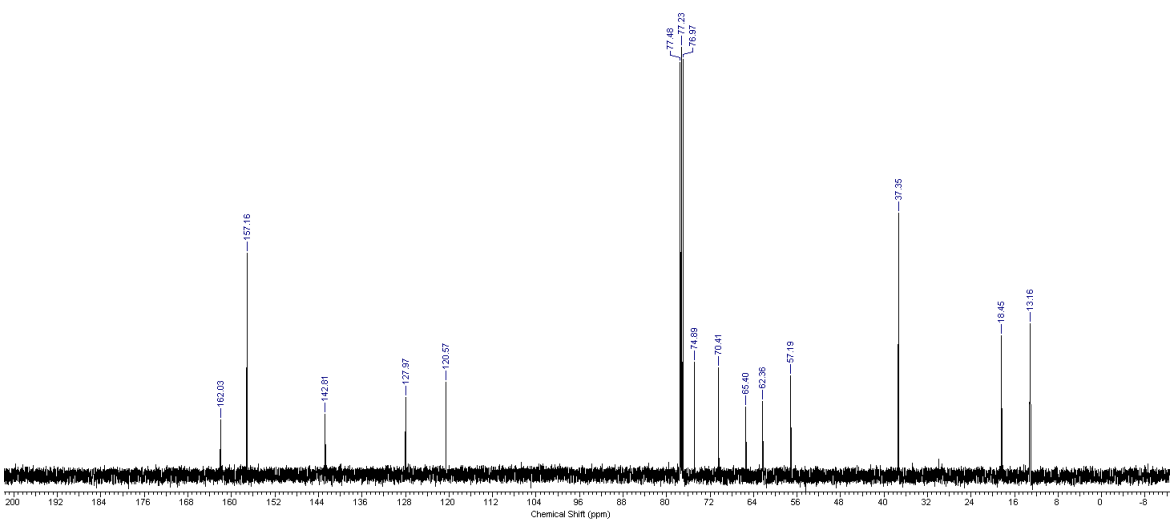
77.48
77.23
76.97
162.03
157.16
142.81
127.97
120.57
74.89
70.41
65.40
62.36
57.19
37.35
18.45
13.16
Chemical Shift (ppm)

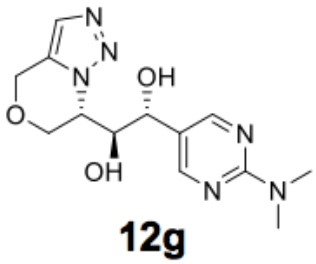
N
N
N
OH
O
OH
N
N
N

12g

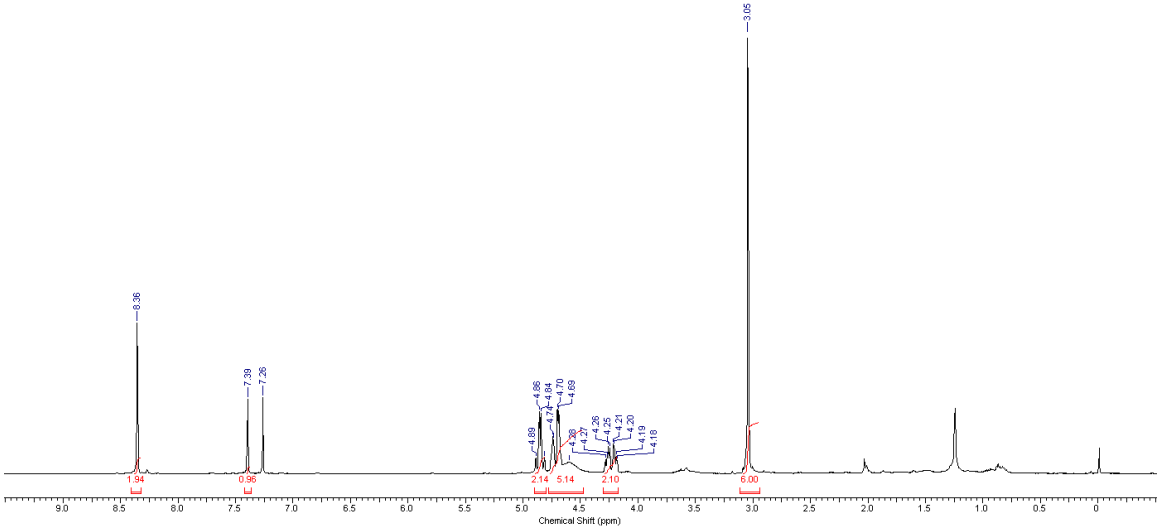
8.36
7.39
7.26
4.88
4.84
4.74
4.70
4.69
4.89
4.27
4.26
4.25
4.21
4.20
4.19
4.18
3.05
1.94
0.96
2.14
5.14
2.10
6.00
Chemical Shift (ppm)

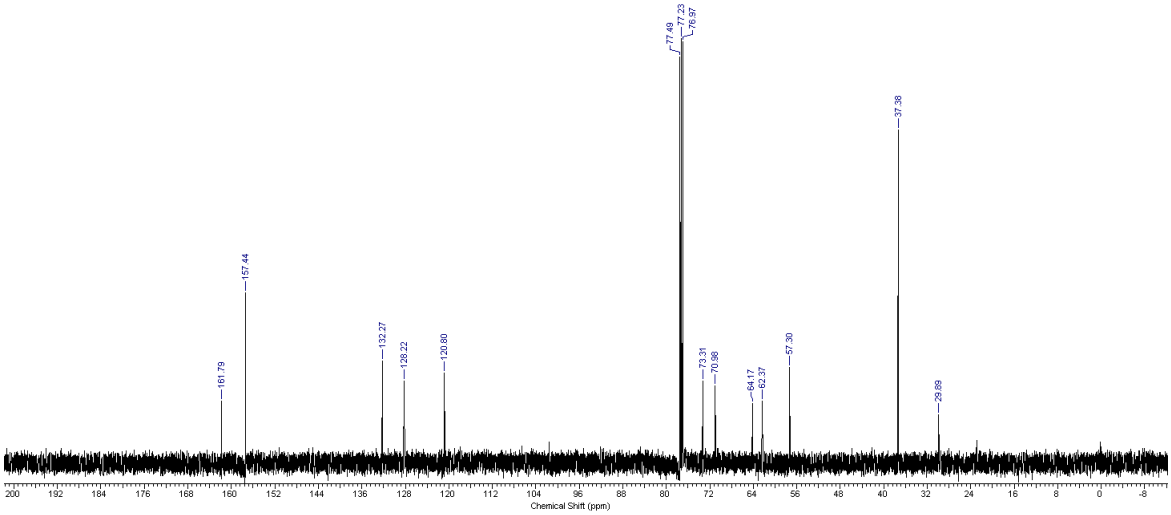
161.79
157.44
132.27
128.22
120.80
77.49
77.23
76.97
73.31
70.98
64.17
62.37
57.30
37.38
29.89
Chemical Shift (ppm)

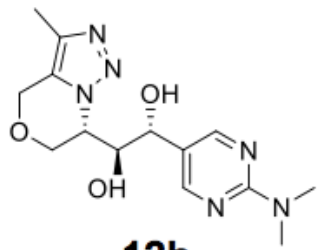
N
N
N
OH
O
OH
N
N
N

12h

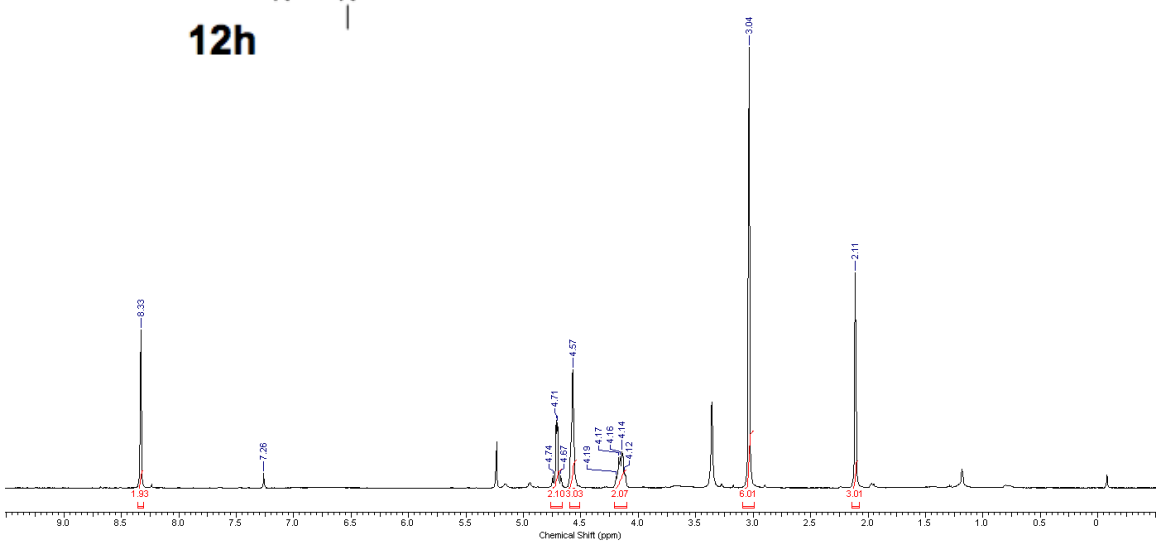
8.33
7.26
4.74
4.71
4.67
4.57
4.19
4.17
4.16
4.14
4.12
3.04
2.11
1.93
2.10
3.03
2.07
6.01
3.01
Chemical Shift (ppm)

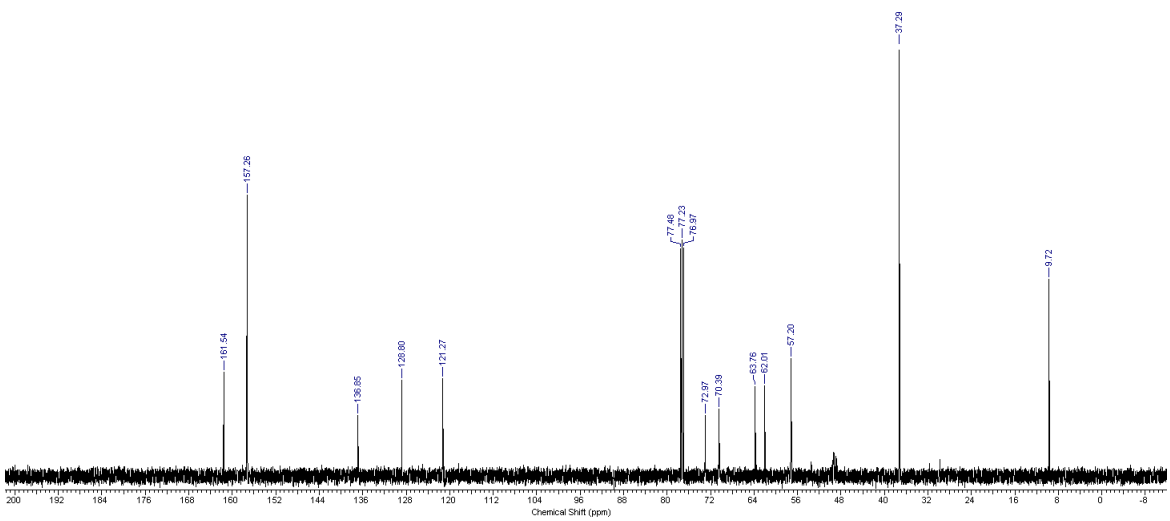
181.54
157.26
136.85
128.80
121.27
77.48
77.23
76.97
72.97
70.39
63.76
62.01
57.20
37.29
9.72
Chemical Shift (ppm)

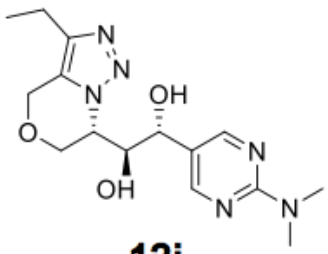
N
N
N
OH
O
OH
N
N
N

12i

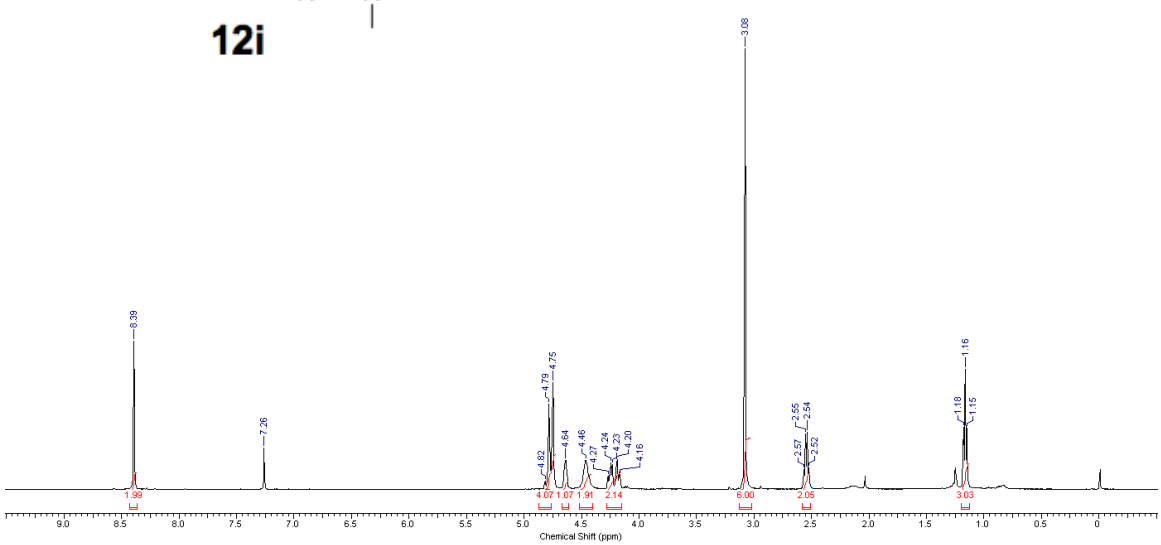
8.39
7.26
4.82
4.79
4.75
4.64
4.46
4.27
4.24
4.23
4.20
4.16
3.08
2.57
2.55
2.54
2.52
1.18
1.16
1.15
1.99
4.07
1.07
1.91
2.14
6.00
2.05
3.03
Chemical Shift (ppm)

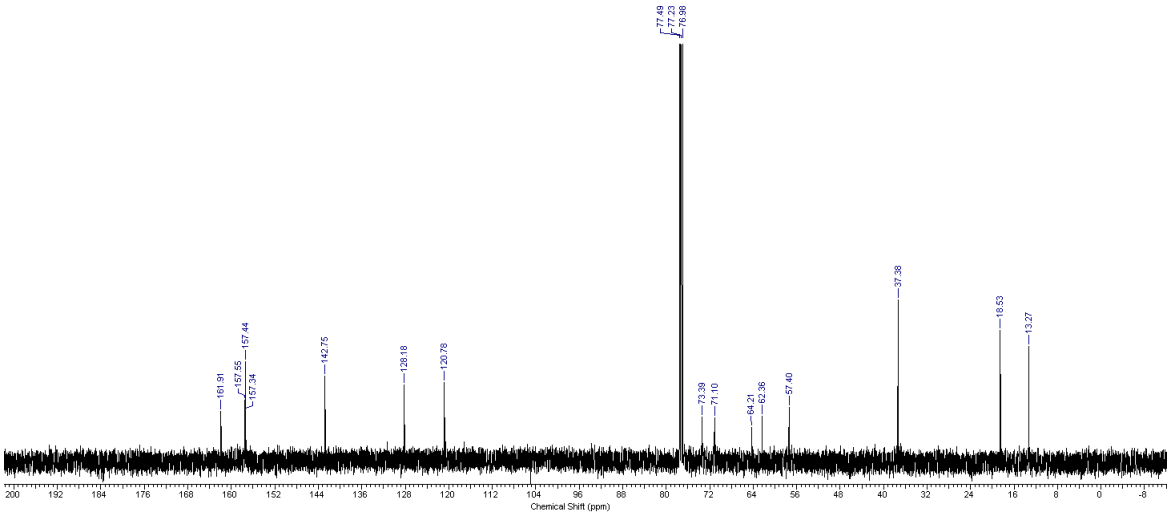
77.49
77.23
76.98
161.91
157.55
157.34
157.44
142.75
128.18
120.79
73.39
71.10
64.21
62.36
57.40
37.38
18.53
13.27
Chemical Shift (ppm)

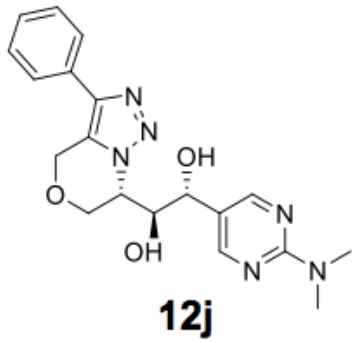
N
N
N
OH
O
OH
N
N
N

12j

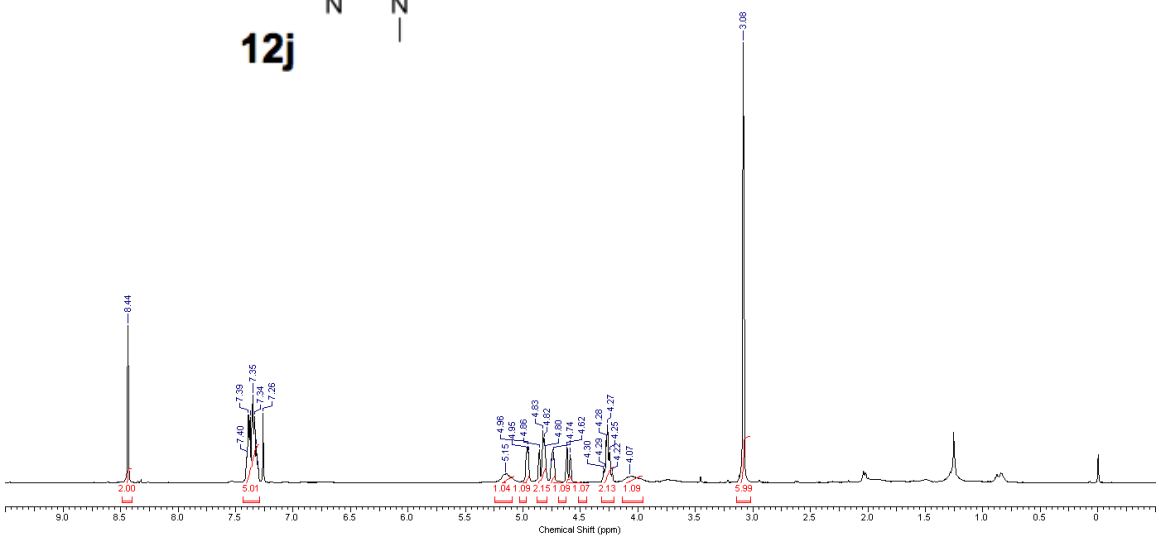
8.44
7.40
7.39
7.35
7.34
7.26
5.15
4.96
4.95
4.86
4.83
4.82
4.80
4.74
4.62
4.30
4.29
4.28
4.27
4.25
4.22
4.07
3.08
2.00
5.01
1.04
1.09
2.15
1.09
1.07
2.13
1.09
5.99
Chemical Shift (ppm)

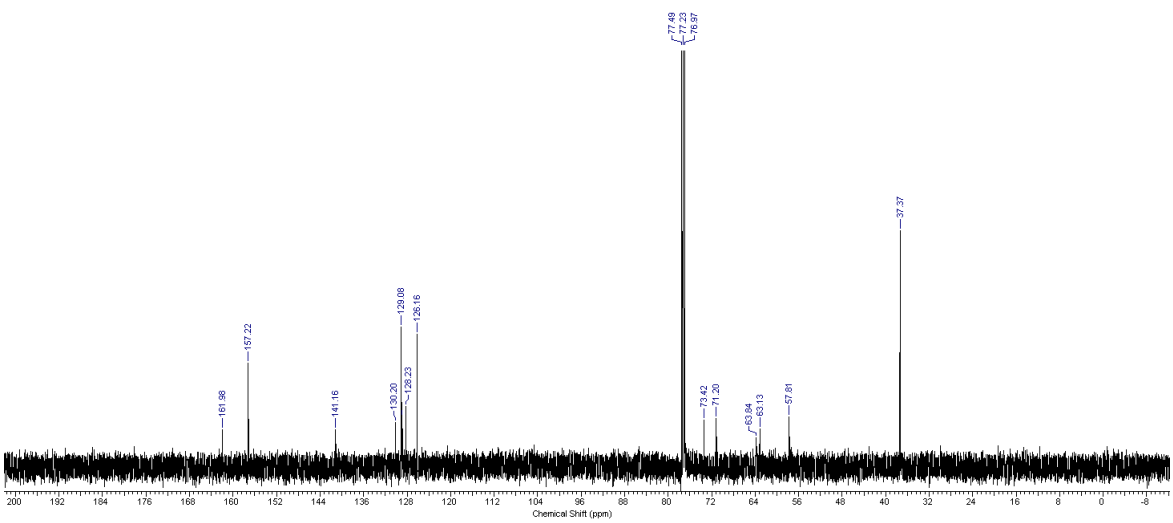
161.98
157.22
141.16
130.20
129.08
128.23
126.16
77.49
77.23
76.97
73.42
71.20
63.84
63.13
57.81
37.37
Chemical Shift (ppm)

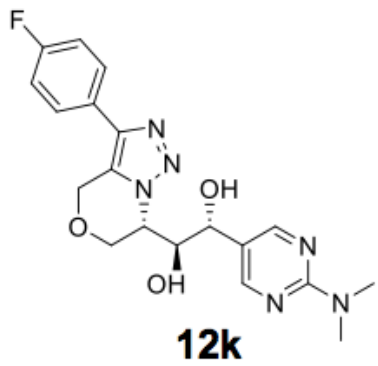
F
N
N
N
O
OH
OH
N
N
N

12k

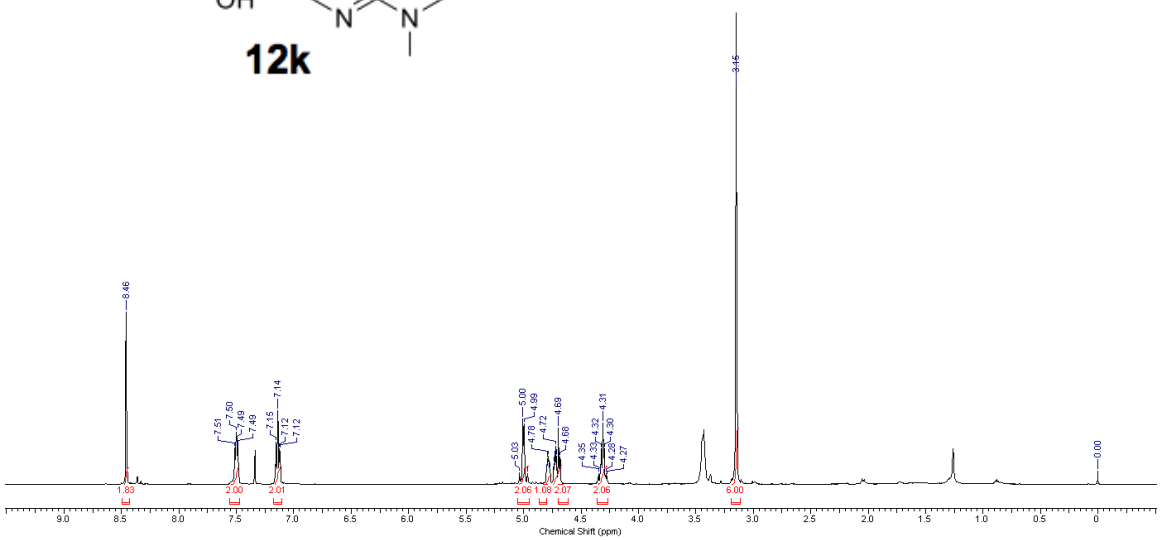
8.46
7.51
7.50
7.49
7.48
7.15
7.14
7.12
7.12
5.03
5.00
4.99
4.76
4.72
4.69
4.68
4.35
4.33
4.32
4.31
4.30
4.28
4.27
3.45
0.00
1.83
2.00
2.01
2.06
1.08
2.07
2.06
6.00
Chemical Shift (ppm)

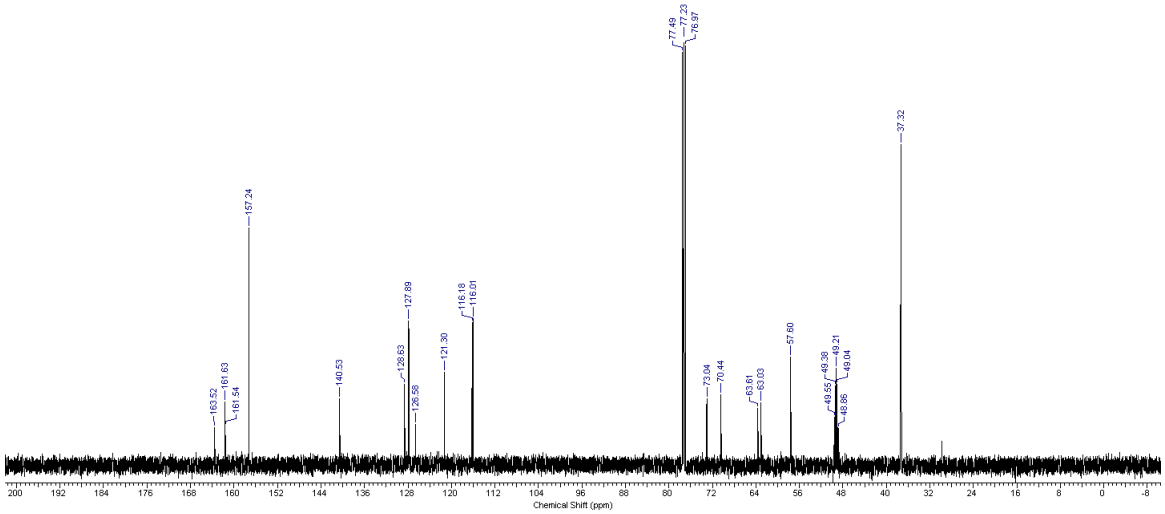
157.24
163.52
161.63
161.54
140.53
129.63
127.89
126.98
121.30
116.18
116.01
77.49
77.23
76.97
73.04
70.44
63.61
63.03
57.60
49.55
49.38
49.21
49.04
48.86
37.32
Chemical Shift (ppm)

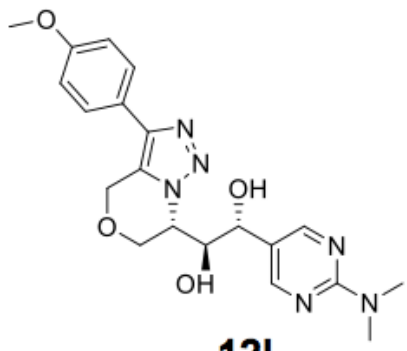
O
N
N
N
OH
O
OH
N
N
N

12l

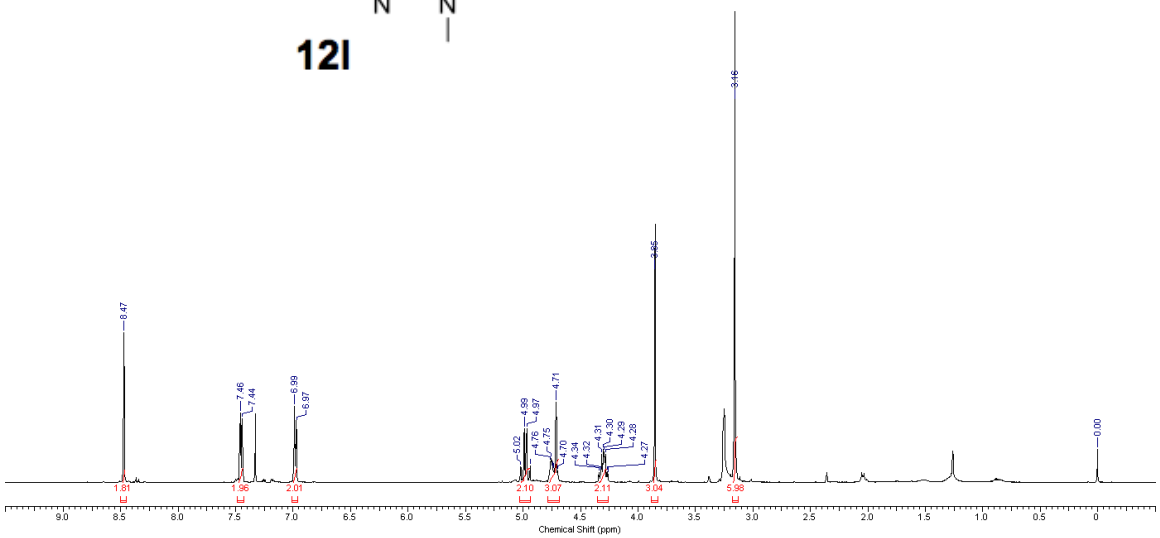
8.47
7.46
7.44
6.99
6.97
5.02
4.98
4.97
4.76
4.75
4.71
4.70
4.34
4.32
4.31
4.30
4.29
4.28
4.27
3.85
3.46
0.00
1.81
1.96
2.01
2.10
3.07
2.11
3.04
5.98
Chemical Shift (ppm)

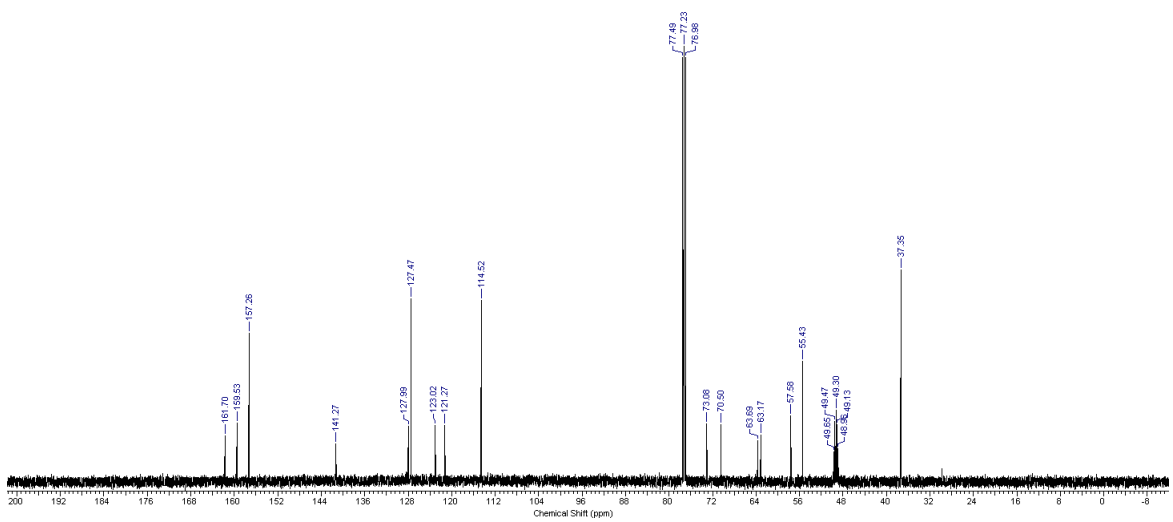
77.49
77.23
76.98
161.70
159.53
157.26
141.27
127.99
127.47
123.02
121.27
114.52
73.08
70.50
63.69
63.17
57.58
55.43
49.65
49.47
49.30
49.13
37.35
Chemical Shift (ppm)

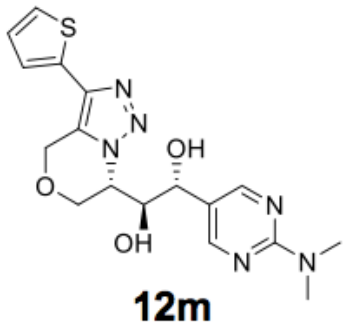
S
N
N
N
OH
O
OH
N
N
N

12m

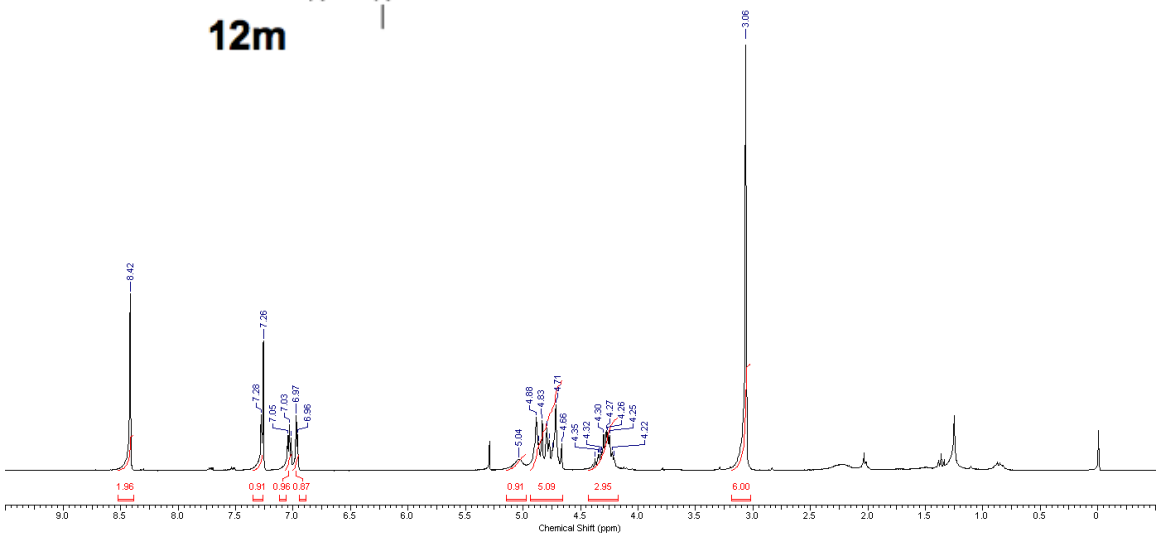
8.42
7.26
7.28
7.05
7.03
6.97
6.96
4.88
4.83
4.71
4.66
5.04
4.35
4.32
4.30
4.27
4.26
4.25
4.22
3.06
1.96
0.91
0.96
0.87
0.91
5.09
2.95
6.00
Chemical Shift (ppm)

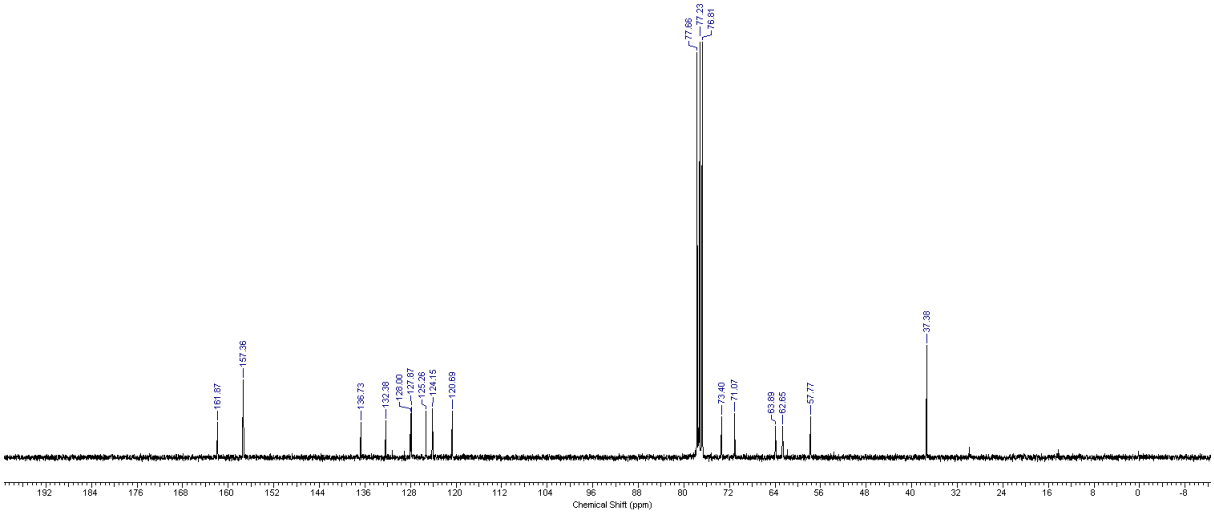
77.66
77.23
76.81
161.87
157.36
136.73
132.39
128.00
127.87
125.26
124.15
120.69
73.40
71.07
63.89
62.65
57.77
37.38
Chemical Shift (ppm)

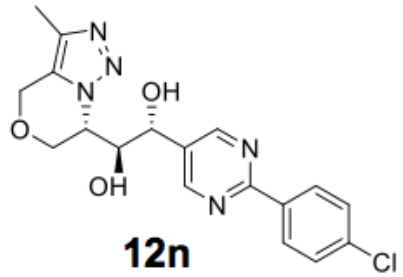
N
N
N
OH
O
OH
N
N
Cl

12n

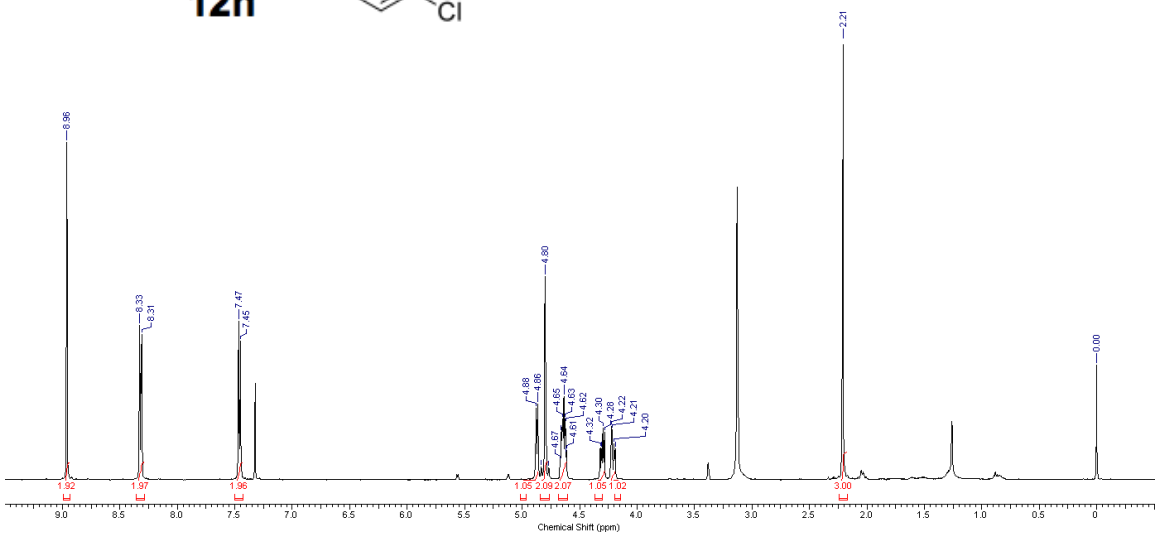
8.96
8.33
8.31
7.47
7.45
4.90
4.88
4.86
4.65
4.64
4.63
4.62
4.61
4.57
4.32
4.30
4.28
4.22
4.21
4.20
2.21
0.00
1.92
1.97
1.96
1.05
2.09
2.07
1.05
1.02
3.00
Chemical Shift (ppm)

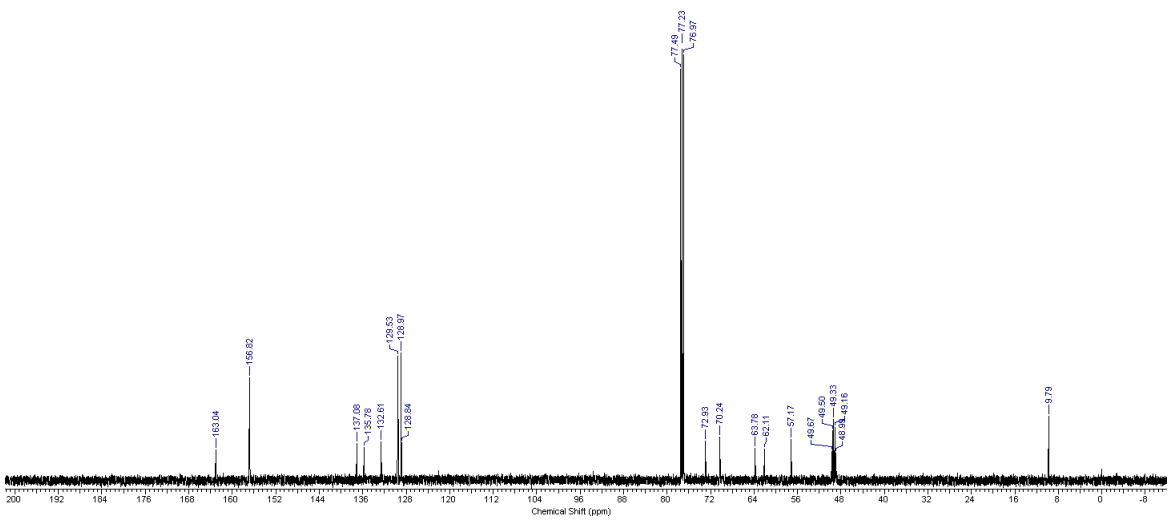
77.45
77.23
76.97
156.82
163.04
137.08
135.78
132.61
129.53
128.97
128.84
72.93
70.24
63.78
62.11
57.17
49.67
49.50
49.33
49.16
9.79
Chemical Shift (ppm)

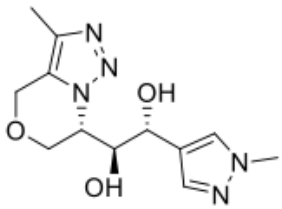
N
N
N
OH
O
OH
N
N

12o

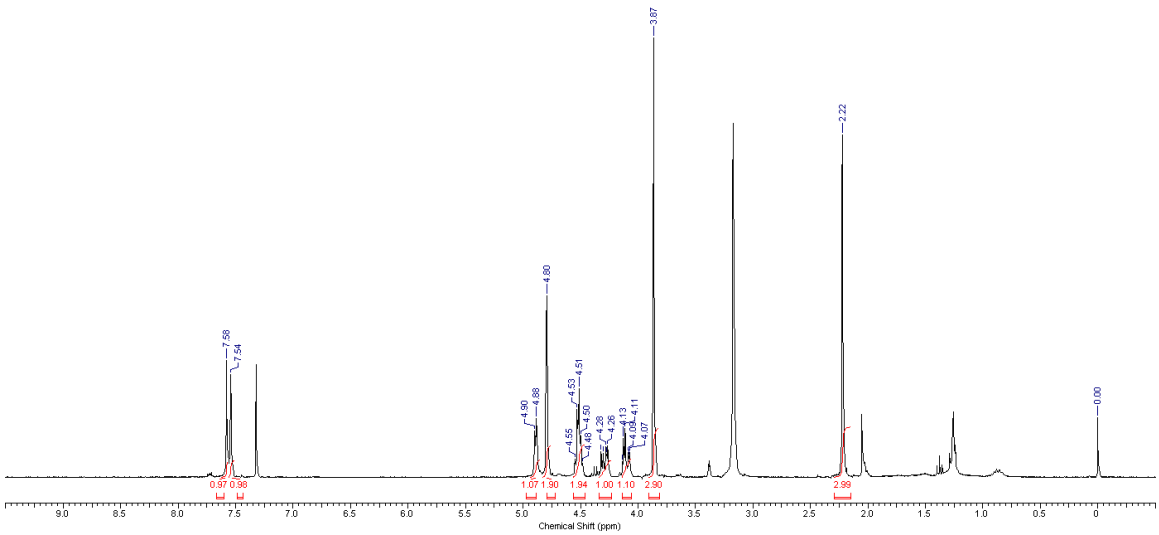
7.58
7.54
4.90
4.88
4.80
4.55
4.53
4.51
4.50
4.48
4.28
4.26
4.13
4.11
4.07
3.87
2.22
0.00
0.97 0.98
1.07 1.90
1.94
1.00 1.10
2.90
2.99
Chemical Shift (ppm)

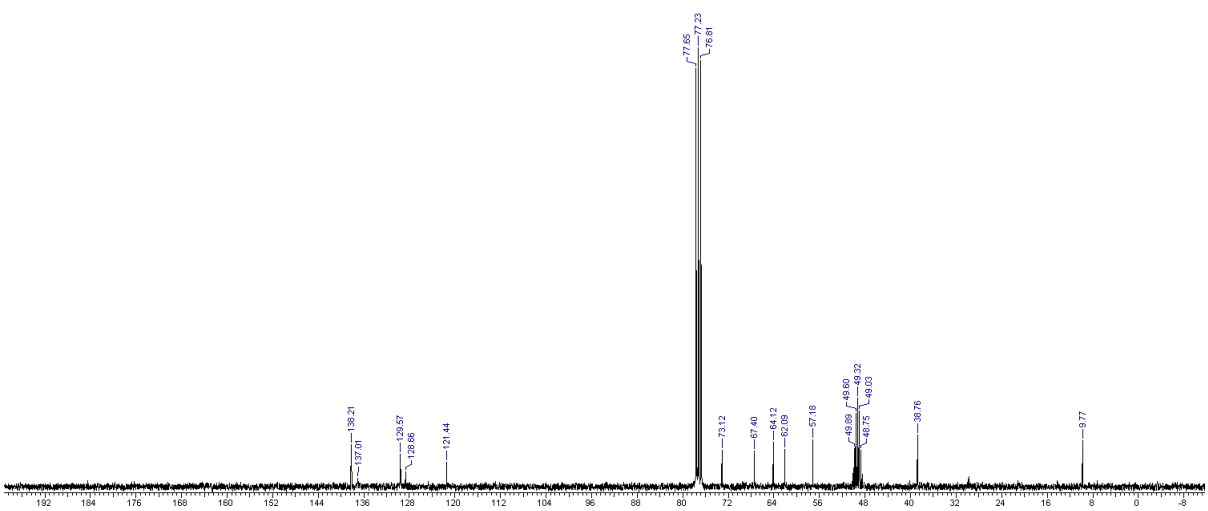
77.65
77.23
76.81
138.21
137.01
129.57
128.66
121.44
73.12
67.40
64.12
62.09
57.16
49.60
49.32
49.03
48.89
48.75
38.76
9.77
Chemical Shift (ppm)

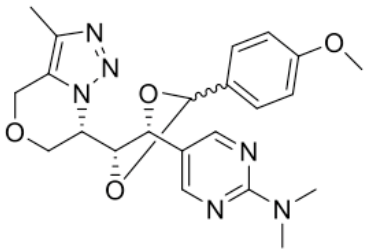

13b obtained by DDQ treatment

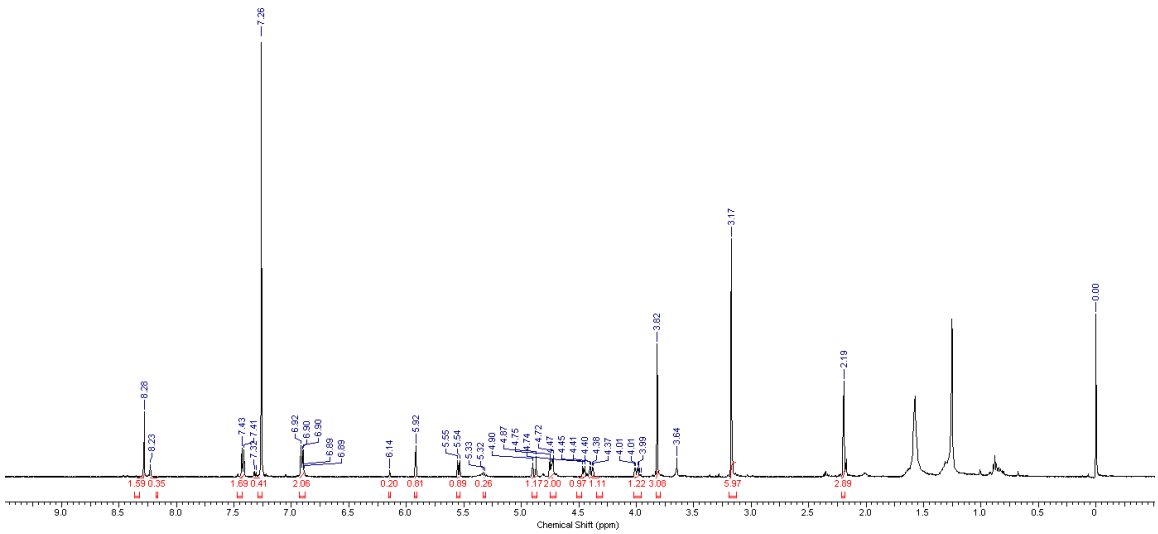

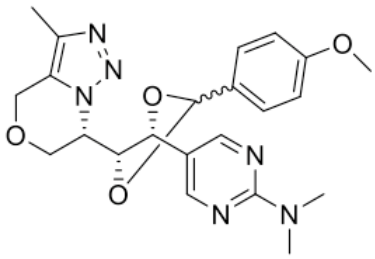

13b obtained by acetal exchange

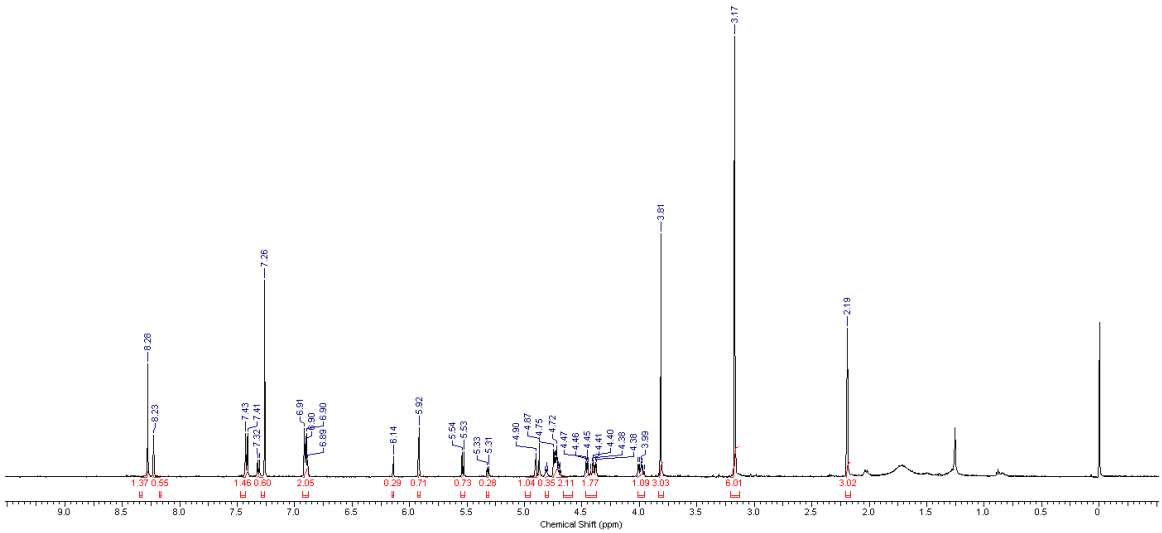

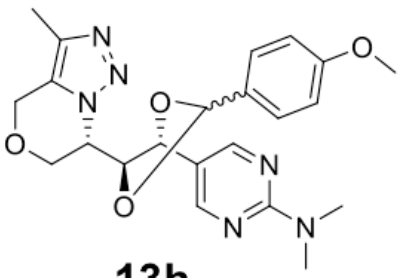

13h

Diastereomer 1 (**13h-1**)

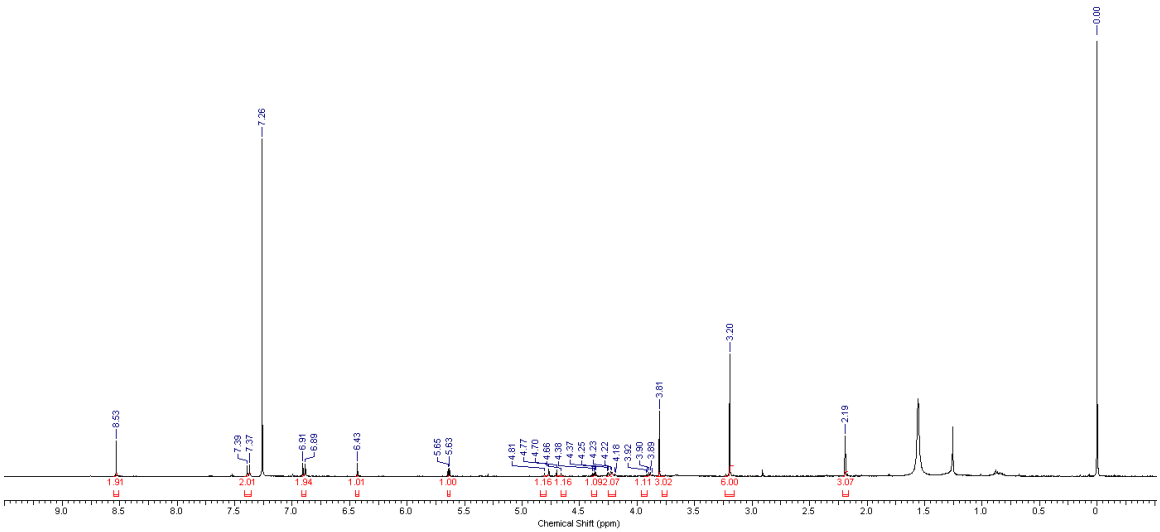

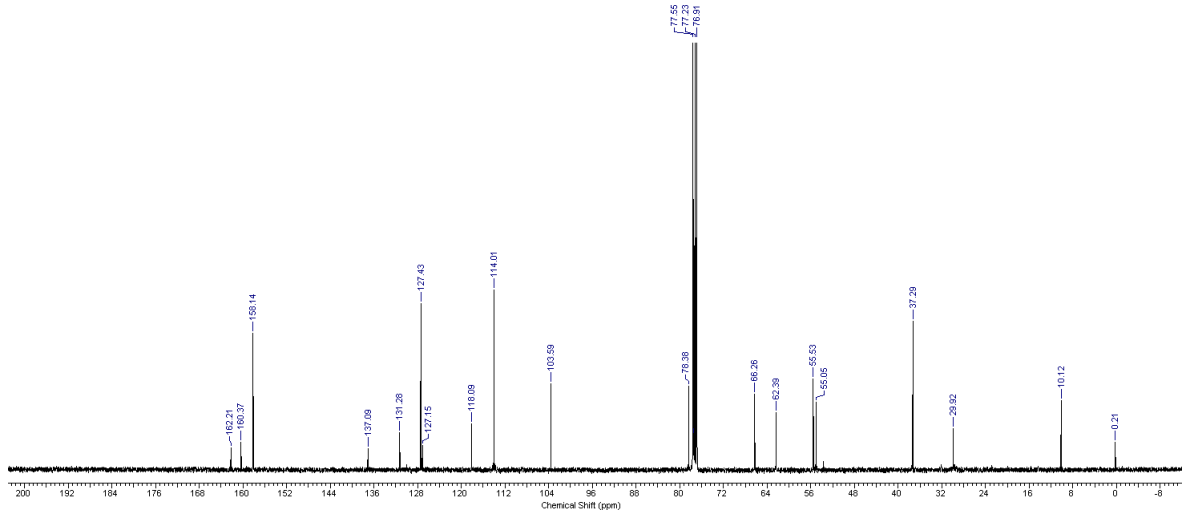

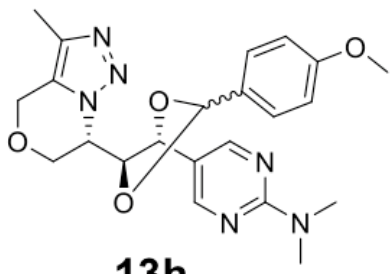

13h

Diastereomer 2 (**13h-2**)

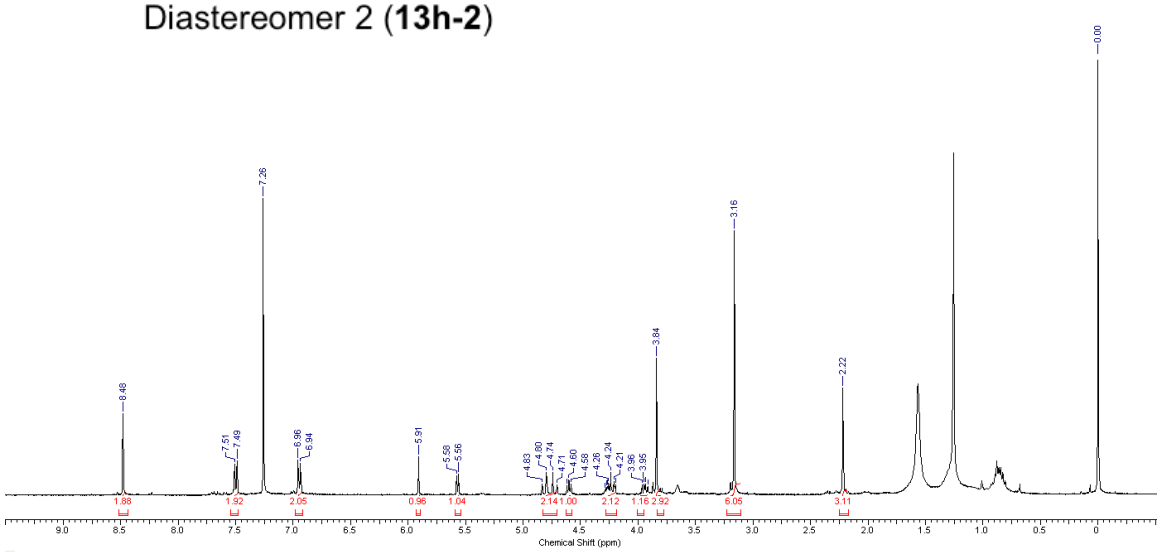

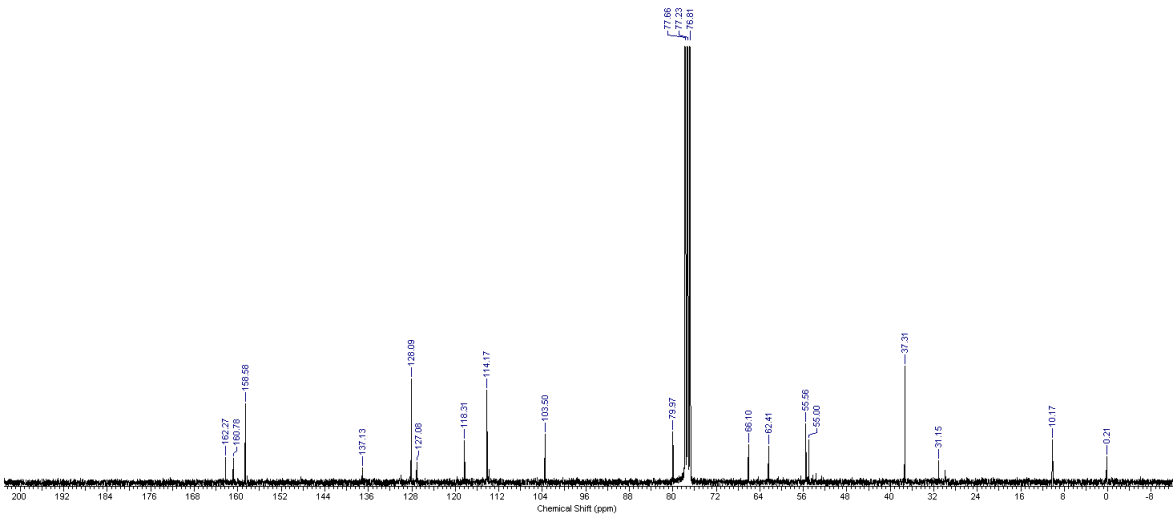

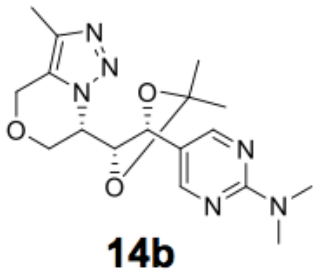

14b

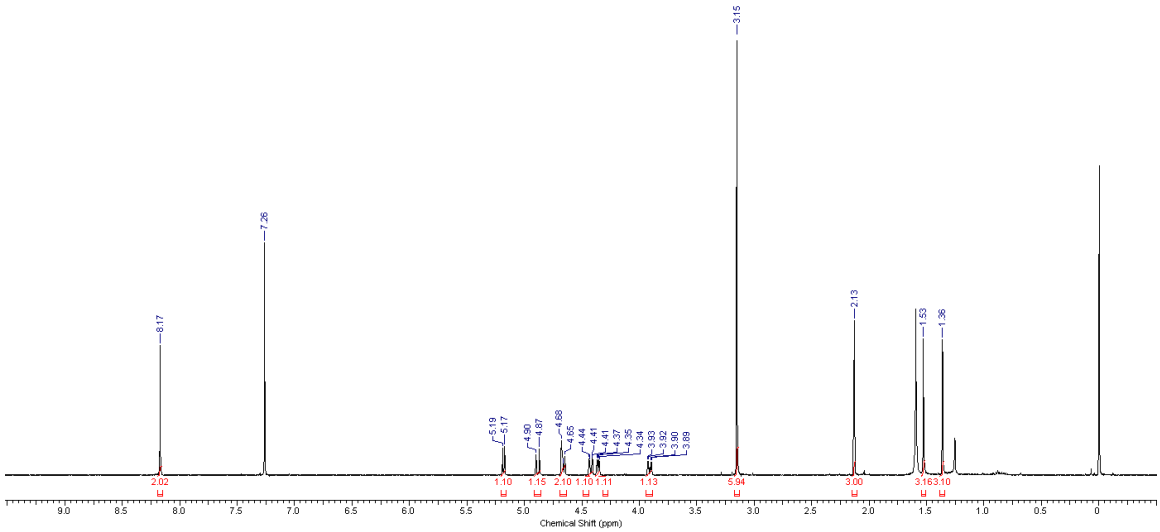
8.17
7.26
5.19
5.17
4.90
4.87
4.68
4.65
4.44
4.41
4.41
4.37
4.35
4.34
3.93
3.92
3.90
3.89
3.15
2.13
1.53
1.36
2.02
1.10
1.15
2.10
1.10
1.01
1.11
1.13
5.94
3.00
3.16
3.10
Chemical Shift (ppm)

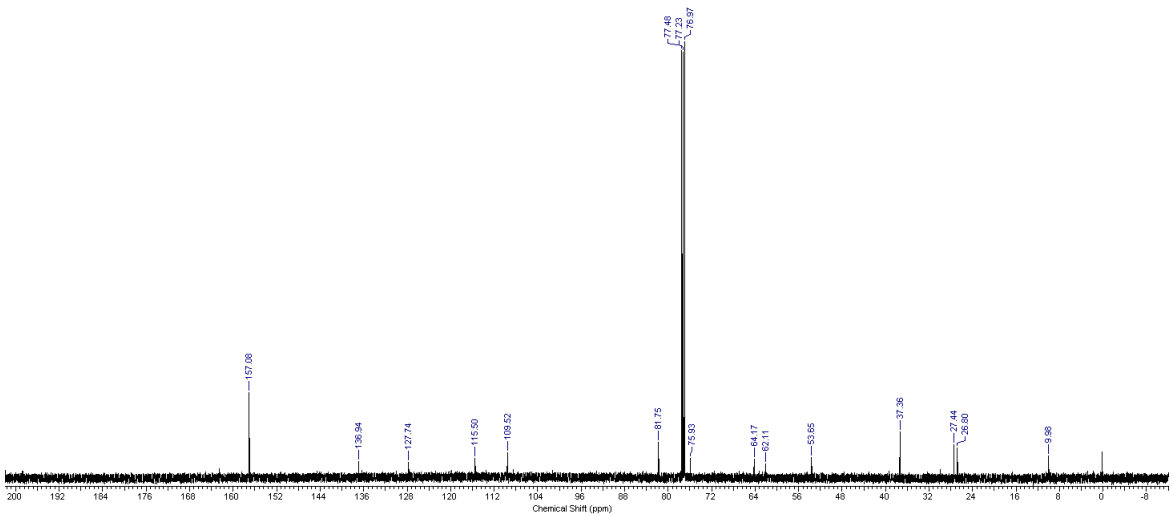
77.48
77.23
76.97
157.09
138.94
127.74
115.50
109.52
81.75
75.93
64.17
62.11
53.65
37.36
27.44
26.80
9.98
Chemical Shift (ppm)

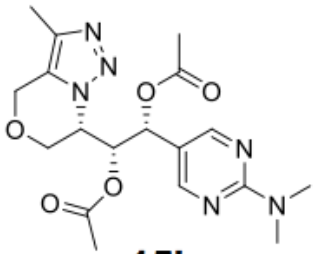

15b

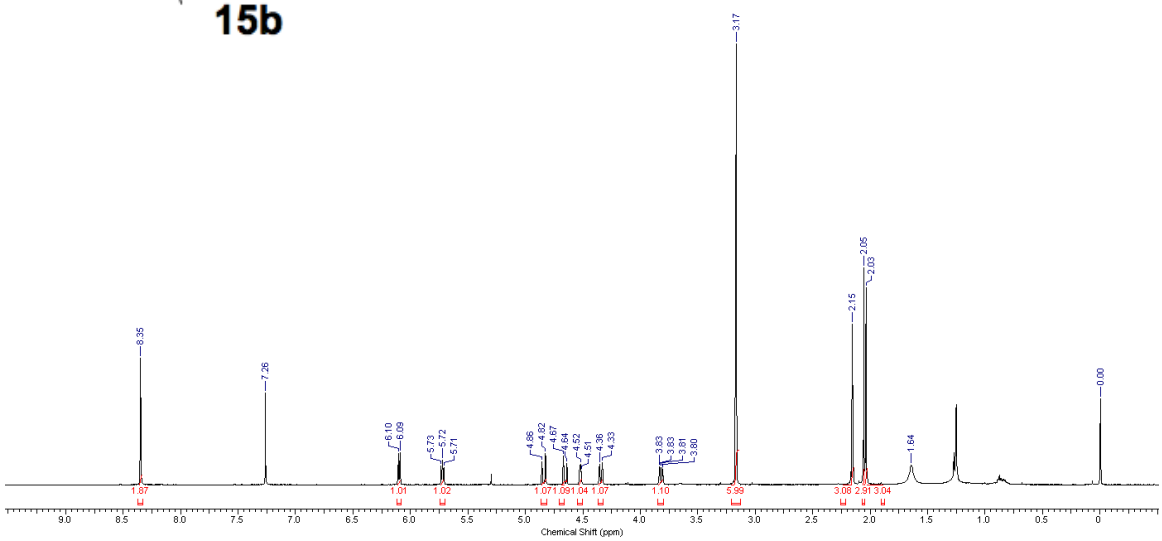
8.35
7.26
6.10
6.09
5.73
5.72
5.71
4.86
4.82
4.67
4.64
4.52
4.51
4.36
4.33
3.83
3.83
3.81
3.80
3.17
2.15
2.05
2.03
1.64
0.00
1.87
1.01
1.02
1.07
1.09
1.04
1.07
1.10
5.99
3.06
2.91
3.04
Chemical Shift (ppm)

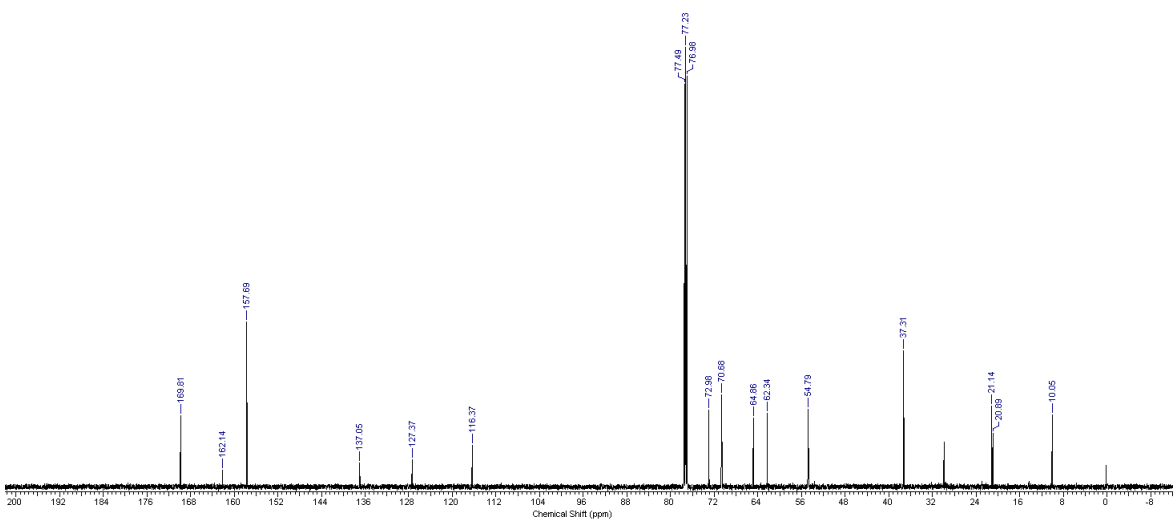
169.81
162.14
157.69
137.05
127.37
116.37
77.49
77.23
76.98
72.98
70.88
64.86
62.34
54.79
37.31
21.14
20.89
10.05
Chemical Shift (ppm)

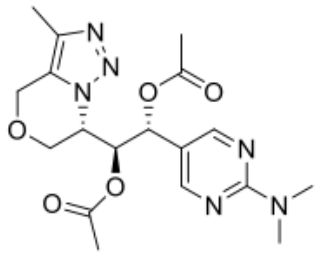

15h

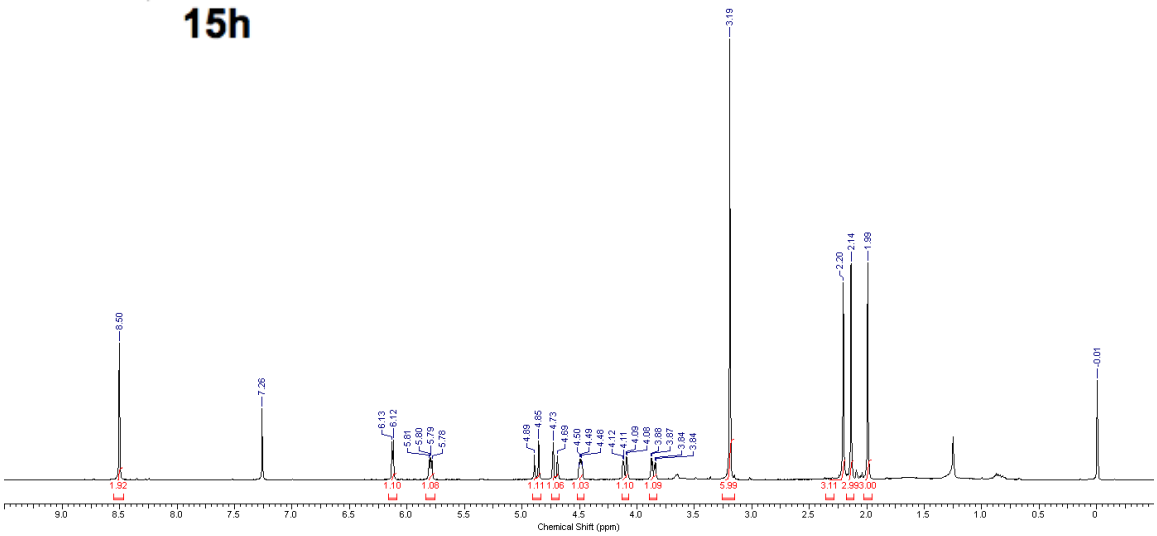
8.50
7.26
6.13
6.12
5.81
5.80
5.79
5.78
4.89
4.85
4.73
4.69
4.50
4.49
4.46
4.13
4.11
4.09
4.08
3.88
3.87
3.84
3.19
2.20
2.14
1.99
0.01
1.92
1.10
1.08
1.11
1.06
1.03
1.10
1.09
5.99
3.11
2.99
3.00
Chemical Shift (ppm)

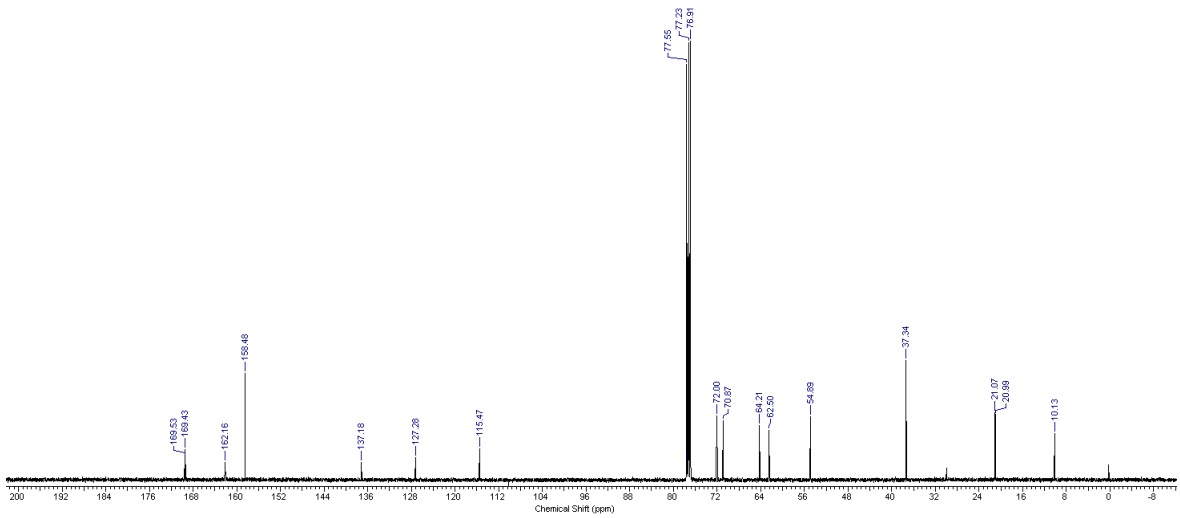
169.53
169.43
162.16
158.48
137.18
127.28
115.47
77.55
77.23
76.91
72.00
70.87
64.21
62.50
54.89
37.34
21.07
20.99
10.13
Chemical Shift (ppm)

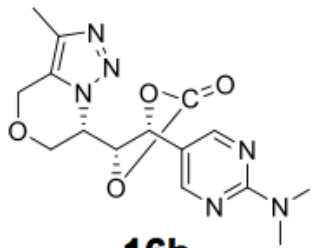

16b

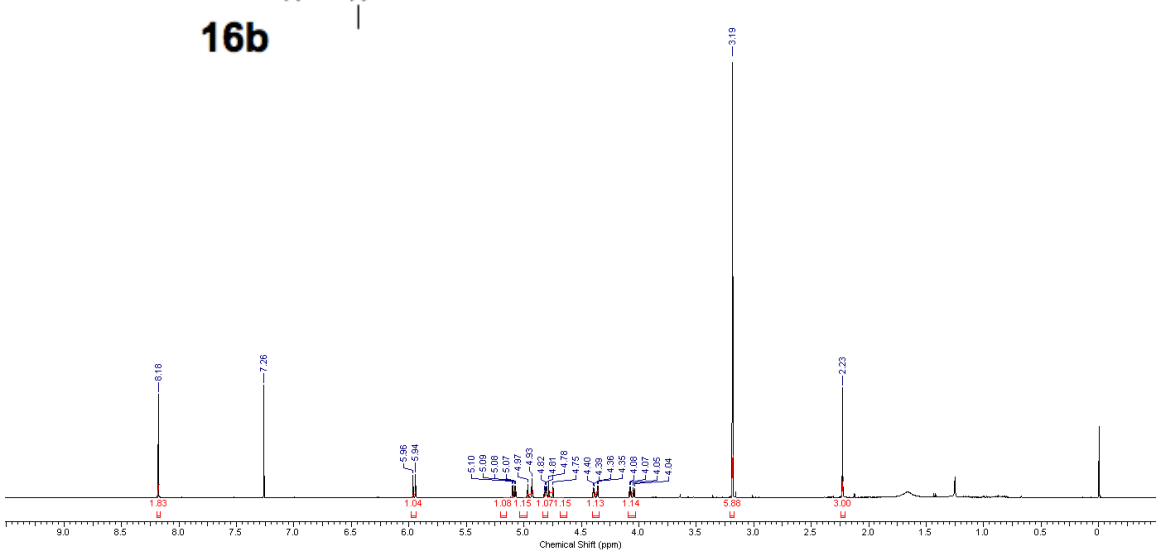
8.18
7.26
5.96
5.94
5.10
5.09
5.08
5.07
4.97
4.93
4.82
4.81
4.78
4.75
4.40
4.39
4.36
4.35
4.06
4.07
4.05
4.04
3.19
2.23
1.83
1.04
1.08
1.15
1.07
1.15
1.13
1.14
5.88
3.00
Chemical Shift (ppm)

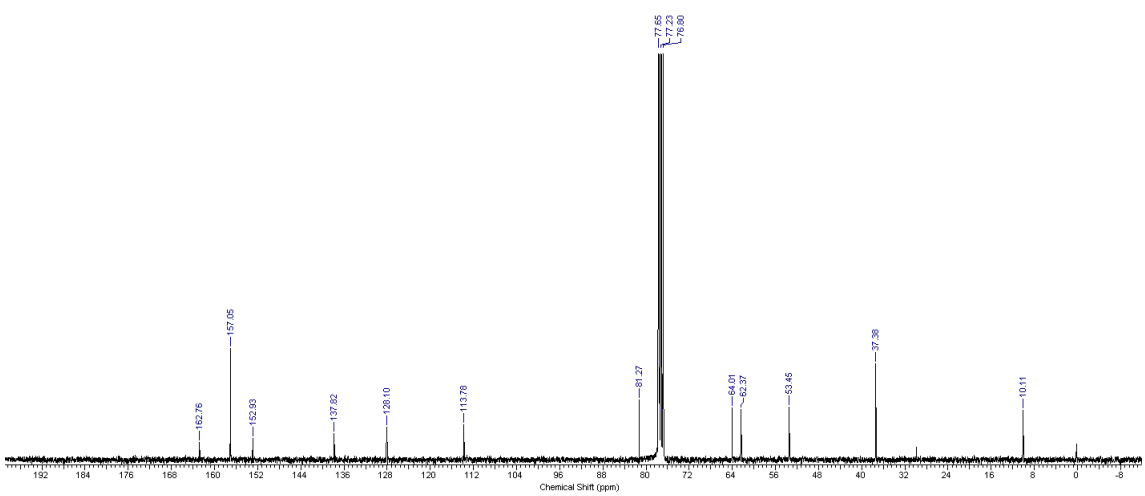
77.65
77.23
76.80
157.05
152.76
152.93
137.62
128.10
113.78
81.27
64.01
62.37
53.45
37.26
10.11
Chemical Shift (ppm)

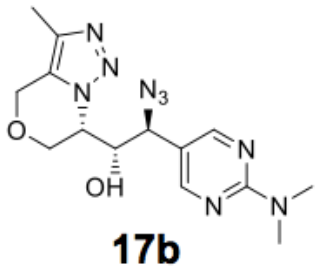
N
N
N
N3
O
OH
N
N
N

17b

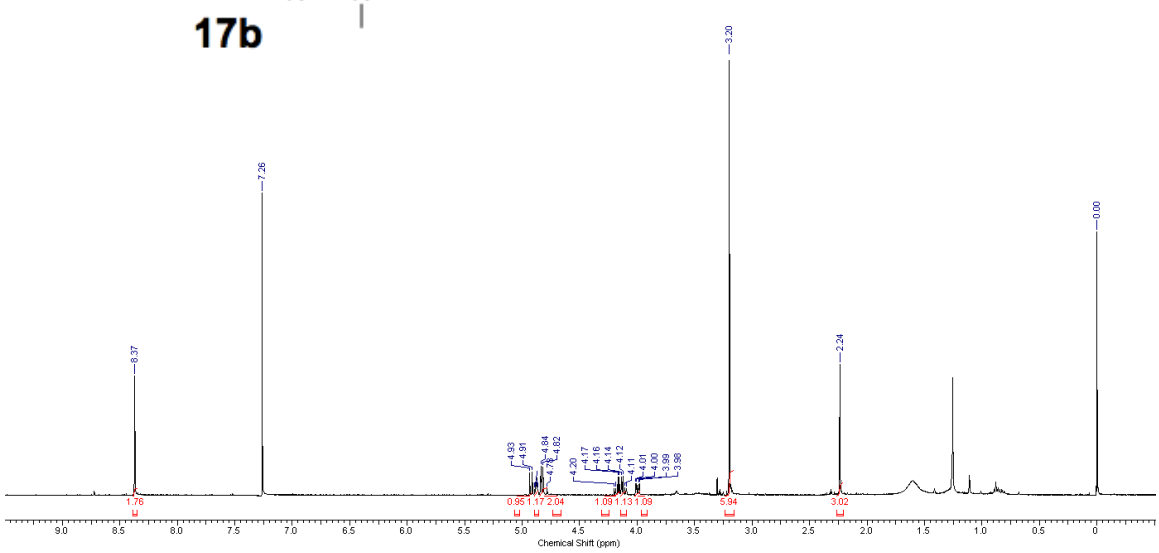
8.37
7.26
4.93
4.91
4.84
4.82
4.20
4.17
4.16
4.14
4.12
4.11
4.01
4.00
3.99
3.98
3.20
2.24
0.00
1.76
0.95
1.17
2.04
1.09
1.13
1.09
5.94
3.02
Chemical Shift (ppm)

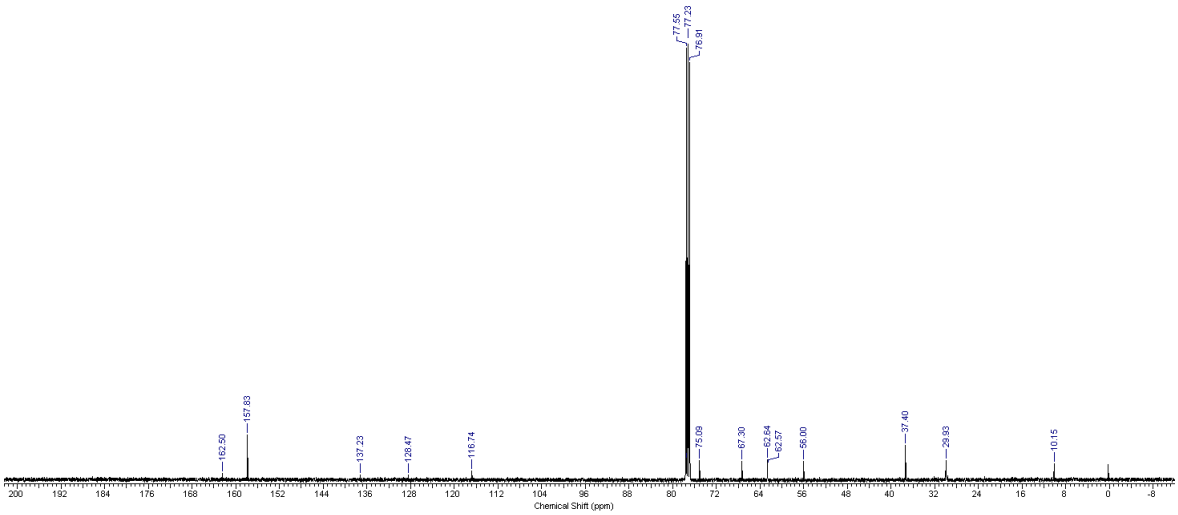
77.55
77.23
76.91
162.50
157.83
137.23
128.47
116.74
75.09
67.30
62.64
62.57
56.00
37.40
29.93
10.15
Chemical Shift (ppm)

NMR spectra of new compounds in Chapter 3

Compound **7bE**

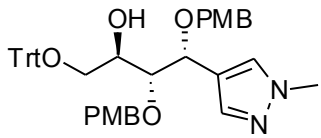

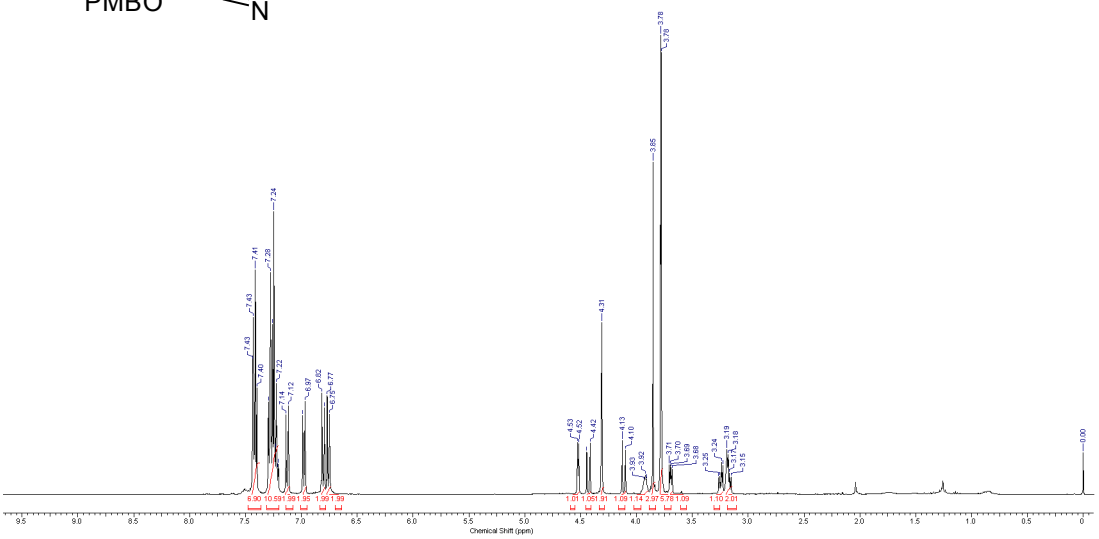

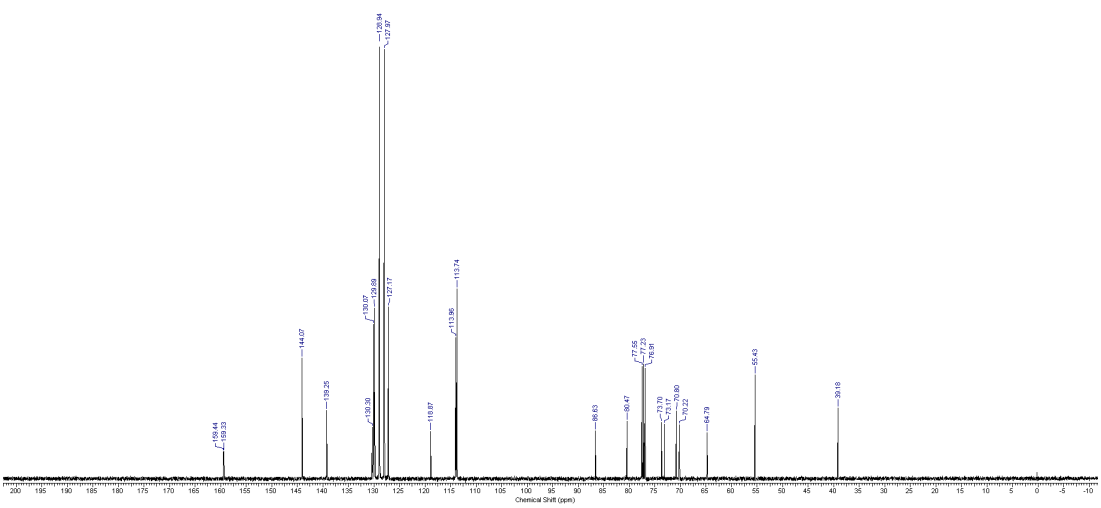

Compound **8aA**

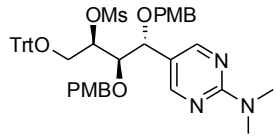

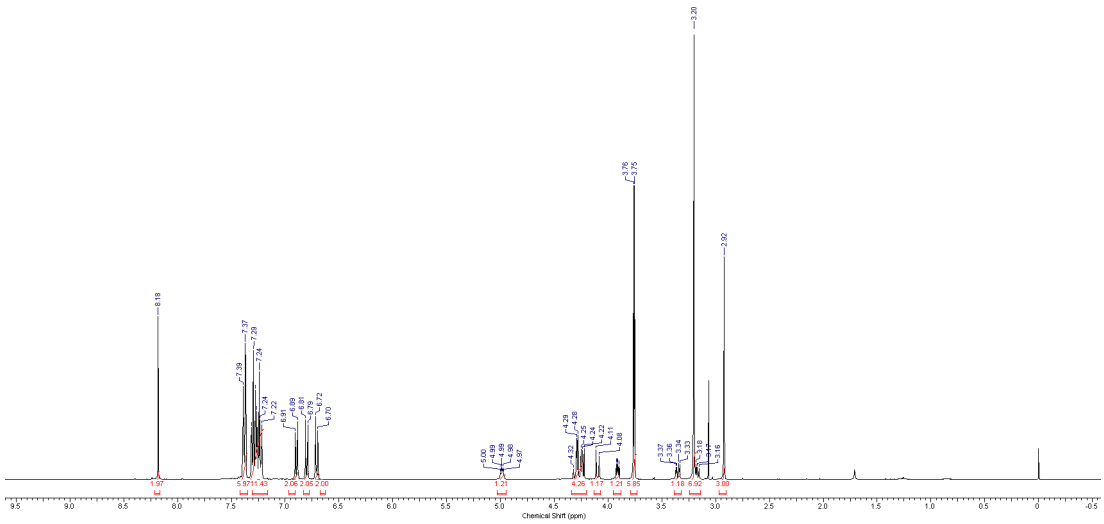

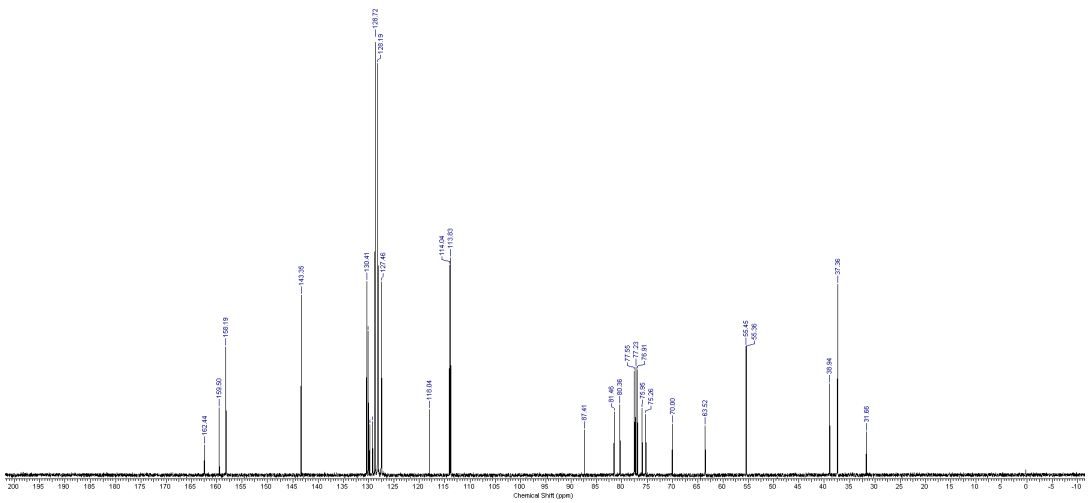

Compound **8aC**

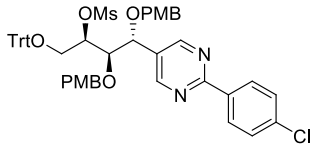

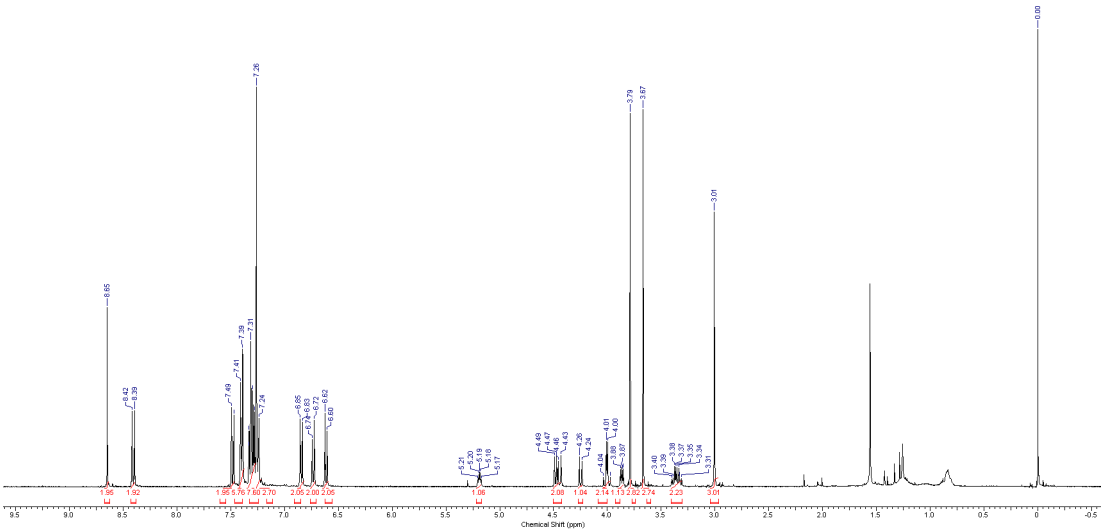

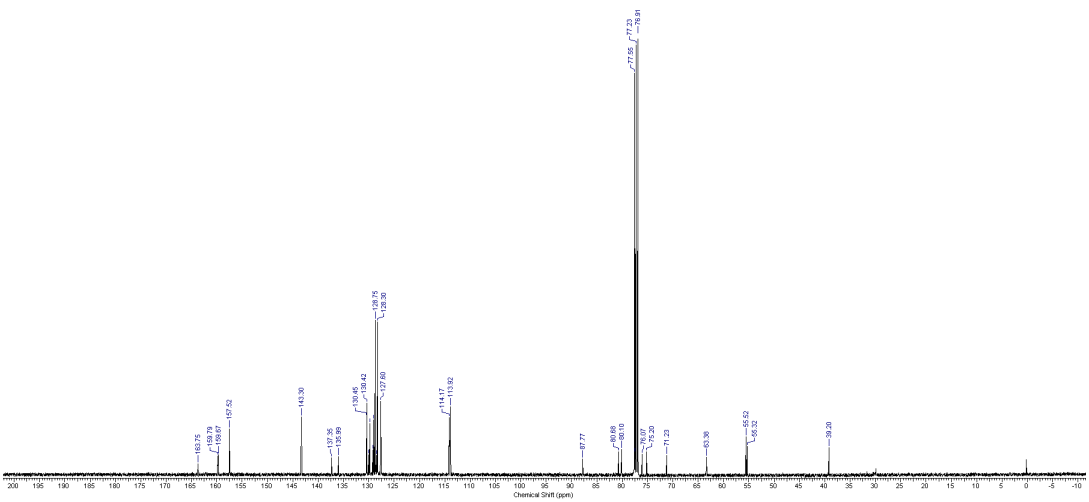

Compound **8aD**

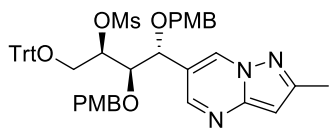

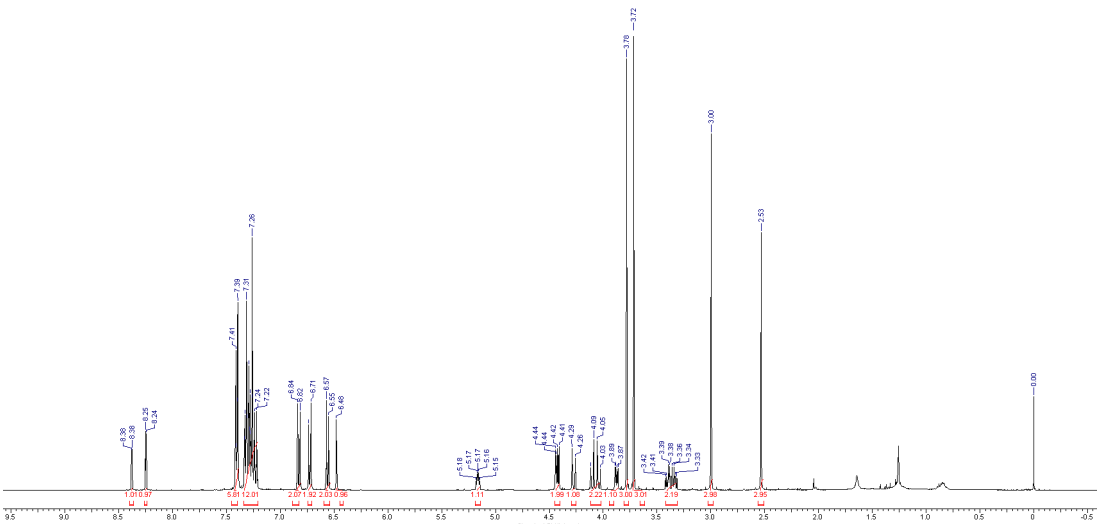

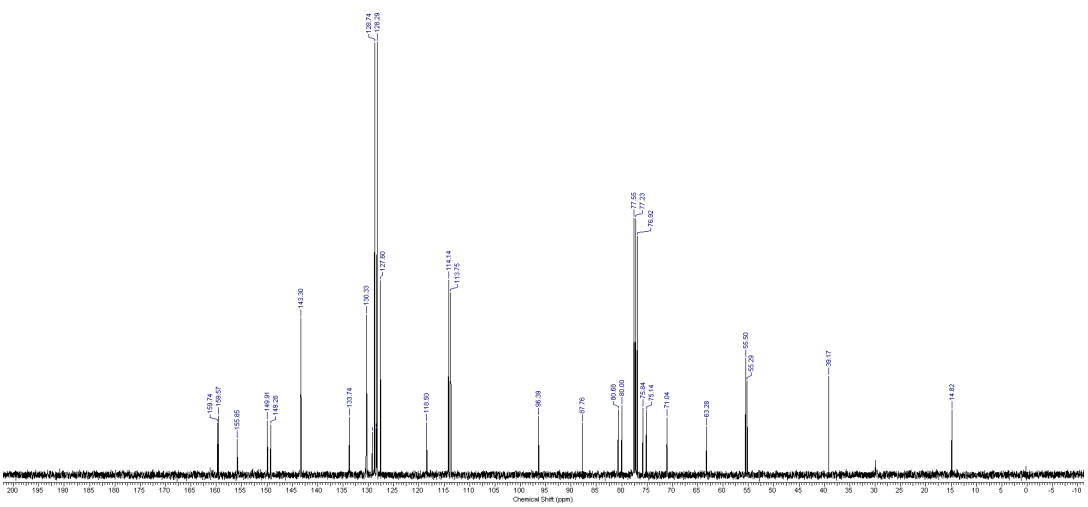

Compound **8aE**

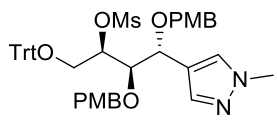

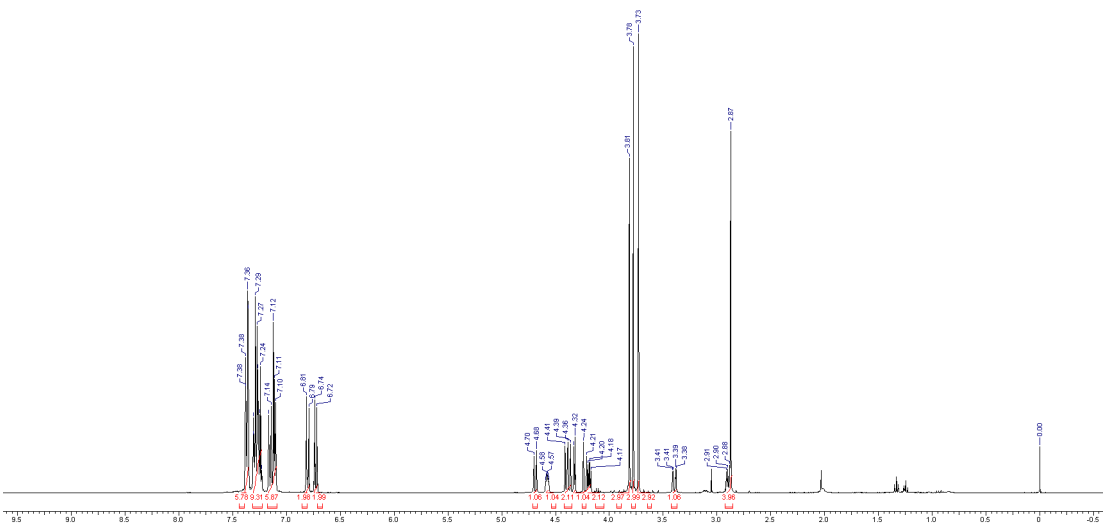

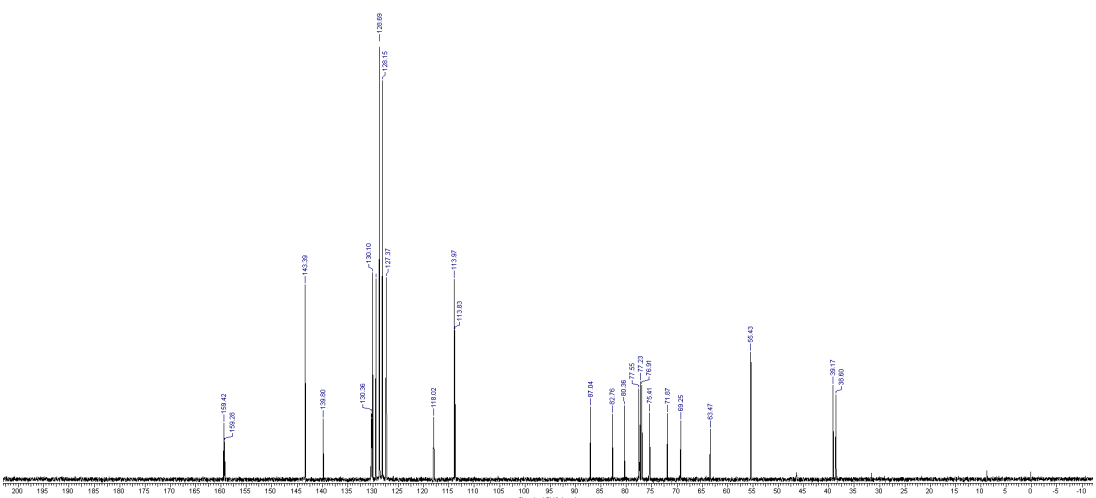

Compound **8bA**

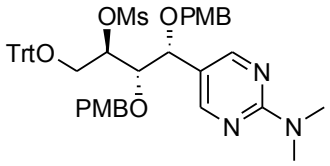

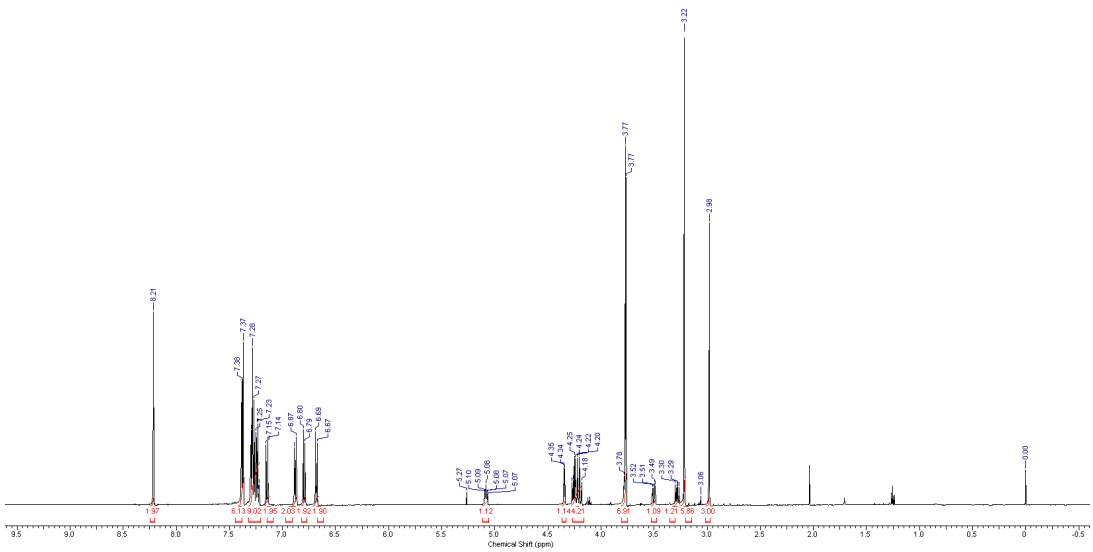

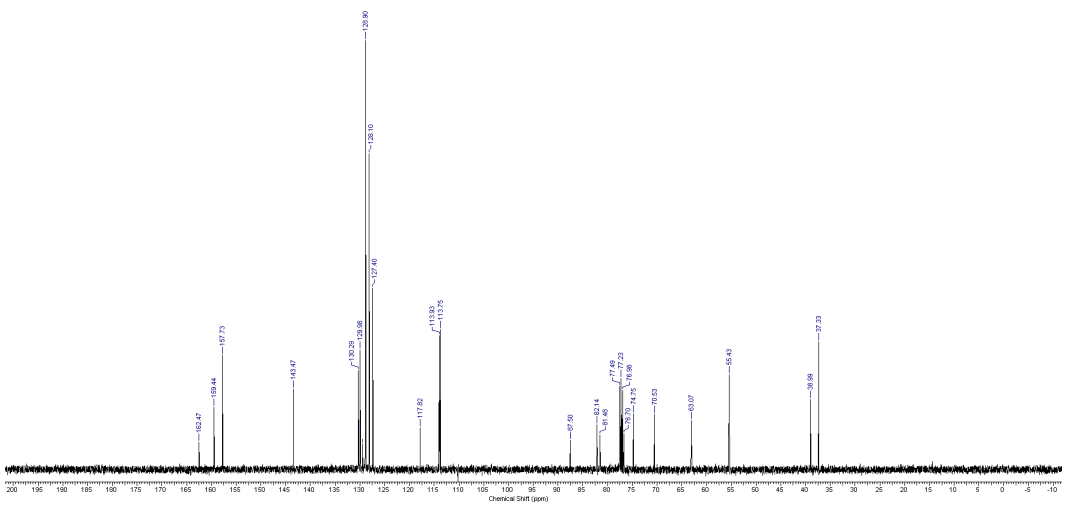

Compound **8bE**

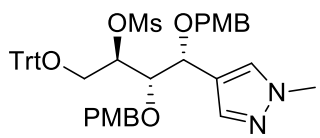

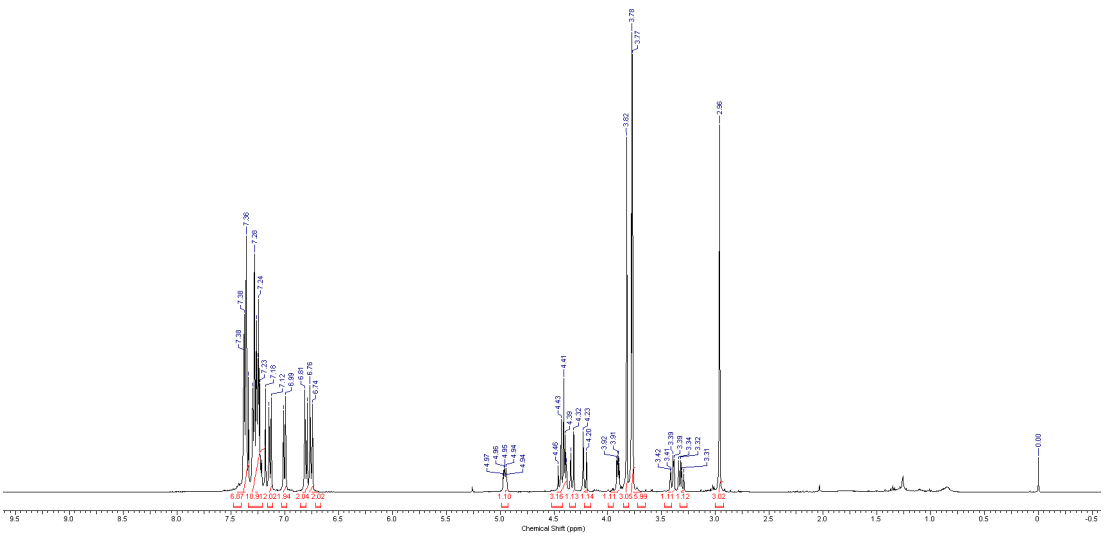

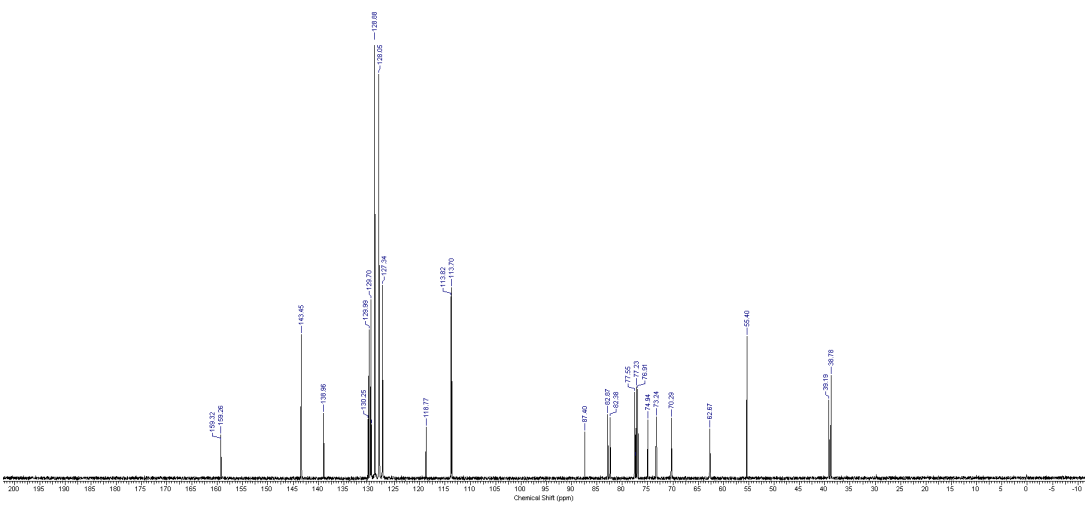

Compound **9aA**

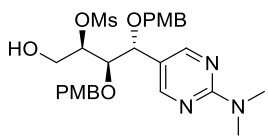

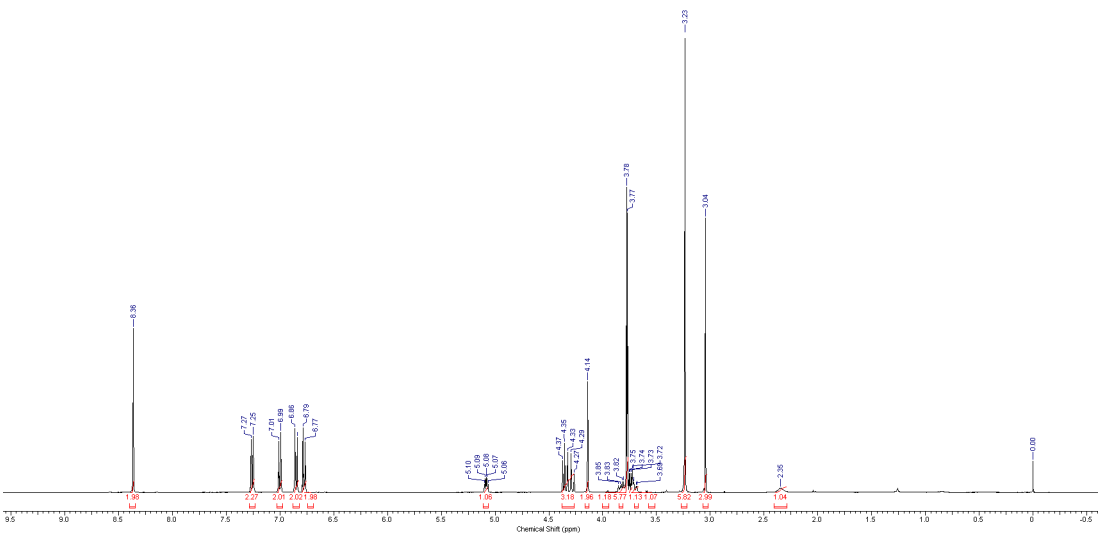

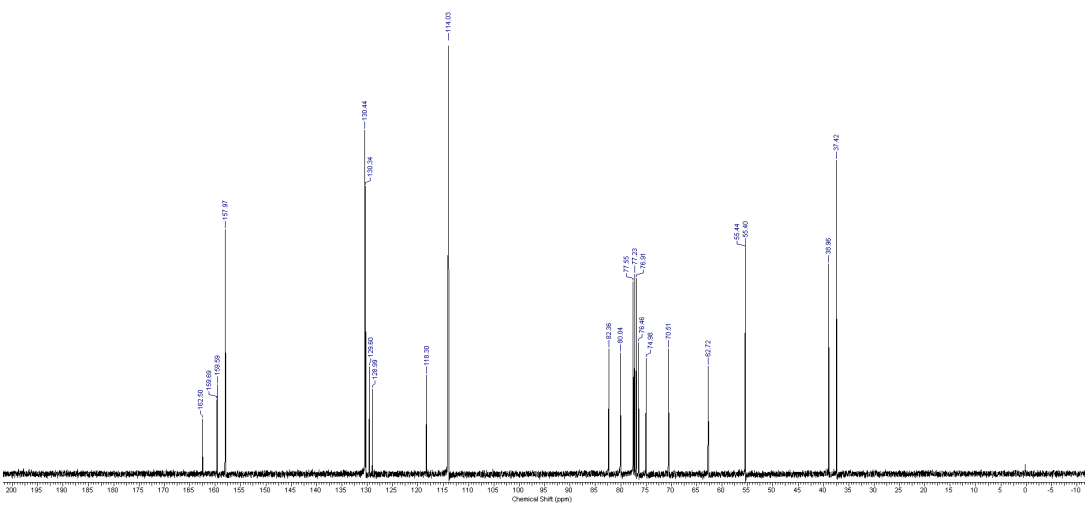

Compound **11aA**

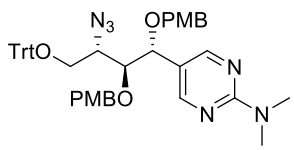

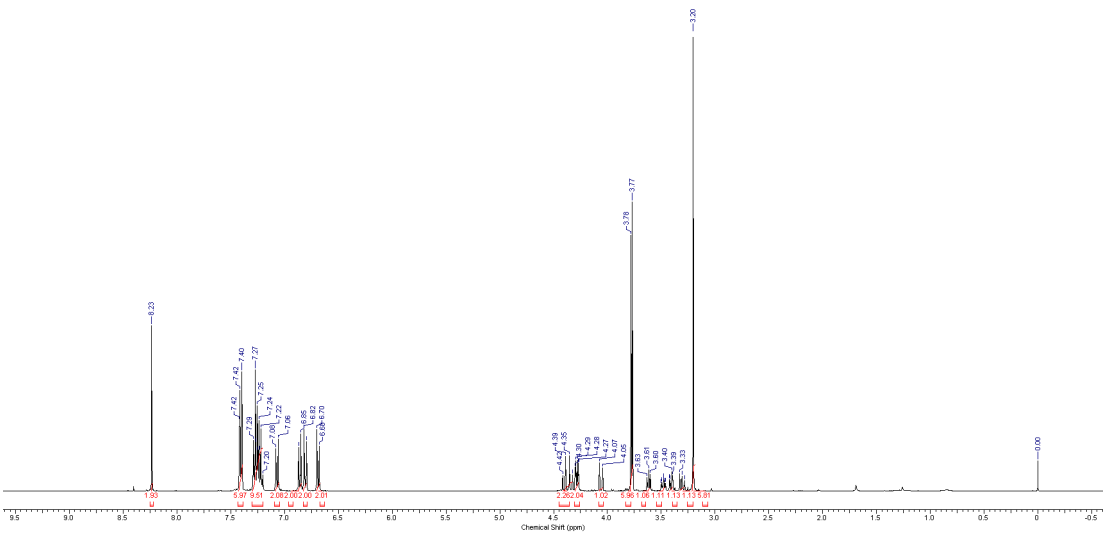

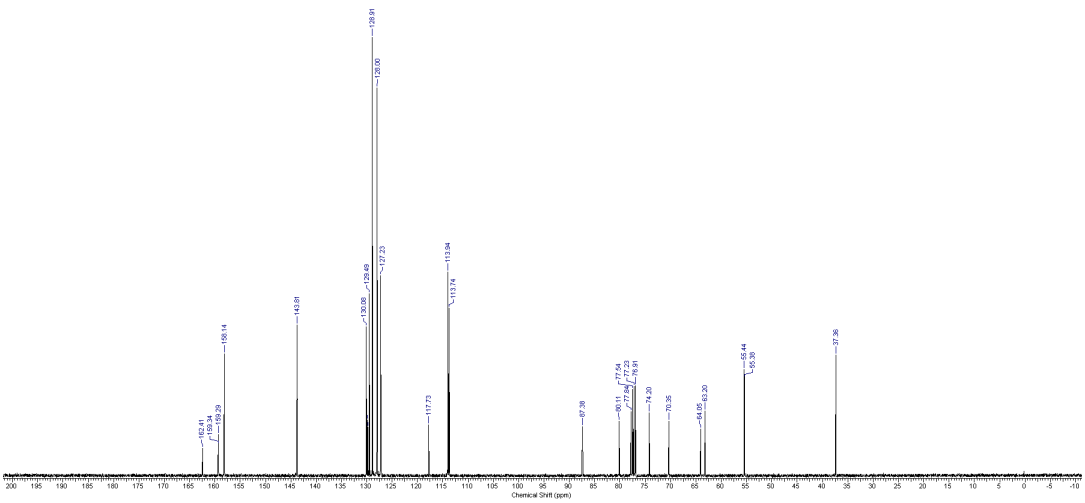

Compound **11aE**

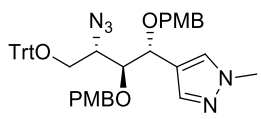

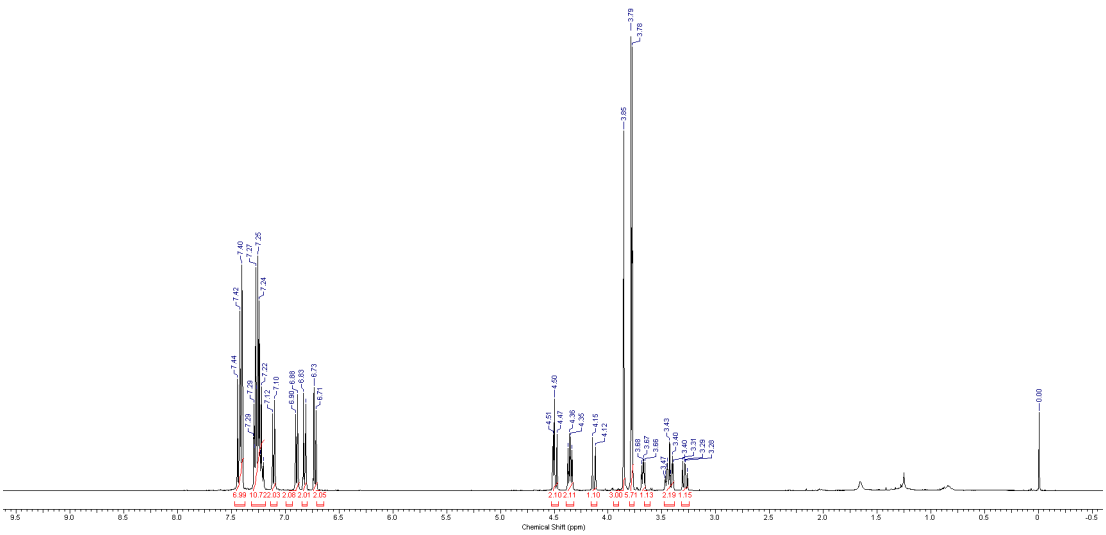

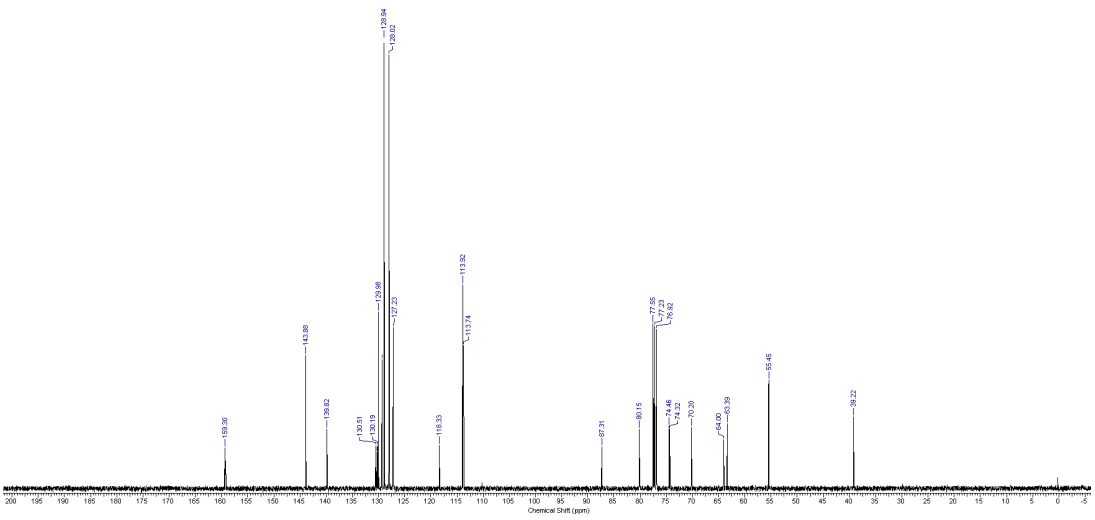

Compound **11bA**

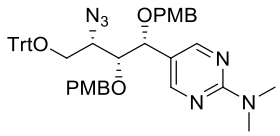

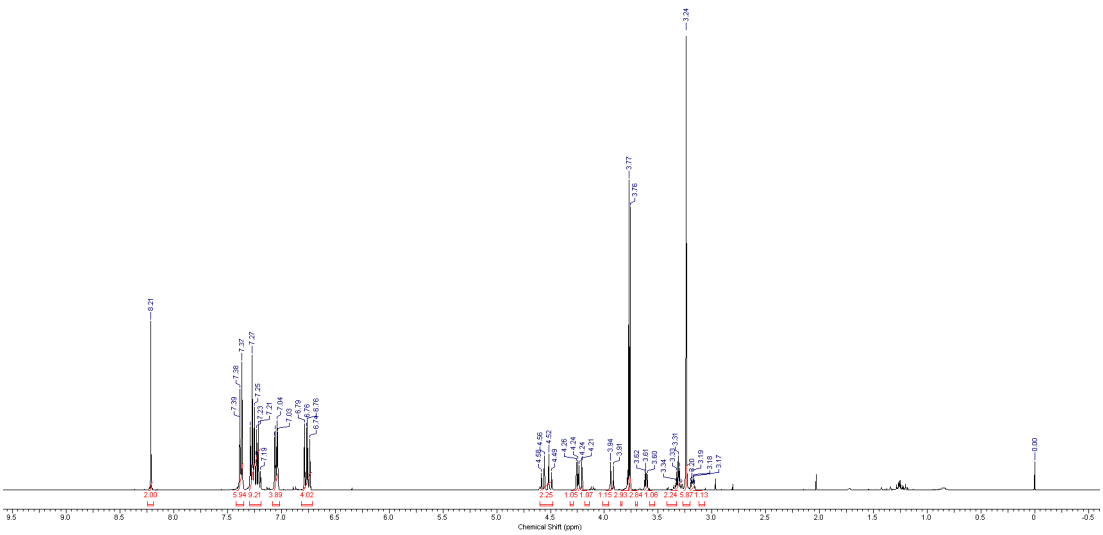

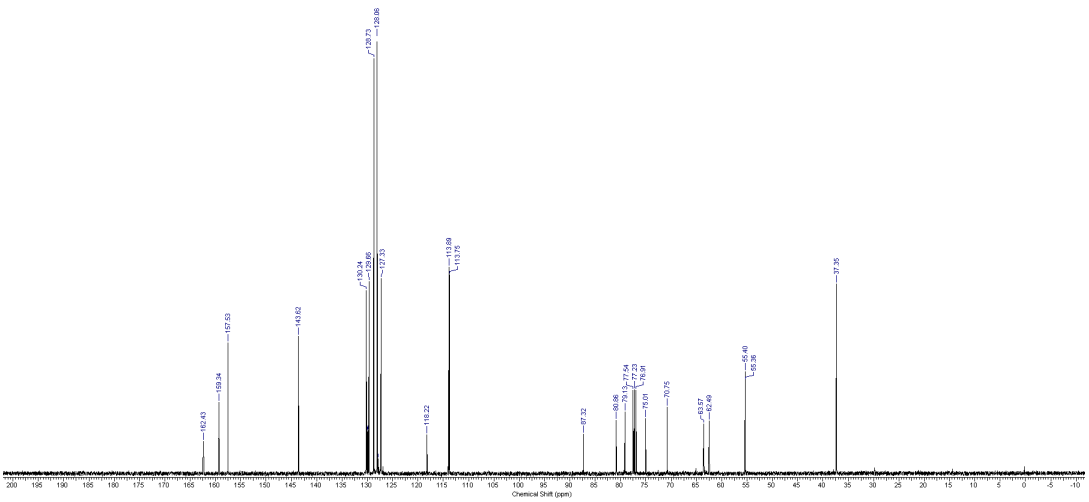

Compound **11bE**

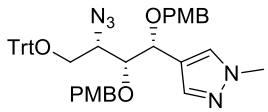

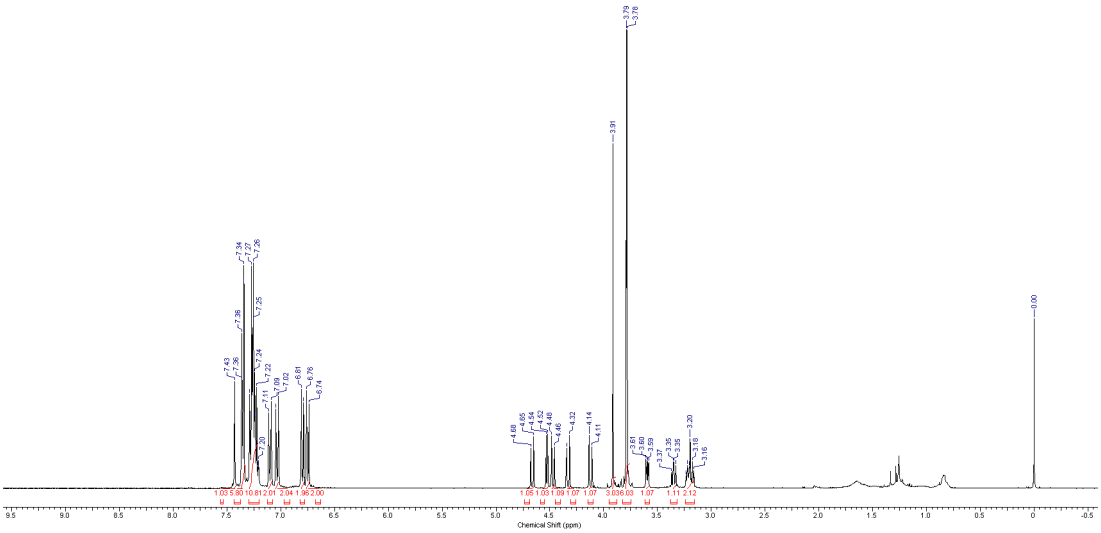

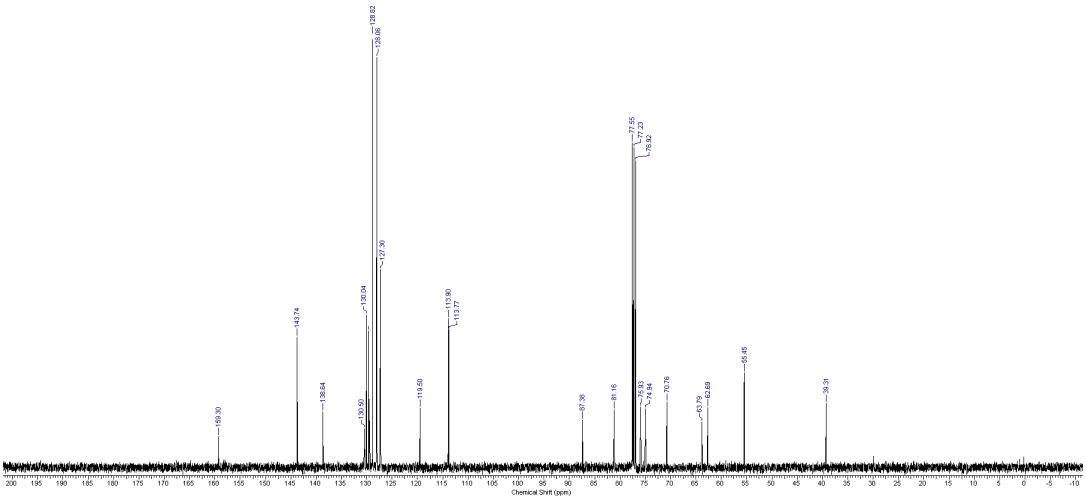

Compound **12aA**

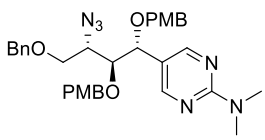

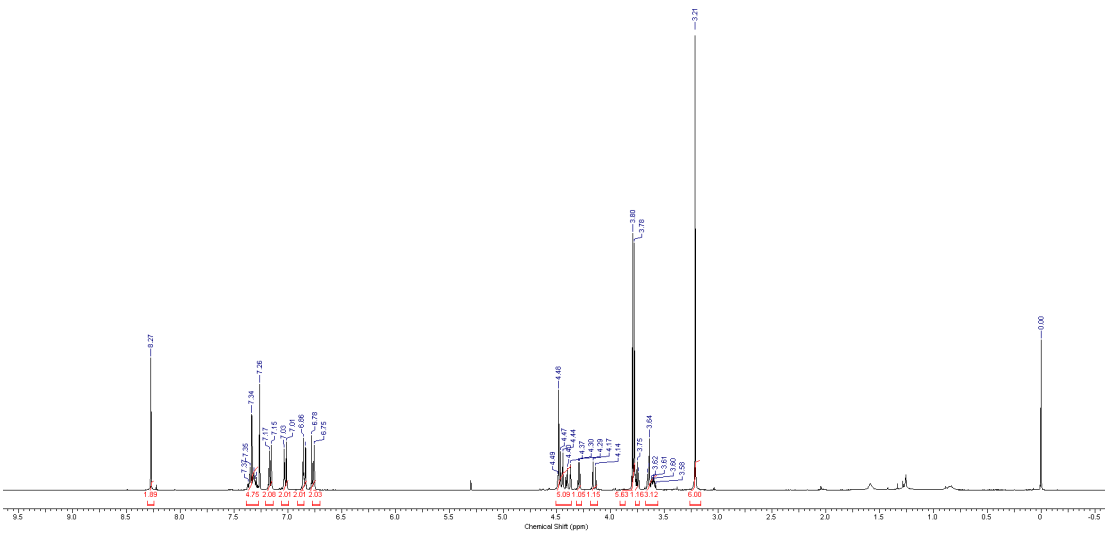

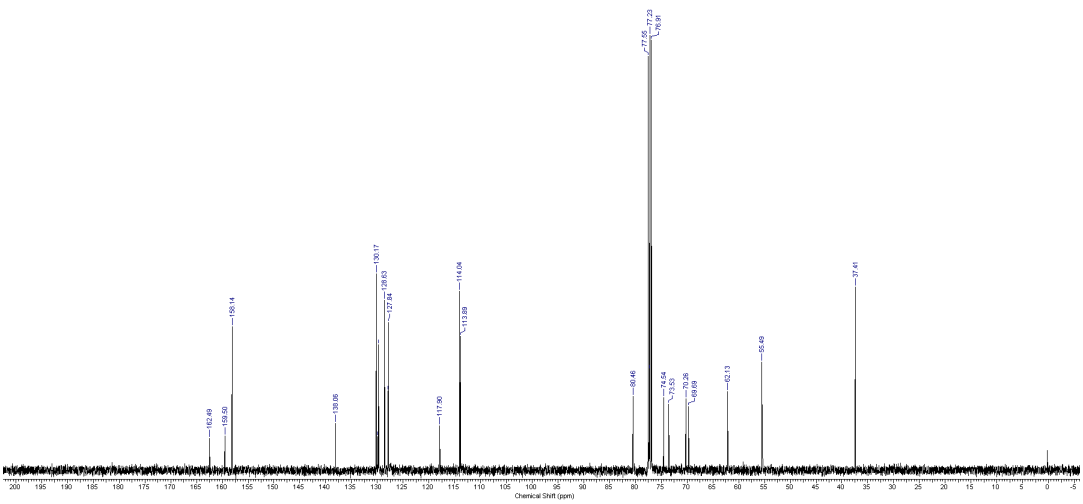

Compound **12aE**

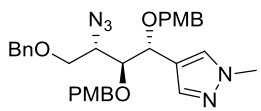

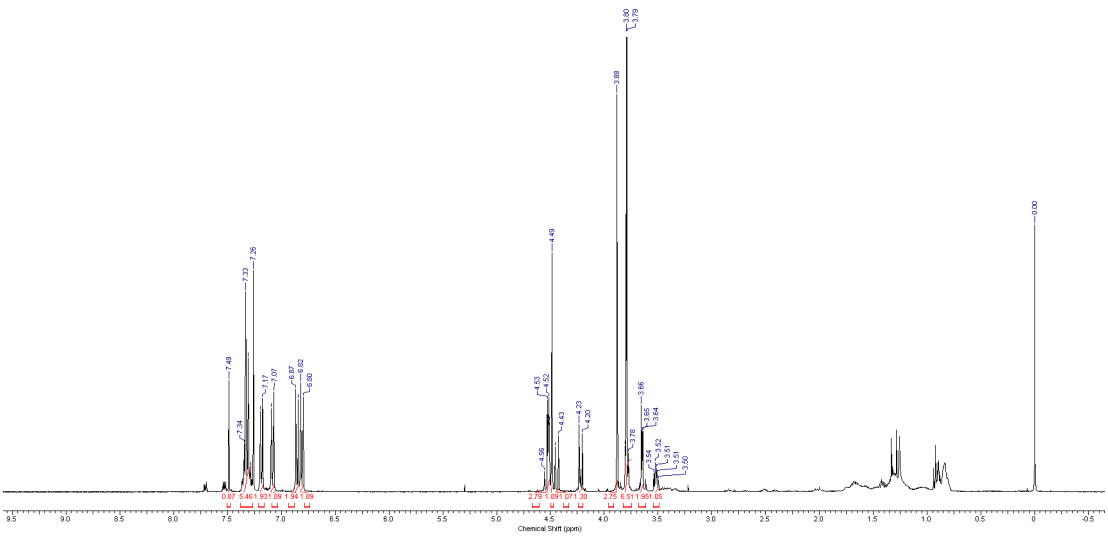

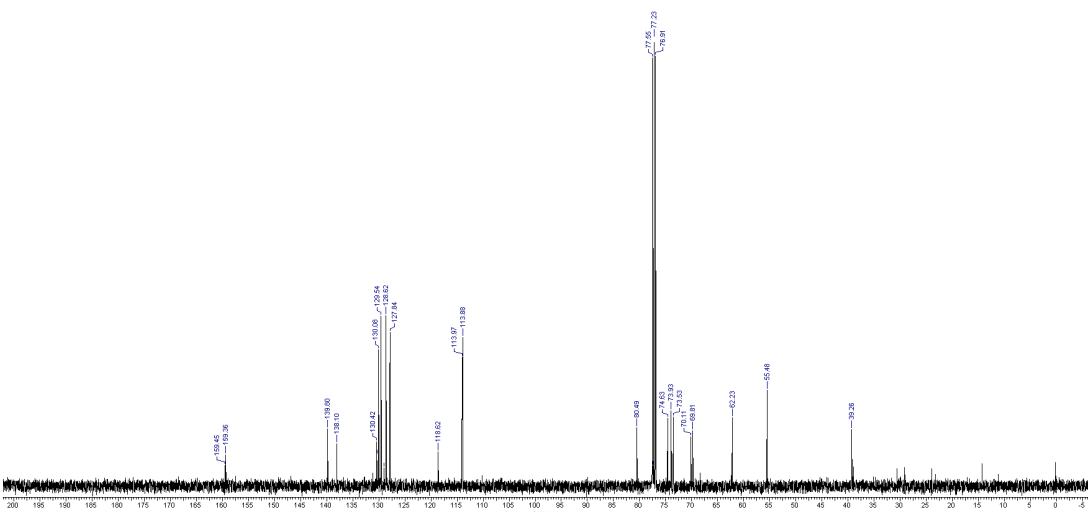

Compound **12bA**

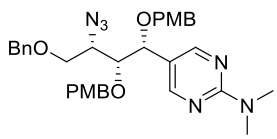

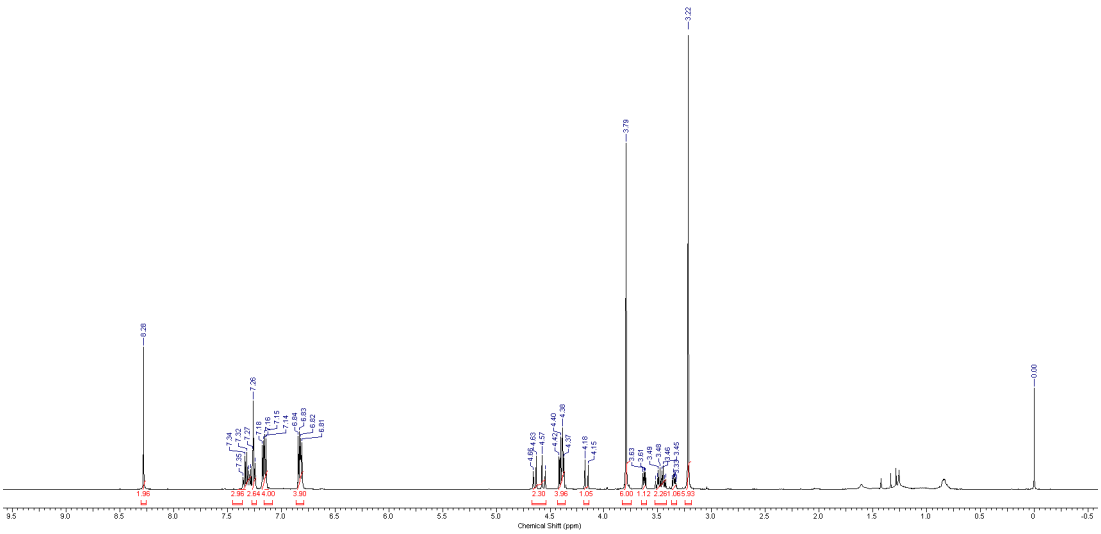

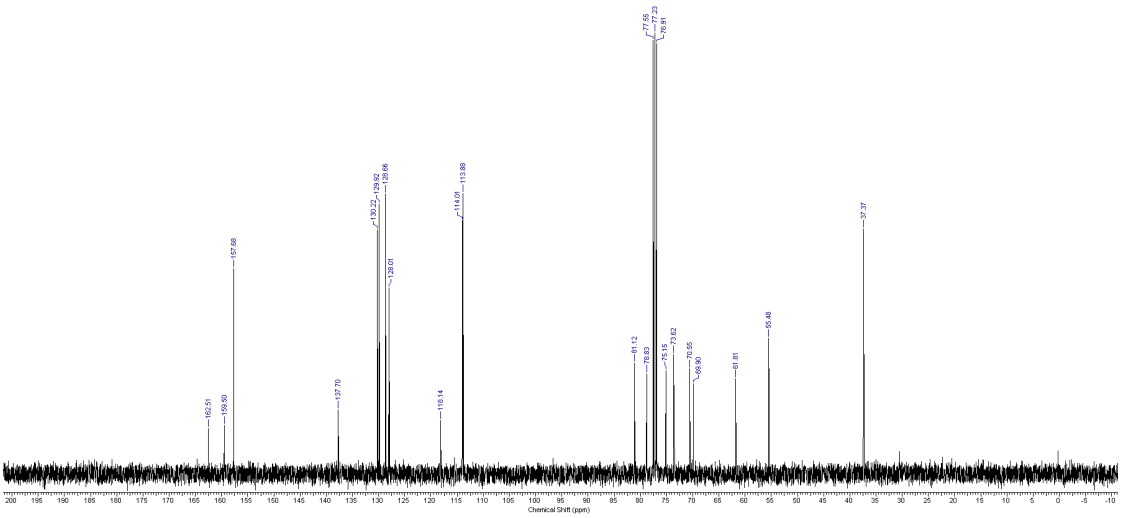

Compound **13aA**

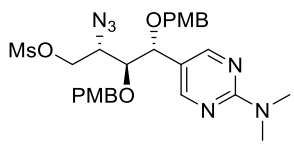

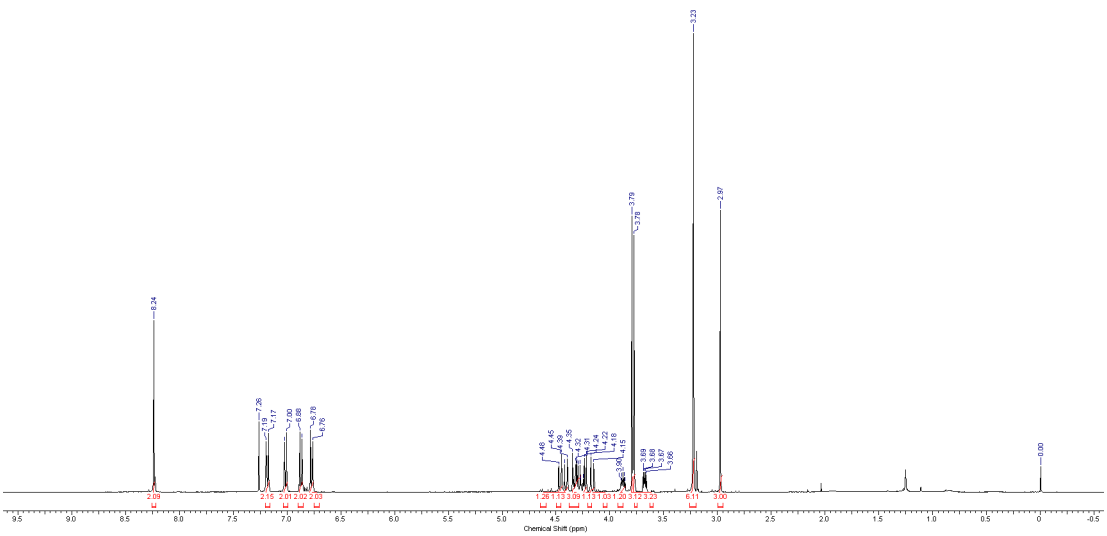

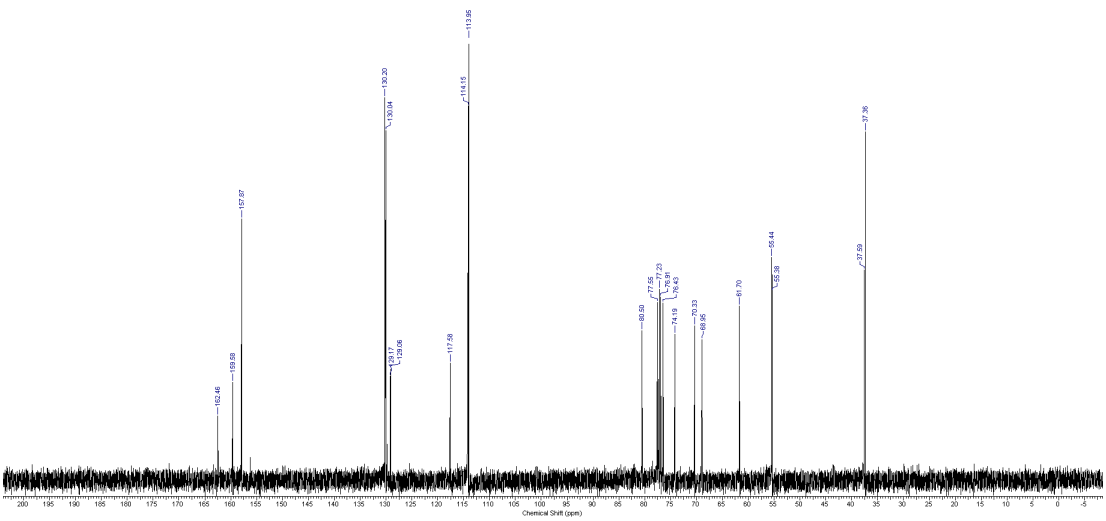

Compound **13bA**

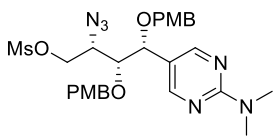

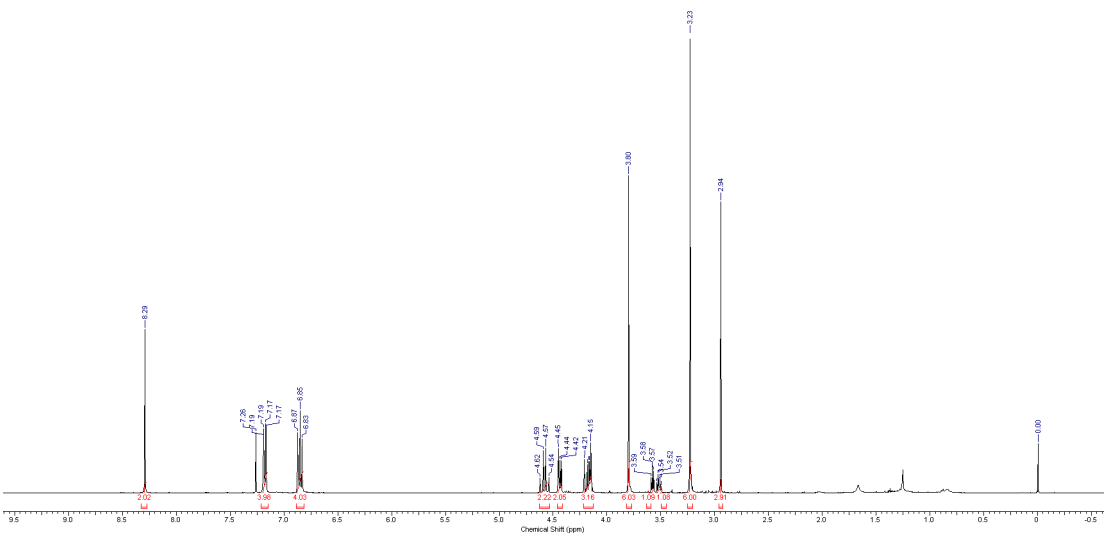

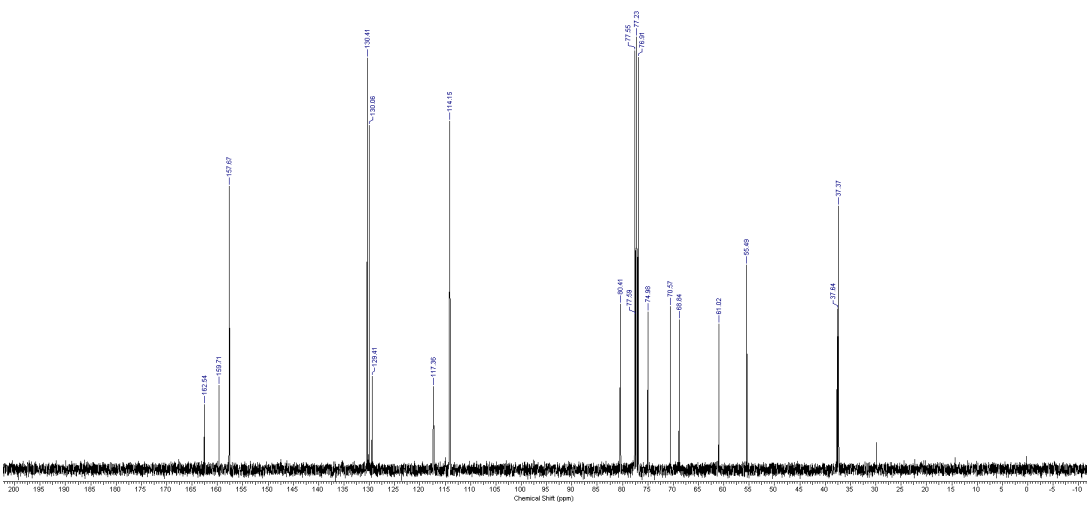

Compound **14bA**

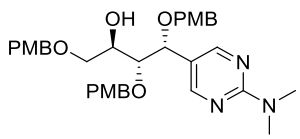

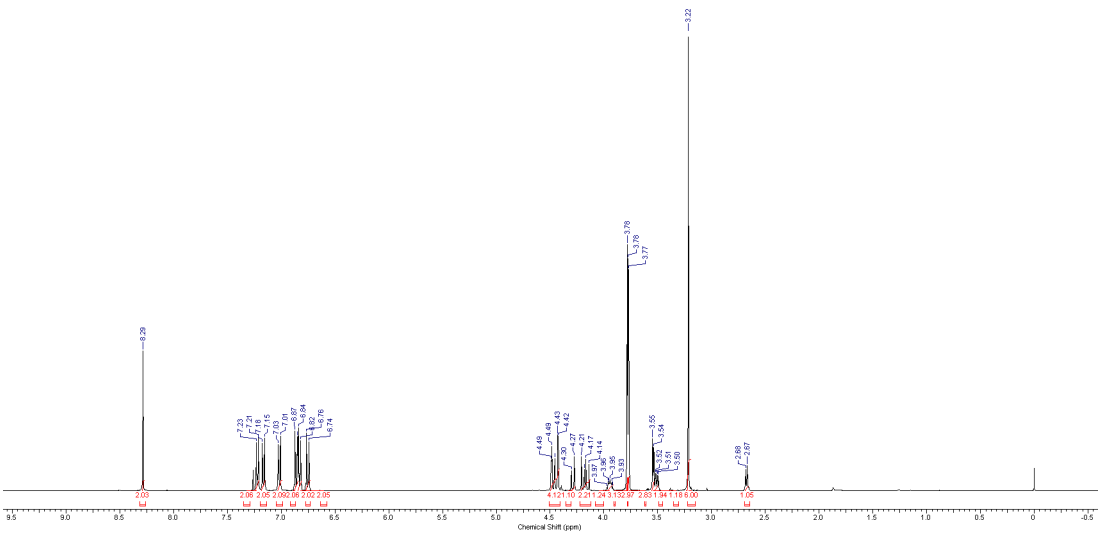

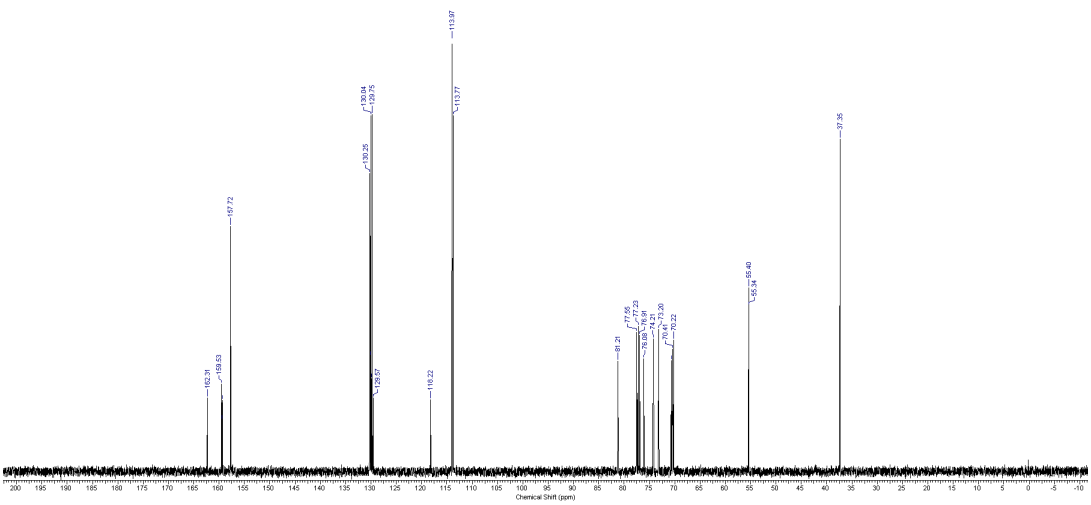

Compound **15bA**